Heuristics and metaheuristics in the design of sound-absorbing porous materials.

Submitted in partial fulfillment of
the conditions for the award of the degree

Doctor of Philosophy in Computer Science

Vivek Thaminni Ramamoorthy
14341798

Supervised by Ender Özcan, Andrew J. Parkes

School of Computer Science
University of Nottingham

I hereby declare that this dissertation is all my own work, except as indicated in the text:

Signature P.R. Vivek

Date April 4, 2023

I hereby declare that I have all necessary rights and consents to publicly distribute this dissertation via the University of Nottingham's e-dissertation archive.

Abstract

Inexact optimisation techniques such as heuristics and metaheuristics that quickly find near-optimal solutions are widely used to solve hard problems. While metaheuristics are well studied on specific problem domains such as travelling salesman, timetabling, vehicle routing etc., their extension to engineering domains is largely unexplored due to the requirement of domain expertise. In this thesis, we address a specific engineering domain, namely, the design of sound-absorbing porous materials. Porous materials are foams, fibrous materials, woven and non-woven textiles, etc., that are widely used in automotive, aerospace and household applications to isolate and absorb noise to prevent equipment damage, protect hearing or ensure comfort. These materials constitute a significant amount of dead weight in aircraft and space applications, and choosing sub-optimal designs would lead to inefficiency and increased costs. By carefully choosing the material properties and shapes of these materials, favourable resonances can be created making it possible to improve absorption while also reducing weight. The optimisation problem structure is yet to be well-explored and not many comparison studies are available in this domain. This thesis aims to address the knowledge gap by analysing the performance of existing and novel heuristic and metaheuristic methods. Initially, the problem structure is explored by considering a one-dimensional layered sound package problem. Then, the challenging two-dimensional foam shape and topology optimisation is addressed. Topology optimisation involves optimally distributing a given volume of material in a design region such that a performance measure is maximised. Although extensive studies exist for the compliance minimisation problem domain, studies and comparisons on porous material problems are relatively rare. Firstly, a single objective absorption maximisation problem with a constraint on the weight is considered. Then a multi-objective problem of simultaneously maximising absorption and minimising weight is considered. The unique nature of topology optimisation problem allows it to be solved using combinatorial or continuous, gradient or non-gradient methods. In this work, several optimisation methods are studied including solid isotropic material with penalisation (SIMP), hill climbing, constructive heuristics, genetic algorithms, tabu search, covariance matrix adaptation evolution strategy (CMA-ES), differential evolution, non-dominated sorting genetic algorithm (NSGA-II) and hybrid strategies. These approaches are tested on a benchmark of seven acoustics problem instances. The results are used to extract domain-specific insights. The findings highlight that the problem domain is rich with unique varieties of solutions, and by using domain-specific insights, one can design hybrid gradient and non-gradient methods that consistently outperform the state-of-the-art ones.

Acknowledgements

First and foremost, I am thankful for the guidance and nurturing provided by my supervisors, Ender Özcan and Andrew J. Parkes. After every supervision meeting, I gained new perspectives on metaheuristics and research in general. Their support has helped me grow exponentially in these few years.

I am grateful to my industrial supervisors from Matelys Research Lab, Luc Jaouen and François-Xavier Bécot, for their dedication to research and teaching. They have introduced me to the breadths and depths of the world of acoustic porous materials. They have also provided training, transferable skills, and software access to carry out research seamlessly.

I am thankful for the European Union's Marie Skłodowska-Curie Actions initiative, which made such an interdisciplinary project with industry collaboration possible. I am fortunate to have engaged with remarkable fellow early-stage researchers in the No2Noise project, Abhilash and Arasan, whose collaboration and friendship constitute a large part of the time spent during my PhD. I am thankful to the No2Noise supervisory board, including Jelena Ninic, Dimitrios Chronopoulos, Savvas Triantafyllou, Gregor Tanner and Fabien Chevillotte, for their numerous interactions and guidance throughout the project. I also thank the administrative staff, Sarah, Paul and Manuela, for their persistent support.

I am thankful for the kind interactions and fruitful discussions with Derya, Elif, Han, Lam, Manikumar, Mehdi, Peng (Simon), Rebecca, Udit, Vinicius, Warren, Weijie, Weiyao, Yun and others. I am fortunate to have had the opportunity to interact with the remarkable faculty members of the COL group, including Dario, Rong, Jason, Isaac, Geert, Ferranti, Bob and others. Thanks to Vik and Kiran, who worked in the background to facilitate seamless access to the University's computational resources.

I am thankful to my parents, Bharathi and Ramamoorthy, and my brother, Gowtham, for their unconditional love and support in all my endeavours. Finally, a special thanks to my long-term partner and now wife, Preethi Rajendram Soundararajan, for her unfettered love, encouragement and support, without whom this effort would not have been possible.

I dedicate this thesis to all my teachers.

Contents

Abstract i

Acknowledgements iii

1 Introduction 1
- 1.1 Introduction . . . 1
- 1.2 Motivation . . . 2
- 1.3 State of the art . . . 2
- 1.4 Gaps in knowledge . . . 5
- 1.5 Focus of the current thesis . . . 6
- 1.6 Contributions in this thesis . . . 7
- 1.7 Thesis structure . . . 8
- 1.8 Publications from this research . . . 9

I Literature review chapters 11

2 Metaheuristics literature 12
- 2.1 Introduction . . . 12
- 2.2 Local search . . . 14
  - 2.2.1 Hill Climbing . . . 14
  - 2.2.2 Iterated local search . . . 15
- 2.3 Simulated annealing . . . 15
- 2.4 Tabu search . . . 16
- 2.5 Genetic algorithms . . . 16
- 2.6 Memetic algorithms . . . 17
- 2.7 Differential evolution . . . 18
- 2.8 Surrogate modelling methods . . . 19
- 2.9 Metaphor controversy . . . 19
- 2.10 Hyper heuristics . . . 20
- 2.11 Use in topology optimisation . . . 20
- 2.12 Conclusions . . . 21

3 Acoustic porous material literature 22
- 3.1 Introduction . . . 22
- 3.2 Basics of acoustics . . . 23
- 3.3 Material models for dissipative media . . . 24
  - 3.3.1 Motionless skeleton models . . . 25
  - 3.3.2 Poroelastic materials . . . 29

3.4 Properties of porous media . . . 29
3.4.1 Open porosity . . . 30
3.4.2 Static airflow resistivity . . . 30
3.4.3 High-frequency limit of the tortuosity . . . 30
3.4.4 Viscous characteristic length . . . 30
3.4.5 Thermal characteristic length . . . 31
3.4.6 Static thermal permeability . . . 31
3.4.7 Static viscous tortuosity . . . 32
3.4.8 Static thermal tortuosity . . . 32
3.5 Geometric modelling methods . . . 32
3.5.1 Transfer matrix method (TMM) . . . 32
3.5.2 Finite element method (FEM) . . . 34
3.6 Conclusions . . . 36

4 Topology optimisation literature **37**
4.1 Introduction . . . 37
4.2 The compliance minimisation problem . . . 39
4.2.1 What is compliance? . . . 39
4.2.2 Problem formulation . . . 40
4.2.3 Topology optimisation methods . . . 41
4.3 Extension to acoustic problem domains . . . 43
4.3.1 Gaps in knowledge . . . 48
4.4 Conclusions . . . 48

II Contribution chapters **50**

5 Multilayered sound package optimisation **51**
5.1 Introduction . . . 51
5.2 Problem description . . . 55
5.3 Two-layered porous and screen . . . 57
5.3.1 Problem description . . . 58
5.3.2 Modelling the fibrous/foam layer . . . 58
5.3.3 Modelling the screen . . . 59
5.3.4 Results . . . 60
5.4 Three-layered porous absorption package . . . 63
5.4.1 Problem description . . . 63
5.4.2 Genetic algorithm . . . 64
5.4.3 Results . . . 65
5.4.4 Fitness landscape analysis . . . 67
5.4.5 Guidelines for algorithm selection . . . 70
5.5 Conclusions . . . 70

6 Single-objective topology optimisation **72**
6.1 Introduction . . . 72
6.1.1 Heuristics . . . 73
6.1.2 Metaheuristics . . . 73
6.1.3 Acoustic topology optimisation . . . 74
6.1.4 Contributions in this chapter . . . 74

6.1.5 Organisation of this chapter . . . 74
6.2 Problem description . . . 75
6.2.1 Optimisation formulation . . . 75
6.2.2 Computing the fitness function: sound absorption . . . 77
6.2.3 Computing gradient of sound absorption . . . 79
6.2.4 Verification of the modelling procedure . . . 83
6.2.5 Fitness computation performance improvements . . . 83
6.2.6 Computational complexity . . . 86
6.2.7 Benchmark problem instances . . . 89
6.3 Experimental design . . . 90
6.4 Heuristics . . . 92
6.4.1 Hill climbing (HC) . . . 92
6.4.2 Constructive heuristics (CH1 & CH2) . . . 93
6.4.3 Solid isotropic material with penalisation (SIMP) . . . 94
6.5 Metaheuristic approaches . . . 95
6.5.1 Genetic algorithm (GA) . . . 96
6.5.2 Tabu search (TABU) . . . 99
6.5.3 Covariance-matrix-adaptation evolution strategy (CMA) . . . 102
6.5.4 Discrete variant of CMA evolution strategy (CMAd) . . . 102
6.5.5 Differential evolution (DE) . . . 103
6.5.6 Discrete variant of differential evolution (DEd) . . . 105
6.6 Results and discussion . . . 106
6.6.1 Run time performance comparison . . . 106
6.6.2 Final solution quality comparison . . . 108
6.6.3 Performance across problem instances . . . 110
6.6.4 Best shapes obtained from algorithms . . . 113
6.6.5 Statistical test: Wilcoxon signed-rank test . . . 114
6.6.6 Landscape analysis . . . 115
6.7 Conclusions . . . 118

7 Multi-objective topology optimisation 119
7.1 Introduction . . . 119
7.2 Methodology . . . 121
7.2.1 Problem formulation . . . 121
7.2.2 Computing the objective function . . . 123
7.2.3 Benchmark problem instances . . . 124
7.2.4 Approaches for multi-objective topology optimisation . . . 124
7.3 Experimental design . . . 125
7.4 Solid-isotropic-material-with-penalisation . . . 127
7.4.1 SIMPrestart . . . 127
7.4.2 SIMPsweep . . . 130
7.4.3 Comparison between SIMPsweep and SIMPrestart . . . 130
7.5 Constructive heuristic using gradient (CHg) . . . 133
7.6 Comparison of gradient-based algorithms . . . 135
7.7 Hill climbing with scalarisation (HC) . . . 135
7.7.1 Weighted-sum vs. Chebyshev scalarisation . . . 139
7.8 Non-dominated sorting genetic algorithms (NSGA-II) . . . 140
7.9 Random Search (RAND) . . . 141

7.10 Comparison of non-gradient algorithms . . . 145
7.10.1 Performance per trial . . . 145
7.10.2 Performance across 15 trials . . . 145
7.11 Hybrid algorithm 1: CHg+HC . . . 147
7.12 Hybrid algorithm 2: CHg+NSGA-II . . . 148
7.13 Overall comparison . . . 152
7.13.1 Trial-averaged performance for 4096 budget . . . 152
7.13.2 Combined performance of 15 trials each with 4096 budget . . . 153
7.13.3 Pareto front comparison for all algorithms combined across 15 trials . . . 153
7.14 Conclusions . . . 154

8 Conclusions and perspectives **156**
8.1 Multilayered sound package optimisation study . . . 156
8.1.1 Summary . . . 156
8.1.2 Contributions . . . 156
8.2 Single objective topology optimisation study . . . 157
8.2.1 Summary . . . 157
8.2.2 Contributions . . . 158
8.3 Multi-objective topology optimisation study . . . 158
8.3.1 Summary . . . 158
8.3.2 Contributions . . . 159
8.4 Reflections and future work prospects . . . 160
8.5 Final remarks . . . 162

Bibliography **162**

Appendices **183**

A Database of porous materials **183**

B Topology optimisation **191**
B.1 Runtime progress: all problem instances . . . 191
B.2 Final solution absorption-distribution from trials . . . 195
B.3 Final solution absorption vs. volume fraction . . . 196
B.4 Final solutions across trials . . . 196

C Multi-objective optimisation **204**
C.1 Pareto plots for 15-trial-combined results . . . 204

List of Tables

4.1 Topology optimisation applications. . . . 39
4.2 A list of most acoustic topology optimisation publications 45

5.1 Material parameters required by each acoustic model. . . . 56
5.2 Genetic algorithm standard parameters. . . . 65
5.3 Best multilayered system 69

6.1 Time complexity comparison absorption vs. compliance problem domains . . . 88
6.2 Benchmark problems for single objective topology optimisation 89
6.3 Properties of materials used in benchmark problems 89
6.4 Optimisation approaches used in the single objective topology optimisation study 91
6.5 Final algorithm ranks for single objective topology optimisation 111
6.6 Wilcoxon signed-rank test problem instance 6 115

7.1 Classification of multi-objectives approaches for topology optimisation 124
7.2 Multiobjective optimisation approaches and their settings. . . . 126
7.3 Hypervolume comparison of gradient methods 135
7.4 Comparison of scalarisation methods 139
7.5 Per-trial hypervolume comparisons for all algorithms 152
7.6 Combined-15-trial hypervolumes covered by all multi-objective algorithms . . 153

A.1 Air 183
A.2 Air dissipative 183
A.3 Felt 62 kg·m^{-3} 183
A.4 Felt 93 kg·m^{-3} 184
A.5 Foam 55 kg·m^{-3} 184
A.6 Foam Agglomerate, Gourdon and Seppi [93] 184
A.7 Foam Backrest 185
A.8 Foam Agglomerate, Gourdon and Seppi [93] 185
A.9 Foam cushion 185
A.10 Foam Headliner 185
A.11 Foam R1 Perrot *et al.* 2012 [190] 185
A.12 Glasswool Thermal 186
A.13 Glasswool 16 kg·m^{-3} 186
A.14 Glasswool 18 kg·m^{-3} 186
A.15 Glasswool 18 kg·m^{-3} visco 187
A.16 Glasswool 27 kg·m^{-3} 187
A.17 Glasswool 8 kg·m^{-3} 187
A.18 Melamine foam 188

A.19 Mineral wool Villot *et al.* 2001 [248] 188
A.20 Perforated Plate circular 188
A.21 Polymer foam 27 kg·m^{-3} 189
A.22 PU foam Groby *et al.*, JASA 2010 189
A.23 PU foam Groby *et al.*, JASA 2010 189
A.24 Rock wool 189
A.25 Screen 10 190
A.26 Screen with high porosity, Jaouen & Bécot 2011 [108] 190
A.27 Screen with low porosity, Jaouen & Bécot 2011 [108] 190
A.28 Scrim headliner 190
A.29 Wood fiber 190

List of Figures

1.1 Context of the current work . . . 3

2.1 Method of moving asymptotes . . . 19

3.1 A schematic of the transfer matrix method . . . 33
3.2 Finite element discretisation illustration . . . 35

4.1 Illustration of topologies . . . 38
4.2 Optimal shape of a bridge across a river . . . 38
4.3 Schematic of a generic compliance minimisation topology optimisation problem 41

5.1 Acoustic energy balance . . . 52
5.2 Application of sound absorbing materials in automotive and building applications 53
5.3 Schematic of a multilayered sound absorbing package . . . 55
5.4 Two-layered sound absorption system schematic . . . 58
5.5 Fitness landscape for two layered system . . . 60
5.6 The evolution of absorption landscapes for two-layered system . . . 62
5.7 Three-layered sound absorption system. . . . 63
5.8 Comparison between tournament selection and roulette-wheel selection. . . . 66
5.9 Effect of population size . . . 66
5.10 Comparison of average fitness progress between strong and weak elitism. . . . 67
5.11 Frequency of occurrences of different materials in best solutions . . . 68
5.12 Material choice landscape . . . 68
5.13 Fitness landscape across layer thicknesses . . . 69

6.1 Optimisation problem formulation . . . 75
6.2 Verification of absorption computation with existing literature . . . 84
6.3 Verification of analytical gradients . . . 85
6.4 Comparison of a full vs. half-symmetric model of the LKKK shape . . . 85
6.5 Effect of varying the thickness of the front air layer. . . . 86
6.6 Effect of number of elements along air layer in front of design domain. . . . 86
6.7 Genetic algorithm: effect of different mutation rates . . . 97
6.8 Genetic algorithms: effect of various population sizes . . . 98
6.9 An illustration of rounding optimised shapes . . . 103
6.10 Differential evolution parameter tuning . . . 105
6.11 Run time progress of best absorption for problem instance 6 . . . 107
6.12 Trial averaging illustration . . . 108
6.13 Run time progress of best absorption for problem instance 1 . . . 108
6.14 Distribution of best-solution absorption across trials for problem instance 6. . . . 109
6.15 Impact of trials on the best shapes produced . . . 109

6.16 Sound absorption curves of optimal shapes from selected algorithms 110
6.18 Absorption vs. volume fraction of optimal shapes for problem instance 6 114
6.19 Landscapes for fully-filled shape problem instance 6 115
6.20 Example of an anomalous gradient methods getting stuck at a local optimum . . 117
6.21 Proof that SIMP is a heuristic. 117

7.1 Schematic of the problem and its representation 122
7.2 An Illustration of the hypervolume metric 127
7.3 Illustration of SIMPrestart 128
7.4 SIMPrestart trade-off solutions for all problem instances 129
7.5 SIMPsweep trade-off solutions for all problem instances. 131
7.6 Comparison of Pareto fronts: SIMPrestart vs. SIMPsweep 132
7.7 Constructive heuristic with gradients (CHg) solution progress 134
7.8 Comparison of gradient algorithm solutions in objective space 136
7.9 Isolines of combined objective in weighted-sum scalarisation 137
7.10 HC solution progress in the objective space compared with CHg. 138
7.11 Isolines of combined objective in Chebyshev scalarisation 140
7.12 Why weighted sum performs better than Chebyshev 141
7.13 NSGA-II Pareto progress across generations 142
7.14 NSGA-II trade-off solutions for all problem instances 143
7.15 Random search results in objective space 144
7.16 Comparison of Pareto fronts of non-gradient algorithms 146
7.17 Illustration of one trial of hybrid algorithm 1 147
7.18 HA1 trade-off solutions for all problem instances 149
7.19 Illustration of one trial of hybrid algorithm 2 150
7.20 HA2 trade-off solutions for all problem instances 151
7.21 Comparison of all Pareto fronts in problem instance 1 154

B.1 Runtime progress of all algorithms on problem instance 1 191
B.2 Runtime progress of all algorithms on problem instance 2 192
B.3 Runtime progress of all algorithms on problem instance 3 192
B.4 Runtime progress of all algorithms on problem instance 4 193
B.5 Runtime progress of all algorithms on problem instance 5 193
B.6 Runtime progress of all algorithms on problem instance 6 194
B.7 Runtime progress of all algorithms on problem instance 7 194
B.8 Distribution of best absorption from all trials 195
B.9 Clustering of solutions in absorption vs. volume fraction space 196
B.10 Final solutions for problem instance 1 197
B.11 Final solutions for problem instance 2 198
B.12 Final solutions for problem instance 3 199
B.13 Final solutions for problem instance 4 200
B.14 Final solutions for problem instance 5 201
B.15 Final solutions for problem instance 6 202
B.16 Final solutions for problem instance 7 203

C.1 Comparison of all Pareto fronts in problem instance 2 204
C.2 Comparison of all Pareto fronts in problem instance 3 204
C.3 Comparison of all Pareto fronts in problem instance 4 205
C.4 Comparison of all Pareto fronts in problem instance 5 205

C.5 Comparison of all Pareto fronts in problem instance 6 205
C.6 Comparison of all Pareto fronts in problem instance 7 206

Chapter 1

Introduction

1.1 Introduction

Noise control is an essential aspect of engineering, which arguably plays as important a role as efficiency in the success of a technology. It is one of the reasons why supersonic air travel was abandoned, and passenger drones are not commonplace yet. Noise control can be achieved either through active or passive means. In active control, opposing sounds are produced to cause destructive interference to reduce sound levels. Noise-cancelling headphones are an example. In passive control, porous materials such as foams and fibrous materials are typically used to absorb and limit sound levels within an environment. Common materials such as those used in carpets, vehicle upholstery and car headliners are examples. In some cases, sound isolation and scattering strategies are used in passive noise treatment to reflect or deflect sounds from reaching a region of interest. Examples include double-glazed windows and architectural walls in theatres and halls. Of interest in this study is the porous sound treatment.

Porous materials constitute a significant amount of dead weight in several passive noise control applications. In aircraft, porous insulating materials are placed throughout the outer walls to prevent the extreme noise from the engine and wind sheer from entering the passenger cabin. The payload compartment of space shuttles needs to be isolated to prevent the equipment from being damaged by extreme noise and vibration levels during launch.

Typically, placing more sound absorbing materials reduces noise levels, however, this is not always the case. While it may seem counter-intuitive, in some cases, removing acoustic material can result in improved absorption. By carefully introducing pockets of air within porous materials, favourable resonances can be created that concentrate the acoustic pressure fields in some regions, effectively improving sound absorption at specific frequencies. However, finding the best acoustic material shapes that maximise absorption is a challenging optimisation problem. With expensive fitness evaluations, large search spaces and multi-modal landscapes, exact methods that guarantee to find the best solutions are impractical, and heuristics are the only viable alternatives. This thesis deals with understanding the problem structure and identifying more effective heuristic and metaheuristic strategies that find near-optimal acoustic shapes in a reasonable time.

1.2 Motivation

The urgent need to tackle the aforementioned problem is fuelled by climate change, which is one of the serious concerns of the current time. The aviation and transport industries are taking rapid initiatives to curb CO_2 emissions, and one of the focuses is on light-weighting technologies. Government research grants in recent years have also prioritised technologies that address this problem. The European Strategic Research and Innovation Agenda (SRIA) predicts that the available technologies and procedures will allow a 75% reduction in CO_2 emission per passenger kilometre, 90% reduction in NO_x emissions, and 65% reduction in perceived noise emissions by the year 2050. One such technology is composite materials.

In recent years, composite structures have been widely used in aerospace, automotive and construction applications due to their higher strength-to-weight ratio than their metallic counterparts. The recent builds of two international airline manufacturing giants, Boeing 787 and Airbus 350, significantly replaced metals with fibre-reinforced composites. Massive fuel savings, reduction in emissions and travel costs are foreseen in the coming decades, out of which a significant fraction is expected to be due to the use of composite materials [242]. However, composite materials have poor noise isolation capacity compared to conventional metals partly due to their lightweight. To keep the noise at the same level, additional sound packages are typically used along with composites to absorb and dissipate sound energy. However, if not sufficiently sound treated, such composite structures could lead to significantly higher noise and discomfort in the passenger and the payload compartments. Thus, this is a classic trade-off problem. Choosing sub-optimal designs could result in additional weight negating a significant amount of light-weighting benefits. Over many flight hours, these inefficiencies add up, and the costs are eventually transferred to the public. Hence, it is worth investigating the optimisation problems that arise in porous material design.

The optimisation of acoustic porous materials involves domain-specific challenges, and the optimisation theory related to this field is yet to be well developed. The computation of sound absorption coefficient requires physics knowledge, unlike in problems such as boolean satisfiability or travelling salesman problem, which do not require any expert knowledge. This work is a step towards better understanding the interdisciplinary challenges so that better heuristics and metaheuristics may be developed. This work is carried out under the framework of the No2Noise (no2noise.eu) project, an Innovative Training Network under the European Union's Horizon 2020 research and innovation programme under the Marie Skłodowska-Curie grant agreement number 765472.

1.3 State of the art

This thesis is an investigation at the intersection of three well-established fields (see Figure 1.1):

1. Acoustic porous material modelling
2. Topology optimisation
3. Metaheuristics

According to web of science, tens of thousands of publications exist that deal with metaheuristics and their application to other fields, thousands exist that deal with topology optimisation techniques, and hundreds of publications exist that deal with acoustic porous material modelling. At the intersection of metaheuristics and topology optimisation about a hundred publications exist and a majority of others deal with conventional gradient-based search methods.

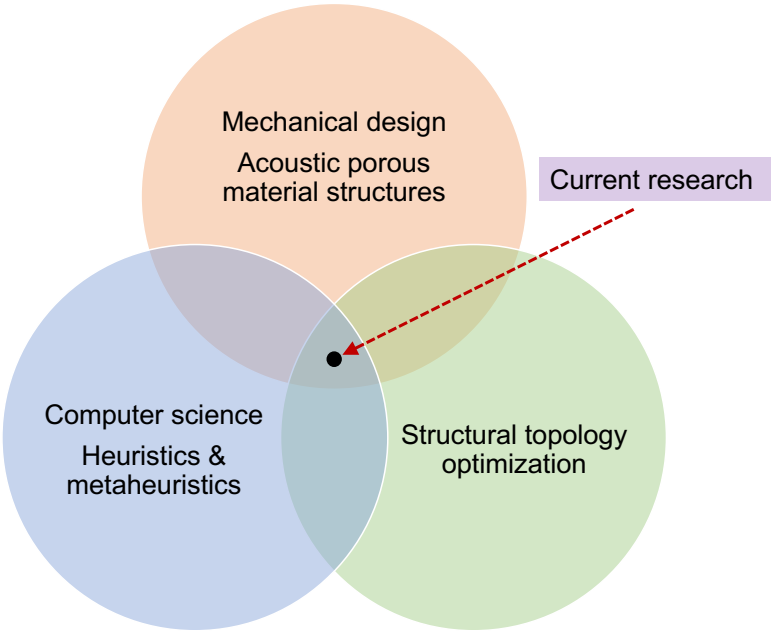

Figure 1.1: Context of the work presented in this thesis.

About fifty publications exist that deal with applying topology optimisation in the design of acoustic porous materials and metamaterials. A few tens of publications deal with applying metaheuristics in acoustic material modelling. At the intersection of these three fields, no previous publications exist that analyse and compare the performance of several metaheuristics including against conventional methods on acoustic material topology optimisation. This will be further discussed in the chapters under part I, which will review the existing work. A brief overview of the current state-of-the-art of these topics is introduced to the reader in what follows.

Metaheuristics: While many optimisation problems can be solved using exact approaches that guarantee to find the best possible solution, for many others, such exact methods are too expensive to be practical. Examples includes problems in NP-complete and NP-hard classes. For such problems, inexact methods or *heuristics* are the only viable option. Metaheuristics are problem-independent guidelines for designing heuristic algorithms [226]. Metaheuristic strategies have been the *go-to* approaches for combinatorial optimisation, and in some cases, for global optimisation of continuous variable problems. Examples include genetic algorithms, tabu search, simulated annealing, covariance matrix adaptation evolution strategy etc. Metaheuristics research forms a constituent part of developments in artificial intelligence as they provide automated problem-solving tools. The recent research focus is on fully automated algorithm design using hyper heuristics that operate across the search space of heuristics [181, 39, 192].

Acoustic porous materials: In order to optimise the design of porous sound-absorbing materials, it is first necessary to accurately model the propagation of sound waves in them. For elastic solids and non-Newtonian fluids, which do not dissipate the wave energy in any form, it is relatively easy to describe the motion of the wave. The propagation of sound waves in such media can be mathematically described by solving the wave equation, often referred to as the Helmholtz equation.

For porous materials, which dissipate sound energy, the governing laws were developed in the latter half of the 20th century. Some of the notable works include the Biot theories, which introduced the first formulations to model poroelastic materials that encompass an elastic solid part in a saturated fluid medium [26, 27, 25]. Delany, Bazley, and Miki introduced the first set of empirical models to estimate the complex dynamic bulk modulus and density for fibrous materials [70, 164, 163] which can be used to describe wave propagation with dissipation. Incrementally improving the model with help from theoretical modelling, Johnson, Champoux, Allard, Pride, Lafarge, and their co-authors derived what are now known as semi-phenomenological models [111, 43, 8, 196, 134]. Allard and Atalla published one of the first books on the propagation of sound in porous materials [7], which is considered a standard textbook for students and practitioners.

Multilayered sound packages: Typically acoustic porous materials are used in the form of multilayered packages, with each layer possessing different material properties. Layered sound-absorbing panels are easier to describe using acoustic wave equations. The transfer matrix method is a powerful analytical tool to model wave propagation in such materials. Typically, each layer will be represented by a transfer matrix which governs the variation of acoustic pressure or velocity across the layer. The material properties of the porous materials can be tuned during manufacturing. Choosing the best material properties for a given application for each layer is of interest to acoustic engineers. The thickness and the set of material properties for each layer are typically the design variables to be optimised, and the fitness function is typically the sound absorption or sound transmission loss. Once these properties are known, one can compute the fitness function using engineering modelling methods which are well established and validated with experiments. A quick yet comprehensive summary of the field may be found in the https://apmr.matelys.com maintained by Matelys Research Lab [107]. Based on the micro-structural complexity of the porous materials, there exist various material models to describe the behaviour of the material in flat layered structures using the transfer matrix method. These methods are explained in further detail in the literature review part under chapter 3.

Acoustic topology optimisation: Topology optimisation is a field which specialises in finding the optimal shapes and topologies of mechanical structures by distributing a given amount of material in a region in space. Topology optimisation is a challenging problem as the number of design variables needed to describe a shape can be thousands to millions in industrial cases. One of the unique attributes of this problem is the possibility to compute the gradient of the fitness function with respect to the design variables in quick time. Often with conjugate gradient [81] or adjoint [87] techniques, the gradients can be computed with the same time complexity as the fitness functions. This enables applying quick gradient-based algorithms. One such gradient method is the solid isotropic material with penalisation (SIMP), which is the most widely used across many problem domains. In addition to SIMP, there also exist a wide variety of other methods, such as the bi-directional evolutionary structural optimisation method (BESO) method and the level set method. BESO is a constructive approach that fills material in regions where stresses are high and removes material where stresses are low. In level set method, a scalar field is associated with the design region and the presence or absence of material is determined by whether or not the scalar value crosses a threshold. The scalar field is then optimised to optimise the shape and topology.

Knowledge of the gradient does not make topology optimisation akin to conventional convex optimisation, and there are some stark differences. The design variables are essentially a continuous relaxation of the decision variables, which determine the presence or absence of materials at each discretised element in the region. Rather than finding an interior optimum, a boundary optimum that has the highest fitness is of interest. The optimality criteria method, which is used along with SIMP, is similar to conventional constraint-included convex optimisation, which involves computing gradients and meeting the Karush Kuhn Tucker (KKT) necessary conditions for optimality. Such procedures would guarantee finding the true optimal solution in the continuous space if and only if the fitness function is convex over the design variables. However, the convexity of the fitness landscape is not guaranteed in most of the practical problem domains for which topology optimisation is used. Hence in almost all cases, SIMP is only a heuristic approach.

Once a shape is determined, an engineering modelling procedure is used to find its fitness. The physical laws governing wave propagation are represented in the form of partial differential equations (PDEs). Based on the geometry of the acoustic system, these PDEs are typically solved using the transfer matrix method (TMM) or the finite element method (FEM). TMM is an analytical method applicable to flat layered structures, where each layer is modelled as a transfer matrix that relates the wave amplitudes at one face to the other. The elements of this matrix incorporate closed-form solutions to the PDE derived in terms of the material's characteristic properties which are described using an acoustic material model. FEM is a numerical method that can solve PDEs in intricate geometries, where the structure is discretised into smaller pieces (called finite elements) of regular geometries (such as triangles, quadrilaterals, tetrahedrons etc.) and the governing partial differential equations applied on these pieces are converted to matrix equations using weak formulations. The matrix dimensions are linked to the number of vertices (nodes) in the discretised structure. Using the finite element method, the physics of many real-world systems can be accurately captured as long as certain numerical guidelines are followed. This has made FEM a workhorse for engineering analysis in the modern world. Since the 1960s when FEM was introduced, computers have become faster, allowing FEM and its extensions to be used widely in industrial applications. One of the quirks of FEM is that solving the system of matrix equations becomes expensive as the the matrix size (discretisation) increases, and the optimisation becomes time consuming. There exists a trade-off between accuracy and time when using FEM.

1.4 Gaps in knowledge

The existing work in optimisation with regard to multilayered porous package optimisation focuses mainly on the physics modelling or extending the methodology to more applications. Only a small number of works focus on optimisation aspects specific to porous materials, and the choice of optimisation algorithms relies on studies using mathematical benchmark problems. Understanding the fitness landscapes would help design more effective algorithms for problems involving a large number of layers. There have been very few studies [240, 148] dedicated to understanding the fitness landscapes of sound absorption or other acoustic indicators in multilayered porous structures. This is discussed further in chapter 3. However, the fitness evaluation is relatively less expensive in the multilayered optimisation problem as compared to that in topology optimisation. In some cases, the multilayered problem can be solved using simple heuristics or by brute-force. Hence, in this thesis, the multilayered optimisation problem

is addressed only as a formative study.

On the other hand, topology optimisation is challenging firstly because of the large number of decision variables in the original combinatorial form of the problem, and secondly, the expensive nature of fitness evaluation. Acoustic topology optimisation has been an emerging field since the early 2000s. An extensive literature survey covered in chapter 4 indicates that the number of publications in acoustic topology optimisation has seen tremendous growth in the last few years. Many publications focus on implementing topology optimisation using SIMP for specific problem cases. Specifically, these works include deriving the finite element formulations, computing the sensitivities, extending finite element-based to isogeometric analysis-based meshes etc. In other publications the focus has mainly been on gaining insights from the optimised shapes for specific use cases which are useful to the acoustic community. However, the question as to which optimisation strategies are more effective in obtaining better quality solutions in less time in porous material topology optimisation remains unanswered. Comparisons of different heuristics and metaheuristics have been previously made by other researchers in the compliance minimisation problem domain [205]. However, there is little effort towards comparison studies on problems in the acoustic domain. Chapter 4 provides a detailed account of the available studies to emphasise this gap in knowledge.

In addition, to design efficient algorithms, it is essential to have an understanding of the fitness function landscapes across the design/decision variables. The existing literature does not seem to have investigated this research area. In this thesis, an initial analysis of the nature of the fitness landscapes is performed. This knowledge is expected to greatly help in improving the convergence rate and solution quality by modifying available optimisation strategies.

The computational complexities of finding the absorption coefficient and that of its gradient have not been assessed in previous work. The relative complexity of the fitness function to its gradient will greatly affect the relative performance of gradient and non-gradient methods. This thesis also aims to address this question by analysing the procedures involved in the fitness computation.

1.5 Focus of the current thesis

The main aim of this work is to better understand the performance of existing and novel heuristics and metaheuristics in the design of sound-absorbing structures. The objective to arrive at a set of guidelines for novel, more efficient heuristics in this domain. As a formative study, the one-dimensional multilayered sound package optimisation will be considered. Then, the two-dimensional shape and topology optimisation of acoustic foams will be studied. Since there are no practically viable exact optimisation methods in this domain, the work will focus on heuristic and metaheuristic optimisation methods.

In multilayered sound absorption packages each layer of the sound package may be constituted of poroelastic materials, perforated plates, solid elastic materials, plaster boards, and woven or non-woven textiles. The choice of materials in each layer, their thickness and material properties govern the sound absorption properties of the multilayered system. Identifying the discrete material choices and continuous thickness and material parameters makes this a mixed discrete-continuous problem. As a first approach, an integer representation genetic algorithm is applied. A discussion on the objective function landscape across different parameters of multilayered

sound absorption problems is provided.

It is known that introducing air cavities in materials (often called Helmholtz resonators) may enhance or suppress the absorption at different frequencies depending on the shape of the cavity. Often, fully filling porous materials in the available space is not often the most absorbing solution. There exist potential weight savings while obtaining more noise attenuation. To explore optimal shapes of air cavities in porous materials, various topology optimisation approaches including several heuristic and metaheuristics are studied. The time complexities of the fitness and gradient computation are compared and contrasted with those of compliance minimisation. The absorption landscapes across the design variables are analysed to gain insights for algorithm design. Then, a multi-objective optimisation problem of simultaneously maximising the absorption properties while minimising weight is considered. The main focus will be on comparing gradient and non-gradient methods through empirical optimisation experiments. The results will also be subject to statistical tests. Further, from the knowledge obtained from these tests, hybrid algorithms will be designed and tested. The research outcome will be a set of initial guidelines to design efficient heuristic algorithms tuned to the acoustics problem domain.

1.6 Contributions in this thesis

The specific contributions of this thesis in terms of addressing the knowledge gap are as follows:

1. In a novel effort, an extensive multilayered sound package optimisation using 29 existing porous materials with recent advanced material models is carried out for absorption maximisation in a three-layered sound package using a genetic algorithm (Chapter 5).
2. The fitness landscape in multilayered optimisation problems is explored, and it is identified that the landscapes are smooth over the material property variables. Memetic algorithms that perform local search over the material properties are then suggested for this application (Chapter 5).
3. A comparison of several topology optimisation strategies is performed for the first time for optimal two-dimensional distribution of poroelastic material and air for sound absorption maximisation. The study included state-of-the-art topology optimisation strategies and popular metaheuristics. Some of the heuristics are novel, and some already-existing metaheuristics which are applied have not been used on this specific problem before (Chapter 6).
4. Notably, evidence shows that state-of-the-art algorithms are often outperformed by certain newly tested methods. However, no algorithm clearly outperforms all others across all the benchmark problem instances considered (Chapter 6).
5. Each algorithm finds a unique set of optimal solutions, exploring different regions of the search space. One of the general lessons is to use multiple well-performing strategies together and pick the best results for manufacturing (Chapter 6).
6. The problem structure of the above topology optimisation, including the fitness landscapes, is explored in detail for the first time, and new insights for designing better strategies are identified (Chapter 6).
7. A comparison of multi-objective strategies is performed in a first-of-its-kind study in acoustic topology optimisation. The objectives are to maximise absorption while minimising weight. The algorithm pool includes state-of-the-art and novel gradient-based, gradient-free and hybrid strategies, including SIMP and NSGA-II (Chapter 7).
8. It is observed that while gradient methods are quick to obtain near-optimal solutions, non-gradient methods outperform them given sufficient time (Chapter 7).

9. Two hybrid strategies are proposed that consistently outperform all other methods, including the state-of-the-art, over all the problem instances. These hybrid strategies use gradient methods as initialisers and non-gradient methods as improvers (Chapter 7).
10. A simple new Pareto-slope-based scalarisation technique is proposed and applied for the first time and seems to perform well as an improver (Chapter 7).

1.7 Thesis structure

In this thesis, there are mainly three literature review chapters and three contribution chapters. Due to the multidisciplinary nature of the work, an individual chapter is dedicated to overview relevant literature in the three fields—metaheuristics, acoustic porous materials and topology optimisation.

- **Chapter 1: Introduction**

  PART I: LITERATURE REVIEW CHAPTERS

- **Chapter 2: Metaheuristics literature**
  This chapter introduces a brief account of the state-of-the-art of metaheuristics, with descriptions of popular strategies.

- **Chapter 3: Acoustic porous-material literature**
  This chapter will describe the available tools to compute the objective function, i.e. sound absorption or transmission loss. In addition, brief accounts of the various properties of porous materials, how they are measured in practice, and how they affect their behaviour are provided in this section.

- **Chapter 4: Topology optimisation literature**
  This chapter introduces topology optimisation and provides a brief account of the current state of the art, including available techniques, the wide variety of applications it has found, and the potential benefits it offers. In this chapter, an extensive account of existing acoustic applications of topology optimisation research is also provided.

  PART II: CONTRIBUTION CHAPTERS

- **Chapter 5: Multilayered sound package optimisation**
  This chapter will cover the one-dimensional acoustic material design optimisation methods in multilayered packages seeking the best sequencing of given materials and synthesis of material properties for new materials. This work is done as a formative study to gain insights for topology optimisation.

- **Chapter 6: Single-objective topology optimisation for absorption maximisation**
  Heuristic and metaheuristic approaches, which do not exploit any information but the fitness (and its derivatives) of the problems, will be compared on benchmark problem instances. State-of-the-art heuristics and some well-known metaheuristics will be compared with originally proposed heuristics.

- **Chapter 7: Multi-objective topology optimisation for absorption maximisation and weight minimisation**

In this chapter, the use of multiple objectives (noise and weight reduction) in acoustic porous material topology optimisation and how different approaches compare against each other will be discussed. There are many applications where the weight minimisation is indirectly set as an inequality constraint, and the noise is optimised. Although there are many works on multi-objective structural topology optimisation, there are no works in the porous materials domain dealing with these objectives simultaneously, which makes this venture novel.

- **Chapter 8: Conclusions and future work**
  This chapter summarises the current work, highlights the novel contributions of the work carried out and discusses possible future work prospects.

1.8 Publications from this research

Journal articles:

1. **Vivek T. Ramamoorthy**, Ender Özcan, Andrew J. Parkes, Abhilash Sreekumar, Luc Jaouen and François-Xavier Bécot, Comparison of heuristics and metaheuristics for topology optimisation in acoustic porous materials, The Journal of Acoustical Society of America, Vol. 150, Issue 4, pp. 3164-3176, (October 2021).
   (DOI: https://doi.org/10.1121/10.0006784)

2. **Vivek T. Ramamoorthy**, Ender Özcan, Andrew J. Parkes, Luc Jaouen and François-Xavier Bécot, Multi-objective topology optimisation of acoustic porous materials for minimum weight and maximum absorption (submitted to The Journal of Acoustical Society of America).

Conferences:

1. **Vivek T. Ramamoorthy**, Ender Özcan, Andrew J. Parkes, Luc Jaouen and François-Xavier Bécot, Metaheuristic Optimisation of multilayered porous materials, International Congress on Acoustics, Aachen, Germany (September 2019).

2. **Vivek T. Ramamoorthy**, Ender Özcan, Andrew J. Parkes, Abhilash Sreekumar, Luc Jaouen and François-Xavier Bécot, Acoustic topology optimisation using CMA-ES, proceedings of ISMA2020 International Conference on Noise and Vibration Engineering and and USD2020 International Conference on Uncertainty in Structural Dynamics (September 2020).

3. **Vivek T. Ramamoorthy**, Ender Özcan, Andrew J. Parkes, Abhilash Sreekumar, Luc Jaouen, François-Xavier Bécot, On the topology optimisation of acoustic porous materials, e-Forum Acusticum, (December 2020).

4. **Vivek T. Ramamoorthy**, Ender Özcan, Andrew J. Parkes, Luc Jaouen, François-Xavier Bécot, Metaheuristics in topology optimisation of sound absorbing materials, The OR society conference-OR63, (September 2021).

Part I

Literature review chapters

Chapter 2

Metaheuristics literature

Optimisation techniques can be broadly classified into exact methods and heuristics. Exact methods guarantee that the found solution is indeed the optimal solution. Examples of exact algorithms are enumerative search (searching through all possible solutions), branch and bound, and dynamic programming. However, for some problems with large search spaces and expensive objective functions, such exact methods are often too time-consuming and they are practically unusable. The most notable is the NP-complete class of problems which do not yet have a polynomial time algorithm in the problem size. Heuristic methods are quick alternatives that can find near-optimal solutions in reasonable time. Metaheuristics are certain high-level problem independent guidelines used to design heuristics, such as genetic algorithms. In this chapter, an overview of the field of metaheuristics is provided.

2.1 Introduction

Heuristics are practical approaches, shortcuts or rules of thumb that one can follow to make calculated guesses for solutions to different problems. They are computationally less expensive alternatives to exact methods that provide quick and good solutions to optimisation problems. However, they do not guarantee finding the optimal solutions. Although heuristic problem solving has been used by us humans from time immemorial, in recent decades, they have been formalised under different frameworks as metaheuristics. A heuristic algorithm is an unambiguous set of instructions to solve a specific problem, whereas a metaheuristic is the high-level idea used in the heuristic.

Sörensen [226] defines metaheuristics as problem-independent sets of guidelines for developing heuristic optimisation algorithms that can be thought of as *heuristics to design heuristics* and hence the name. The term metaheuristic was first coined by Glover in 1986 [88] which is derived from the Greek prefix *meta*, which means high level, and *heuristics*, which means to search. An example of a metaheuristic is genetic algorithms wherein the guideline is to pick a population of individuals from feasible solutions, apply selection pressure, crossover the selected good quality solutions, mutate and replace them into the population, repeatedly until a desired outcome is reached. While the guideline is referred to as the metaheuristic in some usages, an implementation of a heuristic based on the guideline is also called a metaheuristic. For instance, an implementation of genetic algorithm following the guideline for a specific problem is also a metaheuristic.

Metaheuristics have been used in many applications to find solutions that are good enough,

quickly enough. Notable metaheuristics include genetic algorithms [102], simulated annealing [125], tabu search [88], etc. The optimisation theories pertaining to popular metaheuristics are so well-studied that several books have been published based on each metaheuristic. Sörensen *et al.* in [227] provided an account of the history of metaheuristics. They describe the evolution of the field from *the early period*, when problem-solving frameworks were being realised (analogy, greedy search, construction etc.), through the *method-centric* period, when these general ideas were still considered to be different algorithms, to the current *framework-centric* period, where the focus is given to the high-level frameworks on which different algorithms are based.

Since porous material layering and topology optimisation involves a large number of design variables, expensive objective functions, and large search spaces, exact algorithms are too time-consuming to be practical. In fact, efforts towards domain-specific extensions of exact methods such as dynamic programming, branch and bound, etc., to porous material design is hard to find in existing literature. Much of the optimisation studies deal with metaheuristic techniques such as genetic algorithms [240], and domain-specific heuristics. Hence, justifiably, this thesis focuses primarily on heuristic and metaheuristic techniques.

The performance of a metaheuristic on a specific problem domain depends on the algorithmic components used, such as move operators (specific procedures involved in finding neighbouring solutions), acceptance criteria (when a solution is accepted), and others. Without empirical testing, it is difficult to ascertain effective outcomes. Techniques such as parameter tuning [114] allow a given metaheuristic to be used in more effective way. Such tuning requires expertise in the field of metaheuristics and algorithm design. While this is not ideal, research into automated selection of algorithms has resulted in the so called *hyperheuristics* which operate in the search space of heuristics.

In choosing metaheuristic algorithms and operators for a problem domain, analysing the fitness landscapes may provide a better understanding of an algorithm's performance [193]. For real-valued problems, fitness landscapes correspond to the scalar field of fitnesses assigned to the design variable space.This notion has been extended to combinatorial problems, where fitness landscapes correspond to the set of fitness values mapped to each solution in the search space connected virtually to other solutions through metrics such as the hamming distance. Performing such an analysis leads to the knowledge of modality (presence of local optimal solutions), presence of basins of attraction (regions that directly lead to the optima), barriers (poor fitness regions which need to be crossed to get to the optimum), ruggedness (a measure of occurrence of local optimal solutions) etc. The presence of a unimodal landscape indicates that the problem could be solved to optimality using most metaheuristics. On the other hand, multi-modal landscapes mean that the problem is difficult to tackle. A popular metric in combinatorial optimisation is the fitness distance correlation which corresponds to the distribution of fitnesses with respect to the distances from the global optimum. This metric has been used successfully in many applications to determine the search difficulty and is noted as a *reliable* but not an *infallible* indicator by Jones *et al.* [113].

In the current times, metaheuristics play an integral part of advancements in artificial intelligence in addition to other tools such as machine learning. On the other hand, researchers have also used machine learning techniques at the service of metaheuristics in solving combinatorial optimisation problems [118].

As new methods and extensions to existing methods are being published regularly, it is not practical to provide an account of all the main metaheuristics in detail. For brevity, only some of the well-known methods will be discussed in the subsequent sections. Towards the end, a note on the use of metaheuristics in topology optimisation is provided. Finally, a summary listing the important takeaways is provided.

2.2 Local search

Local search is a simple yet powerful heuristic which starts from an arbitrary initial solution, generates a neighbouring solution and accepts it if it is improving [2]. For example, 2-Opt search [62] is a local search heuristic for the travelling salesman problem. The neighbourhood operator chosen will play a vital part in the local search.

2.2.1 Hill Climbing

Algorithm 1: Pseudocode for a local search algorithm

```
1  Generate initial solution s;
2  Evaluate objective function f(s);
3  while Termination criteria is not met do
4  |   s' ← GenerateNeighbour(s);
5  |   Evaluate objective function f(s');
6  |   if f(s') < f(s) then
7  |   |   Set s ← s';
8  |   end
9  end
10 Return s
```

Hill climbing techniques such as steepest descent, random mutation and Davis' bit climbing [64] are some examples of local search. Consider the application of hill climbing to a boolean satisfiability problem. In steepest descent hill climbing, the solution with the highest improvement from all possible neighbours is chosen in each iteration. In random mutation hill climbing, in each move, a bit at random is chosen to be flipped as the neighbourhood operator. Whereas in Davis' bit hill climbing, a random permutation of numbers up to the length of the bit stream is obtained, and in every move, bit flipping is done on the location given by the next number in the permutation while accepting improving moves. A pseudocode for hill climbing or local search is provided in Algorithm 1.

Due to the greedy acceptance of improving moves, local search heuristics have an increased likelihood of getting stuck at a local optimum. A random-restart hill climbing will counter this by restarting the hill climbing from a new solution. A balance between efficiently exploring the search space and exploiting the neighbourhood of good solutions are desirable characteristics of an effective search algorithm.

2.2.2 Iterated local search

A general local search algorithm can be thought of as a function that takes a solution (s) as input and uses specific moves to obtain a local optimum (s^*) in the neighbourhood of s. A nested local search scheme which applies a local search on carefully chosen neighbouring solutions to find neighbouring local optima (s^*) is called an *iterated local search* metaheuristic (ILS) [156]. A pseudocode for iterated local search algorithm is given in Algorithm 2.

Algorithm 2: Pseudocode for iterated local search

```
Pick an initial solution;
Hill climb;
while Termination criteria is not met do
    Pick a neighbouring solution;
    Hill climb;
end
Return s
```

2.3 Simulated annealing

Algorithm 3: Pseudocode for a simulated annealing

```
Pick a solution s randomly from feasible solutions;
Set k ← 0;
Select an annealing schedule t_k : t_k > 0 ∀ k and lim_{k→∞} t_k = 0;
Set M, the number of iterations under each cooling schedule;
while Termination criteria is not met do
    m ← 0;
    while m < M do
        Pick a new solution s' in the neighbourhood of s;
        Calculate Δ = f(s') − f(s);
        if Δ < 0 then
            s ← s';
        else
            s ← s' with a probability exp(−t_k Δ);
        end
        m ← m + 1;
    end
    k ← k + 1;
end
Return s;
```

Simulated annealing was introduced by Kirkpatrick in 1983 [125]. It is one of the old metaheuristics which was formalised before the term *metaheuristics* was coined. It is based on the analogy of the process of slow cooling of metals from a high temperature in order to let the atoms settle in a low energy state (minimising energy). The algorithms start with a single solution and iterate on it, making it a memory-less method. In this, the high-level guideline is to accept worsening moves with a certain probability that slowly reduces. The probability with

which worsening moves are accepted is varied during the algorithm depending on a parameter called the *temperature* and the difference between the previous and the current solution. Typically the temperature is set to approach zero as the iterations progress. A pseudocode for simulated annealing is given in Algorithm 3.

Simulated annealing can be considered a breakthrough for its time, and its use was widespread in many problem domains [236, 9]. The main research focus around simulated annealing includes optimising the annealing schedule and effective hybridisation with other approaches.

2.4 Tabu search

Tabu search was first proposed by Glover in the same article in which the term metaheuristics was coined [88]. In tabu search, a forbidden list (tabu list) of moves is maintained to avoid getting stuck at local optima and cycling through the same set of solutions. Glover considered tabu search not as a heuristic that operates on solutions but rather as a *meta*-heuristic which operates on a local search. A tabu move is liberated from the tabu list after a set number of moves. A pseudocode for tabu search is given in Algorithm 4.

Algorithm 4: Pseudocode for a tabu search algorithm

```
1  Generate initial solution s;
2  Evaluate objective function f(s);
3  UpdateBest: s* ← s, f* ← f(s);
4  while Termination criteria is not met do
5  |  s' ← GenerateNonTabuNeighbour(s);
6  |  if f(s') < f(s*) then
7  |  |  Set s* ← s'; Set f* ← f(s')
8  |  end
9  |  Update Tabulist;
10 end
11 Return s*
```

The advancements of research in tabu search are towards improving the search with better initialisation, parallel search and hybridisation [61, 60, 82], as is stated in the survey article by Gendreau *et al.* [85]. A recent survey on tabu search implementations for the travelling salesman problem is given in [15].

2.5 Genetic algorithms

Genetic algorithms take inspiration from the process of natural evolution, which uses selection pressure, crossover, and mutation to choose better individuals. To perform optimisation, one can pick a set of individuals randomly from the feasible solution space, apply selection pressure to filter good solutions for mating, combine the attributes of good solutions in a crossover operation, modify the solutions with some degree of mutation and find better solutions. This idea of using the process of genetic evolution was first introduced by Holland [102] and, since then, has been used successfully in many applications. Some applications and survey papers on genetic algorithms are [229, 86, 188, 215, 241, 214, 117, 3]. Adaptive versions of genetic algorithms are found to perform better for functions which are more multi-modal [228]. Other metaheuris-

tics, such as hill climbing, can be considered special cases of genetic algorithms, i.e. if only one individual is considered in the population with only the mutation operator. Pseudocode for a sample genetic algorithm is given in Algorithm 5. A simple illustration of a genetic algorithm can be found at VivekTRamamoorthy.github.io/GeneticAlgorithmTutorial that finds the optimal solution of a MAXSUM problem.

Algorithm 5: Pseudocode for a genetic algorithm

```
Pick N members randomly from feasible solutions;
Evaluate their fitnesses;
while Termination criteria is not met do
    Select members as parents with selection pressure;
    Apply crossover on parents to get the offspring;
    Apply mutation with probability MutationRate to the offspring;
    Evaluate the fitnesses of the offspring;
    Replace the offspring in the population;
    Update the best solution;
end
Return the best solution;
```

2.6 Memetic algorithms

Memetic algorithms are extensions to genetic algorithms where local search is performed near the solutions obtained from genetic algorithms. The effectiveness of hill climbing in genetic algorithms is emphasised in several papers [166, 200]. The local search in a memetic algorithm is typically done after the mutation operation of the genetic algorithm. Due to their effectiveness in exploiting locally in conjunction with exploration, memetic algorithms have been successfully used in many applications [40, 126, 179, 275, 151, 180]. An important consideration in memetic algorithms is the interplay between the level of local search and other operators, an example of which is brought out by Freisleben and Merz [83] for the travelling salesman problem. The local search can sometimes be expensive based on the number of iterations needed to reach the local optimum, which is indicated by some theoretical studies [132, 235]. Pseudocode for a memetic algorithm is given in Algorithm 6.

Algorithm 6: Pseudocode for a memetic algorithm

```
pop ←GenerateInitialPopulation();
Evaluate their fitnesses;
while Termination criteria is not met do
    Select parents ⊆ pop;
    CrossOver(parents);
    offspring ← Mutation(parents,MutationRate);
    offspring ← LocalSearch(offspring);
    Evaluate fitnesses of the offspring;
    pop ← Replace(pop,offspring);
    Update(best);
end
Return best;
```

Some continuous optimisation techniques

In porous packaging problems, the parameters for optimisation can be either discrete or continuous. In some cases, considering the continuous variables as discrete is more practical and would reduce the search space. For example, physical variables such as thicknesses or porosities are precise only up to a few significant places: a thickness of 5.477 mm is equivalent to 5.5 mm. Although the above-discussed metaheuristics are applicable to both discrete and continuous optimisation, techniques specific to continuous optimisation have been successfully applied to hundreds of problem cases and are well documented. Differential evolution, and surrogate modelling methods such as covariance matrix adaptation-evolution strategy [100] and method of moving asymptotes [238] are some examples.

2.7 Differential evolution

Differential evolution (DE) is a population-based metaheuristic popular for continuous optimisation proposed by Price and Storn [232, 233]. It is a simple and powerful metaheuristic for real-valued optimisation. A basic example of the method is as follows. Consider the objective function $f(\mathbf{x}) \in \mathbb{R}$ where $\mathbf{x} \in \mathbb{R}^n$. In differential evolution, for every member of the population $\mathbf{x}$ three other unique members $\mathbf{a}, \mathbf{b}, \mathbf{c}$ apart from $\mathbf{x}$ are chosen randomly from the population. A new member $\mathbf{y}$ is obtained by a simple formula such as $\mathbf{y} = \mathbf{a} + F \times (\mathbf{b} - \mathbf{c})$ where $F \in [0, 2]$ is the differential weight. For all $i \in \{1, 2, ...N\}$, with a cross over probability $CR \in [0, 1]$, $\mathbf{y}_i = \mathbf{x}_i$ is set. The objective function is evaluated at the new location, and if it is an improving move, then $\mathbf{x}$ is replaced with the crossover product $\mathbf{y}$. This is repeated until termination criteria are met. Pseudocode for a sample DE is given in Algorithm 7.

Algorithm 7: Pseudocode for differential evolution

```
1  pop x^j ←GenerateInitialPopulation();
2  Evaluate their fitnesses f_j ← f(x^j);
3  while Termination criteria is not met do
4      for j = 0, j < length[pop], j++ do
5          Randomly select a, b, c from pop;
6          y ← a + F × (b − c);
7          for i = 0, i < length[x], i++ do
8              if rand < CR then
9                  y_i ← x_i^j;
10             end
11         end
12         Evaluate f(y) if f(y < f(x) then
13             Replace x^j ← y
14         end
15         Update(best);
16     end
17 end
18 Return best;
```

The key idea in this method is that, as the algorithm picks solutions from a region in the search space and as better solutions are accepted, the span of solutions is widened in the direction of improvement in the population due to step 13 in the pseudocode. Consequently, the differential move operation in step 6 leads to an enhanced search in this direction. Subsequent selection of

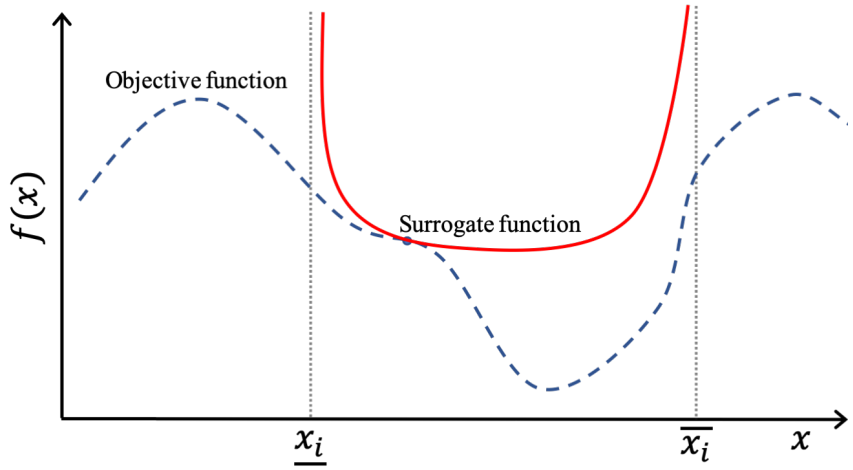

Figure 2.1: Method of moving asymptotes: surrogate function on one of the parameters x_i with lower bound $\underline{x}_i$ and upper bound $\bar{x}_i$.

improved solutions leads to a movement of the population towards higher fitness regions in the search space. This metaheuristic has been successfully applied in many applications [171, 63], and many books have been published on its theory and practise [195, 79, 42]. In acoustic topology optimisation, Khajah *et al.* [121] have applied differential evolution for acoustic horn shapes. Rostami *et al.* [205] in their study of various metaheuristic methods also included differential evolution in their algorithm pool.

2.8 Surrogate modelling methods

In these techniques, a surrogate function is constructed from the available information, such as function values or their derivatives and the surrogate model is optimised to get predictions for the optima. The function values at the predicted solutions are evaluated and checked for improvements. This process is repeated to look for the global optimum. Examples include covariance matrix adaptation-evolution strategy (CMA-ES) [100], method of moving asymptotes (MMA) [238], response surface methods [112] etc. Both CMA-ES and MMA optimise a multi-parameter function $f(\mathbf{x}) \in \mathbb{R}$ where $\mathbf{x} \in \mathbb{R}^n$. While CMA-ES uses a multi-variate Gaussian as the surrogate function, MMA uses a simple asymptotic function based on the constraint to look for the next guess. Figure 2.1 depicts the scheme used in MMA for a minimisation problem on f for a single parameter x_i, where $\underline{x}_i$ is the lower bound and $\bar{x}_i$ is the upper bound.

2.9 Metaphor controversy

While many effective algorithmic frameworks have been inspired by metaphors (simulated annealing, genetic algorithms, particle swarm optimisation), a large number of metaphor-inspired metaheuristics have been published in recent years. Some of these methods have come under criticism for being essentially similar in concept to other existing methods differing only in the metaphor [225]. A list of such metaphor-based methods and their high-level frameworks is available on the Wikipedia page Metaphor-based metaheuristics. An example is harmony search which can be proven to be a special case of $(\mu + 1)$ evolution strategy [253]. Also, as Sörensen points out, a different spectrum of researchers are working along the lines of applying aspects of exact methods to problems and sub-problems, which decompose the methods to

reveal the components actually contributing to their performance.

2.10 Hyper heuristics

In the last two decades, a new field focused on automating the selection of heuristics using higher-level heuristics, called hyper heuristics [58], has emerged. While metaheuristics are higher-level guidelines for designing heuristics, hyper heuristics search across the space of heuristics to automate the algorithm design. They are designed to tackle more general classes of problems making no prior assumptions. Özcan *et al.* [181] presented an analysis of several hill climbers, genetic algorithms and memetic algorithms in the hyper heuristics context. Burke *et al.* [39] presented an overview, including the roots, recent trends and future prospects of the field. Pillay and Qu published the first book on hyper heuristics [192] presenting a summary of the work on hyper heuristics, applications and future work directions. Hyper heuristics can be considered state of the art in automated algorithm design [199, 265].

2.11 Use in topology optimisation

Topology optimisation is a unique problem with a large number of decision/design variables which can be represented in both combinatorial and continuous forms. There exist a plethora of articles applying metaheuristic to topology optimisation.

Guirguis *et al.* [94] recently presented a comprehensive review of blackbox approaches, including metaheuristics, in various topology optimisation applications. Some of the metaheuristics used in these applications are genetic algorithms, covariance matrix adaptation-evolution strategy, differential evolution, particle swarm optimisation, and simulated annealing, to name a few. The variety of applications included structural stiffness, eigenfrequency, micro-mechanical resonators, heat transfer, magnetics, composite structures and photovoltaic panels.

Of the available metaheuristics, the most popular ones are genetic algorithms, CMA-ES and differential evolution. One of the noteworthy comparison studies is the work by Rostami *et al.* [205] which features the application of several metaheuristics using the moving morphable components representation for compliance minimisation topology optimisation.

Metaheuristics being used in compliance minimisation problems came under criticism for being too slow by Sigmund [219] since they require too many function evaluations. Existing state-of-the-art methods use gradient algorithms, and on some occasions, they are an order of magnitude faster than their non-gradient counterparts. Engineering problems have expensive fitness evaluations that are prohibitive for the use of slow-converging approaches in practical scenarios, unlike the benchmark problems used in optimisation literature. However, there are reasons that make a case for using non-gradient metaheuristic strategies: unlike in compliance minimisation, in other problem domains, gradients may not be fast to compute, or the fitness landscapes may be more rugged that the gradients can be misleading. In those cases, metaheuristics may be more viable alternatives than the popular gradient methods. Whether this is the case for acoustic absorption problems is unknown and will be ventured in this thesis. It is also worth noting that deriving these gradients in new problem domains requires expertise in the problem domain and can be quite challenging. If the solutions offered by gradient methods are inadequate, researchers look for other alternatives for global topology optimisation, such as

stochastic gradient-descent [66]. However, there is a lack of benchmark studies on gradient-embedded metaheuristics. For instance, a genetic algorithm can incorporate a gradient-based move operator in crossover or mutation. Such studies will be directly useful for topology optimisation. In this thesis, research into the usefulness of metaheuristics in acoustic topology optimisation will be explored for the first time.

2.12 Conclusions

The points to take away are as follows:

1. Heuristic optimisation techniques are quick alternatives to finding near-optimal solutions for hard optimisation problems.
2. Metaheuristics are a set of problem-independent guidelines to design heuristic approaches that can be thought of as heuristics to design heuristics—hence the name.
3. Metaheuristics are currently the only practical approach to tackling difficult problems, such as those in the NP-hard class, which do not yet have exact approaches that solve in any meaningful amount of time.
4. Metaheuristics are state-of-the-art techniques to solve combinatorial optimisation problems involving design variables that can take discrete values.
5. Popular examples of metaheuristics for combinatorial problems include genetic algorithms and tabu search.
6. There are many hundreds of metaheuristics available, however, some can be thought of as variants of others.
7. Metaheuristics are also available for continuous optimisation. Examples include particle swarm optimisation, covariance matrix adaptation-evolution strategy and differential evolution.
8. Metaheuristics have been used in topology optimisation, although they are not the most popular methods. Often they have come under criticism for being too slow.
9. One reason is that metaheuristics do not use the gradient information available in specific topology optimisation cases.
10. In some topology optimisation problem domains, it has been shown that gradients can be computed quickly using equations obtained from a sensitivity analysis.

Chapter 3

Acoustic porous material literature

This chapter introduces the engineering modelling techniques used to describe the sound absorption behaviour of acoustic porous materials. A complete understanding of these aspects is not essential for understanding the optimisation results. These models will be used in computing the fitness function, and computer scientists can consider them as blackbox functions. This chapter provides an overview of the literature on various levels of abstractions involved in modelling porous materials to lay the foundation for understanding the problem structure. This chapter will serve as a useful reference to readers who do not have a background in poroelastic modelling.

3.1 Introduction

Porous materials are those which have multiple interconnected pores or voids filled with air or other fluids. Porosity is the ratio of the volume of voids to the total volume in these materials. Even though all real materials have some degree of porosity due to the presence of micro-voids, many solids with low porosity could be treated well using continuum approaches. Porous materials commonly refer to those in which the porosities are high enough that the continuum treatments become inapplicable. These materials are found in common use as acoustic and thermal insulation, rubbers, leathers, textiles, filters and home furnishing, to name a few. In this thesis, the focus will be on acoustic porous materials, including fibrous materials (such as glasswool, rockwool) and polymeric or other foams which are specifically used for noise reduction.

For the purpose of this thesis, an overview of the nature of calculations involved in computing the objective function for optimisation is of interest. To help readers from disciplines other than engineering, a brief account of engineering modelling is provided through various levels of abstraction. The important aspects to takeaway are later highlighted in the summary of this chapter. A complete understanding of engineering modelling is not a prerequisite for the readers, although an abstraction would help appreciate the challenges involved in the current work. This chapter will also highlight the aspects that differentiate the problem from other benchmarks commonly dealt with in metaheuristics [16, 203, 74, 175].

Introduced in the 1970s, the finite element method revolutionised the way engineers designed structures [277]. While the field has now diverged into many branches for dealing with specific issues, the core concept remains the same. Many commercial software are available to model and analyse intricate geometries, including modules that provide specific functionalities includ-

ing more physics, ways to deal with boundaries, contact phenomena, and phase interactions, to name a few.

This chapter is organised as follows. In section 3.2, an introduction is given to the field of acoustics leading up to the Helmholtz differential equation used to solve for pressures in a classical fluid medium. In section 3.3, a discussion is provided on how the Helmholtz equation can be modified to model dissipative materials. An overview of such motionless skeleton models published in literature is also provided in this section. In section 3.5, geometric modelling techniques are described, including the transfer matrix method for one-dimensional modelling of layered materials and the finite element method for two- or three-dimensional modelling of intricate porous material structures.

3.2 Basics of acoustics

Physically, sound is the time-varying disturbances in pressure in addition to the atmospheric pressure. The atmospheric pressure at sea level is around 100,000 Pascal (Pa), which converts to 1 kilogram-force acting on every square centimetre of every open surface. A disturbance of 1 Pa over and above this pressure amounts to 93 decibel (dB), which is as loud as a typical lawn mower within a few feet. These variations from the mean atmospheric pressure are referred to as the acoustic pressure.

$$P = P_{atm} + p \tag{3.1}$$

Here, P is the total physical pressure, P_{atm} is the mean atmospheric pressure, and p is the acoustic time-varying pressure, all in Pascals. The human ear can sense disturbances as low as $p_{ref} = 20$ μPa, which is the threshold for human hearing. Human ears are logarithmically sensitive to these pressure variations, and hence a decibel scale is used. The threshold pressure for human hearing is agreed to be the reference pressure for the decibel scale used in practice which relates the sound pressure level to acoustic pressure.

$$L_p(\text{in dB}) = 20 \log_{10} \frac{p}{p_{ref}} \tag{3.2}$$

A calm library is typically between 30 and 40 dB. A conversation between people in a restaurant is around 60 dB. The cabin of an aircraft at cruise altitude without turbulence is between 60 dB and 80 dB. This is one of the reasons why having conversations on a flight is more difficult than at home or a library. The pavement of a busy street has noise levels between 60 and 80 dB. The audience at a rock concert may be subject to as high as 100 dB. A lawn mower at arm's length is around 90 dB. The sound during rocket launch can be high as 220 dB.

The frequency of sound is the number of pressure oscillations in one second measured in Hertz (Hz). Sounds we hear in normal life are composed of several frequencies, and the human audible frequency range is from 20 Hz to 20,000 Hz. Any pressure disturbance beyond this range is not sensed by our ear. As we age, our capacity to hear high frequencies tend to deteriorate. Factory workers exposed to louder than 80 dB for long periods of time develop premature hearing loss. One-time exposures of 85 dB for more than 8 hours can cause permanent damage to the ear. Thus, it is easy to get exposed to excessive levels of noise in day-to-day life.

Sound waves propagate in different media at different speeds. In air, at standard temperature and pressure at sea level, the speed of sound waves is around 340 m·s^{-1}. The propagation of

sound in an infinite block of a medium is governed by the wave equation, which is often referred to as the Helmholtz equation. In cartesian coordinates, the Helmholtz equation may be written as:

$$\left(\frac{\partial^2}{\partial x^2}+\frac{\partial^2}{\partial y^2}+\frac{\partial^2}{\partial z^2}\right)p=\frac{1}{c_m^2}\frac{\partial^2 p}{\partial t^2} \tag{3.3}$$

where x, y, and z refer to the spatial coordinates, t refers to time, and c_m is the speed of sound in the medium. In a one-dimensional duct, the equation reduces to:

$$\frac{\partial^2 p}{\partial x^2}=\frac{1}{c_m^2}\frac{\partial^2 p}{\partial t^2} \tag{3.4}$$

A known solution for pressure p that satisfies the above condition is the following:

$$p(x,t)=Au(x-c_m t)+Bv(x+c_m t) \tag{3.5}$$

Here $u(x-c_m t)$ and $v(x+c_m t)$ are forward and backward propagating waves of any wave form, and A and B are arbitrary constants.
If we consider sound at a specific angular frequency $\omega=2\pi f$, where f is the frequency in Hz, then using $p=\tilde{p}(\omega)\exp(-i\omega t)$, the expression 3.3 can be rewritten in the frequency domain as follows:

$$\frac{\partial^2 \tilde{p}}{\partial x^2}+\frac{\omega^2}{c_m^2}\tilde{p}=0 \tag{3.6}$$

For non-dissipative fluid media, the above equation can be solved for a given geometry using the corresponding values of c_m for different materials to find the acoustic propagation. Considering the relation between the speed of sound, bulk modulus and density of the medium given by $c^2=K/\rho$, materials which have a higher density to bulk modulus ratio tend to have higher sound speeds and vice versa. Propagation in elastic solids can also be reduced to the above form using constitutive relations. In the following sections, we will consider dissipative materials. For consistency of notations with existing literature, henceforth, we will replace the frequency domain notation of $\tilde{p}$ with p.

3.3 Material models for dissipative media

In this section, the modelling approaches for porous materials are discussed. Porous materials have networks of interconnected pores filled with a fluid (typically air), often in intricate geometries. This makes modelling their physics more challenging compared to homogeneous materials such as metals and ceramics. When an acoustic loading is given to a porous medium, both the solid and fluid phases allow for the propagation of waves. Coupled interactions could take place between the solid and the fluid phase in frequency regimes where the bulk stiffness and mass density of the solid phase and fluid phase are comparable. The viscous interaction between the solid phase and fluid phase occurs when there is relative motion between these two. This effect dissipates part of the acoustic energy into heat. Such dissipation is commonly referred to as the viscous effect. When waves propagate in porous media, the pressure, density and, therefore, the temperature of the fluid phase vary temporally and spatially. Such fluctuations in temperature in the fluid part cause heat transfer between the two phases and this is termed as the thermal interaction. Both these effects lead to the dissipation of the wave energy as it propagates, giving rise to the common application of porous materials in acoustic treat-

ments. Many researchers have proposed models to approximate the physics in porous materials in the last 70 years to predict their acoustic response. These models can be classified into analytical models, empirical models and semi-phenomenological models.

While analytical models are only available for regular pore geometries, such as cylindrical fluid cavities in a solid matrix, empirical models are developed through measurements of existing porous materials. Semi-phenomenological models are those that break down complex porous structures using theoretical models to relate the equivalent characteristic properties that may not be measured directly to other measurable properties. A brief account of such models is given in this chapter. A more detailed account of these models may be found at apmr.matelys.com created by Luc Jaouen from Matelys research lab [107].

If the stiffness of the solid phase is orders of magnitude higher than the fluid phase, then the energy of wave propagating in the solid phase is insignificant compared to that in the fluid phase. In such materials, the porous media can be considered to be an equivalent fluid, and those models are often referred to as motionless skeleton models. Those models which treat wave propagation in both solid and fluid phases are referred to as bi-phasic models, and an example is the Biot theory [27].

3.3.1 Motionless skeleton models

Zwikker and Kosten model

An approximation of some types of porous media would be to consider them as an array of tubes of fluid phase in a solid matrix. In 1868, Kirchhoff [124] presented the general theory of propagation of sound in circular tubes accounting for viscous and thermal conductivity effects. In the late 1940s, Zwikker and Kosten [280] showed that for tube radii $r_w > 10^{-3}$ cm and frequencies such that $r_w f^{3/2} < 10^6$ cm $\cdot$ s$^{-3/2}$, the exact theory given by Kirchhoff takes a considerably simpler form. They showed that the viscous and thermal effects could be separated by introducing the complex density ($\widetilde{\rho}$) and the complex compressibility or bulk modulus ($\widetilde{K}$). The resulting wave equation is given in equation 3.7, which is analogous to the Helmholtz equation.

$$\left(\frac{\partial^2}{\partial x^2} + \frac{\partial^2}{\partial y^2} + \frac{\partial^2}{\partial z^2}\right) p + \omega^2 \frac{\widetilde{\rho}}{\widetilde{K}} p = 0 \tag{3.7}$$

Stinson [230] derived the Zwikker and Kosten approximation for intermediate frequencies starting from Kirchoff theory. Stinson also presented a general approach to describe sound propagation in a uniform tube cross-section. From this theory, one could analytically derive the complex compressibility, complex density, characteristic impedance and propagation constants for tubes with arbitrary cross-sections. Certain models [26, 13] account for variations from pore shape by using shape factors, which can be calculated. The approaches to calculating such shape factors were also given by Stinson.

Delany Bazley model

Delany and Bazley performed experiments on a series of fibrous materials with low mass density [70]. They observed that the acoustical properties normalise as a function of f/σ, the ratio of frequency (f) and the flow resistance (σ) . The variation of characteristic impedance (Z), and the wavenumber (k) with (f/σ), closely resembled a straight line in a log-log plot against the real and imaginary parts of acoustic impedance and wavenumber. This indicated that there

exists a power-law relation between them. The study also verified the contemporary theories, which also predicted such normalisation on (f/σ) but cautioned against extrapolation. Due to the empirical relations, the acoustic properties of such fibrous absorbent materials can be determined only with the knowledge of static airflow resistivity (or flow resistance, denoted by σ). The resulting relations for characteristic impedance and wavenumber for fibrous materials are expressed in equations 3.8 and 3.9.

$$Z_c = \rho_0 c_0 \left[1 + 9.08 \left(10^3 \frac{f}{\sigma}\right)^{-0.75} - j11.9 \left(10^3 \frac{f}{\sigma}\right)^{-0.73}\right] \tag{3.8}$$

$$k = \frac{\omega}{c_0} \left[1 + 10.8 \left(10^3 \frac{f}{\sigma}\right)^{-0.70} - j10.3 \left(10^3 \frac{f}{\sigma}\right)^{-0.59}\right] \tag{3.9}$$

Delany-Bazley-Miki model (DBM)

About 20 years after Delany and Bazley presented their model for fibrous materials, Yasushi Miki [164] modified them in order to meet the positive condition for the real part of the impedance. Miki took the analogy of a one-port electric circuit and used mathematical conditions to make the characteristic impedance positive real. Using these properties, Miki made an adjustment which ensures the positive real part of the impedance. The proposed empirical relations for $(+j\omega t)$ sign convention are given in equations 3.10 and 3.11.

$$Z_c = \rho_0 c_0 \left[1 + 5.50 \left(10^3 \frac{f}{\sigma}\right)^{-0.632} - j8.43 \left(10^3 \frac{f}{\sigma}\right)^{-0.632}\right] \tag{3.10}$$

$$k = \frac{\omega}{c_0} \left[1 + 7.81 \left(10^3 \frac{f}{\sigma}\right)^{-0.618} - j11.41 \left(10^3 \frac{f}{\sigma}\right)^{-0.618}\right] \tag{3.11}$$

The boundaries of validity for the DBM model is $0.01 < (f/\sigma) < 1$.

Miki model

Miki generalised the Delany Bazley formulations, including porosity, tortuosity, and the pore shape factor ratio [163]. In comparison to the DBM model, the generalised Miki model can be applied to a wider range of materials and not only fibrous ones. The propagation constant obtained from the Miki model showed agreement with that obtained from Attenborough's model [13] using the same parameters. This showed that the Miki model could be used to describe the acoustical properties of a wide variety of ground surfaces.

Johnson-Champoux-Allard model (JCA)

The Johnson-Champoux-Allard (JCA) model is based on the work by Johnson, Koplik and Dashen (JKD) [111] to describe visco-inertial dissipative effects inside the porous media and the work by Champoux and Allard [43] to describe the thermal dissipative effects. JKD used a semi-phenomenological model to describe the complex density of an acoustical porous material

with a motionless skeleton having arbitrary pore shapes, as given in equation 3.12.

$$\widetilde{\rho}(\omega) = \frac{\alpha_\infty \rho_0}{\phi}\left[1 + \frac{\sigma\phi}{j\omega\rho_0\alpha_\infty}\sqrt{1 + j\frac{4\alpha_\infty^2\eta\rho_0\omega}{\sigma^2\Lambda^2\phi^2}}\right] \tag{3.12}$$

The four parameters involved in the calculation of this dynamic density are the open porosity ϕ, the static airflow resistivity σ, the high-frequency limit of the tortuosity α_∞ and the viscous characteristic length Λ. Here η is the dynamic viscosity of air, ρ_0 is the mass density of air at rest, and ω is the angular frequency. One of the limitations of this description worth noting is that the low-frequency limit of the real part of the dynamic mass density is not exact.

Champoux and Allard [43] introduced an expression as given in equation 3.13 for the dynamic bulk modulus for the same kind of porous material based on the previous work by Johnson *et al.* to describe the thermal effects.

$$\widetilde{K}(\omega) = \frac{\gamma P_0/\phi}{\gamma - (\gamma-1)\left[1 - j\frac{8\kappa}{\Lambda'^2 C_p\rho_0\omega}\sqrt{1 + j\frac{\Lambda'^2 C_p\rho_0\omega}{16\kappa}}\right]^{-1}} \tag{3.13}$$

In this description, two parameters are needed to calculate the dynamic bulk modulus, namely, the open porosity ϕ and the thermal characteristic length Λ'. Here, C_p is the ratio of specific, and κ is the thermal conductivity of air.

Johnson-Champoux-Allard Lafarge model (JCAL)

In this model, the expression for the mass density $\widetilde{\rho}$ is the same as in the JCA model given in equation 3.12. The description of viscous effects is adopted from JKD [111]. The expression for dynamic bulk modulus $\widetilde{K}$ given by Champoux and Allard was modified by Lafarge *et al.* [134], where the limitations in the low frequencies for thermal effects were highlighted. The modified expression for $\widetilde{K}$ is given in equation 3.14.

$$\widetilde{K}(\omega) = \frac{\gamma P_0/\phi}{\gamma - (\gamma-1)\left[1 - j\frac{\phi\kappa}{k_0' C_p\rho_0\omega}\sqrt{1 + j\frac{4k_0'^2 C_p\rho_0\omega}{\kappa\Lambda'^2\phi^2}}\right]^{-1}} \tag{3.14}$$

It is noted that an additional parameter, the static thermal permeability k_0' is introduced in this model.

Johnson-Champoux-Allard-Pride-Lafarge model (JCAPL)

Based on the JKD description of the viscous effects, the expression for the mass density was modified by Pride *et al.* [196], accounting for pores with possible constrictions in between. In JCAPL, the expression for calculating $\widetilde{\rho}$ is as given in the following equations.

$$\widetilde{\rho} = \frac{\rho_0 \widetilde{\alpha}(\omega)}{\phi} \tag{3.15}$$

$$\widetilde{\alpha}(\omega) = \alpha_\infty \left[1 + \frac{1}{j\bar{\omega}} \widetilde{F}(\omega)\right] \tag{3.16}$$

$$\widetilde{F}(\omega) = 1 - P + P\sqrt{1 + \frac{M}{2P^{\,2}} j\bar{\omega}} \tag{3.17}$$

$$\bar{\omega} = \frac{\omega \rho_0 k_0 \alpha_\infty}{\eta \phi} \tag{3.18}$$

$$M = \frac{8 k_0 \alpha_\infty}{\phi \Lambda^2} \tag{3.19}$$

$$P = \frac{M}{4\left(\dfrac{\alpha_0}{\alpha_\infty} - 1\right)} \tag{3.20}$$

Pride *et al.* [196] modified the expressions describing thermal effects given by Champoux and Allard [43]. Then the modifications of Lafarge *et al.* [134] to include the static thermal permeability (k_0') parameter results in the combined expressions for calculating the dynamic bulk modulus $\widetilde{K}$ are as follows.

$$\widetilde{K} = \frac{\gamma P_0}{\phi} \frac{1}{\widetilde{\beta}(\omega)} \tag{3.21}$$

$$\widetilde{\beta}(\omega) = \gamma - (\gamma - 1)\left[1 + \frac{1}{j\bar{\omega}'} \widetilde{F'}(\omega)\right]^{-1} \tag{3.22}$$

$$\widetilde{F'}(\omega) = 1 - P' + P'\sqrt{1 + \frac{M'}{2P'^2} j\bar{\omega}'} \tag{3.23}$$

$$\bar{\omega}' = \frac{\omega \rho_0 C_P k_0'}{\kappa \phi} \tag{3.24}$$

$$M' = \frac{8 k_0'}{\phi \Lambda'^2} \tag{3.25}$$

$$P' = \frac{M'}{4(\alpha_0' - 1)} \tag{3.26}$$

This combined model is called the Johnson-Champoux-Allard-Pride-Lafarge (JCAPL) model.

Wilson model

In 1993, Wilson developed a propagation model on the basis that the viscous and thermal dissipation of an acoustic wave propagating through a porous medium can be described as a relaxation process. Wilson's model [254] uses four parameters. It is developed to match the middle frequency behaviour where the viscous and thermal boundary layers are of the order of the pore size. Whereas the models by Johnson, Koplik and Dashen for visco-inertial effects and models by Champoux-Allard or Champoux-Allard-Lafarge for thermal effects are developed to match the low and high-frequency behaviours of materials. The expression for complex mass density and bulk modulus in Wilson's model are given in equations 3.27 and 3.28.

$$\widetilde{\rho}(\omega) = \rho_\infty \frac{(1 + j\omega\tau_{\text{vor}})^{1/2}}{(1 + j\omega\tau_{\text{vor}})^{1/2} - 1} \tag{3.27}$$

$$\widetilde{K}(\omega) = K_\infty \frac{(1 + j\omega\tau_{\text{ent}})^{1/2}}{(1 + j\omega\tau_{\text{ent}})^{1/2} + \gamma - 1} \tag{3.28}$$

where ρ_∞, τ_{vor}, K_∞ and τ_{ent} are the four parameters of Wilson's model and γ is the ratio of specific heats.

3.3.2 Poroelastic materials

In the previous section, we have seen models which treat porous materials as equivalent fluids that have dissipative behaviours. However, there exist several materials wherein, at specific frequencies, such assumptions are no longer sufficient. Porous materials have a solid matrix with interconnected pores filled with a fluid medium. Although other works which describe the porous material acoustics taking into account the elasticity of the solid part exist, Biot theory has been the most popular. Many useful developments on the method have been made and validated with experiments [29, 11, 17]. Biot theory, in conjunction with other acoustic models, improves the accuracy of predictions of the acoustic behaviour of a class of materials commonly known as poroelastics or poroelastic materials.

Biot theory

The Biot theory considers that the solid part can deform elastically under the influence of forces. Biot published two articles in 1956 [26, 27] on wave propagation in fluid-saturated porous media. The theory was based on an elegant Lagrangian model where the stress-strain relations are derived from the potential energy of deformation. Biot theory predicted the existence of a slow compression wave (P_2) in addition to the fast compression wave (P_1) and the shear wave (S). This prediction was later experimentally verified by Plona [194] in ultrasonic frequencies. A reformulated version of the Biot expressions by Bolton *et al.* [29] is given in equation 3.29 and equation 3.30.

$$\text{div}\boldsymbol{\sigma}^s + \omega^2(\rho_{11}\boldsymbol{u} + \rho_{12}\boldsymbol{U}) - j\omega b(\boldsymbol{u} - \boldsymbol{U}) = 0 \tag{3.29}$$

$$\text{div}\boldsymbol{\sigma}^f + \omega^2(\rho_{12}\boldsymbol{u} + \rho_{22}\boldsymbol{U}) + j\omega b(\boldsymbol{u} - \boldsymbol{U}) = 0 \tag{3.30}$$

Here $\boldsymbol{\sigma}^s$ represents the partial stress tensor of the solid phase, $\boldsymbol{\sigma}^f$ represents the partial stress tensor of the fluid phase, $\boldsymbol{u}$ is the vector field of solid displacement, $\boldsymbol{U}$ is the vector field of fluid displacement, the parameter b denotes the effect of viscous coupling, and ρ_{11}, ρ_{12} and ρ_{22} denote mass coefficients that account for the effects of nonuniform relative fluid flow through pores between the solid and fluid phases.

3.4 Properties of porous media

At this point, it is worth providing an account of various properties used to characterise porous materials in the models discussed in the previous section.

3.4.1 Open porosity

Open porosity (ϕ), commonly called porosity, is the ratio of the volume of the fluid part to the total volume of porous material as given in equation 3.31. It is a scalar quantity that has no units. Open pores are those pores that are connected to the fluid outside the porous material through the network of interconnected pores. The pores which are closed and have no fluid transfer from outside are called closed pores and are considered part of the skeleton. The closed pores do not allow fluid motion and do not play any significant role in an acoustic fluid motion.

$$\phi = \frac{\text{Volume of fluid part}}{\text{Total volume of porous sample}} \tag{3.31}$$

There are direct ways to measure open porosity. The simplest method involves saturating the pores with water or other liquid and measuring the volume of the liquid required to saturate the medium. For the measurement, the material is placed inside a container, and the liquid is poured to fill the pores in the material. Open porosity may then be computed using equation 3.32.

$$\phi = \frac{\text{Volume of porous sample - (Volume of container - Volume of liquid)}}{\text{Volume of porous sample}} \tag{3.32}$$

The value of porosity for most fibrous materials and plastic foams is close to 1 (around 0.90–0.99) [7].

3.4.2 Static airflow resistivity

Static airflow resistivity (σ) is the amount of pressure gradient required to create unit porous volume velocity in the porous material, expressed by Darcy's flow as given in equation 3.33.

$$\sigma\phi\vec{v} = -\vec{\nabla}p \tag{3.33}$$

Here, ϕ is the open porosity, $\vec{v}$ is the acoustic particle velocity, and $\vec{\nabla}p$ is the pressure is the gradient of pressure. The S.I. unit of σ is N·s·m^{-4}.

3.4.3 High-frequency limit of the tortuosity

The high-frequency limit of tortuosity (α_∞) is a measure of disorderliness in the path of the fluid flow. It is the ratio of the mean square value of the velocity to the average velocity vector of the fluid. For a straight inviscid flow through a duct, this value will be 1. The expression for tortuosity in a volume V of a given porous material is given by equation 3.34. Here, V is the total volume of the porous material system, v is the local velocity.

$$\alpha_\infty = \frac{\frac{1}{V}\int_V v^2 dV}{\left(\frac{1}{V}\int_V \vec{v} dV\right)^2} \tag{3.34}$$

3.4.4 Viscous characteristic length

Viscous characteristic length is a scalar quantity denoted by Λ. As defined by Champoux and Allard [43], it is numerically equal to twice the weighted average of squares of the velocities

$\boldsymbol{v}(\boldsymbol{r})$ over the volume of the pore to the weighted average of squares of the velocities $\boldsymbol{v}(\boldsymbol{r_w})$ over the walls as described in equation 3.35.

$$\Lambda = \frac{2\int_V |\boldsymbol{v}(\boldsymbol{r})|^2 dV}{\int_A |\boldsymbol{v}(\boldsymbol{r_w})|^2 dA} \tag{3.35}$$

The velocities in the numerator and denominator $\boldsymbol{v}(\boldsymbol{r})$ and $\boldsymbol{v}(\boldsymbol{r_w})$ are those of an inviscid (ideal) fluid and thus do not depend on the characteristics of the fluid. The viscous characteristic length can be estimated from the measurements of the dynamic density $\rho(\omega)$ of a porous medium with prior knowledge of the static air flow resistivity and the open porosity. The method, introduced by Olny, Panneton and Tran-van [177] and further described by Panneton and Only [184], allows estimations of the high-frequency limit of the dynamic tortuosity and the viscous characteristic length from the measurement of the dynamic mass density.

3.4.5 Thermal characteristic length

Thermal characteristic length is a scalar quantity denoted by Λ'. As defined by Champoux and Allard [43], it is numerically equal to twice the ratio of volume to the average surface area of the pores as given in equation 3.36. Here, V is the volume inside the pore and A is its surface area.

$$\Lambda' = \frac{2\int_V dV}{\int_A dA} \tag{3.36}$$

This property is useful in describing the excess temperature in the pore and hence associated with the thermal effects analogous to the viscous characteristic length. If the pores are spherical, Λ' is close to the value of the radius of the pore. The thermal characteristic length may be obtained by 2D or 3D microstructure images.

3.4.6 Static thermal permeability

The static thermal permeability (commonly denoted as k_0') is a parameter that is used to describe the thermal exchanges between the skeleton and saturating fluid of the porous material at low frequencies, when the pore size is in the same order as the thermal boundary layer. As described by Lafarge *et al.* [134], it is the lower asymptotic value of the dynamic thermal permeability and is expressed as below.

$$k_0' = \lim_{\omega \to 0} k'(\omega) = \lim_{\omega \to 0} \frac{\phi \kappa \tau}{\partial p / \partial t} \tag{3.37}$$

where, κ and τ are the thermal conductivity of air and excess temperature in the porous material, respectively. Static thermal permeability (k_0') can be estimated using impedance tube or ultrasonic measurements from dynamic bulk modulus $\widetilde{K}(\omega)$ if the open porosity of the medium (ϕ) is known, using the works of Olny and Panneton [177, 184].

3.4.7 Static viscous tortuosity

The static viscous tortuosity (introduced in [174] as an inertial factor and usually denoted by α_0) is a parameter used to describe the pore fluid-structure interaction at low frequencies and expressed as follows:

$$\alpha_0 = \frac{m\phi}{\rho_f} = \frac{\frac{1}{V}\int_V v_0^2 dV}{\left(\frac{1}{V}\int_V \vec{v_0} dV\right)^2} \tag{3.38}$$

where m is the effective density of the pore space, ρ_f is the density of the pore fluid, v_0 is the relaxed velocity in the pore space and V is the porous volume. The lower limit of static viscous tortuosity is 1. This parameter has been used in multi-periodic composites [137] to determine the absorption coefficient, but experimental methods to find this parameter are not available in the literature. Alternatively, Sadouki [210] proposed a least square fit technique to compute the porosity and viscous tortuosity of a rigid porous material using reflected wave signals at low frequencies (100–400 Hz).

3.4.8 Static thermal tortuosity

The thermal counterpart of the static viscous tortuosity is called static thermal tortuosity (commonly denoted by α_0'), which is expressed as follows:

$$\alpha_0' = \frac{\frac{1}{V}\int_V \tau_0^2 dV}{\left(\frac{1}{V}\int_V \tau_0 dV\right)^2} \tag{3.39}$$

where τ_0 is the relaxed excess temperature in the pore space and V is the porous volume. It must be noted that $\alpha_0 \geq \alpha_0' > 1$ for any geometry of the pore. Further, $\alpha_0 = \alpha_0'$ in the case of aligned cylindrical pores [196].

3.5 Geometric modelling methods

In the previous section, the available approaches to model acoustic materials were discussed. Geometric modelling methods were briefly mentioned in the introduction section of this chapter. In the following, a more detailed account is provided.

3.5.1 Transfer matrix method (TMM)

The general principle behind transfer matrix methods is to establish a relationship between an input state of a system to its output state after being subject to a process by using a transfer matrix. Each state can have a set of parameters which are usually represented in the form of a vector $\mathbf{s}^{[0]}$, and the transfer matrix is a square matrix of the same size. The series of processes can be abstracted within the transfer matrices, and the state after a number of such processes can be written as in equation 3.40. Given one of the states, it is then possible to retrieve all other states if the transfer matrices are known. If two states are known, then the transfer matrix corresponding to the states can be constructed by solving the inverse problem. For this method

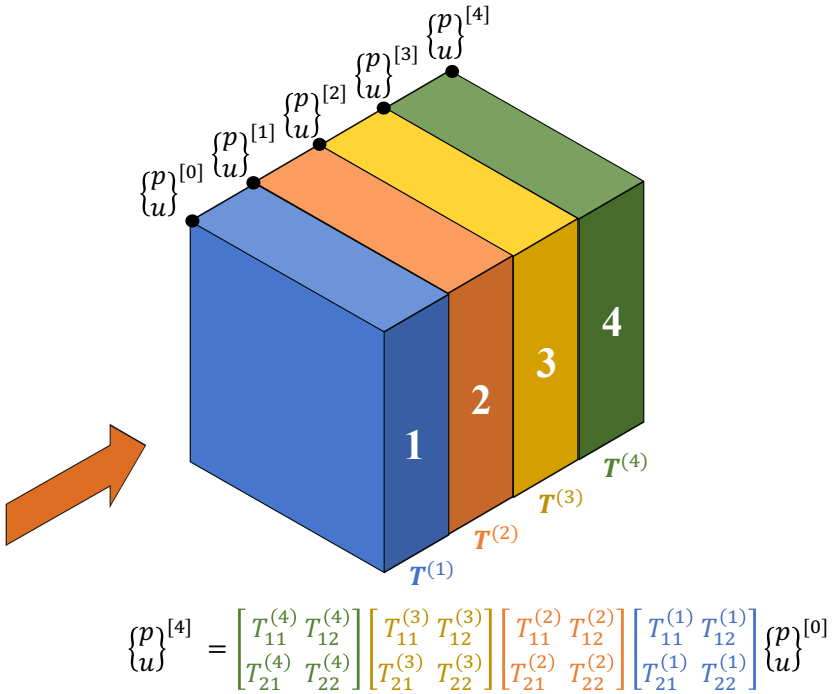

Figure 3.1: A schematic of the transfer matrix method for a multilayered system composed of a series of fluid layers.

to work, the assumption of linear relationship between the states must be valid. Once this is ensured, TMM provides a high-level abstraction to an otherwise complex problem.

$$\mathbf{s}^{[n]} = [\mathbf{T}]^{(n)} \dots [\mathbf{T}]^{(2)} [\mathbf{T}]^{(1)} \mathbf{s}^{[0]} \tag{3.40}$$

Transfer matrix methods are widely used in many fields such as optics [31], wave propagation in homogeneous media [212], muffler acoustics [167] etc. For multilayered porous media, the transfer matrix method has been extended by a series of researchers since the 1990s [8, 245], and since then, it has been successfully applied by researchers to many applications [224, 136, 246, 186]. Chapter 11 in Allard and Atalla's book [7] provides a compilation of transfer matrices for fluid, solid and porous media. The state of plane waves in a classical fluid medium can be represented by just two variables, say, acoustic pressure p and velocity u, since fluids propagate only longitudinal waves. The transfer matrix for a fluid layer is hence a 2×2 matrix. For a series of fluid layers, the equations can then be represented using the transfer matrix expression, as shown in Figure 3.1. Whereas, for solid and porous media, compressional and shear waves need to be taken into account. Consequently, the matrix sizes are larger for solid and poroelastic media. For interfaces between dissimilar layers, the state variables are not readily compatible. To link the state variables among fluid, solid and porous layers, the transfer matrices would need to be rectangular. To avoid this, constraints can be used on the interface state variables, and a global transfer matrix can be assembled for the entire multilayer system. This is discussed in detail in Allard & Atalla's book and is not elaborated here. For the purposes of this research, abstracting the computations involved helps in understanding the optimisation problem structure. Mainly, it should be noted that the computation involves the assembly of the global transfer matrix for the multilayered system and solving the system of linear equations. The size of the global matrix is in the order of the number of layers. The book also outlines the procedure to compute the specific impedances and the acoustic indicator for diffused field acoustic sources. The method has been validated for several multilayered systems with experi-

ments by many researchers. Due to the simplicity and the well-documented accuracy of transfer matrix methods to model the impedance predictions, they are the most preferred methods used by researchers working on acoustic porous media. These procedures for several acoustic material models are also implemented by Matelys Research Lab in a commercial software named AlphaCell.

3.5.2 Finite element method (FEM)

As briefly described before, the finite element method is an approach to find numerical solutions to partial differential equations (PDE) in complex geometries. The main idea is to discretise the real-world system with intricate shapes into a finite number of smaller elements of standard shapes such as triangles, quadrilaterals, tetrahedrons etc. An interpolation function for the field variable of the PDE is assumed across these finite geometries. The differential equation of the problem is rewritten in a weak form for these known geometries in the form of element matrix equations. In weak formulations, instead of setting the differential equation to zero at all points within the element, the residual or the error of the differential equation is set to zero and solved. This formulation essentially facilitates the conversion of the PDE into matrix equations, allowing the use of linear algebra to solve the problem. These element matrix equations are then combined into large global matrix equations to satisfy the field value constraint at the interface of the elements. By solving the linear algebra problem, a weak solution to the PDE is obtained, which may be sufficient for engineering practice. The method can also be easily extended to include a variety of complicated material behaviours such as non-linearities, plasticity, and visco-elasticity in their finite elements. Although the method has its origins in the 1940s [105, 57], it was formalised after the 1960s by Zienkiewicz and colleagues [277]. With the advent of powerful computers in the 1990s, the use of FEM surged, and previously unsolvable problems were being solved. The field of FEM has been extended to all possible domains, including acoustics.

Biot laid the theoretical foundations for modelling wave propagation in porous materials [26, 27] in the 1960s. Up to the 1990s, many researchers focussed on deriving numerical formulations to solve porous media problems. The initial models included equivalent fluid approaches models [59], and later sophisticated models using the Biot theory were developed [116, 182, 183] involving the classical $(\underline{u}, \underline{U})$ formulation, which solves for both the displacement of the porous skeleton$(\underline{u})$ and the displacement of the fluid part $(\underline{U})$. Göransson *et al.* [91] proposed a simpler $(\underline{u}, \underline{p})$ formulation which solves for the pressure instead of displacements in the fluid part, reducing the number of equations to be solved. Atalla *et al.* [11] included the strain couplings between the solid and the fluid phases and reformulated them into the exact $(\underline{u}, \underline{p})$ formulation. Bécot and Jaouen [17] have recently presented a way to account for the elastic frame effects in porous materials modelled using the equivalent fluid model. These new and improved finite element models have been rigorously validated over the years with experimental results on multilayered systems.

Figure 3.2 shows a schematic of a car cavity and its discretisation into smaller triangular and quadrilateral elements for illustration. While the system shown uses either air or poroelastic foam, the existing finite element formulations can also model elastic materials. By solving for the pressure fields of the fluid part and the displacements of the solid part using the $(\underline{u}, \underline{p})$ formulations, one can estimate the amount of sound energy absorbed by the foam, the sound pressure levels at various points within the car cavity, and further, optimise the placement of

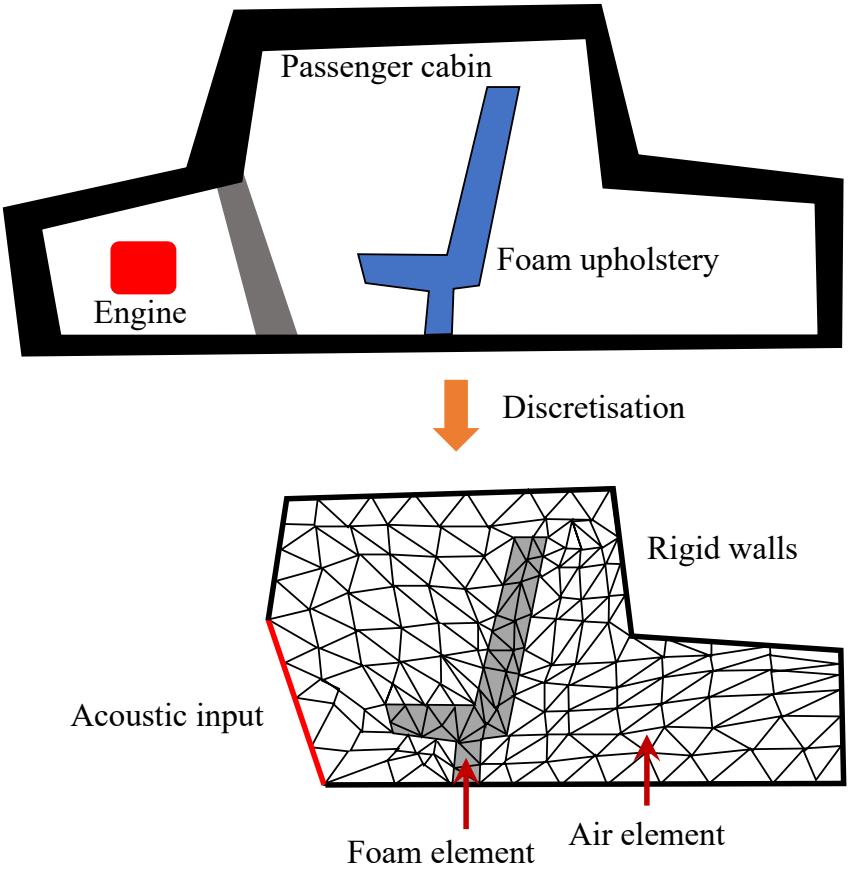

Figure 3.2: Finite element discretisation of a schematic car cabin.

additional sound-absorbing materials as per needs. Also, note that the engine noise in this example is abstracted into the dashboard surface, wherein the acoustic loads are subjected, and the other walls are assumed to be rigid. The abstraction may be done using measurements or solving for another finite element model considering the engine cavity alone. FEM also allows modelling the engine cavity in this example by including the elastic/poroelastic properties of the dashboard. These procedures may be easily extended to three dimensions to model a real-world car cavity or aircraft passenger cabin, wherein the properties of each surface and material can be chosen. Thus, we illustrate the geometric modelling capabilities of finite element tools.

When using finite element methods, the accuracy of the solutions and whether the modelling procedure followed sufficiently represents the real system is often a question. A general guideline is to use finer meshes with smaller element sizes and limit the aspect ratio of the smaller finite elements to ensure accuracy. To model a real-world system, it is necessary to ensure that loads, boundary conditions and material properties are included accurately.

Governing differential equations to numerical matrix equations: The physics of most engineering problems can be represented in the form of governing differential equations with boundary conditions. Since the geometries are complex, analytical solutions are not available in most cases. The finite element method provides a way to convert these differential equations into matrix equations that can be solved to find numerical solutions. The matrix sizes are typically very large and of the order of the number of nodes (vertices or corner points of an element)

of the finite element model.

Smaller the elements –higher the accuracy: The accuracy of a finite element model is typically better if the discretisation is fine. However, finer mesh also means increased matrix sizes. Hence, the choice of mesh size is a trade-off between accuracy and speed. There also exists a minimum acceptable level of discretisation for each problem. Whereas when considering topology optimisation, the finer the mesh, the higher are the number of design variables. The mesh size also governs the possible shapes that can be explored by the optimisation algorithm. This is called mesh dependence in topology optimisation [221].

Another commonly used geometrical modelling method is the boundary element method (BEM). BEM has similarities to FEM, with the key difference being that instead of modelling the bulk of the system, only the boundary is discretised and modelled. This can save a significant amount of computational effort in modelling such systems, particularly those that involve Laplace-like equations [52].

3.6 Conclusions

The points to takeaway are as follows:

1. Porous materials are those that contain fluid-filled pores in a solid matrix. Of these pores, only the open pores contribute to sound absorption, and the interconnected fluid-filled volume is called the fluid part, while the solid matrix along with closed pores is called the solid part.
2. Researchers have identified various material properties such as open porosity, static airflow resistivity, tortuosity, etc., which affect the propagation of sound in porous media.
3. The behaviour of some porous materials can be approximated by considering the solid part to be rigid by using motionless skeleton models such as DBM, JCA, JCAL etc. These equivalent fluid models can be used with the transfer matrix method to find sound absorption in layered sound absorbing systems.
4. Materials where the solid part is sufficiently elastic that the combined motion of solid and fluid parts influences the absorption of sound are referred to as poroelastic materials. Biot theories provide a framework to model the propagation of sound in poroelastic media.
5. Biot's governing equations have been formulated in the context of finite element method which allows modelling intricate geometries of poroelastic materials. Such models can be used to compute sound absorption in a given poroelastic shape to be used in topology optimisation.
6. The presence of macroscale air cavities or other elastic structures affects the sound propagation behaviour in these materials, resulting in changes in absorption properties. These are often called resonating structures.
7. Given the geometric shape and the material properties, the resulting sound absorption of poroelastics with mesoscale air cavities can be computed by using a combined Biot-Helmholtz approach.

Chapter 4

Topology optimisation literature

This chapter will introduce the concept of topology optimisation, discuss multiple ways to formulate the problem and provide an overview of the various application domains it has been extended to. Further, its use in acoustic porous material design is examined through a review of the existing literature. The current state of the art and gaps in knowledge with regard to optimisation aspects are discussed. It will be evident that only a few previous publications have focussed on studying optimisation strategies in acoustic topology optimisation. Towards the end, a list of the important points is provided to facilitate a quick recap.

4.1 Introduction

Historically, architects and engineers have determined the shapes of mechanical and civil engineering structures through trial and error and incremental improvements to older designs. Romans invented the arch bridge around 1300 BC by finding a way to assemble stones that only resulted in compression. These arch designs have quite literally stood the test of time. The industrial revolution allowed the production of large quantities of steel which crucially can withstand tension, paving the way for steel-reinforced concrete structures that are commonplace in today's infrastructure. The invention of faster computers paved the way for engineers to develop tools such as finite element methods in the 1960s that allowed analysing engineering structures and computing stress fields. New designs were obtained by manually redistributing materials with the knowledge of stress fields. Currently, additive manufacturing technologies such as 3D printing and automated robots allow any shape to be manufactured with fewer limitations than before. Around the 1980s–1990s, early foundations of topology optimisation were laid resulting in a remarkable innovation that can fully automate the structural design.

Topology optimisation is the concept of optimising the shapes and topologies of mechanical structures to optimise a structural performance indicator. In this thesis, topology will be referred to in the context of mechanical structures, which, in essence, is the number of holes in a structure and not the network topology more familiar in communication sciences. On the other hand, shape optimisation is the process of optimising the boundary of the structure, keeping the topology or the number of holes fixed. An illustration is provided in Figure 4.1. The concept of optimising both shape and topology simultaneously was first introduced by Bendsøe and Kikuchi [20, 19] in the 1990s. Topology optimisation has since then been recognised as a field of vast potential, having been extended to a plethora of problem domains involving material and resource distribution problems.

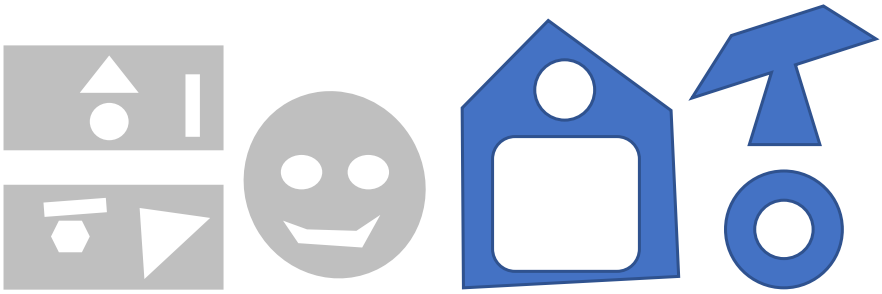

(a) (b)

Figure 4.1: (a) Shapes with the same topology (b) Shapes with different topologies.

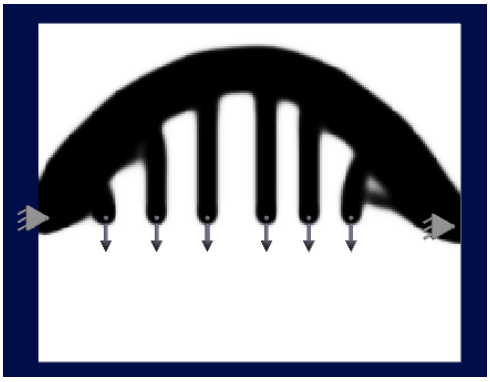

Figure 4.2: Optimal material distribution for constructing a bridge across a river. The triangles indicate the location of the supports, the arrows indicate the location and direction of loads. The optimal shape was generated using an app created by the Technical University of Denmark's topology optimisation group [1].

Topology optimisation can be thought of as a material distribution problem where a limited amount of material is available, and the optimal shape of the material in a given region needs to be found. This problem arises in many contexts and the most popular and well-studied problem is *compliance minimisation*. Compliance is the measure of flexibility of a structure, and mathematically, it is the inverse of stiffness. Let's consider that a certain amount of material is provided to build a bridge across a river which needs to support the weight of the traffic and other loads such as the wind. Topology optimisation aims to find the optimal shape for constructing the bridge with maximum stiffness.

Figure 4.2 shows the optimal shape and topology for given loads and supports distributed mimicking that of a bridge obtained using a mobile app created by the TU Denmark group [1]. Note that this shape resembles a typical arch structure. Romans invented arch bridges around 1300 BC, and today, hand-held devices can reinvent this technology in a few seconds without any prior knowledge. One can consider this achievement to be akin to the AlphaZero AI achieving superhuman Chess skill level in under 24 hours of training with only the rules of the game and self play [223]. Such material distribution problems arise in many engineering domains and they are increasingly making use of topology optimisation. Topology optimisation has also found quick adaptation by industries due to its immense potential benefit. Many commercial finite element software have now implemented variants of the solid isotropic material with penalisation (SIMP) algorithm for rapid and automated generation of mechanical shapes. One study estimates that Airbus' use of topology optimisation for designing lightweight components has

Table 4.1: Topology optimisation applications.

S.No	Application	Examples
1.	Optimal distribution of materials for maximum structural stiffness or minimum compliance.	[19, 256, 133]
2.	Optimal distribution of heat sink materials (fins or radiators) to dissipate heat in applications such as IC engines, computer processors, heat exchangers etc.	[159, 98, 65]
3.	Optimal distribution of front metallisation patterns in solar panels to carry away electrons efficiently while not blocking the light.	[97]
4.	Material distribution for automobile crashworthiness.	[78]
5.	Compliant mechanisms that need to allow flexible motion of structures, such as micromechanical switches and other mechanisms.	[216]
6.	Vibration and eigenfrequency optimisation.	[157, 270]
7.	Optimal shapes of photonic crystal waveguides to significantly enhance the functionality.	[30, 109]
8.	Optimal shapes of acoustic materials such as sound-absorbing materials, rigid scattering materials etc. to maximise the acoustic performance in applications such as mufflers, sound barriers, car cavities, room and auditoriums, etc.	[140, 76, 268]

lead to weight savings in the order of 1000 kg for each A380 aircraft [133]. This is a significant achievement in terms of fuel cost saved, and reiterates the importance of studying this topic. Moreover, topology optimisation can be extended to other domains where a shape or the distribution of materials or resources needs to be optimised. A few example problem domains where topology optimisation has been applied to is given in Table 4.1.

In this chapter, the topology optimisation problem is introduced with a focus on the compliance minimisation problem (Section 4.2). Some of the popular optimisation strategies in use are discussed in 4.2.3. Extension to the acoustics domain is elaborated, and some gaps in knowledge are identified in section 4.3. Then a summary of takeaways is provided in section 4.4.

4.2 The compliance minimisation problem

In this section, we will explore the compliance minimisation problem in more detail since the pioneering and progressing works in topology optimisation literature deal mainly with this problem domain.

4.2.1 What is compliance?

Compliance of a structure is a quantitative measure of its flexibility. Low compliance is one of the desirable qualities of robust mechanical structures. The compliance of a small bar of a material fixed at one end is the amount of displacement produced by a unit force applied at its other end. A piece of solid not connected to any support can undergo free-body motion and thus has infinite compliance. A perfectly rigid material fixed to a support has zero compliance. Although there are other parameters such as stresses, fatigue, endurance and crack propaga-

tion, which are of practical relevance in engineering, compliance is the performance indicator commonly used in topology optimisation, as it is one of the quantities whose gradients can be computed relatively quickly using adjoint-like methods [34].

To compute compliance of a real structure, one can model the structure by discretising it into finite elements (see 3.5.2), subjecting the model to loads and boundary conditions, and computing the displacements at the nodes. By describing the material behaviour using constitutive modelling, one can write the system matrix equations in the form of $[\mathbf{K}]\{\mathbf{u}\} = \{\mathbf{f}\}$, where $[\mathbf{K}]$ is the global structural stiffness matrix, $\{\mathbf{u}\}$ is the node displacement vector, and $\{\mathbf{f}\}$ is the external force vector. The global stiffness matrix is assembled by merging element stiffness matrices $[\mathbf{K}_e]$ which describe the material at each element. The size of $[\mathbf{K}_e]$ is given by the product of number of nodes per element and the number of degrees of freedom per node. The nodes per element depend on the element geometry i.e., 3 for triangular elements, 4 for quadrilateral elements etc. The number of degrees of freedom refers to the number of ways in which the state of a node can be represented. In a two dimensional problem, a node can have two degrees of freedom corresponding to the horizontal and vertical coordinate locations. Thus, for a two-dimensional 4-noded quadrilateral element, the size of the element stiffness matrix would be 8×8. After assembling the element matrices into the global matrix, the system of linear equations can be solved to find $\{\mathbf{u}\}$. With the nodal displacements, compliance can be computed using the following equation given by Andreassen *et al.* [10].

$$c = \{\mathbf{u}\}^T[\mathbf{K}]\{\mathbf{u}\} \tag{4.1}$$

The size of the matrices correspond to the number of nodes in the finite-element discretisation. Thus, if the discretisation is fine, the matrix sizes will become large, requiring more computational time to solve the equations and vice versa.

4.2.2 Problem formulation

Consider a structure as shown in Figure 4.3 demarcated into a fixed domain (white and black) and a design domain (grid area). The design domain (Ω) is the region where the shape and topology have to be optimised while the fixed domain is kept unchanged. A generic topology optimisation (TO) is to find the optimal assignment of material properties at every point in the design domain such that a desired structural parameter is optimised [19]. When the structure is discretised into finite elements, each element in the design domain is assigned materials. Usually, the material choice is binary, but multi-material topology optimisation is also being studied [279]. In the standard compliance minimisation problem, the two material choices are solid ($x = 1$) and void ($x = 0$). The volume fraction of the solid in the design is typically limited by an inequality constraint (V_f). This problem is formulated mathematically in equation 4.2.

$$\begin{aligned} \min_{\mathbf{x}} \quad & c(\mathbf{x}) \\ \text{subject to:} \quad & \frac{1}{N}\sum_{i=1}^{N} x_i \leq V_f \\ & \mathbf{x} : x_i \in \{0, 1\} \end{aligned} \tag{4.2}$$

The optimisation problem is to find the assignments x_i for each element in the design domain such that the compliance of the structure c is minimised, while limiting the maximum solid

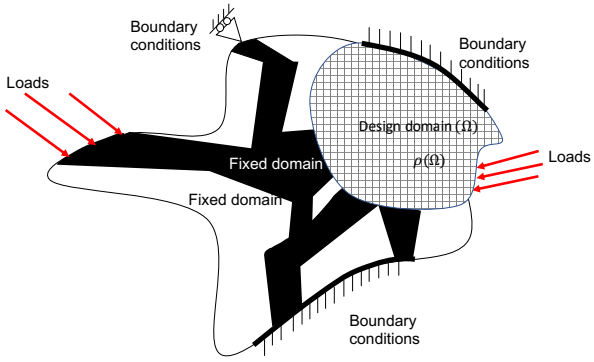

Figure 4.3: Schematic of a generic compliance minimisation topology optimisation problem. Black colours correspond to solid material and white corresponds to void (no material). Design domain marked by the grid pattern is where one needs to optimally assign solid or void such that a structural parameter is optimised.

volume fraction. Here N is the total number of finite elements in the design domain. It is worth noting that enumerating all solutions is impractical, even for small problem instances in this domain, as the search space size (2^N) grows immensely as N increases.

The presence or absence of material in a given finite element is a binary choice. The problem posed in 4.2 is hence combinatorial and, in general, difficult to solve. More often than not, the problem is relaxed to the continuous domain by allowing intermediate materials between solid and void to be filled. Rewriting the problem with $x_i \in \{0, 1\}$ replaced by the continuous design variable $\rho_i \in [0, 1]$, we have:

$$\begin{aligned} \min_{\boldsymbol{\rho}} \quad & c(\boldsymbol{\rho}) \ : \ \mathbb{R}^N \to \mathbb{R} \\ \text{subject to:} \quad & \frac{1}{N}\sum_{i=1}^{N} x_i \leq V_f \\ & \boldsymbol{\rho} : \rho_i \in [0, 1] \end{aligned} \tag{4.3}$$

The above continuous relaxation for two material compliance minimisation is commonly called density-based topology optimisation since the design variables can be thought of as the density of the fictitious intermediate material or as the thickness of a 2D plate. To model the system, the material properties for intermediate materials can be given by a material interpolation scheme:

$$E_i = E_{void} + \rho_i^p (E_{solid} - E_{void})$$

where E_{void} and E_{solid} are the elastic moduli of void and solid respectively, and E_i gives the elastic modulus to be assigned to the i^{th} element. If ρ_i is 0, then the element i would be assigned an elastic modulus of 0, and if ρ_i is 1, the element i would be assigned the elastic modulus of the solid material.

4.2.3 Topology optimisation methods

Solid isotropic method with penalisation (SIMP)

SIMP is the most popular topology optimisation method. In this method, the discrete material distribution problem is converted to a continuous problem by using a power-law interpolation

scheme. This is one of the pioneering approaches proposed by Bendsøe and Kikuchi [20, 19].

Sigmund popularised the strategy for compliance minimisation through his 99-line educational Matlab code in 2001 [217]. Publishing such educational examples of topology optimisation strategies and applications has been quite common in literature. This educational code had a far-reaching impact in the research community, especially for beginners. Then, an update to the code was published by Andreassen *et al.* [10]. More recently, Ferrari and Sigmund [80] published an even more efficient version which also includes its extension to three-dimensional problems. Recently Zhou *et al.* [274] published complementary lecture notes to elaborate on some of the less well-known aspects of the optimality criteria method used in Andreassen *et al.* [10] and others. Wang *et al.* [250] present a comprehensive review of such Matlab codes in literature.

Instead of a linear relaxation, the intermediate material properties are arrived at using generalised interpolation schemes like the SIMP scheme [22] (not to be confused with the SIMP approach). In the SIMP scheme, interpolation is done using a penalty exponent $E_i = E_{void} + \rho_i^p(E_{solid} - E_{void})$ where $p > 1$, usually $p \geq 3$. The reasoning stated is that unless ρ_i is 1, the benefit of the solid will be penalized (say $\rho_i = 0.5$, $p = 2$ then $E_i = 0.25E_{solid}$). This is supposedly to penalise intermediate materials which have $\rho_i \in (0, 1)$. A SIMP 'approach', on the other hand, is to optimise a topology optimisation problem by starting from an initial guess, using an interpolation scheme (with $p \geq 1$) for intermediate materials, computing derivatives of the objective function with respect to the design variables ($\frac{dc}{d\rho_i}$) and making moves in the gradient direction using an optimiser. The optimisers are gradient-based move operators, some examples of which are the optimality criteria method [21] and the method of moving asymptotes [238].

Bidirectional evolutionary structural optimisation (BESO)

Not to be confused with evolutionary optimisation, evolutionary structural optimisation (ESO) is a constructive heuristic for compliance minimisation topology optimisation. This method was first introduced by Xie and Steven [256, 257]. It is one of the simplest and most intuitive strategies for topology optimisation. The initially introduced version, ESO, uses a material removal heuristic that starts from a fully-filled design domain and incrementally removes material from locations where the stresses are low. This was later extended to include bi-directional moves wherein materials can also be added. The bi-directional ESO, often abbreviated as BESO, is the second most popular topology optimisation strategy. ESO and BESO require the use of problem-specific information, namely the stress fields, to make move operations. For readers new to engineering, stress can be contrived as a measure of force per unit area. Materials tend to fail (break or deform permanently) when stress exceeds a certain limit. The general idea is to remove materials where they are not needed (low-stress regions) and add materials where they are needed (high-stress regions). BESO can be extended easily to other domains if a field variable akin to stress can be established. In many cases, the sensitivities of the fitness function to the design variables are computed by researchers for various problem domains, and these gradients can be used to make the moves.

Level set method

The level-set topology optimisation method uses a higher-dimensional scalar field described in the design domain space and uses a threshold value of this scalar field to represent the presence or absence of material at a given point. Some of the first publications of this work were by Allaire *et al.* [5, 6, 4] and Wang *et al.* [251].

Blackbox metaheuristics

Many researchers have studied metaheuristics on the topology optimisation problems. An extensive review of such blackbox topology optimisation algorithms may be found in Guirguis *et al.* [94]. Blackbox algorithms are those that do not use any problem information other than fitness. Such blackbox algorithms include metaheuristics such as genetic algorithms, covariance matrix-adaptation evolution strategy, simulated annealing etc. Metaheuristics are known to have notably poor convergence rates for topology optimisation algorithms, often requiring many function evaluations before a reasonably fit shape can be obtained. Research focus has also been devoted to improving the performance of such metaheuristics. Some researchers also have been critical of using non-gradient algorithms for compliance minimisation as gradients are fast to compute. A full research article dedicated to this issue has been published by Sigmund [219] and is worth highlighting.

Moving morphable components-based topology optimisation

Moving morphable components (MMC) [96] is an alternative representation scheme for topology optimisation, wherein the number of design variables can be substantially reduced. The key idea is to assume that the topology and shape are given by a union of small components of known shapes and optimising the size, shape and dimensions of these components. Such methods are often used to speed up metaheuristic algorithms [205]. MMC is a topic of interest to topology optimisation researchers, and a subfield has emerged around this technique with numerous publications [123].

4.3 Extension to acoustic problem domains

It is common knowledge that the acoustics of a room can be improved by introducing intrusions/niches or projections on the reflecting walls. The acoustic performance of porous materials also depends on their geometric shape. The shape of porous absorbers can be optimised to obtain better performance without adding to the weight or material costs. Numerous previous works have provided solutions to shape optimisation in porous materials. Acoustic testing is commonly done in *anechoic* (meaning *without echo*) chambers which typically feature large wedge-shaped foams that absorb and scatter almost all of the impinging sound waves. Beranek *et al.* [24] in 1946 published a seminal work on the experimental assessment of different acoustical foam shape designs to be used in anechoic chambers. They showed that a linear wedge shape is the best among other contemporary designs [178, 162]. Through extensive experiments, different dimensions of the wedge were tested, and a reference chart for the cut-off frequencies for different geometrical parameters of the linear wedge shape was obtained. The absorption curve of a linear wedge shape typically is low at low frequencies and increases after a certain cut-off frequency and stays nearly flat at higher frequencies. The cut-off frequencies define the frequencies above which more than 90% of the incident sound pressure of normal incidence is absorbed. While the charts given in [24] are for glasswool, those of Koidan *et al.*

[127] are generalised for more materials. These charts have mainly been obtained by extensive experiments which need large impedance tubes for low frequencies.

Boutin and colleagues [33, 176, 213] have shown that porous materials with mesoscale pores (shapes cut out from the materials) can be tuned to have improved acoustic performance at low frequencies than uncut specimens. These materials are sometimes referred to as double porosity materials due to the presence of networks of multiple interconnected pores with different characteristic sizes. Bécot *et al.* [18] have successfully applied the double porosity theory to non-planar shapes, including an anechoic wedge.

In Lee *et al.* [140], a shape optimisation for the foams used in anechoic chambers was performed. The authors consider the Biot theory for the poroelastic foam and Helmholtz equation for the air. An interpolation scheme is proposed, which uses an interpolation parameter χ_e in a unified model. The technique involves setting $\chi_e = 0$ for air and $\chi_e = 1$ for the porous medium. The unified model was validated for tested foam shapes, including and other than the wedge shape. Then an optimisation scheme is used to find better foam shapes under certain constraints. They consider two objectives and optimise the weighted sum. The first objective is to minimize the absorption and the second is to minimise $\chi_e(1 - \chi_e)$ from $\chi_e \in [0, 1]$. The second objective will require χ_e to be set to 0 or 1. However, this can be improved by choosing discrete values for χ_e from either 0 or 1, and removing the second objective. For discrete optimisation, metaheuristic algorithms such as genetic algorithm [102] and simulated annealing [125] could be used effectively.

Yoon [266] proposed a new acoustic topology optimisation (ATO) framework for fibrous materials using the Delany Bazely model [70]. With the use of a SIMP interpolation scheme, the acoustic topology optimisation of both the fibrous material and the interior solid structure was performed. A numerical example of a simple expansion muffler was considered, and the optimal shape were found.

Wadbro *et al.* [249] performed shape optimisation of an acoustical horn for maximising sound transmission using a gradient-based method of moving asymptotes [238]. Other relevant works, for example, Duda [75] are also available for shape optimisation in acoustic foam applications.

Xu *et al.* [258] used Matlab evolutionary optimisation toolbox to optimise a flat three-layered porous material that achieves close to the performance of linear wedge shape. In this case study, some pursuits of acoustic researchers to find optimal shapes for maximal absorption coefficient in wedges are provided. The motivation is to arrive at better foam shapes for different applications, taking the anechoic chamber wedge as a benchmark. This presents a venture for further research in devising generalised algorithms for porous shape optimisation. The contributions foreseen from No2Noise include testing different optimisation algorithms which are efficient in finding the best foam shape in benchmark applications such as anechoic wedge shape optimisation. The better-performing algorithms could then be deployed for obtaining optimal shapes in different applications.

Many researchers have published applications of topology optimisation on acoustic porous material problems in the last two decades. This could be achieved due to the fact that both porous media modelling and structural topology optimisation matured around the 2000s. A review of the literature indicates that acoustic topology optimisation is only an emerging field: there

have only been about 100 publications with *acoustic topology optimisation* in their title or abstract in Web of science search. On the other hand, the total number of topology optimisation publications vastly outnumbers this, with around 10,000 articles (Web of science search as of May 2020). Out of acoustic topology optimisation articles, a brief account of about thirty more relevant articles is listed in Table 4.2.

Table 4.2: A comprehensive list of relevant acoustic topology optimisation publications.

No.	Publication	Year	Description	Method
1.	Wadbro and Berggren [249]	2006	Acoustic horns: Optimising acoustic horns to minimise the reflection coefficient	SIMP
2.	Lee *et al.* [140]	2008	Anechoic chamber foam shape optimisation	SIMP
3.	Dühring *et al.* [76]	2008	Room ceiling foam shape optimisation	SIMP
4.	Lee *et al.* [142]	2009	Distribution of rigid material in mufflers	SIMP
5.	Yamamoto *et al.* [261]	2009	Multimaterial topology optimisation of a soundproof panel	SIMP
6.	Kook *et al.* [130]	2013	Car cavity	SIMP
7.	Yoon [266]	2013	Mufflers with porous and rigid materials using Delany-Bazley-Miki model	SIMP
8.	Isakari *et al.* [106]	2014	Optimal placement of scatterers in a rectangular cavity	Levelset
9.	**Lee *et al.*** [138]	2015	Distribution of air, poroelastic and rigid material in a muffler	SIMP
10.	Yedeg *et al.* [263]	2016	Mufflers	SIMP
11.	Kook *et al.* [129]	2017	Periodic microstructure-enhanced loss factor using acoustic-structure interaction	SIMP
12.	Zhao *et al.* [271]	2017	Sound barriers using porous materials and boundary element method	SIMP
13.	Chen *et al.* [46]	2018	Porous material sound barriers using boundary element method	SIMP
14.	Azevedo *et al.* [14]	2018	Porous material in an impedance tube	BESO
15.	Noguchi *et al.* [173]	2018	Negative bulk modulus acoustic metamaterial	Levelset
16.	Dilgen *et al.* [71]	2019	Impedance tube	Levelset
17.	Yoon *et al.* [268]	2020	Impedance tube by distributing porous and rigid materials	SIMP
18.	Gonçalves *et al.* [90]	2020	Identification problem: Synthesise input from the output	SIMP
19.	Wang *et al.* [252]	2020	Component mode synthesis (Craig-Bampton) for vibroacoustic topology optimisation	BESO
20.	Chen *et al.* [47]	2020	An approach for exterior acoustic distribution of sound-absorbing materials using the boundary element method with isogeometric analysis-based basis functions	SIMP
21.	Khajah *et al.* [121]	2021	Shape optimisation of horn using scaled boundary finite element modelling	Differential evolution

22.	Li, Tahar and Sui [146]	2021	Sound transmission loss of open acoustic barrier	Genetic algorithm
23.	Qin *et al.* [197]	2021	Robust topology optimisation considering acoustic sources with stochastic frequencies	Levelset
24.	Gao *et al.* [84]	2021	Acoustic phononic structures using level set with boundary element method	Levelset
25.	Gao *et al.* [104]	2021	Acoustic phononic structures using level set with boundary element method	Levelset
26.	Yu *et al.* [269]	2021	Optimal distribution of acoustic material	SIMP
27.	Chen *et al.* [49]	2022	Sound absorbing materials using isogeometric BEM	SIMP
28.	Qin *et al.* [198]	2022	Extension of the robust topology optimisation method to viscoelastic structures	Levelset
29.	Dilgen *et al.* [72]	2022	Three dimensional hearing aid vibroacoustic topology optimisation	SIMP
30.	Chen *et al.* [48]	2022	Bi-material topology optimisation coupled structural acoustic system using FEM-BEM	SIMP
31.	Pereira *et al.* [189]	2022	Multi-constrained BESO method for two acoustic systems respectively with rigid material and poroelastic material	BESO
32.	Kim and Yoon [123]	2022	Moving morphable components in neural network based design	SIMP, MMC
33.	Guo *et al.* [95]	2022	Acoustic metasurface for reflected wavefront modulation	Levelset

Horns: In one of the earliest studies, Wadbro *et al.* [249] applied topology optimisation for distributing sound-hard materials in front of a regular triangular horn to optimise the reflection coefficient of acoustic horns. Acoustic horns are one-dimensional ducts with an increasing area that can amplify sound energy radiated from vibrating surfaces placed in its throat. They are typically used in old loudspeakers, air horns etc. The mechanism behind this device is to increase the specific impedance at the vibrating surface such that a given vibrational velocity of the sound-producing membrane transmits more acoustic energy. The gradually increasing area of a horn provides impedance matching so that reflections caused by sudden area changes are avoided. By optimising the shape of rigid scattering materials using topology optimisation, the performance of the horn can be improved. The objective function is to minimise the reflection coefficient at a specific frequency. The system was modelled using the finite element method to compute the fitness. Khajah *et al.* [121] have used the differential evolution metaheuristic to study the shape of acoustic horns.

Impedance tubes: Impedance tubes are often used to characterise and measure acoustic materials. They are also used to test poroelastic shapes experimentally to obtain their absorption characteristics and as a representative canonical system that can be used for studying topology optimisation. One can consider the impedance tube system as a template or a unit cell which is a constituent part of an application. Several topology optimisation studies have been conducted on impedance tubes. Notably, one of the first such studies for poroelastic materials is Lee *et al.* [140], who presented an application of a SIMP algorithm to optimise the topology and shape

of anechoic foam wedges. The material distributed was a poroelastic modelled using a unified Biot-Helmholtz modelling approach. This unified approach considers air as a poroelastic material with negligible solid part elastic modulus. This approach was further verified with the conventional mixed model using Helmholtz equations for air and Biot equations for poroelastic material with the necessary interface conditions. The goal of this study was to improve the low-frequency performance of anechoic chamber wedges. Hence, sound absorption under a broad frequency range from 100 to 1500 Hz was considered as the objective function. However, the material optimised was a fictitious material with a high tortuosity of 7.8, which is uncommon in real materials. Nevertheless, the study set forth a valuable precedent for a research of this kind. This modelling approach has been widely adopted in the current work for computing sound absorption and its gradients in chapters 6 and 7. Further, many of the applications listed in Table 4.2 have been studied on impedance tube-like systems with topics including multi-material topology optimisation [138] and total sound absorption at a single target frequency [268] using porous and rigid materials.

Mufflers: Mufflers are sound attenuation devices that are typically fitted to automotive exhaust. The function of a muffler is to allow exhaust gases to flow out, while preventing the high amplitude combustion noise from reaching the environment. A primitive muffler design is a simple expansion chamber placed in the exhaust duct. When sound waves from the engine enter the expansion chamber, depending on the frequency and the area change in the expansion chamber, a part of the sound energy is reflected, and a part is transmitted. Transmission loss through a muffler is a frequency-dependent quantity which refers to the ratio of the energy transmitted to the total incident energy at that frequency. A high transmission loss across a wide range of frequencies is indicative of good performance. Transmission loss depends on the area ratios, the shape of the expansion chamber and the material inside it. Often, perforated plates, porous materials or rigid scatterers are placed to alter and improve the transmission loss [167]. This is achieved typically by an expansion chamber. Before 2009, optimising muffler designs did not involve topology optimisation, with some of them using metaheuristic techniques such as genetic algorithms [44, 45, 264]. In 2009, Lee and Kim [143] applied topology optimisation for muffler design using the SIMP approach. In 2022, Qin *et al.* [198] extended their robust topology optimisation method to design viscoelastic structures that involve acoustic-elastodynamic coupling.

Sound barriers: Sound barriers are typically high-rise walls adjacent to highways that prevent road noise from entering residential and other protected biodiversity areas. The cross-sectional shape and material used for the construction of sound barriers along the long portions of roadways can contribute to high economic costs to the public. Topology optimisation has been extended to sound barrier design by several researchers. Zhao *et al.* [271] used topology optimisation to distribute sound absorbing material within a sound barrier using a boundary element method to model the system. Chen *et al.* [46] used an isogeometric boundary element method to optimise the topology of a sound barrier of a different shape. They extended the isogeometric analysis method further for exterior acoustic distributions [47, 48, 49].

Car or room cavities A cavity in acoustics is a connected region of air in a structure. The passenger cabin in a car or an aircraft or rooms in buildings must not exceed specific noise levels to ensure comfort. Placing sound-absorbing foams in these cavities is a common way to

reduce noise levels. However, finding the optimal locations to place these foams is a challenge. Also, based on the shapes of these foams, the sound level distribution in the cavity will vary. Topology optimisation is a naturally suited tool to simultaneously find the shape and placement of foams in such cavities. One of the notable initial works is by Düring *et al.* [76], wherein a cuboidal room ceiling was considered to be the design domain, and the optimal placement of a foam material was studied. The optimal solution was found to fill foams along the corners of the ceiling. Isakari *et al.* [106] studied the placement of rigid scattering materials on a three-dimensional cavity using a level set method and a fast multipole boundary element method, and derived the sensitivities for the problem. Car cavity foam shape optimisation is of interest to automotive engineers. Kook *et al.* [130] presented an efficient approach to compute the sensitivities using Padé approximants when using Zwikker's loudness as an acoustic indicator. They modelled a car cavity using their approach and optimised the distribution of acoustic materials on the floor, ceiling and rear shelf.

4.3.1 Gaps in knowledge

From Table 4.2, one may observe that SIMP-based gradient methods are the most popular. BESO and level set are also used often, and the use of metaheuristics is less common. One of the reasons is thought to be the faster convergence rates offered by these methods from studies on compliance minimisation problems. Also, note that in most of these applications, the focus is on extending topology optimisation strategies to new domains, and comparison studies are lacking. While there of many problem domains for which topology optimisation formulations do not yet exist and research in this direction is essential, comparison studies can only reveal which algorithms perform better for a problem domain. Such comparison studies have been performed extensively for the compliance minimisation domain [94, 37, 205]. However, for acoustics problems, extensive comparison studies seem to be unavailable as per our knowledge. The optimisation problem structure is yet to be explored thoroughly and remains a gap in knowledge. Understanding the problem structure thoroughly is helpful in designing better optimisation strategies in these problem domains. It is of interest to know how metaheuristics compare against commonly used gradient-based strategies such as SIMP.

4.4 Conclusions

The highlights from the literature survey presented in this chapter are as follows.

1. Structural topology optimisation is finding the optimal distribution of a given amount of material within a design region of a structure such that its performance is optimised, thereby simultaneously optimising both the shape and the topology of the structure.
2. Optimising material distribution for minimising the compliance of a structure is the most studied problem within topology optimisation research.
3. Solid isotropic material with penalisation method (SIMP) is the commonly adopted approach to perform topology optimisation for compliance minimised structures.
4. SIMP is a gradient-based method which requires computing the sensitivity of the objective function with respect to the design variables.
5. Other notable approaches include a constructive approach known as bi-directional evolutionary structural optimisation (BESO), a level-set method that optimises a higher-dimensional scalar field.
6. Metaheuristics for topology applications have been relatively rare.

7. Several application domains of topology optimisation include heat transfer, solar panel collectors, photonic and phononic crystals.
8. In acoustics, a few tens of applications of topology optimisation have been published so far, and the number of publications each year is rising rapidly every year.
9. A review of the literature quickly indicates that the most commonly used approach for acoustic topology optimisation has been SIMP, followed by BESO.
10. A variety of applications within the acoustic domain have found a use for topology optimisation, including acoustic horns, mufflers, impedance tube foams, scatterers, room cavities, and car cavities, to name a few.

Part II

Contribution chapters

Chapter 5

Multilayered sound package optimisation

The optimisation of multilayered sound packaging involves choosing the best/optimal material properties and thicknesses for each layer. As the number of layers increase, the search space size becomes too large to handle by brute force. In this study, the application of metaheuristics to configure multilayered porous materials for maximising their overall sound absorption coefficient is studied. A layer of the multilayered system may be composed of facing screens (such as woven or non-woven textile or perforated plates) or thicker porous materials, chosen from a database of common acoustic materials. Firstly, we consider a two-layered system with a fibrous porous material layer modelled using the Delany-Bazley-Miki model and a facing screen modelled by Johnson-Champoux-Allard model, and optimise different material properties for maximising the sound absorption. Secondly, for multilayered systems with more than two layers, a genetic algorithm is presented to explore the thickness and acoustical properties that maximise the sound absorption coefficients for a frequency range of interest. The problem landscapes are explored revealing that the fitness functions are smooth across the acoustical properties. Based on the insights obtained, guidelines for algorithm selection are obtained.

5.1 Introduction

In many industrial applications, sound-absorbing materials are used in the form of flat-layered packages. In some instances, they are used for sound isolation, for example, behind the dashboard of a car preventing engine noise from entering the cabin, or within the walls of an aircraft behind the plastic lining and the fuselage. Such layered materials are also used to line the payload compartment of space shuttles to prevent extreme launch noise and vibration from damaging sensitive equipment. In other instances, they are used for reducing the noise levels within an enclosure, usually placed in the form of lining materials which also serve aesthetic purposes. Examples include the headliner(the fabric on the roof of a car), the panels placed in the side walls of auditoriums and cinemas, carpets at homes and offices etc., that keep the reverberation at minimal levels. A common aspect in these applications is that they are one-dimensional, i.e., thickness is the important dimension. In this chapter, we will consider the optimisation of such layered sound packages.

The benefit of optimising such layered packages is motivated by the fact that such sound-absorbing layers are often used in large quantities in many applications constituting a significant amount of dead weight. If these sound packages are not optimised, they can contribute to economic losses, reduced range, increased fuel requirement, especially in aircraft and space applications. Optimising sound packages are also of societal importance to the public: noise

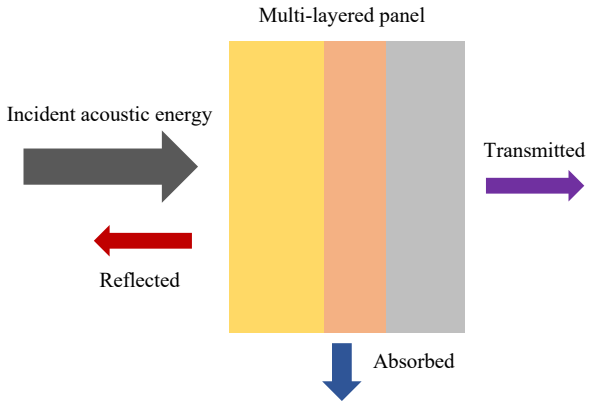

Figure 5.1: Schematic diagram of a multilayered panel depicting acoustic energy balance.

pollution in urban environments lead to increased occurrences of cardio-vascular diseases contributing to reduced life expectancy and undue stresses [168, 169]. Hence, it is essential to have effective strategies tuned to tackle optimisation problems that arise in this domain.

When sound waves are passed through these materials, the sound energy is partly reflected, partly absorbed, and the remaining is transmitted, as depicted in Figure 5.1. The optimisation objective typically falls within two categories based on the application: maximising absorption in the material or minimising transmission through the material.

Absorption maximisation: Within an enclosed cavity such as the passenger compartment of a car or an aircraft, if there is no acoustic dissipation mechanism, the noise generated from a source within the cavity will reverberate and cause discomfort. In such cases, multilayered absorbing panels need to be carefully placed within the cavity to reduce the noise levels. The optimisation goal is to maximise absorption coefficient of the panels. The material should be less reflective so as to allow the sound waves to pass through and get absorbed effectively. For this, the surface impedance of the porous layer should be as close to that of air. Figure 5.2 shows the locations where layered sound-absorbing materials are typically placed to reduce noise in different applications.

Noise absorbing layered panels usually comprise of two to five layers. Two-layered systems are the most common form of panels used in practise. The first layer is typically made of a foam or fibrous material with a thickness of 20 mm or more, followed by a second screen layer of thickness around 1 mm, the purpose of which is mainly to protect the first layer where most of the dissipation takes place. In some cases, an additional screen on the other face of the foam layer may be used forming a three-layered system.

Transmission minimisation: In some applications, noise from the source needs to be isolated from reaching an observation point, for instance, isolating the passenger cabin of an aircraft from engine and wind shear noise (see Figure 5.2c). In these cases, the objective is to minimise the transmission and the materials need to be of high density with a large impedance mismatch so as to cause high reflections or be highly absorbing. The optimisation goal here is to minimise the transmission through the multilayered system. In an aircraft, the outer walls of passenger cabin, called the fuselage, is a multilayered and multi-functional composite structure

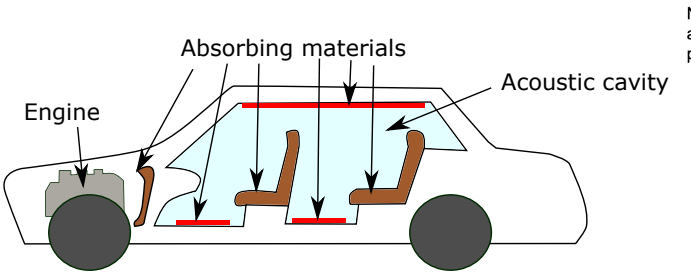

(a) Noise management in a car cavity.

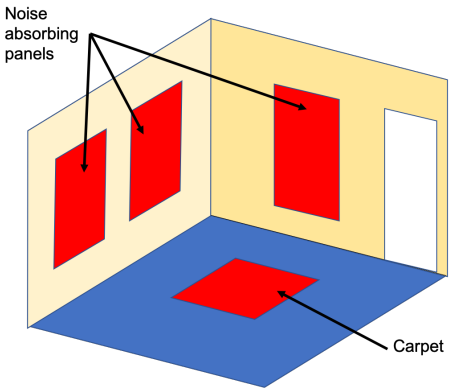

(b) Sound absorbers to prevent reverberation in a room.

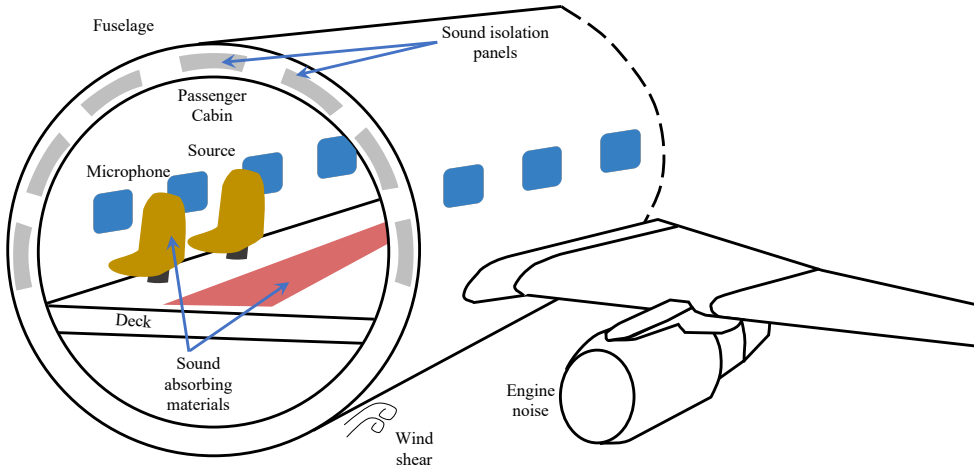

(c) Schematic of an aircraft and the placement of sound absorbing materials.

Figure 5.2: Application of sound-absorbing materials in a automotive and building applications. (a) Car cavity (b) Room in a building (c) Aircraft passenger cabin.

with porous layers to provide acoustic and thermal insulation in addition to maintaining the pressure barrier.

The fuselage, as depicted in Figure 5.2c, generally constitutes an outer structural shell made of aluminium or fibre-reinforced composites. Within this shell is a single/multiple layers of fibrous porous material. The fibrous layers may sometimes be enclosed within a thin covering (usually made of plastic) to protect the fibres from diffusing. These thin coverings are acoustically transparent, i.e., they do not modify the external noise. The porous package with the screen is covered by another layer of plastic or vinyl furnishing which will be the interior lining of the passenger cabin. These porous packages are placed throughout the length of the aircraft constituting significant weight. Although using thick and dense layers that are highly reflective are desirable for minimising transmission, it is not practical in such weight-sensitive applications, and the focus is on improving the absorption in these layers. Thus absorption maximising will be the focus in this study.

Quantification of absorption: Acoustic absorption performance of layered porous materials are typically measured by placing them in impedance tubes with a rigid backing. When an

acoustic source in the form of plane waves is passed on these materials, only absorption and reflection are possible as the rigid backing does not allow any transmission. Hence, by measuring the reflected sound waves, absorption can be estimated. The absorption coefficient α is the ratio of absorbed sound energy to the total incident sound energy. If the absorbing layers are impedance matched and sufficiently thick, there will be no reflected waves and the absorption would be 1. On the other hand, if there is no absorbing material, all the sound is reflected and the absorption would be 0. In addition to modifying the thickness, one can also modify the acoustic properties of the porous layer to improve absorption. Each layer can be modelled using material properties such as porosity, static airflow resistivity, tortuosity etc. A detailed account of porous-material properties and their measurement was provided in chapter 3. These properties can be controlled during manufacturing, for example, for chemically synthesized foams, the reaction conditions can be carefully controlled to alter the acoustic properties. Hence, these properties can be considered as the design variables for optimising the multilayered system in addition to thickness.

Modelling techniques: Many techniques are available to model such multilayered systems acoustically using material models. A review of these models is provided in chapter 3, but for completeness, a short recap is provided as follows. These material models can be broadly categorised into two types: empirical models and phenomenological models. In a seminal work, Delany and Bazley carried out experiments using a variety of fibrous materials with different flow resistivities and observed its relationship with characteristic impedance and propagation coefficient, which can be used to compute sound absorption. Miki [164, 163] extended and generalised the empirical models to non-fibrous materials. While these empirical models relate measurable properties of porous materials directly to their absorption behaviour with no physical links, phenomenological models on the other hand derive physical relations between the pore structure and absorption behaviour. Examples of such models include Biot models [26, 27, 25], Johnson-Champoux-Allard model [111, 43], Wilson model [254], Johnson-Champoux-Allard-Lafarge model [134], to name a few. A compilation of theories including implementing them using transfer matrix method is available in the book by Allard and Atalla [7]. Recent research focus is on extending the modelling tools to unexplored materials and material behaviours. Existing models allow a variety of complex systems to be modelled and some examples are as follows. Parra *et al.* [185] proposed a new method for modelling anisotropic poroelastic materials in multilayered systems. Rhazi and Atalla [204] extended the transfer matrix methodology to model structure-borne mechanical excitations to complement the methodology validated for airborne excitations. While the modelling techniques have been extended to complex acoustic materials, research into optimisation aspects remains to be well-explored.

Previous optimisation studies: Existing optimisation studies in this area report some important findings. Tanneau *et al.* [240] in 2006 demonstrated the use of a genetic algorithm for optimising the transmission loss in aeronautical fuselage application. Their approach is to consider a set of 12 available materials including solids, fluids and foam to optimise the combination of the layers and their thicknesses. This will result is a readily manufacturable layer combination suited to a desired application. Lee *et al.* [141, 139] present a one-dimensional topology optimisation strategy to automatically design a combination of air and a specific porous material to maximise the acoustic performance. They used a method of moving asymptotes-based [238] topology optimisation strategy. The result is a set of alternative layers of air and the specific porous material with different thicknesses. Lind-Nordgren *et al.* [148] presented an optimi-

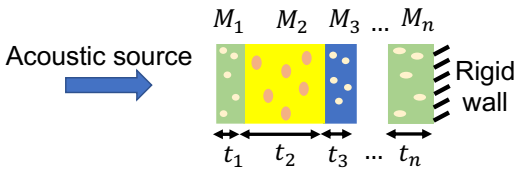

Figure 5.3: Schematic of a multilayered sound absorbing package.

sation of the microstructure of an open foam material using Biot theory-based finite element model with scaling laws to link micro and macro properties. They show that the cost function landscape had a few minima and also noted that the optimisation greatly depends on the cost function. They use the method of moving asymptotes [238] to optimise specific problem cases and have reported the optima. Pichon *et al.* [191] have provided trade-off charts for the visualisation of different categories of acoustic materials to support the optimisation of multilayered acoustic packages. Chen *et al.* [50] presented a design method for computing and optimising the absorption coefficient of multilayered systems involving metallic fibres using a phenomenological model. Boulvert *et al.* [32] presented a procedure for finding the optimal graded properties of porous layers to enhance sound absorption across a broad frequency range. Their work includes manufacturing 3D printed porous solid matrix with varying geometries to achieve the graded behaviour.

Contributions in this chapter: In this work, firstly, an example two-layered system of a fibrous layer with a screen is considered. An oblique incidence sound source is assumed to be passed on the two-layered system, and its absorption over a wide frequency range is optimised. The optimisation problem structure is explored by varying the airflow resistivity of the porous layer and screen, and the porosity of the screen. Secondly, a database of 29 existing acoustic materials is used to explore optimal three-layered configurations similar to Tanneau *et al.* 2006 [240] but for absorption maximisation with more recent and advanced material models. An integer representation genetic algorithm is used to find optimal configurations and thicknesses. A parameter tuning is performed on the genetic algorithm operators. The fitness landscapes of the design variables are studied and it is observed that the landscapes are smooth across the material properties with a finite number of modes that can be easily found by simple optimisation strategies. The observations are used to arrive at guidelines for algorithm design.

Organisation of this chapter: In section 5.2, a general problem formulation is discussed. In section 5.3, a two-layered system with a fibrous layer and a screen is considered, the modelling methodology is described and the landscapes are assessed. In section 5.4, a three-layered system is considered and a genetic algorithm is applied to optimise the layer thickness and material choices. The results are discussed and some guidelines for algorithm selection are provided. In section 5.5, a summary of the findings is reported.

5.2 Problem description

The schematic of a generic multilayered system with n-layers is shown in Figure 5.3. Each layer i is composed of a material M_i described by a set of variables including its thickness t_i and material properties $\{\lambda_1^{(i)}, \lambda_2^{(i)}, \cdots, \lambda_{p_i}^{(i)}\}$, where p_i is the number of properties required for the material model. The optimisation problem can be formulated as follows.

$$\max_{t_i,\lambda_1^{(i)},\lambda_2^{(i)},\cdots,\lambda_{p_i}^{(i)}} \alpha(t_1,\lambda_1^{(1)},\lambda_2^{(1)},\cdots,\lambda_{p_1}^{(1)},\ t_2,\lambda_1^{(2)},\lambda_2^{(2)},\cdots,\lambda_{p_2}^{(2)},\ t_n,\lambda_1^{(n)},\lambda_2^{(n)},\cdots,\lambda_{p_n}^{(n)},\ f) \tag{5.1}$$

$$\begin{aligned} & t_i,\lambda_j^{(i)} \in \mathbb{R} \qquad \forall\, i \in \{1,2,...,n\}\ \&\ \ j \in \{1,...,p_i\} \\ & \alpha \in [0,1] \\ \text{subject to: } & \sum_i t_i \leq L \end{aligned} \tag{5.2}$$

Here, α is the sound absorption coefficient to be maximised which depends on the target frequency f. Each multilayered configuration has its own absorption vs. frequency behaviour often referred to as the *absorption curve*. A constraint on the total length L is typically used to restrict the thickness of the total package from exceeding the available space. For each layer, the thicknesses and material properties are the design variables to be optimised.

To describe the behaviour of a given layer, a suitable acoustic material model needs to be adopted. Depending on the material model used, a number of properties are required to describe the layer. For instance, using the DB or DBM models, only one parameter i.e., the static airflow resistivity (σ), would be necessary to describe the layer. In other models such as JCA or JCAPL more material properties need to be determined. The sets of properties that are required for porous materials in various models are summarised in Table 5.1. Here, ϕ is the open porosity, α_∞ is the high frequency limit of tortuosity, b is the Attenborough's slit thickness parameter, Λ is the viscous characteristic length, Λ' is the thermal characteristic length, k_0' is the static thermal permeability, α_0 is the static viscous tortuosity and α_0' is the static thermal tortuosity.

Table 5.1: Material parameters required by each acoustic model.

Acoustic model	No. of properties	List of parameters
Delany-Bazley (DB) [70]	1	σ
Delany-Bazley-Miki (DBM) [70, 164]	1	σ
Zwikker & Kosten (ZK) [280]	2	σ, ϕ
Miki model [163]	3	$\sigma, \phi, \alpha_\infty$
Attenborough [13]	4	$\sigma, \phi, \alpha_\infty, b$
Johnson-Champoux-Allard-Lafarge (JCAL) model [134]	6	$\sigma, \phi, \alpha_\infty, \Lambda, \Lambda', k_0'$
Johnson-Champoux-Allard-Pride-Lafarge (JCAPL) model [134]	8	$\sigma, \phi, \alpha_\infty, \Lambda, \Lambda', k_0', \alpha_0, \alpha_0'$

Choosing the objective function: The optimisation objective needs to be determined based on the practical considerations. The two main objectives are to reduce the weight and reduce noise, and these are often conflicting. Lets consider the noise-reduction objective as F_1 and the weight/cost objective as F_2. There are several ways to quantify the noise-reduction objective depending on the case. The most common is to sum absorption over different frequencies $\sum_f \alpha_f$. Another strategy is to consider the source frequencies $q(f_i)$ and target the sound package to be more absorbing in those frequencies. The objective could then be the product of absorption and

noise source level over the frequency range of interest as expressed in equation 5.3.

$$\max \qquad F_1 = \frac{1}{N}\sum_{i=1}^{N} \alpha(f_i)q(f_i) \tag{5.3}$$

For an acoustic transmission problem, the noise objective would be as given in equation 5.4.

$$\min \qquad F_1 = \frac{1}{N}\sum_{i=1}^{N} TL(f_i)q(f_i) \tag{5.4}$$

Here TL is the transmission loss in dB. Another way to express the noise reduction objective would be to take into consideration, the noise perceived by humans. Different frequencies cause different levels of loudness to humans. For example, sound beyond 20,000 Hz (ultrasound) cannot be heard by humans, but bats use ultrasound to echolocate obstacles. Elephants use a low frequency of about 10 Hz to communicate over long distances. Humans perceive sounds around 1000 Hz better than other frequencies. Weighting factors such as the A-weighting defined in the international standard IEC 61672:2003 may be used to adjust the raw sound pressure levels as expressed in equation 5.5 . Other weighting factors include B, C, D and Zwikker's loudness (ISO 532B) may be used as the objective depending on the application.

$$\min \qquad F_1 = 10\log_{10}\left(\sum_{i=1}^{N} 10^{[L_p(f_i)+A(f_i)]/10}\right) \tag{5.5}$$

Here L_p is the sound pressure level in dB, and $A(f_i)$ is the A-weighting factor at frequency f_i.

In applications such as building acoustics where cost is more important than weight, one can consider minimising the overall cost of the sound package as expressed in equation 5.6.

$$\min \qquad F_2 = \sum_{i=1}^{\mathrm{N}} \rho_i b h t_i C_i \tag{5.6}$$

Here, ρ_i is the density of the material, t_i is the thickness, C_i is the cost per unit weight, b is the width and h is the height of the i^{th} layer of the multilayered package.

In an aircraft fuselage, sound packages are installed in the form of rectangular blocks as illustrated in Figure 5.2c. It is not necessary that all panels be of the same multilayered configuration. Based on the estimated noise field outside the aircraft, the noise intensity faced by each multilayered panel may be calculated under various scenarios, and each multilayered panel can be optimised for minimal weight, while also minimising the noise levels in the passenger cabin. Thus, the optimisation objective can be formulated suited to specific use cases.

5.3 Two-layered porous and screen

As discussed in the introduction, the most common porous package is a two-layered system consisting of a porous layer and screen. In this section, the fitness function landscapes of the two-layered system is explored for various material properties.

5.3.1 Problem description

Consider a two layered sound absorption system with a screen made of a woven or non-woven textile or a perforated plate for the first layer, and a thick fibrous material or foam for the second layer backed by a rigid impervious wall as shown in the Figure 5.4. This type of system is commonly used in noise absorption packages such as automotive headliners, room absorption panels, upholstery etc., (see Figure 5.2). In order to efficiently optimize the acoustic performance of this two-layered system, it is necessary to understand the objective function landscape before a suitable heuristic can be chosen.

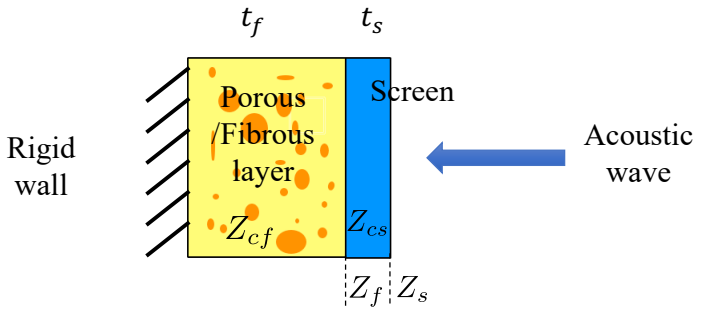

Figure 5.4: Two-layered sound absorption system with a fibrous material and a facing screen.

5.3.2 Modelling the fibrous/foam layer

To model the fibrous layer, a DBM model [164] is considered. The model describes a given porous material with the equations 5.7 and 5.8 for the characteristic impedance Z_{cf} and wave number k_{cf}, respectively.

$$Z_{cf} = \rho_0 c_0 \left[1 + 5.50\left(10^3 \frac{f}{\sigma_f}\right)^{-0.632} - j8.43\left(10^3 \frac{f}{\sigma_f}\right)^{-0.632}\right] \tag{5.7}$$

$$k_{cf} = \frac{2\pi f}{c_0}\left[1 + 7.81\left(10^3 \frac{f}{\sigma_f}\right)^{-0.618} - j11.41\left(10^3 \frac{f}{\sigma_f}\right)^{-0.618}\right] \tag{5.8}$$

In the above equations, f is the frequency in Hz, σ_f is the static airflow resistivity of the fibrous layer in N·s·m^{-4}, ρ_0 is the density of air in kg·m^{-3}, c_0 is the speed of sound in air in m·s^{-1} and $j = \sqrt{-1}$. The properties of air at T $= 20°$C are considered in all the following calculations. The surface impedance (Z_f) at the leading face of the fibrous layer is then found for the oblique incidence scenario using equation 5.9.

$$Z_f = \frac{-jZ_{cf}k_{cf}}{k_3 \tan(k_3 t_f)} \tag{5.9}$$

In the above equation, t_f is the thickness of the fibrous layer and k_3 is the oblique wave number calculated from $k_3 = \sqrt{k_{cf}^2 - \left(\frac{2\pi f \sin(\theta)}{c_0}\right)^2}$, where θ is the angle of oblique incidence.

5.3.3 Modelling the screen

We consider the procedure for modelling facing screens from [12, 108] as briefed below. Transfer matrix method with the JCA model [111, 43, 35] is used to describe the screen layer. In this case, equation 5.10 is used to compute the dynamic mass density of the screen ($\widetilde{\rho}_{cs}$) and equation 5.11 is used to compute its dynamic bulk modulus ($\widetilde{K}_{cs}$).

$$\widetilde{\rho}_{cs}(\omega) = \frac{\alpha_\infty \rho_0}{\phi_s}\left[1 - j\frac{\sigma_s \phi_s}{\omega \rho_0 \alpha_\infty}\sqrt{1 + j\frac{4\alpha_\infty^2 \eta \rho_0 \omega}{\sigma_s^2 \Lambda_s'^2 \phi^2}}\right] \tag{5.10}$$

$$\widetilde{K}_{cs}(\omega) = \frac{\gamma P_0/\phi_s}{\gamma - (\gamma-1)\left[1 - j\frac{8\eta}{\Lambda_s'^2 C_p \rho_0 \omega}\sqrt{1 + j\frac{\Lambda_s'^2 C_p \rho_0 \omega}{16\eta}}\right]^{-1}} \tag{5.11}$$

Here, γ is the adiabatic index for air, P_0 is the atmospheric pressure, η is the dynamic viscosity of air, ω is the angular frequency equal to $2\pi f$, C_p is the specific heat of air at constant pressure and ϕ_s is the porosity of the screen. We compute α_∞ from the equation 5.12.

$$\begin{aligned} &\alpha_\infty = 1 + 2\frac{\varepsilon}{t_s} \\ \text{where} \quad &\varepsilon = \left(1 - 1.13\xi - 0.09\xi^2 + 0.27\xi^3\right)\frac{8r}{3\pi} \\ &\xi = 2\sqrt{\frac{\phi_s}{\pi}} \end{aligned} \tag{5.12}$$

ε is the corrected length accounting for flow distortions near the screen perforations and $\Lambda_s' = r$. The value of r is computed from the relation $r = \sqrt{\frac{8\eta}{\sigma_s \phi_s}}$. Here, σ_s is the static air flow resistivity of the screen. Now, the equivalent characteristic impedance for the screen (Z_{cs}) and equivalent wave number (k_{cs}) may be computed from the relations $Z_{cs} = \sqrt{\tilde{\rho}_{cs}\widetilde{K}_{cs}}$ and $k_{cs} = \omega\sqrt{\frac{\tilde{\rho}_{cs}}{\widetilde{K}_{cs}}}$. For a combination of the two layers, the surface impedance Z_s can be computed from equation 5.13.

$$Z_s = Z_{cs}\frac{-jZ_f + Z_{cs}\tan(k_{cs}t_s)}{Z_f\tan(k_{cs}t_s) - jZ_{cs}} \tag{5.13}$$

Here, t_s is the thickness of the screen. To find the absorption, we use the formula for oblique incidence using the expression 5.14.

$$\alpha(\omega) = 1 - \left|\frac{Z_s(\omega) - \frac{\rho_0 c_0}{\sin(\theta)}}{Z_s(\omega) + \frac{\rho_0 c_0}{\sin(\theta)}}\right| \tag{5.14}$$

For this optimisation, the parameters considered are the thicknesses of the two layers, their static air flow resistivities, and their porosities. To assess the effect of the static air flow resistivities of the facing screen (σ_s) and the fibrous layer (σ_f), we keep all the other parameters fixed while tuning these two. The objective function to be maximized is the root mean square of the absorption coefficients at linearly-spaced frequency intervals between 20 Hz and 5000 Hz. The expression for α_{rms} is given by the equation 5.15.

$$\alpha_{rms} = \sqrt{\frac{1}{N}\sum_{i=1}^{N}[\alpha(f_i)]^2} \tag{5.15}$$

5.3.4 Results

Two parameter optimisation

A test study is considered where the objective function α_{rms} is maximised for different values of σ_s and σ_f while keeping the other parameters unchanged as stated in the equation 5.16.

$$\max_{\sigma_s,\sigma_f} \qquad \alpha_{rms} = \sqrt{\frac{1}{N}\sum_{i=1}^{N}[\alpha(f_i)]^2} \tag{5.16}$$

For this, the thickness of the fibrous layer is arbitrarily set to 20 mm, the thickness of the facing screen to 0.5 mm, and the porosity of the screen to 0.04 and 0.90 (in two separate cases). The absorption coefficients are computed for an oblique incidence of angle 34° (chosen arbitrarily for illustration purposes) and for frequencies from 20 Hz to 5000 Hz in linear steps of 20 Hz. The landscape of the objective function is found to be uni-modal or plateau-like in these two parameters as seen in the Figure 5.5. It is thus noted that a suitable local search heuristic [103] may be used for optimisation. The local search heuristics can be used solely or in conjunction with other metaheuristic methods as they exploit the neighbourhood of good solutions to improvements during optimisation.

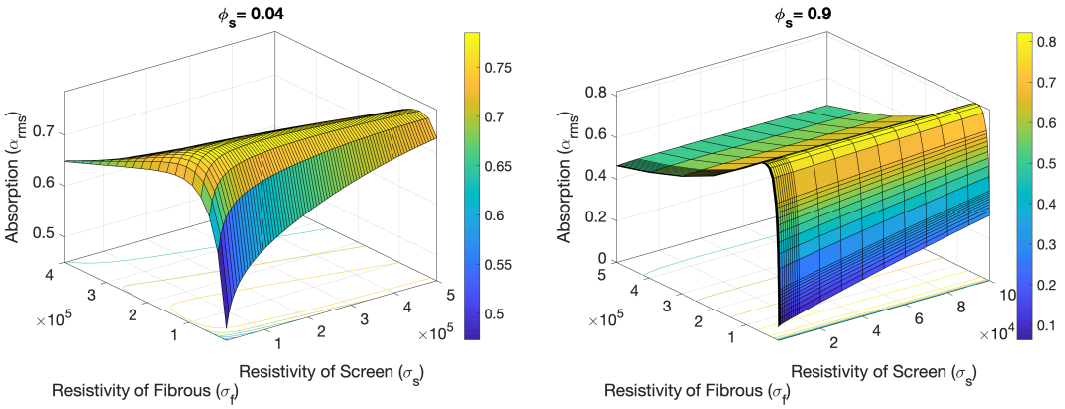

Figure 5.5: Absorption landscape for two-layered system: porous material and screen, over resistivities σ_s and σ_f for $\phi_s = 0.04$ (left) and $\phi_s = 0.90$ (right) for fixed parameters $t_f = 20$ mm, $t_s = 0.5$ mm, at an oblique incidence angle of 34°.

The best α_{rms} obtained using hill climbing for fixed parameters, ϕ_s = 90%, $t_f = 20$ mm, $t_s = 0.5$ mm, at an oblique incidence angle of 34° is 0.846 and it occurs at: σ_s = 19700 N·s·m^{-4} and σ_f = 49000 N·s·m^{-4}.

Three parameter optimisation

The optimisation is extended to include the porosity of the screen ϕ_s as given in equation 5.17. The objective function (α_{rms}) landscapes are plotted versus σ_f and σ_s similar to Figure 5.5 for various values of ϕ_s in Figure 5.6. It may be observed that the landscapes grossly increase up to a certain ϕ_s, and then decrease, indicating the presence of an optimum over this variable. This means that as the screen becomes more porous, the absorption increases, likely due to a better impedance match that fibrous layers provide. Another observation is that the smoothness and the presence of finite modes or plateau-like nature of the landscape is retained when tuning the parameter ϕ_s. For low resistivity values, a kink in the surface is seen which corresponds to sensitivities in the broadband absorption with respect to resistivities.

$$\max_{\sigma_s,\sigma_f,\phi_s} \qquad \alpha_{rms} = \sqrt{\frac{\Sigma_{i=1}^{N}[\alpha(f_i)]^2}{N}} \tag{5.17}$$

For the three parameter problem, the optimum of α_{rms} occurs at $\phi_s = 52\%$, $\sigma_s = 1\,\text{N·s·m}^{-4}$ and $\sigma_f = 71100\,\text{N·s·m}^{-4}$ (rounded to the nearest 100). The objective function value is $\alpha_{rms} = 0.862$ at the optimum. It is noted that $\sigma_s = 1\,\text{N·s·m}^{-4}$ was the lower bound for that parameter in the optimisation. This means that, for the studied configuration, not using a screen is better in terms of absorption, an expected result, as the purpose of the screen is only to protect the porous layer.

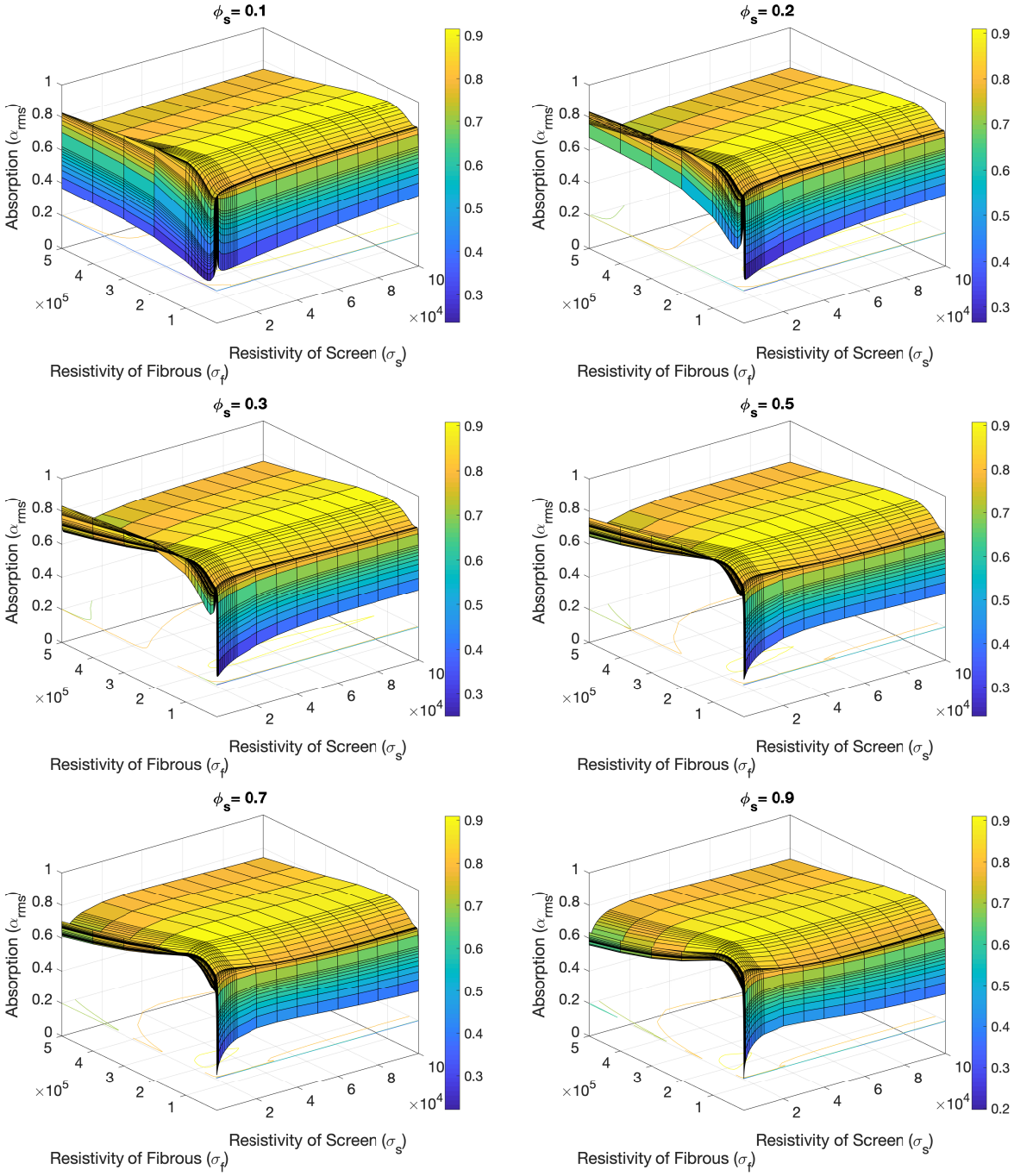

Figure 5.6: The evolution of absorption landscapes for two-layered system: porous material and screen for various ϕ_s values.

5.4 Three-layered porous absorption package

5.4.1 Problem description

In this section, optimising multilayered porous packages with three layers is considered as a case study. Consider the simplified optimisation problem of choosing the optimal material choices and thicknesses for a three-layered absorption package as shown in Figure 5.7. To ensure that non-physical material property combinations are avoided, we will choose the materials from a database of 29 commonly used porous materials with their accurately describing models and properties provided in Appendix A. While the material choices are discrete, the layer thicknesses are continuous values, making this a mixed problem.

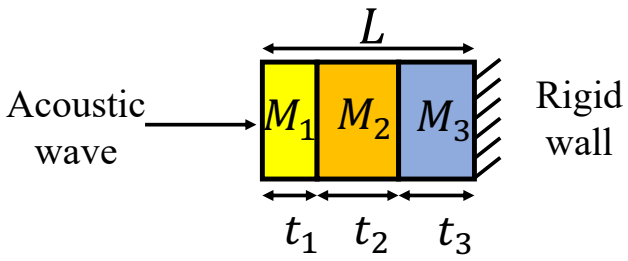

Figure 5.7: Three-layered sound absorption system.

Optimisation formulation: Consider the material-choice decision variables to be M_i, thickness design variables be t_i for each layer, and that the root-mean-square sound absorption α_{rms} of the combined system is to be maximised. We will assume a total thickness constraint of 60 mm, which is typical in practical scenarios. The optimisation problem formulation is expressed as follows:

$$\max_{M_1,M_2,M_3,t_1,t_2,t_3} \quad \alpha_{rms} = \sqrt{\frac{1}{N_f}\Sigma_{j=1}^{N_f}[\alpha(f_j)]^2} \tag{5.18}$$

$$\alpha(M_1, M_2, M_3, t_1, t_2, t_3, f_j) \tag{5.19}$$

$$M_i \in \{1, \cdots, 29\}$$

$$t_i \in \{0, \cdots, L\}$$

$$\text{subject to:} \quad \sum_i t_i = L \tag{5.20}$$

Here, L is the total thickness of the sound package, f_j are the target frequencies at which absorption is to be maximised and N_f is the number of target frequencies. The porous package is assumed to be placed in an impedance tube with a rigid backing and subject to diffuse field acoustic input in the range between 20 Hz and 5600 Hz with 100 linearly-spaced target frequencies.

Implementation: To compute the sound absorption, the AlphaCell software developed by Matelys Research Lab is used. AlphaCell is an implementation of a transfer matrix method (TMM) and finite-size transfer-matrix method (FTMM) solver for modelling multilayered systems that uses recent and advanced acoustic material models. The software has been validated

by Matelys with measurements from a wide range of porous materials and their multilayer combinations, and thus can be readily used for the optimisation studies. The optimisation algorithms are implemented in Matlab with command-line calls to AlphaCell to evaluate the fitness function.

5.4.2 Genetic algorithm

A steady-state genetic algorithm (GA) is applied on the above problem in an initial study. In a steady-state GA, the number of individuals in the population is kept the same over generations. The implementation of the genetic algorithm is detailed as follows.

Representation: For genetic algorithms, a representation scheme needs to be adopted that uniquely encodes any feasible solution to be regarded as the genome of the individual. Material choices for each layer are represented by an integer from 1 to 29 corresponding to the choice from the database. Although thicknesses are real valued and continuous, sub-millimetre differences in thickness neither corresponds to a significant difference in acoustic properties nor is it practical to ascertain in manufacturing the layer. Hence, thicknesses, like material choices, could also be represented using integers. An example of a genome for an individual would be a 6-integer array such as [10 6 15 20 20 20], where the first three integers represent the material choices M_1, M_2 and M_3 respectively, and the last three integers represent thicknesses t_1, t_2 and t_3 respectively in millimetre. Each combination of these 6 integers will be a different multilayered configuration. Note that since a total thickness constraint of 60 mm is considered, the last three integers should add up to 60.

Initialization: Initial population (group of multilayered configurations) is generated randomly using a pseudo random number generator. For each trial, a different random number seed is used, which is saved for reproducibility. For the material choices, a random number from 1 to 29 is chosen. In order to pick the thicknesses from the same distribution for each layer that add up to 60, first, two cutting point integers are randomly chosen from 0 to 60, and the three cut pieces become the thicknesses. For example, if the two cutting points are 15 and 47, the thicknesses are 15, 22 and 13 respectively. In this way, a number of individual solutions are generated that form the initial population. The population size is a parameter that can be tuned. After initiation, each individual corresponding to a multilayered configuration is evaluated to compute its fitness.

Selection: Once the population is generated, in each generation, parents need to be picked with a selection pressure. This step mimics *survival of the fittest* in Darwin's theory of evolution. To enforce a selection pressure for the evolution, two types of selection strategies are implemented. In *tournament* selection, a subset of individuals are randomly picked and the best individual of the subset is chosen as a parent individual. This mimics a typical knockout tournament. Tour size is the size of the subset and in this case, a tour size of 2 is chosen arbitrarily. In *roulette-wheel* selection, the individuals in the population are picked with a probability proportional to their fitness. The name arises due to the fact that it resembles selecting from a roulette wheel with each individual allocated a sector of size proportional to its fitness. In this implementation, two parent individuals ($\mathcal{P}_1$ and $\mathcal{P}_2$) are picked for the cross over operation.

Crossover: This step mimics the crossover of genes during reproduction. The two parent solutions are subject to gene mixing to produce two offspring solutions. A uniform crossover

is applied to the two chosen parents from the selection operation. In this implementation, a uniform crossover with a crossover rate of 0.5 is applied over the material choice parameters. Crossover is not applied over the thicknesses so as to preserve the total thickness constraint. The two new individuals so produced will be the offspring, which represent two new multilayered configurations with characteristics from both the parents.

Mutation: Mutation is performed on the offspring of crossover and a mutation probability of 1/(genome length) is used for each integer in the material choices. In order to maintain the total thickness constraint, the standard perturbation strategy is not suitable. Hence, a *thickness-conserving* mutation operator is implemented on the thickness part of the genome. This operator perturbs one of the layer thicknesses one way and the other layers in the opposite way. For example, to mutate the first element in the thickness part of a genome, say, [17 23 20], this operator will add or subtract [2 -1 -1] resulting in the perturbed thicknesses being either [19 22 19] or [15 24 21]. The direction of move i.e. to add or subtract is chosen with equal probabilities. Likewise, each thickness is mutated with the same mutation probability. If such a mutation results in negative thicknesses or thicknesses more that the constraint, the mutation operation is discarded. The mutated offspring ($\mathcal{C}_1$ and $\mathcal{C}_2$) will then be used to evaluate the objective function α_{rms} using the TMM solver.

Replacement and elitism: The two mutated offspring ($\mathcal{C}_1$ and $\mathcal{C}_2$) from a crossover operation and the two parents ($\mathcal{P}_1$ and $\mathcal{P}_2$) which produced them are pooled, and the best two of in terms of fitness ($\mathcal{B}_1$ and $\mathcal{B}_2$) are chosen to replace the members in the population. Two elitist schemes, namely, strong elitism and weak elitism are implemented. In *weak elitism*, the parent and the offspring solutions are pooled ($\mathcal{P}_1$, $\mathcal{P}_2$, $\mathcal{C}_1$, $\mathcal{C}_2$) and the best two of these will replace the two parents ($\mathcal{P}_1$ and $\mathcal{P}_2$). In *strong elitism*, the two offspring solutions are pooled with the two worst members of the population ($\mathcal{P}_1$, $\mathcal{P}_2$, $\mathcal{W}_1$ and $\mathcal{W}_2$), and the best two among these will replace $\mathcal{W}_1$ and $\mathcal{W}_2$.

5.4.3 Results

In order to study the effect of various GA parameters, multiple optimisation trials are run by varying one parameter at a time while keeping the others fixed. At first, a standard set of GA parameters are used to run five trials. Then, various parameters are modified and the trials are repeated. For the standard run, the parameters are as follows.

Table 5.2: Genetic algorithm standard parameters.

GA Parameter	Value
Population size	4
Selection type	*Tournament*
Crossover type	uniform
Crossover rate	0.5
Mutation type	*randomize* for material choices *perturb* for thicknesses
Mutation rate	1/6
Replacement	*weak elitism*

To study the effect of selection in GA, a tournament selection and a roulette-wheel selection are

run for the same fitness evaluation budget, keeping all other GA parameters fixed. The average fitness evolution across five trials is plotted in Figure 5.8. For the two selection operators, the differences seem to be within 0.1, which is within the accuracy of the material models used.

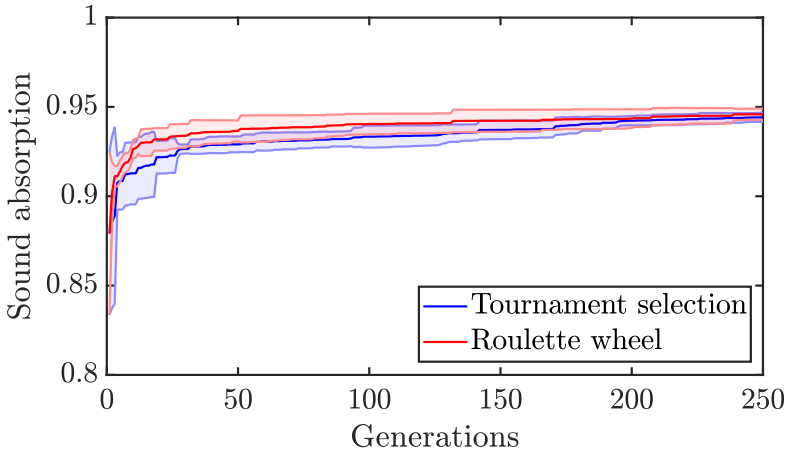

Figure 5.8: Comparison of average fitness progress between tournament selection and roulette-wheel selection.

For the population size, four different values are considered and five trials of GA are run at each population size. The results did not show significant differences as shown in Figure 5.9.

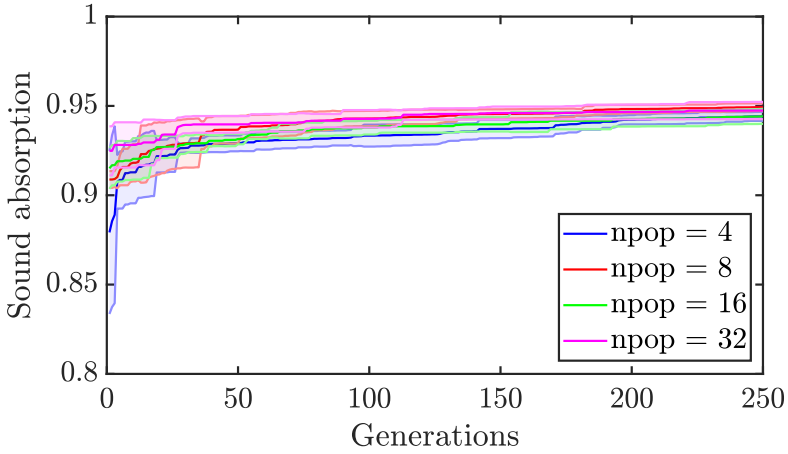

Figure 5.9: Effect of population size on average fitness evolution.

Between the replacement strategies discussed, weak elitism and strong elitism, weak elitism seems to be slightly better as can be observed from the trial-averaged fitness evolutions for five trials shown in Figure 5.10. However, the differences in absorption values are in the order of 0.1 only, which is not significant in terms of practical applications.

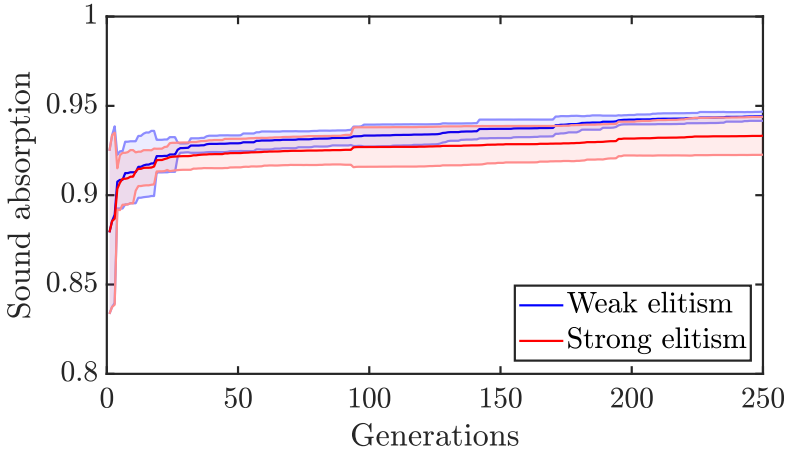

Figure 5.10: Comparison of average fitness progress between strong and weak elitism.

In conclusion, GA is able to quickly find sound packages with around 0.9 absorption within 50 generations. Any improvement after that seems to be less significant for this problem instance. The GA parameters assessed seem to have little effect on the performance.

5.4.4 Fitness landscape analysis

From the GA trials, it is observed that many of the best performing solutions have similar material picks. Figure 5.11 shows the frequency of occurrence of different materials in the initial population vs. in the best solutions across 30 trials. For this comparison, the results for the parameter tuning trials run from 6 sets of hyperparameters are used. The number of occurrences of each material chosen in the initial population is highlighted in blue bars while the number of occurrences in the final best solution are shown using red bars. For each set of hyperparameters, the GA was run using a random number seed picked from a series for each trial to ensure repeatability. Hence for the first trial in each of these hyperparameter sets, the occurences in the initial population are in the multiples of 6. Comparing between the occurences of different materials between the initial population and the final best solutions, it is observed that some materials tend to occur more often than others in the best solutions. For example, foamR1, glasswool8 and glasswool27. Notably, while foamR1 does not occur in any of the initial populations, it seems to be the most preferred constituent material in the best three-layered configurations. The reader is referred to Appendix A.11 for the material properties.

Brute force across all material combinations: Since, some materials occurred more frequently than others in the best solutions from GA, in a separate study, all possible three-layered configurations using 29 layers with each layer having a thickness of 20 mm was studied. The resulting absorption values are plotted in Figure 5.12. The material configuration index in the figure is assigned in the ascending order of permutations for choosing three layers from 29. It may be observed that even from a random guess it is possible to find configurations with absorption above 0.85. This could explain the good performance of GA irrespective of the parameters since it is easy to find a well performing material configuration. Out of all the three-layered combinations, a system with Rockwool, Glasswool and FoamR1 in that order from the rigid backing had the highest absorption.

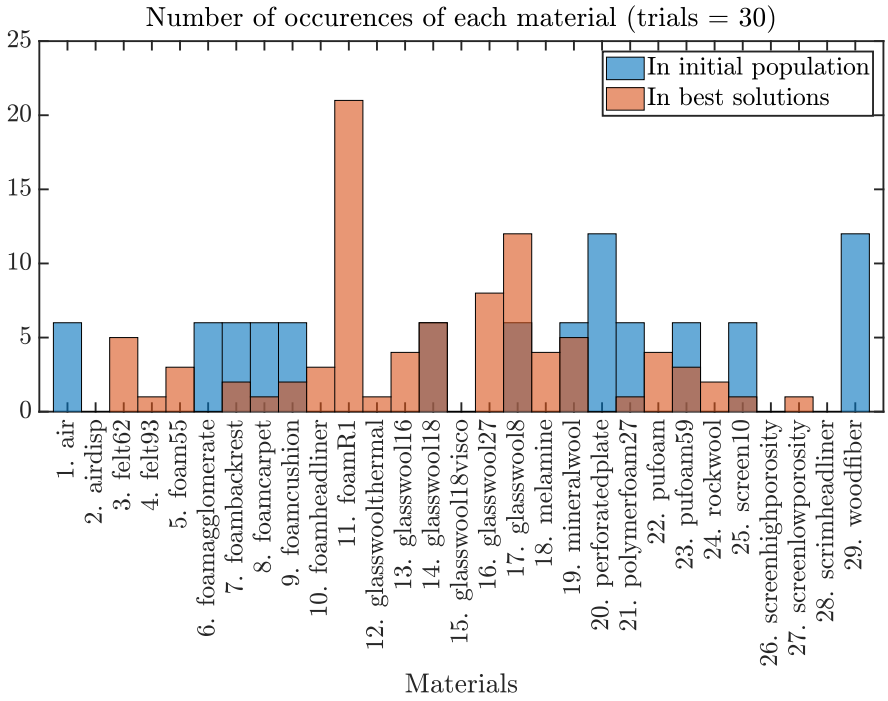

Figure 5.11: Frequency of occurences of materials in initial population and in best solutions across 30 trials. For the material properties, the reader is referred to Appendix A.

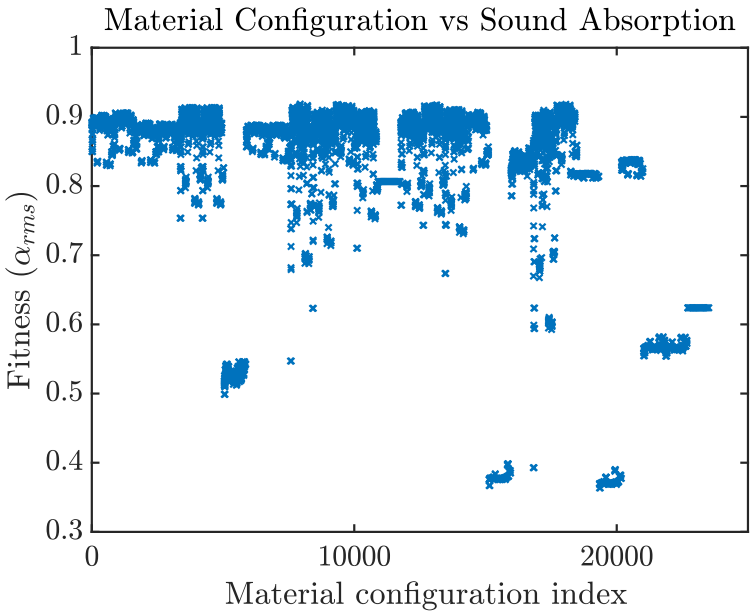

Figure 5.12: Fitness landscape over all possible material choice combinations of three-layered systems from 29 materials with each layer having a thickness of 20mm.

Thickness landscape of the best three-layered system: With the best three-layered material configuration having 20 mm thickness for each layer identified, the landscape of absorption over the thickness space of this three-layered system is computed and shown in Figure 5.13. With a constraint on the total thickness, the first two thicknesses t_1 and t_2 are varied and the other thickness is computed as $t_3 = 60 - t_1 - t_2$. In this thickness space, the sound absorption is observed to be smooth and unimodal. The smoothness of the fitness landscape for thicknesses is expected, since the material models involve analytical expressions. Such fitness landscapes can be effectively exploited by using suitable algorithms such as hill climbing, covariance matrix adaptation evolution strategy or a stochastic local search heuristic.

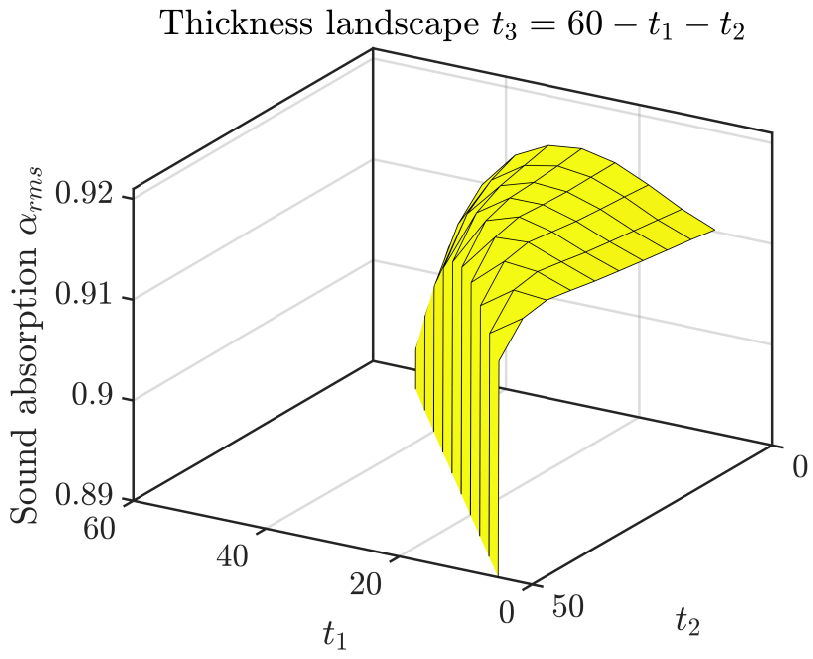

Figure 5.13: Fitness landscape across layer thicknesses.

For a total thickness constraint of 60 mm, the best thickness combination is reported in Table 5.3. In the table, the layering order is from the material next to the rigid wall to the material facing the acoustic wave. It may be noted that FoamR1 features as the first material facing the acoustic wave. Also, notice that the static airflow resistivity of the layers facing the sound source gradually increase from 7000 N·s·m^{-4} for FoamR1 to 20,000 N·s·m^{-4} for Glasswool to 120,000 N·s·m^{-4} for Rockwool, thus facilitating a gradual change in impedance. A gradual impedance change produces less reflections, allowing more sound to pass through and get absorbed in the subsequent layers.

Table 5.3: The best configuration found for a total thickness constraint of 60 mm, with $\alpha_{rms} = 0.919$.

Material	Model	t (mm)	ϕ	σ (N·s·m^{-4})	Λ (μm)	Λ' (μm)	α_∞	k_0' (10^{-10} m^2)	α_0	α_0'
Rockwool	JCAL	19	0.95	120000	12	20	1.08	10	-	-
Glasswool	JCA	23	0.99	20000	26	135	1.11	-	-	-
FoamR1	JCAPL	18	0.9	7000	129	440	1.12	83	1.22	1.13

5.4.5 Guidelines for algorithm selection

From the above results, it can be concluded that the multilayered sound package problem is easy to tackle with numerous good quality solutions. Since the thickness and property landscapes are known to be smooth with finite modes, a random search on the material choices followed by a local search or pseudo-gradient algorithms across the material properties may be sufficient. For problems with larger number of layers, memetic algorithms seems to be a natural choice to explore further. Memetic algorithms are extensions to genetic algorithms which embed local search. Due to their robustness, memetic algorithms have been successfully used in many applications [170] including university time tabling [40], nurse rostering [179], flow-shop scheduling [151] etc. A memetic algorithm with GA for the material configuration will retain the combinations that tend to have high absorption providing pathway to a near-optimal solution, and the local search will quickly find the optimum in the thickness and material property space.

While the multilayered problem discussed in this chapter has numerous practical use cases, the landscapes of the fitness function are smooth making it easy to optimise. The computation of the fitness function is also not expensive and hence the problem is not very difficult to solve to optimality. Only when the number of layers increase, the material choices being combinatorial pose difficulties in finding the global optima. Since there is a practical limit on the number of layers that can be physically bundled in a sound package, by limiting the number of layers, finding the global optimum would not be very difficult. In practise, the material choices are also limited, further simplifying the problem. Once the available material choices are established, the material property design variables can be optimised using a suitable algorithm such as hill climbing with restarts, CMA-ES, differential evolution, particle swarm etc., These algorithms can operate as local exploiters in a memetic algorithm. The choice of materials is a discrete variable and optimising across this choice is a bit challenging. Although, by sorting the material database, based on key acoustic material properties such as porosity, static airflow resistivity or tortuosity, one can create an artificial correlation between the material choice variable and the nature of the material to be chosen. With such encoding schemes, applying algorithms such as genetic algorithms on the material choices might prove to be an effective search strategy.

5.5 Conclusions

In this chapter, the optimisation of one-dimensional multilayered sound absorption packages was studied. Multilayered sound packages containing several layers of acoustic porous materials are the prevalent form of sound treatment in the industry. We noted that acoustic material models such as DBM, JCA, used along with a geometric modelling method such as the transfer matrix method allows a quick computation of sound absorption. A two-layered system was considered to study the landscapes of acoustic design variables, static airflow resistivity and porosity. Using a steady-state genetic algorithm (GA), a three-layered system with a total thickness constraint was considered and the material choices from 29 available materials were optimised for maximising sound absorption under diffused field excitation. Various parameters of GA were explored. Then, a brute force search over all possible material configurations was performed. From the best material configuration, the fitness landscape over the thickness variables were studied. From the insights obtained some guidelines for algorithm selection were provided. The key findings are highlighted as follows.

1. Upon studying a simple two-layered system, the fitness function across the acoustic design variables—static airflow resistivity and porosity—seemed to be smooth, often form-

ing unimodal or landscapes or few modes with plateaus and valleys indicating the relative ease of optimising using a suitable continuous optimisation approach.
2. Genetic algorithms applied on a three-layered problem over material choices and thicknesses were able to quickly find close to 0.9 sound absorption in under 50 generations. Any improvements beyond 0.9 seemed to be insignificant and hard to obtain.
3. It was observed that specific materials such as FoamR1 and Glasswool occurred more frequently as constituent layers in the best three-layered solutions from GA.
4. The choice of GA parameters seemed to have little effect on the performance.
5. Brute force search over the available material choice configuration for equal thickness layers seemed to suggest that numerous combinations exhibited absorption above 0.85, indicating the ease of finding good quality solutions.
6. The best three-layered configuration consisted of FoamR1, Glasswool, and Rockwool in that order facing the acoustic source with gradually increasing static airflow resistivities. Such gradual change in resistivities is known to facilitate impedance matching that allows more sound to pass through and get absorbed.
7. For the above material configuration, the fitness landscapes over the thickness was smooth and unimodal indicating that a local search could be used for exploitation to quickly reach an optimum.
8. From the insights obtained from the landscapes, it seems that a memetic algorithm, with genetic algorithm over the material configuration and a local search across the acoustic design variables, may be a natural choice to explore as the number of layers increase.

Chapter 6

Single-objective topology optimisation for absorption maximisation

When designing sound packages in the form of composite walls with porous infill, often fully filling the available space with acoustic materials is not the most absorbing solution. Better solutions can be obtained by creating cavities of air pockets. Determining the most optimal shape and topology that maximises sound absorption is a challenging task. This chapter deals with the shape optimisation of acoustic porous materials focussing on maximising sound absorption without considering the weight-reduction objective. As established in chapter 4, many recent topology optimisation applications in acoustics use heuristic methods such as solid-isotropic-material-with-penalisation (SIMP) to quickly find near-optimal solutions. In this chapter, the application of seven heuristic and metaheuristic optimisation approaches including SIMP will be studied. The approaches tested are hill climbing, constructive heuristics, SIMP, genetic algorithm, tabu search, covariance-matrix-adaptation evolution strategy (CMA-ES), and differential evolution. All the algorithms are tested on seven benchmark problems varying in material properties, target frequencies, and dimensions. The empirical results show that hill climbing, constructive heuristics, and a discrete variant of CMA-ES outperform the other algorithms in terms of the average quality of solutions over the different problem instances. Though gradient-based SIMP algorithms converge to local optima in some problem instances, they are computationally more efficient. One of the general lessons is that different strategies explore different regions of the search space producing unique sets of solutions. Parts of this work are published in the Journal of Acoustical Society of America [202].

6.1 Introduction

Historically, shape designs in engineering have been arrived at via trial-and-error, intuition, incremental improvements to old designs, human decision-making from numerical analyses, and recently, solely by computer analyses. Superior-to-human engineering designs have been achieved by computers using technologies such as structural topology optimisation. Topology optimisation involves finding the optimal topology (number of holes) and shape (size, dimensions) for a structure such that a given performance indicator is either maximised or minimised. Bendsøe and Kikuchi [20] introduced the concept of simultaneously optimising both shape and topology in the late 1980s. Since then, many theoretical developments have been made, and a community of researchers have actively been working in this field. One of the ways to formulate a topology optimisation problem is finding the optimal assignment of materials in each finite element of a discretised structure. In principle, this formulation is discrete optimisation, and

finding the exact global optimum is challenging. Exact optimisation techniques that guarantee to find the global optimum remain prohibitively expensive. Evaluating all possible solutions becomes impractical due to the large search space sizes and the expensive finite element evaluations. A noteworthy effort towards topology optimisation using an exact approach was by Stolpe and Bendsøe [231] on the Zhou and Rozvany problem instance [273]. But justifiably, the focus of previous work has mainly been on the inexact or *heuristic* optimisation approaches.

6.1.1 Heuristics

Heuristics are techniques that find solutions close-enough to the global optimum in reasonable time. Though heuristics do not guarantee to find the optimal solution, they are well-established and often the only viable option to address hard problems, such as those in NP-complete and NP-hard classes. The three most popular heuristic approaches applied to topology optimisation problems are SIMP [20, 19, 272, 217] (solid-isotropic-material-with-penalisation), BESO [256, 257, 262] (bi-directional evolutionary structural optimisation), and the level-set method [251, 6, 38]. These approaches have been described in more detail in chapter 4, and they are briefly recalled here for completeness. Among these, SIMP is the most commonly used and well-studied approach. In this approach, the discrete problem is relaxed to the continuous space by allowing intermediate materials between solid and void. A penalty-based material interpolation scheme is used to represent intermediate materials and gradient-based optimisation strategies such as optimality criteria [21] or method of moving asymptotes [238] is used to move across the design variable space to find a near-optimal design. As SIMP is a derivative-based technique, it requires that a sensitivity analysis be carried out. BESO, not to be confused with evolutionary algorithms despite its name, is a type of constructive approach which iteratively adds material where stresses are high and removes material where stresses are low to arrive at a design. In the level-set method, a scalar field is associated with the design domain region and the iso-surfaces of this scalar field are made the boundaries of the topology. This scalar field is then optimised to optimise the topology.

6.1.2 Metaheuristics

While heuristics are quick strategies to find near-optimal solutions, it was realised by Glover [89] that many powerful heuristic approaches follow certain higher-level guidelines. These guidelines can be considered heuristics to design heuristic algorithms, and hence are termed as *meta*heuristics. A popular example of a metaheuristic is genetic algorithms, wherein the guideline is to initiate a population of solutions, apply selection pressure to pick good individuals, recombine the selected individuals, mutate them and replace them into the population. Numerous metaheuristic techniques, such as genetic algorithms and CMA-ES, have also been studied on structural topology optimisation problems [94]. However, such blackbox metaheuristics are not the most common in usage since gradient methods that make the search quick are available. Theoretical developments in structural topology optimisation have focused on the classical problem of compliance minimisation [23, 221]. Nevertheless, the application of topology optimisation techniques to other problem domains is steadily on the rise [207, 23, 68]. These techniques have already been extended to acoustics, giving rise to a sub-field called acoustic topology optimisation.

6.1.3 Acoustic topology optimisation

Previously, topology optimisation has been performed on a variety of acoustic applications, including horns, mufflers, rooms and sound barriers [249, 76, 140, 143, 131, 266, 138, 122, 263, 46, 128, 268, 259, 47, 260]. A majority of these applications use the gradient-based SIMP method or its variants, while a small fraction of them use BESO or level-set methods. These applications can be categorised into acoustic fluid-structure interaction problems and porous material problems. In acoustic fluid-structure interaction problems, the material choices are non-porous solid and fluid phases, and the wave propagation is modelled using mixed formulations [220, 267]. Within acoustic fluid-structure interaction, problems other than topology optimisation such as material parameter estimation [92] have also found application of gradient-based methods such as the method of moving asymptotes [239]. In porous material topology optimisation problems, the material choices also include poroelastic materials, and specialised Biot formulations [11, 17] are generally used. In some applications [46, 106], the boundary element method is used to optimise the boundary topology instead of the bulk topology. In this report, poroelastic material topology optimisation is in focus. Specifically, topology optimisation is referred to in the context of finding optimal mesoscale shapes and topologies, i.e., in the order of magnitude of the material thickness, and not the optimisation of their microstructures, which is a different research area.
Although metaheuristics have been previously tested on classical structural topology optimisation problems [94, 205], their use has been limited in acoustic topology optimisation applications [201]. Only a few optimisation approaches have been tested, and optimisation theory exclusive to this problem domain remains yet to be well explored. The present work is a step in this direction.

6.1.4 Contributions in this chapter

The goal of the present chapter is to investigate the performance of alternative heuristic optimisation approaches, including a few well-known metaheuristic approaches on a set of benchmark problems. The purpose is to arrive at guidelines for designing better approaches for the absorption maximisation problem. The approaches compared are hill climbing, constructive heuristics, SIMP, genetic algorithms, tabu search, CMA-ES and differential evolution. While SIMP and its variants use gradients, none of the other approaches use any domain-specific information from the problem other than the objective function. Optimisation tests show how different approaches perform for various CPU time budgets. Notably, while SIMP algorithms produce good-quality solutions at low CPU time budgets, certain other algorithms such as hill climbing, constructive heuristics and CMA-ES outperform at higher computational budgets. The findings reported in this chapter may serve as a useful prelude to develop better strategies for topology optimisation in acoustic porous materials.

6.1.5 Organisation of this chapter

The chapter is organised as follows: An acoustic topology optimisation problem for maximising sound absorption is described in detail in section 6.2. This section also includes insights about the problem structure, including the modelling methodology, fitness landscapes and computational complexity. Concise descriptions and settings of the optimisation approaches are given in section 6.3. In section 6.4, a set of five heuristic algorithms that include hill climbing, two variants of constructive heuristic and two variants of SIMP are described. In section 6.5, a set of six metaheuristic-based algorithms that include a genetic algorithm, a tabu search, two

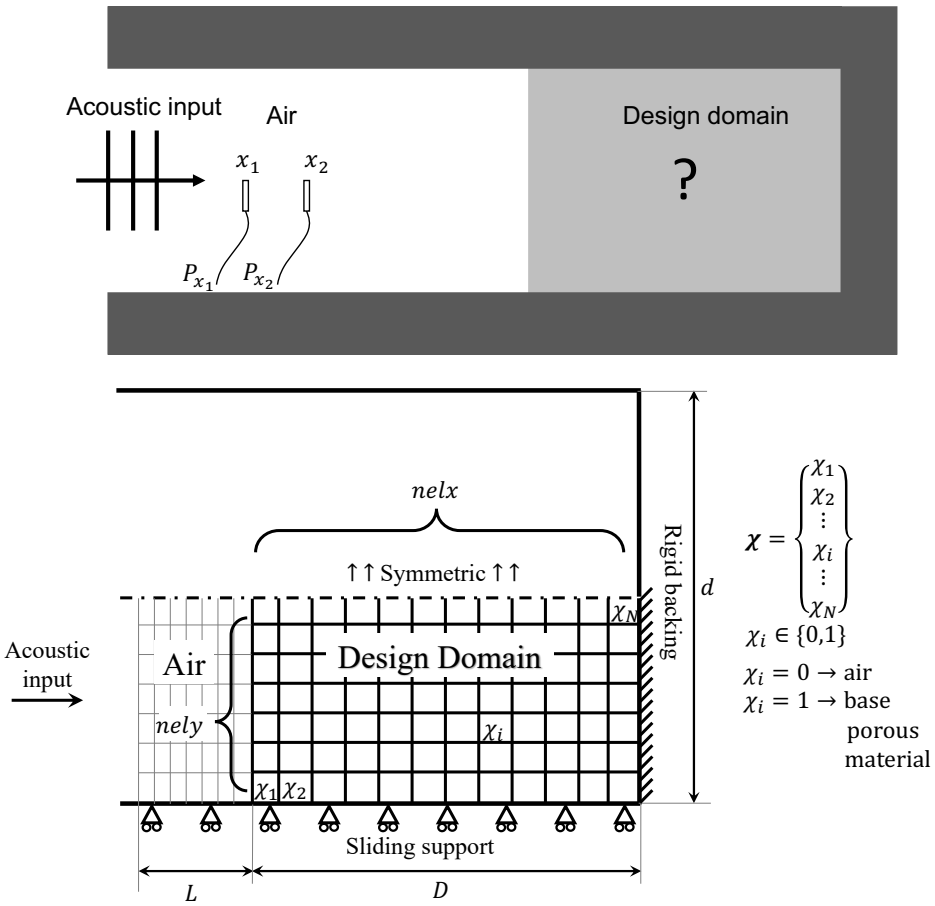

Figure 6.1: Optimisation problem formulation—the finite element model of a unit cell of a porous absorbing wall used to generate benchmark problems (see Section 6.2.7 in page 89).

variants of CMA-ES and two variants of differential evolution are described. The results from the optimisation tests and comparisons are provided in section 6.6 that includes statistical tests and landscape studies. A summary of the findings and some conclusive remarks are provided in section 6.7.

6.2 Problem description

6.2.1 Optimisation formulation

The objective in a quintessential topology optimisation problem in porous-material acoustics is the maximisation of the sound absorption coefficient. Given an acoustic system discretised into finite elements such as an impedance tube system shown in Figure 6.1, consider the problem of finding the best assignment of either air or a given porous material for each element in a design domain to maximise the sound absorption in the material. The optimisation formulation for this can be written as:

$$\begin{aligned} \max_{\chi_i} \quad & \overline{\alpha}(\boldsymbol{\chi}) = \frac{1}{n}\sum_{f=f_1}^{f_n} \alpha(\boldsymbol{\chi}, f) \\ & \boldsymbol{\chi} : \chi_i \in \{0,1\} \quad \forall \quad i = 1, 2, \ldots, N \\ & \overline{\alpha} \in [0,1] \end{aligned} \tag{6.1}$$

Here, $\alpha(\boldsymbol{\chi}, f)$ is the sound absorption coefficient in normal incidence for a given shape $\boldsymbol{\chi}$ for frequency f, χ_i are the decision variables representing the choice between air and porous material for the i^{th} element, N is the number of elements in the design domain, and $f_1, f_2, ..., f_n$ are the target frequencies for which the mean absorption is to be maximised (where n is the number of frequencies considered). The symbol $\overline{\alpha}$ is used to refer to the mean of sound absorption coefficient (α) across the target frequencies. In this report, $\overline{\alpha}$ may be referred to as simply *absorption* or *fitness*, which is to be maximised.
Note that in problem 6.1, a volume fraction constraint is not included, which is unlike in usual topology optimisation problems. One reason is because in porous material topology optimisation, often the optimal shapes need to be carved out from a large block of the base porous material. The removed material may not often constitute material-saving, as the cost of recycling the carved out material could negate the material-saving benefit. Another reason for not including a volume fraction constraint is that more optimisation approaches can be tested as the formulation would resemble a conventional discrete optimisation problem. Without the volume constraint, the search space size becomes 2^N since two choices are available (air or the base porous material) for each of the N elements in the design domain. If a limit V_f is imposed on the ratio of porous volume to the total volume in the design domain ($\frac{1}{N}\sum_{i=1}^{N}\chi_i = V_f$), the search space size would become ${}^{N}C_{(V_f N)}$. In both these cases, the number of feasible solutions grows quickly with increase in N. Since discrete optimisation problems are considered difficult to solve, the problem is usually relaxed to a continuous problem allowing χ_i to take values between 0 and 1, in other words allowing intermediate materials between air and porous material in the design domain. The problem is then solved using continuous optimisation approaches. Intermediate materials given by $\chi_i \in (0,1)$ are modelled using interpolation schemes. One such interpolation scheme is the SIMP scheme (not to be confused with the SIMP approach). Using this scheme, a material property, say, ψ for the intermediate material is given by equation 6.2.

$$\begin{aligned} \psi_i &= \psi_{air} + \chi_i^p[\psi_{por} - \psi_{air}] \\ \psi &\in \{E, \nu, \widetilde{\rho}, \widetilde{\gamma}_s, \widetilde{\rho}_{eq}, \widetilde{K}_{eq}\} \end{aligned} \tag{6.2}$$

Here, ψ could be any property from Young's modulus (E), Poisson's ratio (ν), modified Biot density ($\widetilde{\rho}$), coupling factor ($\widetilde{\gamma}_s$), dynamic mass density ($\widetilde{\rho}_{eq}$), dynamic bulk modulus ($\widetilde{K}_{eq}$) etc. The value ψ_{air} is the value of the material property for air, ψ_{por} is the value for the porous material considered, and ψ_i is the interpolated material property assigned to i^{th} element through the design variable χ_i. It satisfies that $\chi_i = 0 \Rightarrow \psi = \psi_{air}$ and $\chi_i = 1 \Rightarrow \psi = \psi_{por}$.

$$E_i = E_{air} + \chi_i^p (E_{por} - E_{Air}) \tag{6.3}$$
$$\nu_i = \nu_{air} + \chi_i^p (\nu_{por} - \nu_{Air}) \tag{6.4}$$
$$\widetilde{\rho}_i = (\widetilde{\rho})_{por} + \chi_i^p [(\widetilde{\rho})_{por} - (\widetilde{\rho})_{air}] \tag{6.5}$$
$$\widetilde{\gamma}_{(s)i} = (\widetilde{\gamma}_s)_{air} + \chi_i^p [(\widetilde{\gamma}_s)_{por} - (\widetilde{\gamma}_s)_{air}] \tag{6.6}$$
$$\widetilde{K}_{(eq)i} = (\widetilde{K}_{eq})_{air} + \chi_i^p [(\widetilde{K}_{eq})_{por} - (\widetilde{K}_{eq})_{air}] \tag{6.7}$$
$$\widetilde{\rho}_{(eq)i} = (\widetilde{\rho}_{eq})_{air} + \chi_i^p [(\widetilde{\rho}_{eq})_{por} - (\widetilde{\rho}_{eq})_{air}] \tag{6.8}$$

Since filters in topology optimisation themselves play a role in the optimisation performance, no filters or manufacturability restrictions are considered in this study with the view that these can be done in post-processing. However, for a fair comparison between discrete and continuous approaches, a simple round-off filter is applied to the solutions from continuous approaches. This ensures that only solutions from the same search space, i.e. discrete, are compared.

6.2.2 Computing the fitness function: sound absorption

To compute sound absorption, the poroelastic system constituting the fixed and design domains is modelled using the Biot assumptions of poroelastic material [27]. For modelling the two-dimensional system, an alternative Biot finite element formulation described by Bécot and Jaouen [17] is used. This formulation is based on the mixed $\{\mathbf{u}, \tilde{\mathbf{p}}\}$ formulations by Göransson [91] and Atalla *et al.* [11]. To naturally account for the interface between porous and air regions, the unified analysis approach proposed and verified by Lee *et al.* [140] is adopted. For intermediate material properties between air and porous material, the SIMP interpolation scheme [22] is used. The poroelastic system governing equations can be expressed in matrix form as in equation 6.9.

$$\underbrace{\begin{bmatrix} \tilde{\mathbf{K}} - \omega^2 \tilde{\mathbf{M}} & -\tilde{\mathbf{C}} \\ -\tilde{\mathbf{C}}^T & \tilde{\mathbf{H}}/\omega^2 - \tilde{\mathbf{Q}} \end{bmatrix}}_{\tilde{\mathbf{S}}(\omega)} \underbrace{\begin{Bmatrix} \{\tilde{\mathbf{u}}\} \\ \{\tilde{\mathbf{p}}\} \end{Bmatrix}}_{\tilde{\mathbf{X}}(\omega)} = \underbrace{\begin{Bmatrix} \tilde{\mathbf{f}}_{\mathrm{u}} \\ \tilde{\mathbf{f}}_{\mathrm{P}}/\omega^2 \end{Bmatrix}}_{\tilde{\mathbf{f}}} \tag{6.9}$$

Here, $\tilde{(\cdot)}$ denotes the complex-valued nature of its argument. The expressions for the state matrices $\tilde{\mathbf{K}}$, $\tilde{\mathbf{M}}$, $\tilde{\mathbf{H}}$, $\tilde{\mathbf{Q}}$ and $\tilde{\mathbf{C}}$ are functions of the topological design/decision variables $\boldsymbol{\chi}$. The construction of these matrices are followed from Atalla *et al.* [11]. The vectors $\{\tilde{\mathbf{u}}\}$ and $\{\tilde{\mathbf{p}}\}$ denote the solid phase displacement and fluid phase pressure degrees of freedom in the poroelastic system, respectively. The associated global stiffness matrix $\tilde{\mathbf{S}}(\omega)$ and the acoustic load vector $\tilde{\mathbf{f}}$ are iteratively assembled over each angular frequency $\omega = 2\pi f$ to yield a system of linear equations. These equations are solved as given in equation 6.10 to obtain the solution vector $\tilde{\mathbf{X}}(\boldsymbol{\chi}, \omega)$, which will contain the displacement and pressure fields of the solid and fluid parts of the poroelastic material, respectively.

$$\{\tilde{\mathbf{X}}(\boldsymbol{\chi}, \omega)\} = [\tilde{\mathbf{S}}(\boldsymbol{\chi}, \omega)]^{-1} \{\tilde{\mathbf{f}}\} \tag{6.10}$$

The system matrix is given by,

$$\tilde{\mathbf{S}} = \begin{bmatrix} \tilde{\mathbf{K}} - \omega^2 \tilde{\mathbf{M}} & -\tilde{\mathbf{C}} \\ -\tilde{\mathbf{C}}^T & \tilde{\mathbf{H}}/\omega^2 - \tilde{\mathbf{Q}} \end{bmatrix} \tag{6.11}$$

From Atalla *et al.* [11], the element stiffness matrix equations are given by:

$$\tilde{\mathbf{K}}_{ei} = \int [B]^T [D]_i [B] dV \tag{6.12}$$

Here, $[D]_i$ depends on the Young's modulus E_i and Poisson's ratio ν_i of the material used in the element i. Whereas, $[B]$ is the solid part strain-displacement matrix that depends only on the shape function and does not depend on χ_i. Likewise, the other element matrices can be expressed from Biot equations using weak formulations as follows.

$$\tilde{\mathbf{M}}_{ei} = \widetilde{\rho}_i \int_{\Omega_e} [N]^T [N] dV \tag{6.13}$$

$$\tilde{\mathbf{C}}_{ei} = \widetilde{\gamma}_{(s)i} \int_{\Omega_e} N^T \nabla N_p dV \tag{6.14}$$

$$\tilde{\mathbf{H}}_{ei} = \frac{1}{\widetilde{\rho}_{(eq)i}} \int_{\Omega_e} \nabla [N]_p^T \nabla [N]_p dV \tag{6.15}$$

$$\tilde{\mathbf{Q}}_{ei} = \frac{1}{\widetilde{K}_{(eq)i}} \int_{\Omega_e} [N]_p^T [N]_p dV \tag{6.16}$$

The properties of the material $\{E_i, \nu_i, \widetilde{\rho}_i, \widetilde{\gamma}_{(s)i}, \widetilde{\rho}_{(eq)i}, \widetilde{K}_{(eq)i}\}$ assigned to element i depend on the design variable χ_i through equations 6.3 to 6.8. The corresponding properties of the porous material may be obtained using a suitable acoustic model, for example, the Johnson-Champoux-Allard-Lafarge or JCAL model [111, 43, 134]. These element matrices are then assembled into the corresponding degrees of freedom in the global matrices $\tilde{\mathbf{K}}$, $\tilde{\mathbf{M}}$, $\tilde{\mathbf{C}}$, $\tilde{\mathbf{H}}$, and $\tilde{\mathbf{Q}}$. Once these global matrices are computed, the system matrix $\tilde{\mathbf{S}}$ can be constructed and equation 6.10 can be solved to obtain the pressures and displacements at all nodal points in the impedance tube system.

Once the pressures and displacement fields are known, computing absorption may be done in several ways. Two of the procedures that one can follow are provided below:

1. Two microphone method
2. Surface impedance method

Two-microphone method

Two-microphone method is a simple and commonly used procedure to compute absorption which needs the pressure field values at only two points in the acoustic system [54]. It is widely used in experimental measurements since only two devices are needed. The method assumes plane waves in the air region in front of the design domain. Considering two closely spaced points x_1 and x_2 in the air region (as shown in Figure 6.1 in page 75), the complex pressure amplitudes in frequency domain $\tilde{P}_{x_1}$ and $\tilde{P}_{x_2}$ can be obtained from $\{\tilde{\mathbf{p}}\}$ in $\tilde{\mathbf{X}}$. The plane wave reflection coefficient $\tilde{R}_c$ can then be computed from these pressures as,

$$\tilde{R}_c(\boldsymbol{\chi}, \omega) = \frac{\tilde{P}_{x_1}(\boldsymbol{\chi}, \omega) e^{(-ikx_2)} - \tilde{P}_{x_2}(\boldsymbol{\chi}, \omega) e^{(-ikx_1)}}{-\tilde{P}_{x_1}(\boldsymbol{\chi}, \omega) e^{(ikx_2)} + \tilde{P}_{x_2}(\boldsymbol{\chi}, \omega) e^{(ikx_1)}} \tag{6.17}$$

Here, k is the wave number given by ω/c_{air} with c_{air} being the speed of sound in air. The sound absorption coefficient α is then given by:

$$\alpha(\boldsymbol{\chi}, \omega) = 1 - |\tilde{R}_c(\boldsymbol{\chi}, \omega)|^2 \tag{6.18}$$

Thus, the sound absorption can be computed for a given shape $\boldsymbol{\chi}$ at a given frequency f.

Surface impedance method

Alternatively, one can use the surface impedance at a certain cross section in the air layer to compute the average impedance at the source layer [7]. The surface impedance can computed at an incident surface Γ_I in the air layer away from the porous medium as:

$$\tilde{Z}_{sn}(\omega) = -\frac{\mathrm{P}|_{\Gamma_I}}{\mathrm{V}_n|_{\Gamma_I}}, \tag{6.19}$$

where $\mathrm{P}|_{\Gamma_i}$ and $\mathrm{V}_n|_{\Gamma_i}$ are the mean fluid pressures and normal velocities at the incident surface Γ_I, respectively. The mean normal fluid velocity is computed as:

$$\mathrm{V}_n|_{\Gamma_I} = j\omega \mathrm{U}_n|_{\Gamma_I}, \tag{6.20}$$

Here, $\mathrm{U}_n|_{\Gamma_I}$ the mean of normal fluid displacements at Γ_I is evaluated as:

$$\mathrm{U}_n|_{\Gamma_I} = \frac{\sum \mathbf{F}_g|_{\Gamma_I}}{H|_{\Gamma_I}} \tag{6.21}$$

Here, H is the chamber height and the intermediate quantity $\mathbf{F}_g$ is computed from the unconstrained system matrix using the following expression.

$$\mathbf{F}_g = \underbrace{\tilde{\mathbf{S}}(\omega)}_{\text{unconstrained}} \cdot \tilde{\mathbf{X}}(\omega)/\omega^2 \tag{6.22}$$

Then, from $\tilde{Z}_{sn}(\omega)$, the sound absorption coefficient $\alpha(\omega)$ is computed as follows:

$$\alpha(\omega) = 1 - |\tilde{R}_c|^2 = 1 - \left| \frac{\tilde{Z}_{sn}(\omega) - Z_{\text{air}}}{\tilde{Z}_{sn}(\omega) + Z_{\text{air}}} \right|^2 \tag{6.23}$$

Here, Z_{air} represents the characteristic impedance of air. The surface impedance method is considered to be more accurate, since it avoids the dependence on local pressure field variations the two-microphone method is prone to. We have verified that these two methods produce close results in most cases. Since two microphone method is cheaper for computing gradients, this method is used in the optimisation trials.

6.2.3 Computing gradient of sound absorption

Gradient of absorption using the two microphone method

In this section, we will derive the equations to compute the gradient of sound absorption α with respect to the design variables χ_i. We have seen that α can be computed from the complex reflection coefficient $\tilde{R}_c$ as:

$$\alpha = 1 - |\tilde{R}_c|^2 \tag{6.24}$$

Using chain rule:

$$\frac{\partial \alpha}{\partial \chi_i} = -2|\tilde{R}_c|\frac{\partial |\tilde{R}_c|}{\partial \chi_i} \tag{6.25}$$

To find the derivative of absolute value of $\partial|\tilde{R}_c|\partial\chi_i$ using commonly known rules, we can use the formula:

$$\frac{\partial |\tilde{R}_c|}{\partial \chi_i} = \frac{\Re(\tilde{R}_c \times \overline{\frac{\partial \tilde{R}_c}{\partial \chi_i}})}{|\tilde{R}_c|} \tag{6.26}$$

Here, $\Re(\cdot)$ is the real part, $\overline{(\cdot)}$ is the complex conjugate operators. To compute the gradient of the reflection coefficient, we can consider the equation 6.17, to be of the form

$$\tilde{R}_c = \frac{N_R}{D_R} \tag{6.27}$$

where

$$N_R = (\tilde{P}_{x_1} e^{(-ikx_2)} - \tilde{P}_{x_2} e^{(-ikx_1)}) \tag{6.28}$$

$$D_R = (-\tilde{P}_{x_1} e^{(ikx_2)} + \tilde{P}_{x_2} e^{(ikx_1)}) \tag{6.29}$$

Computing the derivative, we have,

$$\frac{\partial \tilde{R}_c}{\partial \chi_i} = \frac{(D_R \frac{\partial N_R}{\partial \chi_i} - N_R \frac{\partial D_R}{\partial \chi_i})}{D_R^2} \tag{6.30}$$

$$\frac{\partial N_R}{\partial \chi_i} = \left(\frac{\partial \tilde{P}_{x_1}}{\partial \chi_i} e^{(-ikx_2)} - \frac{\partial \tilde{P}_{x_2}}{\partial \chi_i} e^{(-ikx_1)} \right) \tag{6.31}$$

$$\frac{\partial D_R}{\partial \chi_i} = \left(-\frac{\partial \tilde{P}_{x_1}}{\partial \chi_i} e^{(ikx_2)} + \frac{\partial \tilde{P}_{x_2}}{\partial \chi_i} e^{(ikx_1)} \right) \tag{6.32}$$

Note that N_R, D_R, $\frac{\partial N_R}{\partial \chi_i}$ and $\frac{\partial D_R}{\partial \chi_i}$ are intermediate variables and need to be recalculated for each element i. The pressure field values $\tilde{P}_{x_1}$ and $\tilde{P}_{x_2}$ are elements of $\tilde{\mathbf{p}}$ vector which is part of $\tilde{\mathbf{X}} = \begin{Bmatrix} \tilde{\mathbf{u}} \\ \tilde{\mathbf{p}} \end{Bmatrix}$. Hence, $\frac{\partial \tilde{P}_{x_1}}{\partial \chi_i}$ and $\frac{\partial \tilde{P}_{x_2}}{\partial \chi_i}$ can be obtained from $\frac{\partial \tilde{\mathbf{X}}}{\partial \chi_i}$ as shown in equation 6.33.

$$\tilde{\mathbf{X}} = \begin{Bmatrix} \tilde{\mathbf{u}} \\ \tilde{\mathbf{p}} \end{Bmatrix} = \begin{Bmatrix} \tilde{u}_1 \\ \vdots \\ \tilde{u}_{2n} \\ \tilde{P}_1 \\ \vdots \\ \tilde{P}_{x_1} \\ \vdots \\ \tilde{P}_{x_2} \\ \vdots \\ \tilde{P}_n \end{Bmatrix} \qquad \frac{\partial \tilde{\mathbf{X}}}{\partial \chi_i} = \frac{\partial}{\partial \chi_i} \begin{Bmatrix} \tilde{\mathbf{u}} \\ \tilde{\mathbf{p}} \end{Bmatrix} = \begin{Bmatrix} \frac{\partial}{\partial \chi_i} u_1 \\ \vdots \\ \frac{\partial}{\partial \chi_i} u_{2n} \\ \frac{\partial}{\partial \chi_i} P_1 \\ \vdots \\ \frac{\partial}{\partial \chi_i} \tilde{P}_{x_1} \\ \vdots \\ \frac{\partial}{\partial \chi_i} \tilde{P}_{x_2} \\ \vdots \\ \frac{\partial}{\partial \chi_i} P_n \end{Bmatrix} \tag{6.33}$$

To find $\frac{\partial \tilde{\mathbf{X}}}{\partial \chi_i}$, equation 6.10 is differentiated to get the following expression.

$$\frac{\partial}{\partial \chi_i}\tilde{\mathbf{X}}(\boldsymbol{\chi},\omega) = [\tilde{\mathbf{S}}(\boldsymbol{\chi},\omega)]^{-1}\frac{-\partial[\tilde{\mathbf{S}}(\boldsymbol{\chi},\omega)]}{\partial \chi_i}\tilde{\mathbf{X}} \tag{6.34}$$

The above equation is again a linear system ($\mathbf{x} = \mathbf{A^{-1}b}$) which is expensive, and needs to be computed at every element i in the design domain. However, there is an efficient way to compute this using an adjoint-based approach similar to the one introduced by Lee, Göransson and Kim [138] for multi-material topology optimisation. Since only two elements in $\frac{\partial \tilde{\mathbf{X}}}{\partial \chi_i}$ i.e., $\frac{\partial \tilde{P}_{x_1}}{\partial \chi_i}$ and $\frac{\partial \tilde{P}_{x_2}}{\partial \chi_i}$ are required, one can premultiply equation 6.34 by the term $\frac{\partial \tilde{P}_{x_1}}{\partial \mathbf{X}}$, which is a vector of 0s except for one element with a value of 1 corresponding to the $\tilde{P}_{x_1}$ degree of freedom in equation 6.36.

$$\begin{aligned}\frac{\partial \tilde{P}_{x_1}}{\partial \chi_i} &= \left\{\frac{\partial \tilde{P}_{x_1}}{\partial \mathbf{X}}\right\}^T \frac{\partial \tilde{\mathbf{X}}}{\partial \chi_i} \\ &= \left\{\frac{\partial \tilde{P}_{x_1}}{\partial \mathbf{X}}\right\}^T [\tilde{\mathbf{S}}]^{-1}\frac{-\partial[\tilde{\mathbf{S}}]}{\partial \chi_i}\tilde{\mathbf{X}} = \lambda_{x_1}^T\frac{-\partial[\tilde{\mathbf{S}}]}{\partial \chi_i}\tilde{\mathbf{X}}\end{aligned} \tag{6.35}$$

$$\left\{\frac{\partial \tilde{P}_{x_1}}{\partial \mathbf{X}}\right\}^T = [\cdots\cdots\ 1\ \cdots] \tag{6.36}$$

Then, one can find a fictitious response vector $\lambda_{x_1} = [\tilde{\mathbf{S}}]^{-1}\frac{\partial \tilde{P}_{x_1}}{\partial \mathbf{X}}$ and compute $\frac{\partial \tilde{P}_{x_1}}{\partial \chi_i}$ for each i by computing $\lambda_{x_1}^T\left(\frac{-\partial[\tilde{\mathbf{S}}]}{\partial \chi_i}\tilde{\mathbf{X}}\right)$ quickly. This avoids solving system of equations repeatedly for each element or performing explicit matrix inversions. The above step is crucial for speeding up gradient methods. Thus, in addition to solving $[\tilde{\mathbf{S}}(\omega)]^{-1}\tilde{\mathbf{f}}$, two additional instances of solving system of equations is involved in finding λ_{x1} and λ_{x2}. Assuming all other steps are time insignificant, **function evaluation with gradients are approximately three times as expensive as evaluating without gradient**.
Note that this procedure has to be repeated at each frequency f and for fine frequency steps, the calculation would become expensive. Although not implemented in this work, it is worth noting that there exist various expansion methods [144, 209, 208] to speed up the computation by interpolating values between frequencies. Further, the gradients $\frac{-\partial[\tilde{\mathbf{S}}]}{\partial \chi_i}$ are obtained by applying chain rule all the way up to the material properties, which depend on the design variables $\boldsymbol{\chi}$.

In the remainder of this section, the full sensitivity computation is included even though these computations do not take significant amount of computational time. The derivative of the global assembled matrix $\frac{-\partial[\tilde{\mathbf{S}}]}{\partial \chi_i}$ is computed as follows:

$$\frac{\partial \tilde{\mathbf{S}}}{\partial \chi_i} = \begin{bmatrix} \frac{\partial \tilde{\mathbf{K}}}{\partial \chi_i} - \omega^2\frac{\partial \tilde{\mathbf{M}}}{\partial \chi_i} & -\frac{\partial \tilde{\mathbf{C}}}{\partial \chi_i} \\ -\frac{\partial \tilde{\mathbf{C}}^T}{\partial \chi_i} & \frac{1}{\omega^2}\frac{\partial \tilde{\mathbf{H}}}{\partial \chi_i} - \frac{\partial \tilde{\mathbf{Q}}}{\partial \chi_i} \end{bmatrix} \tag{6.37}$$

For the sub matrices, the derivatives are propagated as follows. Calculating solid part element stiffness matrix $\tilde{\mathbf{K}}_{ei}$ derivative, from equation 6.12, we have:

$$\frac{\partial \tilde{\mathbf{K}}_{ei}}{\partial \chi_i} = \int_{\Omega_e}[B]^T\frac{\partial [D]_i}{\partial \chi_i}[B]dV \tag{6.38}$$

The above integration is done numerically using Gauss integration over the area of the element

Ω_e. Only $[D]_i$ is dependent on χ_i, hence:

$$[D]_i = \frac{E_i}{(1+\nu_i)(1-2\nu_i)} \begin{pmatrix} 1-\nu_i & \nu_i & 0 \\ \nu_i & 1-\nu_i & 0 \\ 0 & 0 & (1-2\nu_i)/2 \end{pmatrix} \tag{6.39}$$

$$\frac{\partial [D]_i}{\partial \chi_i} = \frac{\partial [D]_i}{\partial E_i}\frac{\partial E_i}{\partial \chi_i} + \frac{\partial [D]_i}{\partial \nu_i}\frac{\partial \nu_i}{\partial \chi_i} \tag{6.40}$$

For the element mass matrix $\tilde{\mathbf{M}}$ derivatives, only $\widetilde{\rho}$ depends on χ_i. From equation 6.13,

$$\frac{\partial \tilde{\mathbf{M}}_{ei}}{\partial \chi_i} = \frac{\partial \widetilde{\rho}_i}{\partial \chi_i} \int_{\Omega_e} [N]^T [N] dV \tag{6.41}$$

From equation 6.14, we have,

$$\frac{\partial \tilde{\mathbf{C}}_{ei}}{\partial \chi_i} = \frac{\partial \widetilde{\gamma}_{(s)i}}{\partial \chi_i} \int_{\Omega_e} N^T \nabla N_p dV \tag{6.42}$$

From equation 6.15

$$\frac{\partial \tilde{\mathbf{H}}_{ei}}{\partial \chi_i} = \frac{-1}{\tilde{\rho}^2_{(eq)i}} \frac{\partial \tilde{\rho}_{(eq)i}}{\partial \chi_i} \int_{\Omega_e} \nabla [N]_p^T \nabla [N]_p dV = \frac{-1}{\tilde{\rho}_{(eq)i}} \frac{\tilde{\rho}_{(eq)i}}{\partial \chi_i} \tilde{\mathbf{H}}_{ei} \tag{6.43}$$

where $\tilde{\rho}_{(eq)i}$ is the equivalent density of the porous material. From equation 6.16,

$$\frac{d\tilde{\mathbf{Q}}_{ei}}{d\chi_i} = \frac{-1}{\tilde{K}^2_{(eq)i}} \frac{\partial \tilde{K}_{(eq)i}}{\partial \chi_i} \int_{\Omega_e} N^T \nabla N_p dV = \frac{-1}{\tilde{K}_{(eq)i}} \frac{\partial \tilde{K}_{(eq)i}}{\partial \chi_i} \tilde{\mathbf{Q}}_{ei} \tag{6.44}$$

where $\tilde{K}_{(eq)i}$ is the equivalent bulk modulus of the intermediate material assigned to element i. Derivatives of Young's modulus, Poisson's ratio and other material properties can be calculated from equation 6.3 to equation 6.8 as follows.

$$\frac{\partial E_i}{\partial \chi_i} = p\chi_i^{(p-1)}(E_{por} - E_{air}) \tag{6.45}$$

$$\frac{\partial \nu_i}{\partial \chi_i} = p\chi_i^{(p-1)}(\nu_{por} - \nu_{air}) \tag{6.46}$$

$$\frac{\partial \widetilde{\rho}_i}{\partial \chi_i} = p\chi_i^{(p-1)}[(\widetilde{\rho})_{por} - (\widetilde{\rho})_{air}] \tag{6.47}$$

$$\frac{\partial \widetilde{\gamma}_{(s)i}}{\partial \chi_i} = p\chi_i^{(p-1)}[(\widetilde{\gamma}_s)_{por} - (\widetilde{\gamma}_s)_{air}] \tag{6.48}$$

$$\frac{\tilde{\rho}_{(eq)i}}{\partial \chi_i} = p\chi_i^{(p-1)}[(\rho_{eq})_{por} - (\rho_{eq})_{air}] \tag{6.49}$$

$$\frac{\partial \tilde{K}_{(eq)i}}{\partial \chi_i} = p\chi_i^{(p-1)}[(\tilde{K}_{eq})_{por} - (\tilde{K}_{eq})_{air}] \tag{6.50}$$

Thus, the gradient of absorption with respect to the design variables can be computed for use in gradient algorithms.

A Matlab implementation of the absorption and gradient computations are made available on GitHub at https://github.com/VivekTRamamoorthy/Heuristics-and-metaheuristics-for-Acoustic-Topology-Optimisation.

6.2.4 Verification of the modelling procedure

Absorption verification

In order to verify the accuracy of the engineering model discussed above to compute absorption, let us consider the optimised shape produced by Lee, Kim, Kim and Kang (LKKK) [140] for anechoic chamber wedges. The absorption curve for the optimised shape for a volume fraction constraint of 50% was reproduced by digitally extracting the shape as shown in Figure 6.2(a) left. The optimised porous shape was extracted from the pixel data, and the design variables $\boldsymbol{\chi}$ were determined as shown in Figure 6.2(a) right. The absorption curve extracted from [140] and the one computed using our implementation match satisfactorily as shown in Figure 6.2(b), thus verifying the implementation of absorption computation. The slight variations are thought to be due to errors in digitisation.

Gradient verification

The gradient computation involves intensive calculations as shown in the previous section and is prone to numerical errors. Hence, it is of great importance to ensure the accuracy limits of the linear solver used and verify the gradients before using them in optimisation. One way to verify the gradients is to compute them numerically by perturbing the values of the design variables χ_i and ensuring that the slope of absorption matches the gradient calculated by the analytical equations. For this, we can consider the LKKK shape shown in Figure 6.2(a), and pick an arbitrary element and verify the following:

$$\frac{\partial \overline{\alpha}}{\partial \chi_i} \approx \frac{\overline{\alpha}(\chi_i + \delta\chi_i) - \overline{\alpha}(\chi_i)}{\delta\chi_i} \tag{6.51}$$

Here, $\delta\chi_i$ is a small perturbation in the design variable χ_i. Figure 6.3 shows the variation of $\overline{\alpha}$ with one of the design variables, say, χ_{457} with a blue solid line. For the shape considered, χ_{457} happens to be 1 indicating that the material in the element is porous. The gradient $\partial\overline{\alpha}/\partial\chi_{457}$ computed using the procedure detailed in the previous section is used as the slope to draw a dotted line from $\chi_{457} = 1$. As we can see, the slopes of the lines match at the point indicating that the gradient computed is reasonably accurate. This is generally the case for other elements as well.

6.2.5 Fitness computation performance improvements

Symmetry assumption

Since fitness evaluation is expensive, it was important to ensure performant implementations. Assuming that for sound sources under normal incidence, the shapes are expected to be symmetric about the horizontal centreline in the design domain. It is thus only necessary to model one half of the design domain, reducing the matrix sizes and thereby the fitness evaluation time. Symmetry is applied by imposing u_x-free, $u_y = 0$, P-free boundary conditions at the centreline. It has been verified that modelling only one half of the symmetric design domain gives the same absorptions as obtained when modelling the full unit cell with sliding supports

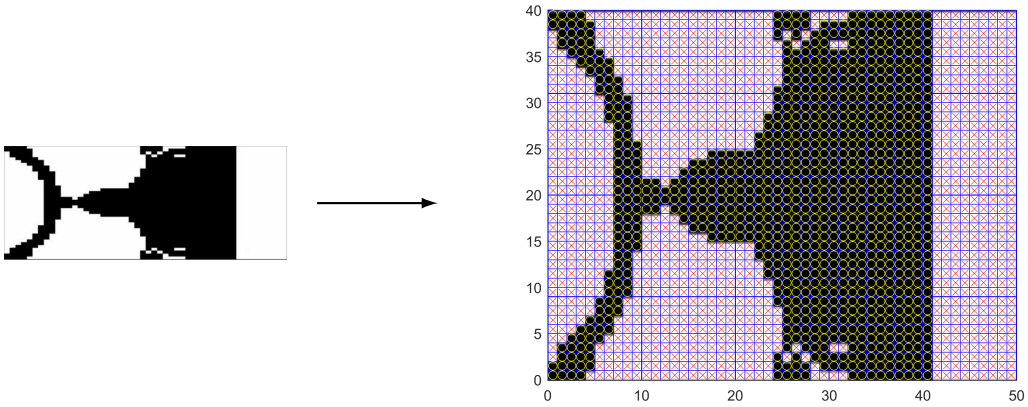

(a) Extracting optimised shape from Lee, Kim, Kim and Kang [140].

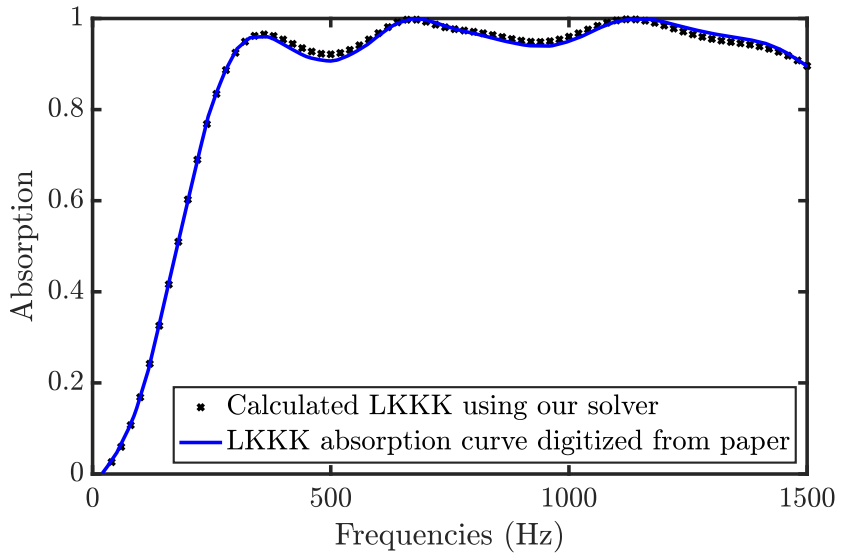

(b) Absorption vs. frequency comparison.

Figure 6.2: Verification of absorption computation with existing literature. A comparison of absorption coefficient between our implementation and that of the article published by Lee, Kim, Kim and Kang [140].

in the top and bottom edges. Figure 6.4 shows a comparison of the absorption spectrum for a given shape modelled in full and modelled in half. The difference is found to be negligible with $\texttt{norm}(|\alpha_{full} - \alpha_{symmetric}|) = 1.24 \times 10^{-10}$ and hence, this symmetric model is used for the optimisation trials to save computational time.

Effect of the air layer

Since the purpose of modelling the air layer in front of the design domain is solely to calculate the absorption coefficient at different frequencies, consideration is given to using minimal number of elements along the length of the air layer. This is to keep the computational effort less while reducing the error due to finite element discretisation. The general rule is to ensure that the element lengths are much smaller than the acoustic wavelengths at the highest frequency. To assess the effect of thickness of the air layer, the design domain is fully filled with porous material, forming a single flat layer. Figure 6.5 shows the variation in absorption curves when the

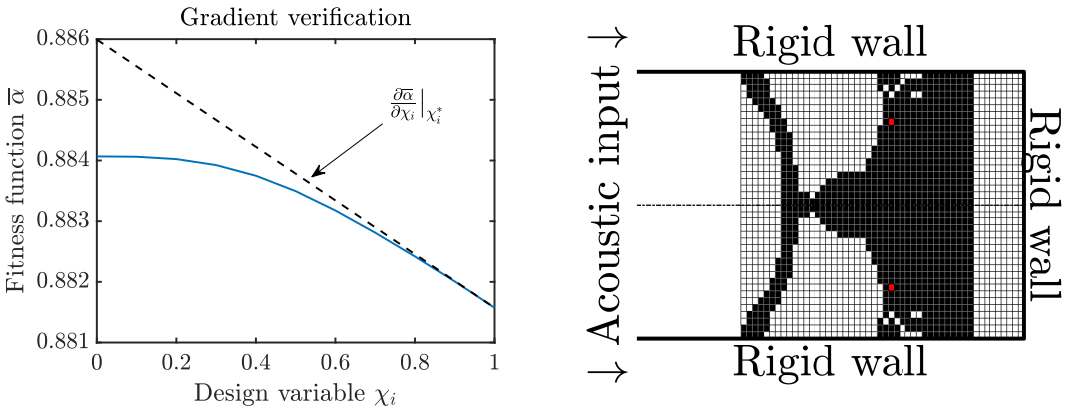

Figure 6.3: Verification of the analytical gradient with numerical gradient: The computed analytical gradient matches the slope of the fitness function. Here, the dotted line is plotted using the analytical gradient computed by our implementation. The blue line corresponds to absorption $\overline{\alpha}$ recomputed at different values for χ_i for $i = 457$.

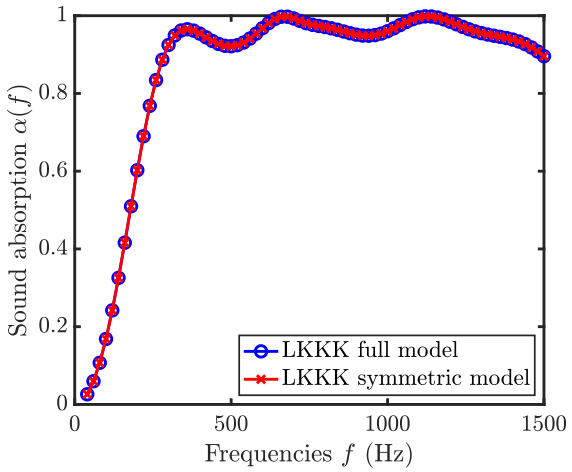

Figure 6.4: Comparison of a full vs. half-symmetric model of the LKKK shape. The absorption differences are negligible.

length of this air layer is increased, while fixing the discretisation of air layer at 10 elements. A comparison with the analytical solution from transfer matrix method calculations is also drawn. As the thickness of the air layer is reduced from 500 mm to 10mm, the accuracy is improved and the sound absorption vs. frequency curve matches with the TMM solution. The line corresponding to an air layer thickness of 500 mm has inaccuracies in the higher frequencies because of the element length being much larger relative to the wavelength and the finite element model being unable to represent the physical wave propagating in the material. An element length of 100mm and lower seems to be able to match closely with the analytical solution from TMM. The error between the finite element and TMM result for different discretisations along the length of the air layer are shown in Figure 6.6. It is observed that the error reduces as the thickness of the air layer reduces. However, it is noted that this is the case for flat layer porous material. To ensure reasonable accuracy while also keeping the number of elements in the FE problem low, the number of elements along the air layer is chosen according to the accuracy desired.

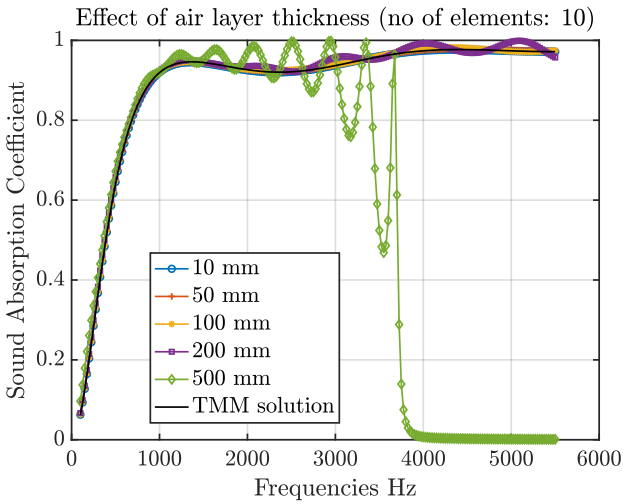

Figure 6.5: Effect of varying the thickness of the front air layer.
Effect of varying the thickness of the front air layer. As the element thickness is reduced from 500 mm to 10 mm, the absorption curve approaches the TMM solution.

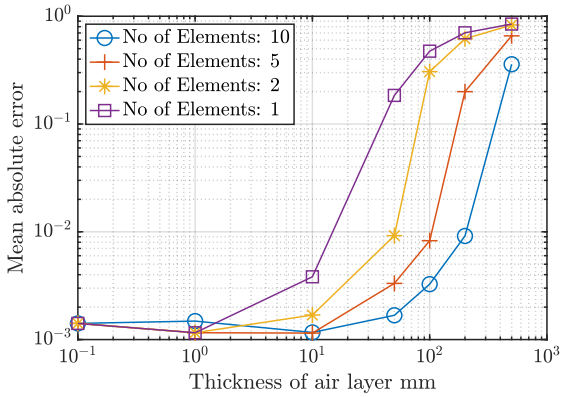

Figure 6.6: Effect of number of elements along air layer in front of design domain. Plot lines show the mean absolute error between finite element solution and transfer matrix method solution for the absorption curve.

6.2.6 Computational complexity

Theoretical time complexity

We have seen how to compute absorption and its gradient, and the nature of computations involved. At this point, it is worth highlighting the computational time complexity of these computations and contrast them with the compliance minimisation problem. Although lots of studies on compliance minimisation are available in the literature, in order for the results to be applicable for absorption maximisation, one of the presumptions would be that the relative expensivenesses of fitness vs. gradient are similar. In this section, we will estimate the theoretical and practical time complexities of fitness vs. gradient for the two problem domains.

(i) Computing the objective function The procedure to compute compliance and its gradient will not be detailed here and can be followed from Andreassen *et al.* [10]. For evaluating the compliance, the significantly expensive operation is solving for the displacements ($\tilde{\mathbf{u}} = \mathbf{K}^{-1}\mathbf{f}$).

Here, $\mathbf{K}$ is the global stiffness matrix in compliance minimisation (not to be confused with $\tilde{\mathbf{K}}$ in absorption maximisation). $\mathbf{K}$ is a real, symmetric and positive definite matrix of dimensions equal to the total degrees of freedom of the system. The precise matrix size depends on the number of nodes N_{node} rather than the number of elements N. Each node has two degrees of freedom corresponding to horizontal and vertical displacements and hence $\mathbf{K}$ has a size of $2N_{node} \times 2N_{node}$. The number of nodes is of the same order as the number of elements making the matrix size $\mathcal{O}(N) \times \mathcal{O}(N)$. Note that we use the same notation N to indicate the number of elements in the design domain in both compliance minimisation and absorption maximisation.

For absorption maximisation, the most significant operation while computing fitness is solving $\tilde{\mathbf{X}} = \tilde{\mathbf{S}}(\boldsymbol{\chi}, \omega)^{-1}\tilde{\mathbf{f}}$. Here $\tilde{\mathbf{S}}$ is a complex symmetric matrix with three degrees of freedom per node corresponding to displacements in two dimensions and pressure field value making the matrix size $3N_{node} \times 3N_{node}$. Complex numbers require 4 times the number of flops for multiplication and twice the number of flops for addition. Since these are constant factors, they don't play a part in the complexity and the dimensions will have the same complexity $\mathcal{O}(N) \times \mathcal{O}(N)$. However, as $\tilde{\mathbf{S}}$ is frequency dependent, the operations need to be repeated at each of the n target frequencies considered.

Finding the vector solution to $\mathbf{K}^{-1}\mathbf{f}$ is equivalent to solving a system of linear equations given by $\mathbf{A}\boldsymbol{x} = \mathbf{b}$. Solving such linear systems is an economically important computational task in engineering. This computation can be performed more efficiently by using special procedures instead of computing the inverse of the matrix explicitly ($\mathbf{A}^{-1}$) and then multiplying it with the vector $\mathbf{b}$. If $\mathbf{A}$ is a square matrix which is invertible with non-zero diagonal elements, the classic Gauss-Jordan elimination can be used which has a complexity of $\mathcal{O}(N^3)$. It is commonly implemented using LU decomposition and requires $\frac{2}{3}N^3$ floating point operations [243], where $\mathbf{L}$ and $\mathbf{U}$ are lower and upper triangular matrices. It has been shown that LU decomposition can be performed with the same complexity as matrix multiplication [36]. Hence, the matrix multiplication complexity of recursive algorithms such as Strassen [234] with $\mathcal{O}(N^{2.807})$ and Coppersmith-Winograd [56] with $\mathcal{O}(N^{2.376})$ can be applied bringing down the theoretical complexity exponent. However, further improvements have stagnated around the Coppersmith-Winograd exponent [244]. Whereas if $\mathbf{A}$ is also symmetric and positive definite, Cholesky decomposition can be used. $\mathbf{A}$ can then be decomposed into $\mathbf{L}\mathbf{L}^*$, where $\mathbf{L}$ is a lower triangular matrix, and $\mathbf{L}^*$ is its Hermitian. Cholesky decomposition is a quicker variant of Gauss elimination requiring $\frac{1}{3}N^3$ flops [243], which makes it about twice as fast as LU decomposition. For sparse symmetric or hermitian positive-definite $\mathbf{A}$, Lipton *et al.* [150] have shown that for matrices arising out of planar graphs such as those from finite element methods, $\boldsymbol{x} = \mathbf{A}\backslash\mathbf{b}$ can be computed with $\mathcal{O}(N^{1.5})$ time complexity. Since in compliance minimisation, it is well-known that the stiffness matrices are symmetric and positive definite, the estimate for the theoretical complexity is that of Lipton. Whereas for absorption maximisation, since the matrix is complex symmetric but not Hermitian, this does not apply and the complexity remains at that of Coppersmith-Winograd. A comparison of these complexities are provided in Table 6.1 for a quick reference.

Although algorithms like Coppersmith-Winograd have smaller complexity exponents, the constant terms are too large to be practical, making it a galactic algorithm [149] i.e., the problem sizes where these algorithms tend to be useful are too large that they are rarely encountered in practise. On the other hand, Strassen algorithm with $\mathcal{O}(N^{\log_2 7})$ is not a galactic algorithm since it is implemented for large values of N. However, in most real life scenarios, non-recursive LU

Table 6.1: Time complexity comparison. Here, N is the number of elements in the design domain and n-number of target frequencies.

Time complexity	Compliance minimisation	Absorption maximisation
Objective function	$\mathcal{O}(N^{1.5})$	$\mathcal{O}(nN^{2.376})$
Gradient	$\mathcal{O}(N)$	$\mathcal{O}(nN^{2.376})$
Objective + gradient	$\mathcal{O}(N^{1.5})$	$\mathcal{O}(nN^{2.376})$

and Cholesky are sufficiently fast and can be used in practise for sparse matrices. For example, writing $\mathbf{A}\backslash\mathbf{b}$ using the *backslash* or *mldivide* operator in Matlab automatically selects from a series of algorithms based on the matrix type as shown in the *mldivide* documentation page [160]. For compliance minimisation, since the matrix $\mathbf{K}$ is symmetric and positive definite, Cholesky decomposition [51] will be picked. However, since $\tilde{\mathbf{S}}$ is not hermitian but complex symmetric, Cholesky cannot be used and instead one has to resort to LU decomposition. This further makes the practical computation of absorption maximisation require twice as many flops. Considering all the differences between compliance minimisation and absorption maximisation, namely, the degrees of freedom per node (2 vs. 3), element space (real vs. complex) and practical floating point operations ($\frac{1}{3}N^3$ vs. $\frac{2}{3}N^3$) required, for the same number of finite elements in the design domain, it is roughly estimated that an absorption maximisation problem with a single target frequency would be $(3/2)^3 \times 4 \times 2 = 27$ times as expensive.

(ii) Computing gradients In compliance minimisation, once the displacements $\tilde{\mathbf{u}}$ are computed, the gradient of compliance can be found using the expression:

$$\frac{\partial c}{\partial x_e} = -p x_e^{p-1}(E_e - E_0)\tilde{\mathbf{u}}_e^T \mathbf{k}_e \tilde{\mathbf{u}}_e \text{ (ref. [10])} \tag{6.52}$$

Note that $\{\tilde{\mathbf{u}}_e\}_{8\times 1}$ and $[\mathbf{k}_e]_{8\times 8}$ are element matrices with fixed matrix sizes. For two-dimensions, a four-noded quadrilateral element would have two displacements per node and correspondingly, the element matrix sizes would be 8. Hence, for computing the gradient at each element in the design domain $\frac{\partial c}{\partial x_e}$ only a fixed number of arithmetic operations $\mathcal{O}(1)$ are required, and computing for all the N elements makes the gradient time complexity $\mathcal{O}(N)$. This implies that, once the objective function is evaluated to find $\tilde{\mathbf{u}}$, the gradient in compliance minimisation can be computed relatively quickly as N increases.

In absorption maximisation, this is not the case. Calculating the gradient $\frac{\partial \overline{\alpha}}{\partial \chi_i}$ requires two instances of solving the system of linear equations. Hence, the gradient has the same time complexity as that of the objective function unlike in compliance minimisation. Additionally, these computations need to be repeated at each frequency, and the overall time complexity to compute both absorption and its gradients is a factor of n higher, where n is the number of target frequencies. Table 6.1 provides an overview of the comparison.

The fact that gradient computation has a higher time complexity in absorption maximisation as opposed to compliance minimisation means that knowledge obtained from testing optimisation algorithms on compliance minimisation may not be scalable to absorption maximisation.

Table 6.2: Benchmark problem instances.

No.	Problem instance name	Mesh size nelx × nely	Length D (m)	Height d (m)	f_{min} Hz	f_{step} Hz	f_{max} Hz	Material ID (see Table 6.3)
1	LKKK material broadband coarse-mesh	10×10	0.135	0.054	100	100	1500	1
2	Melamine - building problem	15×10	0.045	0.1	100	100	1500	2
3	High resistivity foam - low frequency	10×10	0.1	0.1	50	50	500	3
4	Melamine - automotive problem	10×10	0.02	0.1	100	100	1500	2
5	Melamine - high frequency problem	10×10	0.02	0.1	2000	1000	5000	2
6	Melamine -broadband fine-mesh	50×20	0.135	0.054	100	100	1500	2
7	Melamine -single target frequency	10×5	0.135	0.054	500	500	500	2

Table 6.3: Acoustic and elastic properties of materials used in the benchmark problems in Table 6.2.

Material parameters	Material-1	Material-2	Material-3
Material:	LKKK [140]	Melamine	High-resistivity soft foam
Acoustic model:	JCAL	JCAL	JCAL[111, 43, 134]
ϕ	0.9	0.99	0.8
Λ' (μm)	449	196	100
Λ (μm)	225	98	10
σ (N·s·m^{-4})	25000	10000	300000
α_∞	7.8	1.01	3
k_0'	4.75e-09	4.75e-09	4.75e-09
ρ (kg·m^{-3})	31.08	8	80
E (Pa)	800000	160000	30000
(ν)	0.4	0.44	0.44
(η)	0.265	0.1	0.01

6.2.7 Benchmark problem instances

For comparing the performance of various optimisation approaches, seven benchmark problem instances with different characteristics as given in Table 6.2 are considered. In all of these problem instances, the acoustic system is a simple two-dimensional rectangular unit cell of an absorbing wall as shown in Figure 6.1 in page 75. The unit cell's dimensions, its discretisation into finite elements, the base porous material to fill the elements, and target frequencies to be absorbed vary for each problem instance. For each problem instance, the rectangular unit cell backed by a rigid wall on the right is assumed to be of different heights d. The region from the rigid wall up to a length D is designated as the design domain. The design domain is followed by a fixed domain, which is just an air layer with a length L so as to use the two microphone method. The length L is chosen to be the same for each problem instance. The number of finite elements in the design domain along the horizontal and vertical directions are denoted by $nelx$ and $nely$, respectively. A normal incidence sound source is modelled at the left end of the system. Within the unit cell, symmetry is assumed about the central horizontal line, and sliding boundaries (u_x-free, $u_y = 0$, P-free) are assumed at the top and bottom edges. In all the problem instances, the mean sound absorption coefficient under normal incidence across the target frequencies is to be maximised.

Although meant to be arbitrary, the problem instances chosen are picked from practical engineering examples. The material used for optimisation for each problem instance is picked from three choices in Table 6.3. In problem instance 1, a special material previously used by Lee,

Kim, Kim, and Kang [140] (LKKK material) is used on a coarser 10×10 discretisation. Note that the LKKK material may not representative of a physical material due to the high tortuosity value of 7.8. Problem instance 2 features a 45 mm long design domain representative of a typical building application. Problem instance 3 uses an artificial material with a high static airflow resistivity which is expected to have more intricate optimal shapes. In problem instance 4, a thin design domain of 2 cm, representative of a foam layer in an automotive absorber, is considered. In problem instance 5, a thin layer is optimised for high-frequency absorption. Among the problem instances, problem instance 6 has a relatively fine mesh size with 50×20 elements featuring a thicker design domain optimised on a broad frequency range. Other than 1 and 3, all problem instances use Melamine foam for control. In problem instance 7, a single target frequency is considered.

6.3 Experimental design for optimisation computer trials

Several gradient-free heuristic and metaheuristic approaches, including existing and novel methods, are evaluated in this study along with the state-of-the-art gradient-based approach SIMP. Henceforth in this report, all the heuristic and metaheuristic approaches will be referred to as *algorithms*, and they are not to be confused with *exact* algorithms as used by some authors. The algorithms tested and their settings are summarised in Table 6.4.

Five heuristic algorithms namely HC, CH1, CH2, SIMPf0 and SIMPf2 are tested. HC is a first-improvement hill climbing, where each element is flipped between air and porous material, and the new solution is accepted if it is improving. Consecutive elements are flipped like in a raster scan (row-by-row) until the function evaluation budget is used up. CH1 is a constructive heuristic which starts from an air-filled solution and progressively adds porous material in elements of best improvement in absorption. Similarly, CH2 starts from a porous material-filled solution and progressively removes porous material from the elements where the decrease in absorption is the least. SIMPf0 and SIMPf2 are solid-isotropic-material-with-penalisation approaches [10] which use gradients of absorption to modify the solution at each step. While SIMPf2 uses density filtering, SIMPf0 uses no filtering techniques.

Four popular metaheuristic approaches are tested including genetic algorithm (GA), tabu search (TABU), covariance-matrix-adaptation evolution strategy (CMA) and differential evolution (DE). Additionally, discrete variants of CMA and DE, referred to as CMAd and DEd, where the continuous shapes are rounded to discrete before every absorption evaluation, are also tested. It is noted that other variants of CMA were also studied but is not reported in this thesis.

Except for CH1 and CH2, all the other algorithms are non-deterministic as they embed a random component, and each new trial of the non-deterministic algorithm could produce a different near-optimal solution. For these algorithms, 31 trials were run on each problem instance in order to assess their average performance and carry out statistical analysis.

All non-gradient algorithms are allowed 4096 function evaluations during the trials. Since evaluating absorption along with gradient takes approximately thrice the computational time (Equation. 6.35), SIMPf0 and SIMPf2 are allowed 1366 function evaluations.

For a fair comparison, all the algorithms are initialised from randomly generated solutions except for CH1 and CH2 making no assumption about the problem. The discrete algorithms HC,

Table 6.4: Optimisation approaches used in this study, with short pseudocode and some algorithmic and experimental design attributes.

Abbr.	Optimisation approach	Procedure and parameter settings	Algorithm type: Deterministic or Non-deterministic	Trials	Search space	Gradient usage	Fn. eval. budget
		HEURISTICS					
HC	Hill climbing (first improvement)	Start with a random binary array solution; Bit flip the consecutive elements; Accept if improving and move to the next element; Repeat from the start unless fn. eval. budget is used up. Element ordering is like in a raster scan.	Non-deterministic since starting solution is random	31	Discrete	No	4096
CH1	Constructive heuristic: material addition	Start with air-filled design domain; Compute absorption improvement at each element by filling porous material only in that element; Sort elements; Add porous material at best 'm' improving elements; Repeat until design domain is fully porous; Track and return the best solution. m is chosen such that the budget is not exceeded.	Deterministic	1	Discrete	No	4096
CH2	Constructive heuristic: material removal	Similar to CH1. Start from fully porous design domain; Remove porous (replace with air) at 'm' least worsening elements; Repeat until all porous is removed; Track and return the best solution	Deterministic	1	Discrete	No	4096
SIMPf0	SIMP with no filter [10]	Start from a random continuous solution, follow the SIMP procedure [10]; Omit the filtering step. Use SIMP penalty $p = 3$; move update - optimality criteria; move limit $m = 0.2$; Volume fraction limit $V_f = 1$.	Non-deterministic	31	Continuous	**Yes**	1366
SIMPf2	SIMP with density filter [10]	Start from a random continuous solution, follow the SIMP procedure [10]; use density filter `ft=2`. Use SIMP penalty $p = 3$; move update - optimality criteria [101]; move limit $m = 0.2$; Volume fraction limit $V_f = 1$; Filter radius r_{min} =2.	Non-deterministic	31	Continuous	**Yes**	1366
		METAHEURISTICS					
GA	Genetic algorithm [102]	Initialise population with 64 random binary solutions; Selection: tournament–2; Crossover: uniform; Mutation: bitflip; Mutation rate: 1/(N); Replacement: best of parents and offspring replace parents; Repeat from selection, unless budget is used up.	Non-deterministic (uses a random number generator)	31	Discrete	No	4096
TABU	Tabu search [88]	Initiate tabu list; Start with a random binary array solution; Pick a random bit, not in tabu list; Accept if improving and add the bit to tabu list; tabu tenure: 20% of N; Pick another random bit and repeat unless budget is used up.	Non-deterministic (since starting solution and moves are random)	31	Discrete	No	4096
CMA	Covariance-matrix-adaptation evolution strategy [100]	Relax problem to continuous using SIMP interpolation scheme with $p = 3$; Follow CMA procedure [100]; Terminate if budget is used up; Discretise final continuous solution by rounding.	Non-deterministic (uses a random number generator to sample points from the distribution)	31	Continuous	No	4096
CMAd	Discrete variant of CMA	Follow CMA procedure in continuous space; Before fitness evaluation, discretise the sampled continuous solutions by rounding; Return the rounded best solution. Interpolation scheme is not necessary as continuous solutions are never evaluated.	Non-deterministic	31	Discrete	No	4096
DE	Differential evolution [232, 233]	Relax problem to continuous using SIMP interpolation scheme with $p = 3$; Follow differential evolution procedure [232, 233]; Stop if budget is used up. Use population size=32; F=0.2; CR=0.2;	Non-deterministic	31	Continuous	No	4096
DEd	Discrete variant of DE	Follow the differential evolution procedure; Before fitness evaluation, discretise the sampled continuous solutions by rounding; Return the rounded best solution.	Non-deterministic	31	Discrete	No	4096

GA, TABU, CMAd and DEd are initiated from random discrete solutions with equal probability of air and porous material for each element. Continuous algorithms are initiated from random continuous solutions with each element assigned a random number uniformly distributed between 0 and 1.

Some of the approaches, namely, hill climbing, constructive heuristics, and the discrete variants of CMA evolution strategy and differential evolution, in the specific way used, are proposed and tested for the first time. The others are well-established algorithms, and resources including surveys, tutorials and code implementations can be easily found in the literature.

It is noted that a thorough knowledge of all the algorithms is not essential to understand the findings. Readers who are new to metaheuristics may consider these algorithms as black-boxes which optimise the shape design by searching for the optimal assignment of the decision variables $\boldsymbol{\chi}$ to maximise $\overline{\alpha}(\boldsymbol{\chi})$.

6.4 Heuristics

In this section, a concise description of the heuristic procedures used in the study is given. These include hill climbing (HC), constructive heuristics (CH1 and CH2) and solid isotropic material with penalisation (SIMPf0 and SIMPf2).

6.4.1 Hill climbing (HC)

Hill climbing refers to a greedy search procedure that makes a move and only accepts it if it is improving. A *move* in optimisation is an operation that modifies a given solution. In this implementation, initially a random discrete (binary) solution is generated ($\boldsymbol{\chi} : \chi_i \in \{0, 1\}$). The finite elements in the rectangular design domain are ordered row by row like in raster-scanning (as also shown in Figure 6.1). A new solution is generated from the current solution by a bit-flip move operation (air $\rightarrow$ porous, porous $\rightarrow$ air). If the new solution results in an improvement, it is accepted as the current solution. If not, the current solution is unchanged. Then the next bit is flipped. The process is repeated from the first element once all the elements are flipped and checked. If no improvements are obtained in the last N (number of elements in the design domain) steps or if the function evaluation budget is reached, the algorithm is terminated. Note that this procedure does not impose any volume constraint. When used on the MBB beam problem [217] in compliance minimisation, this procedure results in the trivial

fully solid-filled design domain. Pseudocode for this procedure is provided in Algorithm 8.

Algorithm 8: Hill climbing (HC)

Initiate $\boldsymbol{\chi}$ as a random binary vector of size N ;
Evaluate the objective function ($\overline{\alpha}(\boldsymbol{\chi})$) ;
Set counter $feval \leftarrow 1$ and $budget$;
while $feval < budget$ **do**
  for $j = 1, j \leq N, j++$ **do**
    Set $\boldsymbol{\chi}^{new} \leftarrow \boldsymbol{\chi}$;
    Bit flip ${\chi_j}^{new}$;
    Evaluate $\overline{\alpha}(\boldsymbol{\chi}^{new})$; Increment $feval$;
    Accept: $\boldsymbol{\chi} \leftarrow \boldsymbol{\chi}^{new}$ if $\overline{\alpha}(\boldsymbol{\chi}^{new}) > \overline{\alpha}(\boldsymbol{\chi})$;
  end
end
Return $\boldsymbol{\chi}$ as the best shape;

6.4.2 Constructive heuristics (CH1 & CH2)

Material addition (CH1)

In this procedure, a solution is constructed by incrementally adding porous materials, starting from an air-filled design domain. At each step, all remaining air element in the design domain are individually replaced with the porous material, and the corresponding change in absorption is computed. At the end of a step, m best-improving air elements are filled with the base porous material. This step is done repeatedly until all the elements are assigned to the porous material. The best solution is tracked during the process and returned as the optimised shape. The move size m is chosen such that the number of function evaluations necessary to fill the entire design domain does not exceed the budget. A volume fraction constraint can be easily imposed in this method by simply terminating the algorithm after the desired volume fraction is reached. Thus, this method can be used on the classical topology optimisation problems with volume constraint. Pseudocode for this procedure is provided in Algorithm 9.

Algorithm 9: Constructive heuristic: material addition (CH1)

Set the current solution to fully air filled design domain $\boldsymbol{\chi} = \{\mathbf{0}\}$;
Calculate the number of elements to add porous material in each step (m) so as not to exceed budget;
repeat
  for *each remaining air element* $k : \chi_k = 0$ **do**
    Convert the element to porous i.e. : $\boldsymbol{\chi}^{\text{local}} \leftarrow \boldsymbol{\chi}$, $\chi_k^{\text{local}} \leftarrow 1$;
    Evaluate absorption $\overline{\alpha}(\boldsymbol{\chi}^{\text{local}})$;
    Save absorption increments $\Delta\alpha(k) = \overline{\alpha}(\boldsymbol{\chi}^{\text{local}}) - \overline{\alpha}(\boldsymbol{\chi})$;
  end
  Sort elements in descending order of absorption increments $\boldsymbol{k}^s \leftarrow \text{sort}(\boldsymbol{\Delta}\alpha(k))$;
  Select the best m air elements to add porous material $k^s_{1,2,\ldots,m}$;
  Add porous material to the elements $\chi_{k^s_{1,2,\ldots,m}} \leftarrow 1$;
  Evaluate $\overline{\alpha}(\boldsymbol{\chi})$;
  Keep track of step solutions $\boldsymbol{\chi}^{*\text{step}} \leftarrow \boldsymbol{\chi}$
until *the entire design domain is porous*;
return the best step solution $\boldsymbol{\chi}^* \leftarrow \text{best}\ (\boldsymbol{\chi}^{*\text{step}})$;

Material removal (CH2)

In contrast to starting from a fully air-filled design domain and iteratively adding porous material, one can start with a completely porous material-filled design domain and iteratively remove porous material from the elements where the contribution to absorption is the least. The process is repeated until all the porous elements are removed and the best solution found is tracked and returned. At each step, m porous elements are removed, and m is determined such that the budget is not exceeded. This approach would be the fastest for problem instances with porous material-filled design domain as the best solution. The CH1 and CH2 procedures are similar to evolutionary structural optimisation (ESO) [256]. While ESO for compliance minimisation uses stress fields to make modifications to the solution in each step, in CH1 and CH2, the absorption increments are used. Pseudocode for this procedure is provided in Algorithm 10.

Algorithm 10: Constructive heuristic:material removal (CH2)

Set the current solution to fully porous material in the design domain $\boldsymbol{\chi} = \{\mathbf{1}\}$;
Evaluate the objective function $(\overline{\alpha}(\boldsymbol{\chi}))$;
Calculate number of elements to remove porous material from in each step (m) from budget;
repeat
  for *each remaining porous element* $k : \chi_k = 1$ **do**
    Convert element to air i.e. : $\boldsymbol{\chi}^{\text{local}} \leftarrow \boldsymbol{\chi}$, $\chi_k^{\text{local}} \leftarrow 0$;
    Evaluate absorption $\overline{\alpha}(\boldsymbol{\chi}^{\text{local}})$;
    Save absorption increments $\Delta\overline{\alpha}(k) = \overline{\alpha}(\boldsymbol{\chi}^{\text{local}}) - \overline{\alpha}(\boldsymbol{\chi})$;
  end
  Sort elements in descending order of absorption increments $\boldsymbol{k}^s \leftarrow \text{sort}(\boldsymbol{\Delta}\overline{\alpha}(k))$;
  Select the best m elements to remove porous material $k^s_{1,2,\ldots,m}$;
  Remove porous material from those elements and replace with air $\chi_{k^s_{1,2,\ldots,m}} \leftarrow 0$;
  Evaluate $\overline{\alpha}(\boldsymbol{\chi})$;
  Keep track of step solutions $\boldsymbol{\chi}^{*\text{step}} \leftarrow \boldsymbol{\chi}$; `// Each step gives solution with different volume fraction`
until *the entire design domain is air*;
return the best step solution $\boldsymbol{\chi}^* \leftarrow \text{best}\ (\boldsymbol{\chi}^{*\text{step}})$;

6.4.3 Solid isotropic material with penalisation (SIMP)

SIMP is a derivative-based continuous optimisation approach specially designed for topology optimisation with a volume fraction constraint. The principle of this approach is to relax the discrete topology optimisation problem to continuous space using the SIMP interpolation scheme, and use the gradient of the objective function to make incremental moves using a move update scheme. Some examples of move update schemes for SIMP are optimality criteria [101] and method of moving asymptotes [238, 239]. In this implementation, a SIMP penalty of $p = 3$ is used and the procedure by Andreassen *et al.* [10] is followed. The volume fraction limit is set to 1, and the move limit is set to 0.2. In SIMP, after each iteration, a filtering technique is applied to ensure manufacturability, mesh-independence and prevent checkerboard-like solutions [222]. Since manufacturability aspects are not considered for this study, the density filtering step is omitted, and this procedure is called SIMPf0. However, SIMP with a density filter referred to as SIMPf2 is also tested as a control. Although the usage of density filtering

favours discrete solutions, it does not strictly impose discrete solutions. The final shapes from SIMPf0 and SIMPf2 are subject to a simple round-off filter to ensure discrete (0 or 1) solutions. Pseudocode for SIMPf0 and SIMPf2 are provided in Algorithms 11 and 12.

Algorithm 11: Solid isotropic material with penalisation [10] without filter (SIMPf0)

Initiate $\boldsymbol{\chi}_{init} \leftarrow V_f \times$ ones(N,1);
Set $\boldsymbol{\chi} \leftarrow \boldsymbol{\chi}_{init}$;
while *Termination criterion is NOT met* **do**
    Assemble the FE global matrices using $\boldsymbol{\chi}$ and calculated material properties at each frequency;
    Evaluate absorption $\alpha(\boldsymbol{\chi}, f)$;
    Evaluate derivatives at each frequency $(d\alpha/d\boldsymbol{\chi})_f$;
    Set $c = 1 - 1/n_f \sum_f \alpha(\boldsymbol{\chi}, f)$; `// c to be minimised`
    Set the sensitivities $dc/d\boldsymbol{\chi} = -1/n_f \sum_f (d\alpha/d\boldsymbol{\chi})_f$;
    `/* Omit the filtering step */`
    Update design variables $\boldsymbol{\chi} \leftarrow$ OptimalityCriteria$(\boldsymbol{\chi}, c, dc/d\boldsymbol{\chi})$;
end
return Best $\boldsymbol{\chi}^* \leftarrow \boldsymbol{\chi}$;

Algorithm 12: Solid isotropic material with penalisation [10] with density filter (SIMPf2)

Initiate $\boldsymbol{\chi}_{init} \leftarrow V_f \times$ ones(N,1);
Set $\boldsymbol{\chi} \leftarrow \boldsymbol{\chi}_{init}$;
while *Termination criterion is NOT met* **do**
    Assemble the FE global matrices using $\boldsymbol{\chi}$ and calculated material properties at each frequency;
    Evaluate absorption $\alpha(\boldsymbol{\chi}, f)$;
    Evaluate derivatives at each frequency $(d\alpha/d\boldsymbol{\chi})_f$;
    Set $c = 1 - 1/n_f \sum_f \alpha(\boldsymbol{\chi}, f)$; `// c to be minimised`
    Set the sensitivities $dc/d\boldsymbol{\chi} = -1/n_f \sum_f (d\alpha/d\boldsymbol{\chi})_f$;
    Use density filter;
    Update design variables $\boldsymbol{\chi} \leftarrow$ OptimalityCriteria$(\boldsymbol{\chi}, c, dc/d\boldsymbol{\chi})$;
end
return Best $\boldsymbol{\chi}^* \leftarrow \boldsymbol{\chi}$;

6.5 Metaheuristic approaches

Metaheuristics are high-level problem-independent guidelines to design heuristic optimisation approaches [89, 226]. Since topology optimisation can be represented as either discrete or continuous optimisation, two metaheuristics for discrete optimisation, namely, genetic algorithms and tabu search, and two metaheuristics for continuous optimisation, namely, CMA evolution strategy and differential evolution (DE) are studied, along with their discrete variants, CMAd and DEd.

6.5.1 Genetic algorithm (GA)

The notion of mimicking the process of natural evolution to optimise was first introduced by Holland [102], and since then, genetic algorithms have been used successfully in many applications. In the procedure used here, the initial population is obtained by generating random binary arrays. Parameter tuning revealed that for 4096 function evaluations, a population size of 64 gives the best results. Tournament selection is applied with a tour size of 2 to choose parent solutions for recombination. The selected solutions are subject to a uniform crossover to generate the two offspring solutions. With a mutation probability of 1/array length (N), each bit in the offspring is mutated by bit flip operation to generate the two mutated children. The best two out of the parents and mutated offspring are replaced into the population of the next generation. The process is repeated until the function evaluation budget is used up. Pseudocode for this procedure is provided in Algorithm 13.

Algorithm 13: Genetic algorithm (GA)

```
χ^j ←Generate initial population;
Evaluate their fitnesses ᾱ(χ);
repeat
    Apply tournament selection with tour size 2 to pick parent solutions;
    Crossover the selected solutions using uniform cross over;
    Mutate the offspring with a rate of 1/chromosome length;
    Evaluate the fitness of the offspring;
    Replace the best of offspring and parent into the parents in the population;
    Update the best solution;
until Termination criteria NOT met;
Return best;
```

Parameter tuning

In order to tune the parameters used in genetic algorithms, a few sample problem instances with single target frequencies were considered. It was found that a mutation rate of 1/chromosome length gave the best performance across several problem instances. The reason for 1/chromosome length performing the best may be explained as follows. When the genetic algorithm reaches a near optimal solution, the true optimal solution may be a few hamming distances away, with Hamming distance being the number of bits which are different between two solutions. Considering a mutation rate of 1/chromosome length is expected to flip one bit, flipping 2 or more bits in a near optimal solution, is more likely to result in poorer solutions. This is empirically confirmed by parameter tuning studies shown in Figure 6.7. In this figure, five problem instances considered at various target frequencies ranging from 100 Hz to 2000 Hz are optimised using genetic algorithms with different mutation rates keeping all other aspects fixed. At each mutation rate, 31 trials of genetic algorithm were run. The distribution of the optimal solution fitnesses from these trials are plotted in each figure. It may be observed that the fitness values to be maximised are higher for a mutation rate around 1/chromosome length in all the problem instances. Hence, this mutation rate was used in further genetic algorithm studies.

Similarly, parameter tuning is performed on the population size. To study this, the same problem instances were optimised using a genetic algorithm with a fixed mutation rate of 1/chromosome

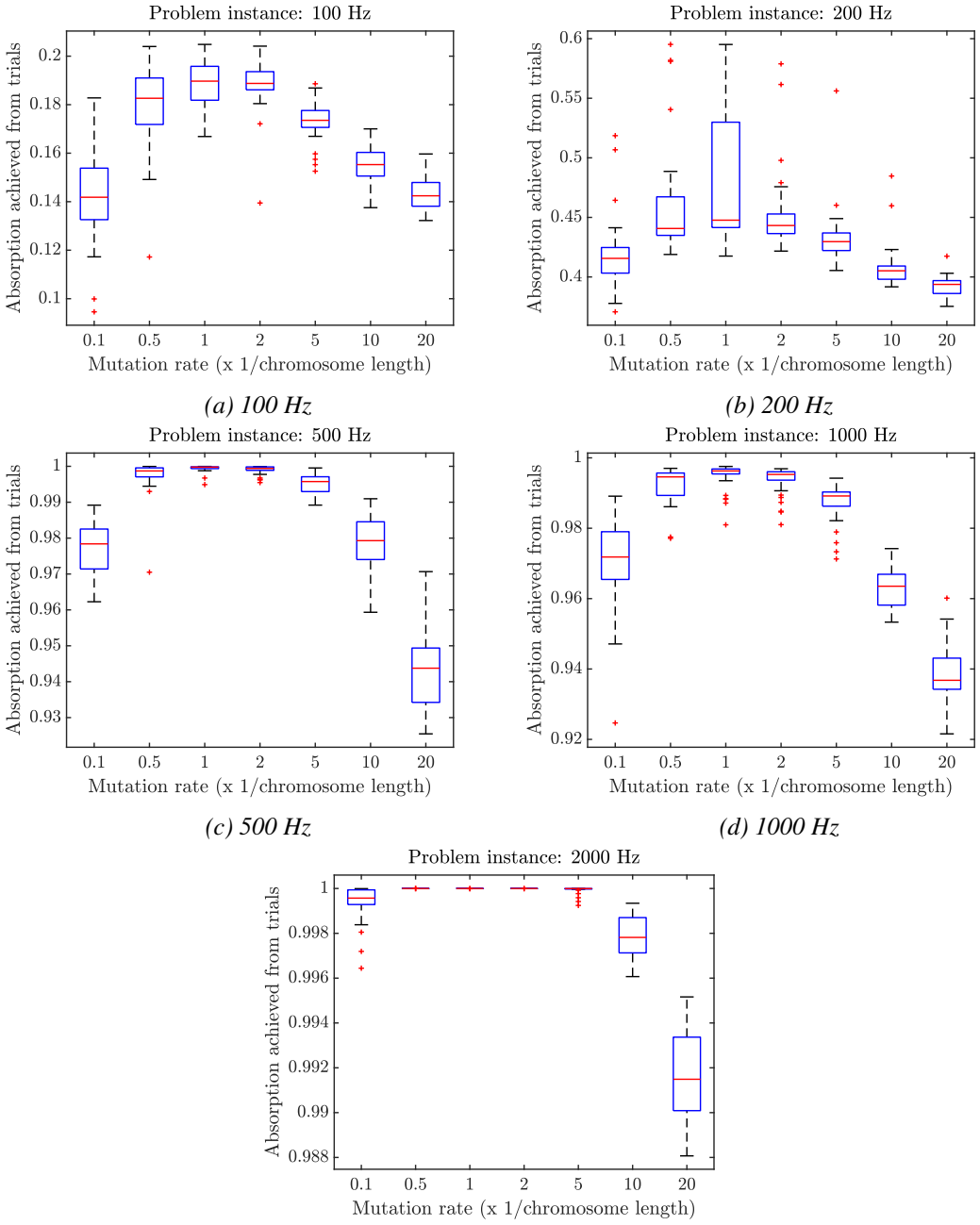

(a) 100 Hz

(b) 200 Hz

(c) 500 Hz

(d) 1000 Hz

(e) 2000 Hz

Figure 6.7: Effect of different mutation rates for a set of problem instances using five different absorption target frequencies, all 10×10 *grid size filled with low resistivity Melamine foam. At each mutation rate 31 trials were run and the distribution of the best fitnesses are shown. The boxes enclose first to third quartiles, the whiskers denote the span and the crosses are the outliers.*

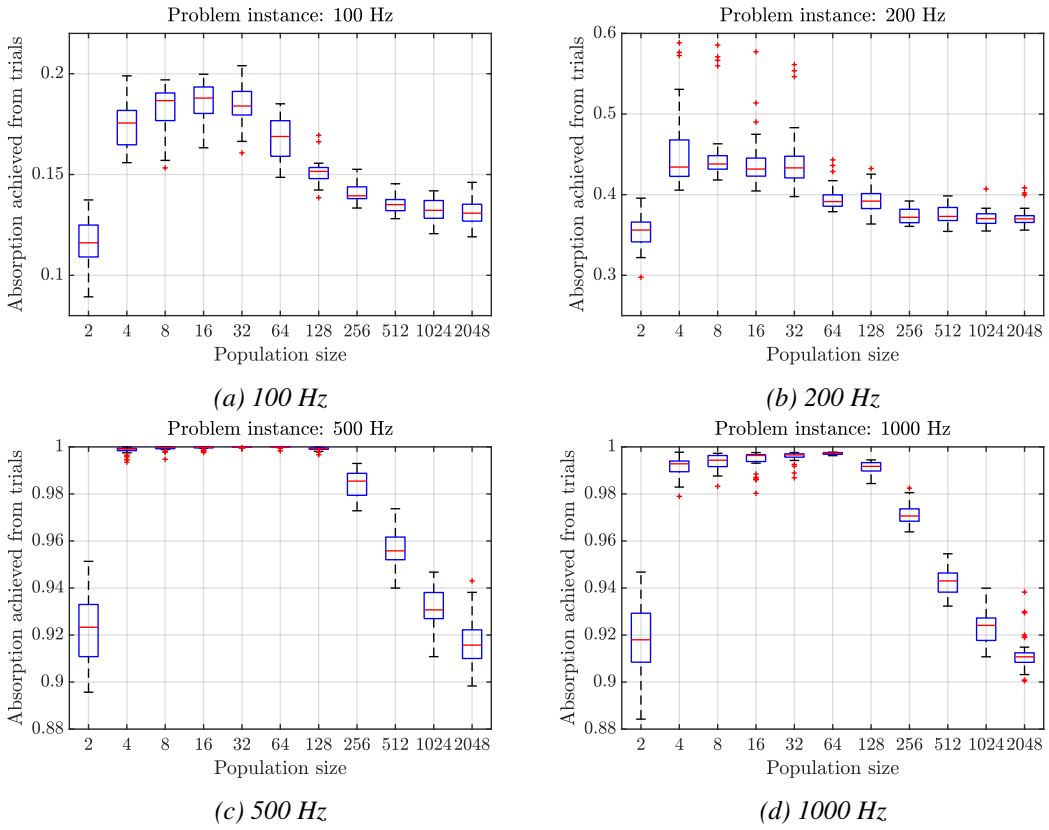

(a) 100 Hz *(b) 200 Hz*

(c) 500 Hz *(d) 1000 Hz*

Figure 6.8: Effect of initial population size in genetic algorithms for (a) 100 Hz, (b) 200 Hz, (c) 500 Hz and (d) 1000 Hz problem instances with the material filled being low resistivity Melamine. At each population size, 31 trials were run and the distribution of the best fitnesses are shown. The maximum function evaluation budget is 2048. The population size of 2048 corresponds to random search trials. The boxes enclose first to third quartiles, the whiskers denote the span and the crosses are the outliers.

length but with various population sizes. Considering population sizes {2, 4, 8, 16, 32, 64, 128, 256, 512, 1024, 2048}, the results with a total fitness evaluation budget of 2048 is studied. The initial population fitness evaluation is included in this budget and until the budget is used up, the genetic algorithms are continued. The distribution of best fitnesses from 31 trials of optimisation at every population size is plotted for a few problem instances in Figure 6.8. The results indicate that a population size of 32 or 64 gives better performance. Using an initial population size of 2048 with a fitness evaluation budget of 2048 is essentially random search as no more fitness evaluations would be allowed after the initial population is evaluated. Comparing the results for 2048 population size with other population sizes, we observe that genetic algorithms perform better than random search on this problem domain.

6.5.2 Tabu search (TABU)

Tabu search is a single point-based local search procedure, first proposed by Glover [88], which uses a high-level procedure that forbids reversing moves for a certain number of subsequent moves. That is, if a bit is flipped from 0 to 1, it will not be flipped back to 0 for a specified number of next moves. Using a forbidden list (tabu list) helps avoid getting stuck at the local optimum and cycling through the same set of solutions. The tabu moves are liberated from the tabu list after a set number of moves called the tabu tenure ($\mathcal{T}$). Here, a random binary initial solution $\boldsymbol{\chi}$ is generated. A tabu length array ($\mathbf{T}$) corresponding to the tabu period for each bit is initiated with zeros. In each step, a randomly chosen element χ_k is picked from those elements which are not tabu (i.e. $\mathrm{T}_k \neq 0$). If bit flipping the chosen element improves the solution, the move is accepted, and the chosen bit is made tabu for the next $\mathcal{T}$ iterations ($\mathrm{T}_k \leftarrow \mathcal{T}$). The tabu length of other bits with non-zero tabu lengths are decremented (i.e. $\mathrm{T}_j \leftarrow \mathrm{T}_j - 1 \; \forall \; j : j \neq k \; \& \; \mathrm{T}_j \neq 0$). A tabu tenure of 20% of the problem size ($\mathcal{T} = 20\%N$) is chosen for this implementation after testing several values. Pseudocode for this procedure is provided in Algorithm 14.

Algorithm 14: Tabu search for acoustic topology optimisation (TABU)

```
Generate initial solution χ ;
Initiate tabulist 𝒯 = {0}_{N×1};
Set tabu tenure t ;
Evaluate objective function ᾱ(χ);
while Termination criteria is not met do
    Generate non-tabu neighbour: χ′
    χ′ ← χ ;
    Pick k such that tabulist(k) = 0 ;
    Bitflip χ′_k ;
    if χ′ better than χ then
        Set χ ← χ′; Set f* ← f(χ′) ;
        Update tabulist 𝒯_k ← 𝒯_k + t;
    end
end
return χ* ← χ ;
```

Algorithm 15: Covariance matrix adaptation-evolution strategy (CMA)

Get finite element mesh, frequencies, material properties and other common parameters;
Initiate $\boldsymbol{\chi}_{mean} \leftarrow$ rand(N,1) , $\sigma \leftarrow 3$ and $B \leftarrow I_{N\times N}$;
Set population size, $\lambda \leftarrow 4 + \lfloor 3\log(N) \rfloor$;
Set strategy parameters for selection;
Set strategy parameters for Adaptation;
Initialize dynamic strategy parameters and constants;
Set $fevals \leftarrow 0$;
while $fevals < budget$ **do**
  for $k = 1, k <= \lambda, i++$ **do**
    $\boldsymbol{\chi}^{(k)} \leftarrow \boldsymbol{\chi}_{mean} + \sigma[B]D \times \texttt{randn}(N, 1)$;
    for $i = 1, i <= N, i++$ **do**
      if $\chi_i^{(k)} < 0$ **then**
        $\chi_i^{(k)} = 0$;
      end
      if $\chi_i^{(k)} > 1$ **then**
        $\chi_i^{(k)} = 1$;
      end
    end
    Assemble FE system matrices;
    Evaluate absorption $\alpha(\boldsymbol{\chi}^{(k)})$;
    Set $fevals \leftarrow fevals + 1$;
    Set $f(\boldsymbol{\chi}^{(k)}) = 1 - \alpha(\boldsymbol{\chi}^{(k)})$;
  end
  Sort and compute weighted mean into $\boldsymbol{\chi}_{mean}$;
  Cumulation: Update evolution paths;
  Adapt covariance matrix $[C]$;
  Adapt step size σ;
  Decomposition of $[C]$ into $[B]\texttt{diag}([D]^2)[B]'$;
  Update best shape $\boldsymbol{\chi}^* \leftarrow$ best$(\boldsymbol{\chi}^*, \boldsymbol{\chi}^{(k)})$
end
return Best $\boldsymbol{\chi}^*$;

Algorithm 16: Discrete variant of CMA-evolution strategy (CMAd)

Get finite element mesh, frequencies, material properties and other common parameters;
Initiate $\boldsymbol{\chi}_{mean} \leftarrow$ rand(N,1) , $\sigma \leftarrow 3$ and $B \leftarrow I_{N\times N}$;
Set population size, $\lambda \leftarrow 4 + \lfloor 3\log(N) \rfloor$;
Set strategy parameters for selection;
Set strategy parameters for Adaptation;
Initialize dynamic strategy parameters and constants;
Set $fevals \leftarrow 0$;
while $fevals < budget$ **do**
  for $k = 1, k <= \lambda, i++$ **do**
    $\boldsymbol{\chi}^{(k)} \leftarrow \boldsymbol{\chi}_{mean} + \sigma[B]D \times \texttt{randn}(N, 1)$;
    for $i = 1, i <= N, i++$ **do**
      if $\chi_i^{(k)} < 0$ **then**
        $\chi_i^{(k)} = 0$;
      if $\chi_i^{(k)} > 1$ **then**
        $\chi_i^{(k)} = 1$;
    Assemble FE system matrices;
    Evaluate absorption of rounded solution $\overline{\alpha}(\lfloor \boldsymbol{\chi}^{(k)} \rceil)$;
    Set $fevals \leftarrow fevals + 1$;
    Set $f(\boldsymbol{\chi}^{(k)}) = 1 - \overline{\alpha}(\lfloor \boldsymbol{\chi}^{(k)} \rceil)$;
  Sort and compute weighted mean into $\boldsymbol{\chi}_{mean}$;
  Cumulation: Update evolution paths;
  Adapt covariance matrix $[C]$;
  Adapt step size σ;
  Decomposition of $[C]$ into $[B]\texttt{diag}([D]^2)[B]'$;
  Update best shape $\boldsymbol{\chi}^* \leftarrow$ best$(\boldsymbol{\chi}^*, \boldsymbol{\chi}^{(k)})$
return Best $\boldsymbol{\chi}^*$;

6.5.3 Covariance-matrix-adaptation evolution strategy (CMA)

Covariance matrix adaptation-evolution strategy is a state-of-the-art black-box optimisation algorithm for continuous optimisation which has outperformed many other evolutionary algorithms in hundreds of applications [99] (black-box means that it only uses the result of the fitness evaluation, and does not use the internal structure of the fitness, in particular, does not use derivatives). CMA-ES constructs a multivariate Gaussian response surface by iteratively sampling points in the search space and adapting the covariance matrix of the multivariate Gaussian to perform the search. The Matlab implementation for CMA-ES provided by Hansen [100] is adapted for performing topology optimisation. The full algorithm and procedure are not discussed in this thesis as it can be found in numerous others. The pseudocode for topology optimisation using CMA-ES is provided in Algorithm 15.

In this application, the unconstrained CMA-ES was modified to include upper and lower limit constraints on the design variables. To ensure χ_i is not below 0 or above 1, after the CMA-ES samples points within the N dimensional hypercube ($\chi_i \in [0,1] \quad \forall \quad i \in 1...N$), the values below 0 are forced to be equal to 0 and the values above 1 are forced to be equal to 1.

In the implementation, the strategy parameters and constants are adopted from the Matlab code by Hansen [100]. The lines 24-28 in the pseudocode 15 are elaborated in the paper by Hansen [100]. In the pseudocode, $I_{N\times N}$ is the identity matrix of size $N \times N$ and λ is the population size. The expression randn$(N,1)$ generates a vector of random numbers of size N from the standard normal distribution. The function diag() returns the elements in the leading diagonal of a square matrix.

The CMA-ES solutions did not result in 0 or 1 shapes in most trials despite using the recommended value for the material interpolation penalty ($p = 3$). Many elements had χ_i between 0 and 1 which correspond to intermediate materials between air and the porous material. Since intermediate materials are not physically realistic, a simple round-off filter was used $\overline{\boldsymbol{\chi}^*} = \lfloor \boldsymbol{\chi}^* \rceil$. The rounding filter is expressed in equation 6.53. An illustration of rounding the best shape from one of the trials is provided in Figure 6.9. Rounding off optimised solutions after termination of the algorithm can result in a small reduction or increase in absorption values. To ensure fairness, the comparison will be made only with rounded solutions from continuous algorithms.

$$\overline{\boldsymbol{\chi}^*} = \text{round}(\boldsymbol{\chi}^*) = \lfloor \boldsymbol{\chi}^* \rceil = \{\lfloor \chi_1^* \rceil \, , \lfloor \chi_2^* \rceil \, ..., \lfloor \chi_i^* \rceil \, ..., \lfloor \chi_N^* \rceil\}^T \tag{6.53}$$

$$\lfloor x \rceil = \begin{cases} 0 & \text{when} \quad 0 < x \leq 0.5 \\ 1 & \text{when} \quad 0.5 < x \leq 1 \end{cases} \tag{6.54}$$

6.5.4 Discrete variant of CMA evolution strategy (CMAd)

In this variant of the CMA evolution strategy, the sampled continuous solutions are rounded to discrete solutions *before* evaluating the fitness function. The procedure is the same as CMA except that the fitness function is $\overline{\alpha}(\lfloor \boldsymbol{\chi} \rceil)$ instead of $\overline{\alpha}(\boldsymbol{\chi})$, where $\lfloor \cdot \rceil$ is the round operator. Even though CMA searches in the continuous space, since the evaluated solutions are always discrete, CMAd essentially searches in the discrete solution space. The best solution returned in the end is the rounded continuous solution ($\lfloor \boldsymbol{\chi}^* \rceil$). Pseudocode for this procedure is provided in Algorithm 16

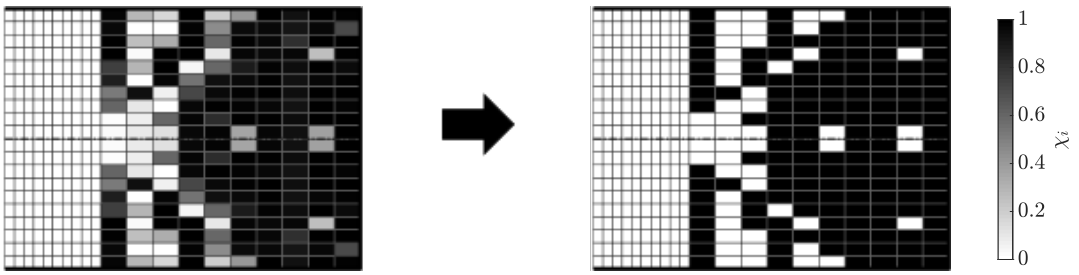

Figure 6.9: An illustration of rounding best shape from trial 14 of CMA to get 0 or 1 shapes on problem instance 1. The values 0 *and* 1 *correspond to air and porous material respectively, and the greys correspond to intermediate materials.*

6.5.5 Differential evolution (DE)

Algorithm 17: Differential evolution (DE) adapted to topology optimisation

```
χ^j ←Generate Initial Population;
Evaluate their Fitnesses ᾱ_j ← ᾱ(χ^j);
while fevals < budget do
    for j = 0, j = length[pop], j++ do
        Randomly select a, b, c from pop;
        y ← a + F × (b − c);
        for i = 0, i = length[χ^j], i++ do
            if rand <CrossoverRate then
                y_i ← χ^j_i;
            end
        end
        Evaluate ᾱ(y);
        if ᾱ(y) is better than ᾱ(χ) then
            Replace χ^j ← y
        end
        Keep track of the best solution χ*;
    end
end
return χ*;
```

Differential evolution is a population-based metaheuristic for real-valued optimisation introduced by Price and Storn [232, 233]. An introduction to DE is provided in chapter 2 and hence not repeated here. Topology optimisation is a unique problem with very large number of decision/design variables and the performance of DE on such problem is not fully explored. In topology optimisation, variations within a design variable are not important and a real-valued optimisation across one of the design variables is a futile exercise as this corresponds ultimately to the binary decision. However, there is benefit to using DE such as the fact that the difference vector is an efficient way to move multiple variables simultaneously, which could help in convergence.

To apply DE in topology optimisation, an initial population of random real-valued solutions representing the design variables ($\boldsymbol{\chi}$) are generated. For every member of the population $\mathbf{x}$, three other unique members $\mathbf{a}, \mathbf{b}, \mathbf{c}$ apart from $\mathbf{x}$ are chosen randomly from the population. A new member $\mathbf{y}$ is obtained by a simple formula such as $\mathbf{y} = \mathbf{a} + F \times (\mathbf{b} - \mathbf{c})$ where $F \in [0, 2]$ is the differential weight. For all $i \in \{1, 2, ...N\}$, with a cross over probability CR $\in [0, 1]$, $\mathrm{y}_i \leftarrow \mathrm{x}_i$ is set. The objective function is evaluated for $\mathbf{y}$ and if it is an improving move, then $\mathbf{x}$ is replaced. This process is repeated until the function evaluation budget is reached. Algorithm 17 provides a pseudocode for the implementation in the context of topology optimisation.

Parameter tuning

To tune the parameters used in differential evolution, tests were performed on a sample problem instance using various initial population sizes, CR and F values. For this, the problem instance 7 was considered, and several trials of DE are run. The results as shown in Figure 6.10 indicate that a population size of 32 lead to better performance, and that CR and F values do not play a significant effect.

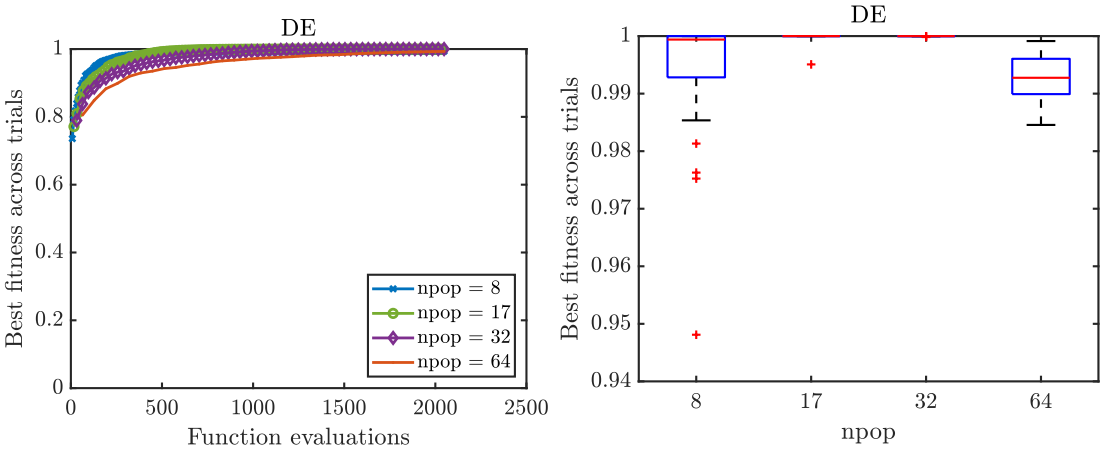

(a) Parameter tuning on population size npop

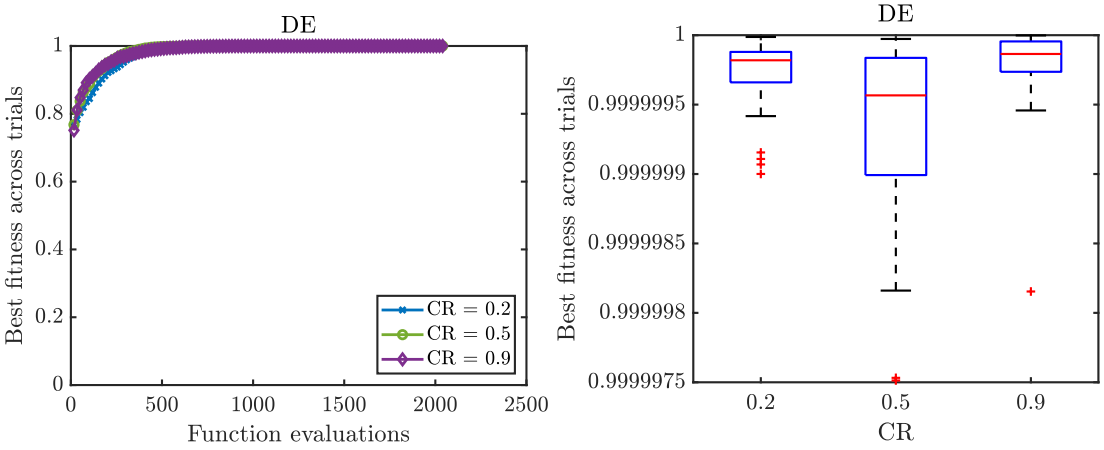

(b) Parameter tuning crossover rate CR

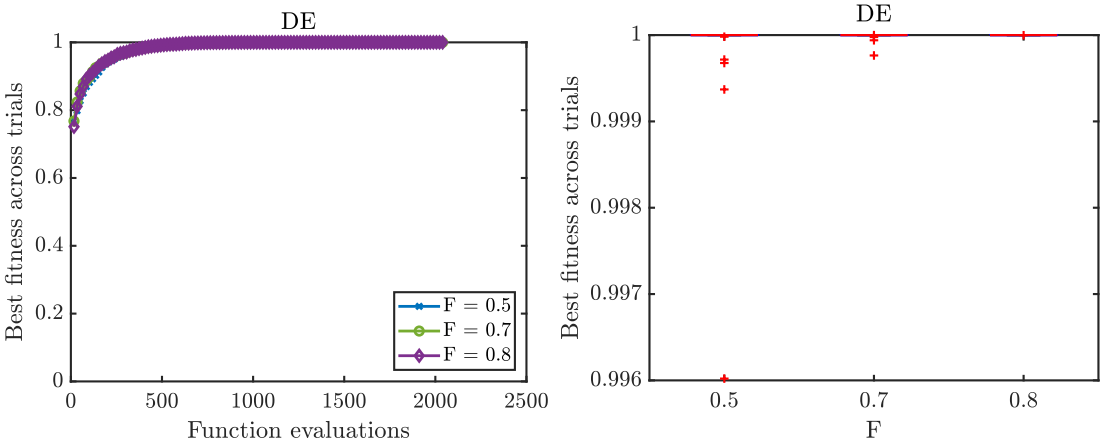

(c) Parameter tuning F

Figure 6.10: Differential evolution parameter tuning studies.

6.5.6 Discrete variant of differential evolution (DEd)

The discrete variant of differential evolution (DEd) is similar to DE except that a round-off filter discretises all solutions before the objective function is evaluated. Even though the algorithm searches in the continuous space $(\boldsymbol{\chi} : \chi_i \in [0, 1])$, the objective function optimised for is the rounded solution $\overline{\alpha}(\lfloor \boldsymbol{\chi} \rceil)$. Thus, DEd is essentially finding solutions in the discrete search space. The best solution returned is the rounded continuous solution $(\lfloor \boldsymbol{\chi}^* \rceil)$. Pseudocode for

this implementation is provided in Algorithm 18.

Algorithm 18: Differential evolution-discrete variant (DEd)

$\boldsymbol{\chi}^j \leftarrow$Generate Initial Population;
Evaluate their Fitnesses $\overline{\alpha}_j \leftarrow \overline{\alpha}(\lfloor \boldsymbol{\chi}^j \rceil)$;
while $fevals < budget$ **do**
  for $j = 0$, $j = length[pop]$, $j++$ **do**
    Randomly select $\boldsymbol{a}, \boldsymbol{b}, \boldsymbol{c}$ from pop;
    $\boldsymbol{y} \leftarrow \boldsymbol{a} + F \times (\boldsymbol{b} - \boldsymbol{c})$;
    for $i = 0$, $i = length[\boldsymbol{\chi}^j]$, $i++$ **do**
      if $rand <$*CrossoverRate* **then**
        $y_i \leftarrow \chi_i^j$;
      end
    end
    Evaluate $\overline{\alpha}(\lfloor \boldsymbol{y} \rceil)$;
    if $\overline{\alpha}(\lfloor \boldsymbol{y} \rceil)$ *is better than* $\overline{\alpha}(\lfloor \boldsymbol{\chi} \rceil)$ **then**
      Replace $\boldsymbol{\chi}^j \leftarrow \boldsymbol{y}$
    end
    Keep track of the best solution $\boldsymbol{\chi}^*$;
  end
end
return $\boldsymbol{\chi}^*$;

6.6 Results and discussion

6.6.1 Run time performance comparison

One of the desired aspects of a good topology optimisation strategy is the ability to find better quality solutions in a limited CPU time. Figure 6.11 compares the progress of the best-so-far absorption values ($\overline{\alpha}$) obtained versus CPU time used by various algorithms on problem instance 6. Multiple machines were used to run the optimisation tests, and in order to remove the machine dependence on runtime in Figure 6.11, the best-so-far absorption values are tracked against the number of function evaluations. The runtimes are then computed by using average time per function evaluation clocked on a reference machine. The reference machine used features an Intel(R) Core(TM) i7-3820 CPU 3.6 GHz processor, 32 GB RAM and a 64-bit Windows 10 operating system running Matlab2019b [161]. Scales indicating the number of function evaluations are also provided for benchmarking purposes. For all non-deterministic algorithms, as multiple trials are run, the absorption values are averaged across the 31 trials after each generation of the algorithm as illustrated in Figure 6.12.

In Figure 6.11, firstly, note that initial absorption levels are different for the algorithms. While the discrete algorithms HC, GA, TABU, CMAd and DEd are initiated from random discrete solutions with $\overline{\alpha}$ around 0.71, the continuous algorithms CMA, DE, SIMPf0 and SIMPf2 are initiated from random continuous solutions with $\overline{\alpha}$ around 0.65. CH2 starts from fully porous design domain with $\overline{\alpha}$ around 0.84 and CH1 starts from an empty (air-filled) design domain with no absorption.

One of the first things to note is that the CH2 does not produce an improvement from the fully

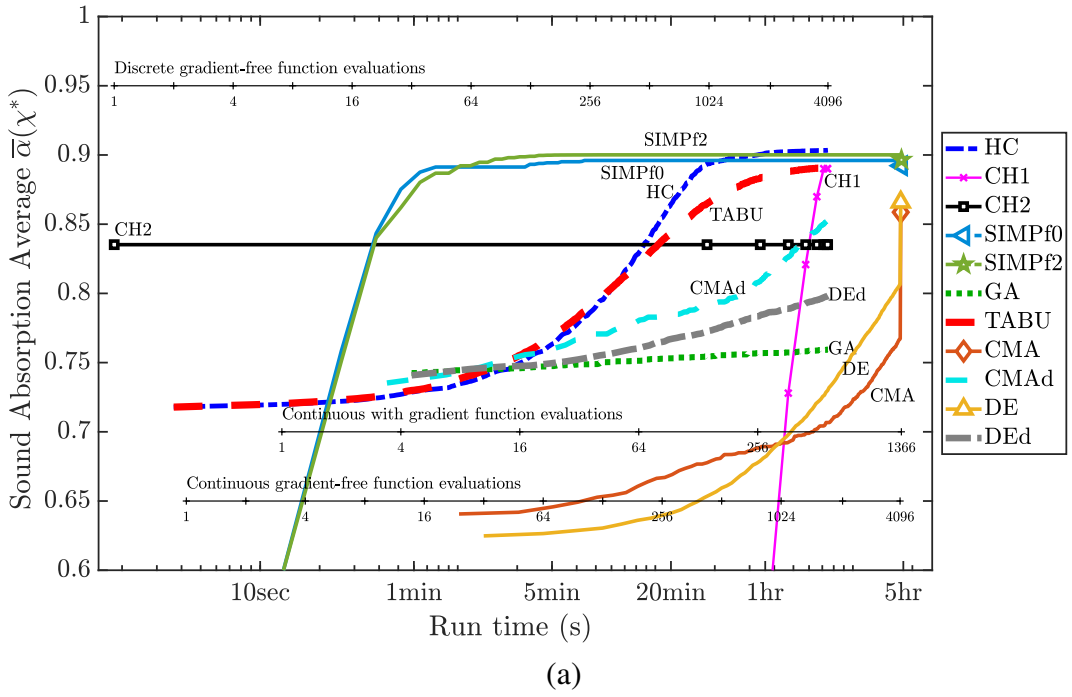

(a)

Figure 6.11: Run time progress of best absorption found (trial-averaged) for problem instance 6.

porous-filled solution and hence the best-so-far absorption value stays the same for this problem. For low CPU-time budgets (up to under half a minute), SIMPf0 and SIMPf2 produce higher quality solutions than all the other algorithms except CH2. SIMPf0 and SIMPf2 converge to a higher absorption than the porous-filled CH2 solution in under 5 minutes on this problem instance highlighting that gradient-based methods can be time-efficient. After about 20 minutes of runtime, HC produces better solutions on average than SIMP, but the difference is small.

After the designated budget (4096 gradient-free function evaluations or 1366 gradient-included function evaluations), HC, SIMPf2, TABU, SIMPf0 and CH1 produce the top tier solutions. CMAd follows closely by producing slightly better-quality solutions compared to fully filled CH2 solution towards the end. Whereas for DEd and GA, the runtime performance was considerably poor.

It is important to appreciate that the solutions from continuous algorithms (CMA, DE, SIMPf0 and SIMPf2) consider intermediate materials, whereas the discrete algorithms consider only porous material or air solutions. Since the solutions are from different search spaces, the absorption levels may not be directly compared between the two. Although, the final shapes from continuous algorithms are desired to be 0 or 1, they are often not. Hence, they are forced to be discrete using a simple round-off filter, and the absorption values are recomputed. Such rounding leads to a drop or surge in the absorption values at the end of all continuous algorithms as can be observed noticeably in CMA and DE plot lines in Figure 6.11. The rounded absorptions indicated by the end markers are also trial-averaged. Rounding leads to no significant changes in SIMPf0 and SIMPf2 solutions for this problem instance. For CMA and DE, the rounded-solution absorption values were poorer to that of SIMP solutions.

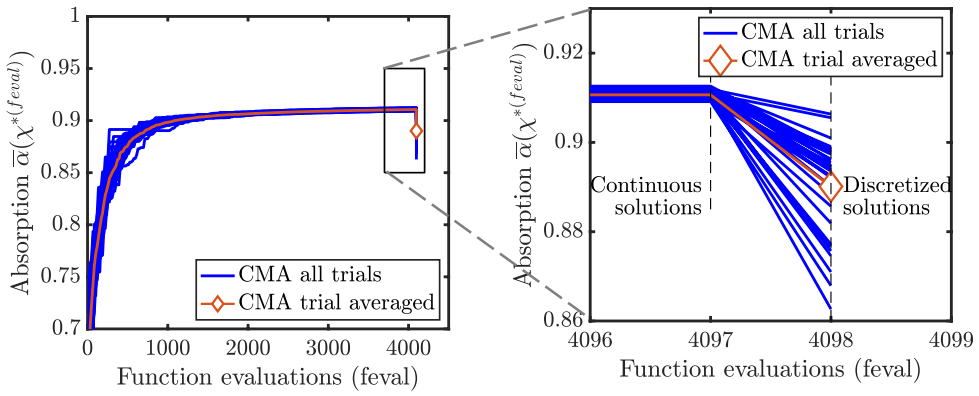

Figure 6.12: An illustration of trial averaging. The blue lines indicate the best-so-far absorption values from CMA in each trial for problem instance 1. These values are averaged to obtain the orange line. After the shapes are discretised, the absorption values are recomputed, and in this case they reduce slightly. Only such trial-averaged plot lines are shown in Figure 6.11 and 6.13.

The above behaviour of continuous algorithms does not seem to be the general trend across all problem instances. When considering the runtime performance of problem instance 1 shown in Figure 6.13, SIMP algorithms produce final solutions with intermediate materials which when rounded result in a significant reduction in absorption. This behaviour is also prominent in other problem instances especially the one with the high resistivity material (problem instance 3).

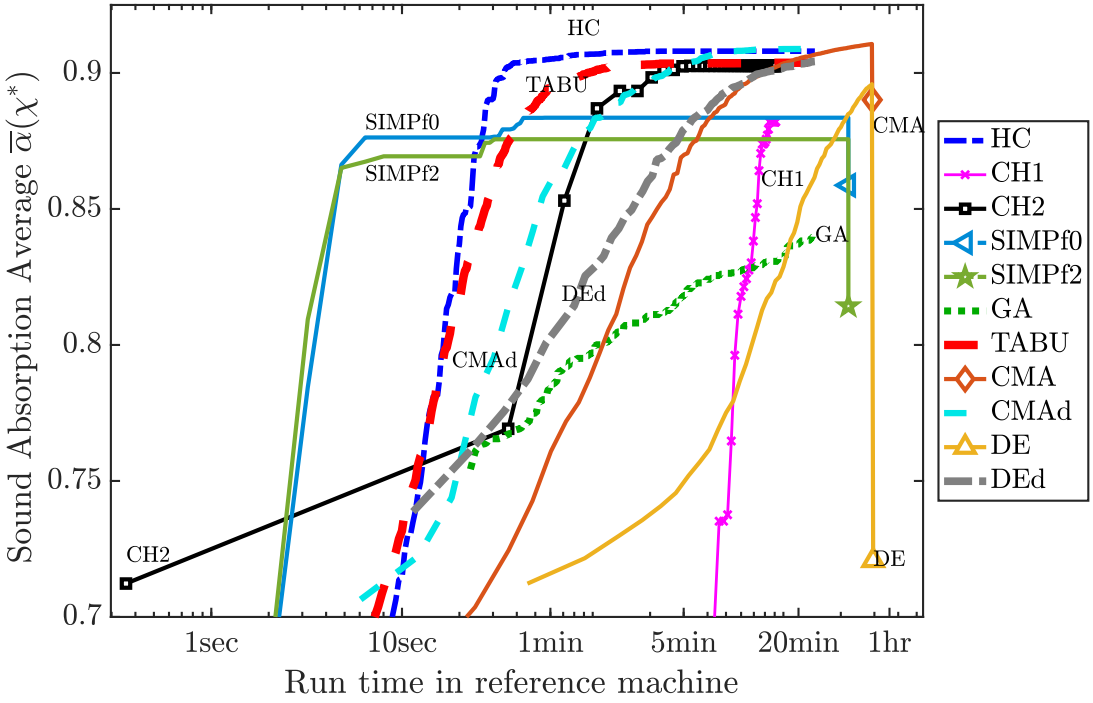

Figure 6.13: Progress of best absorption found vs. runtime: problem instance 1.

6.6.2 Final solution quality comparison

After rounding the continuous algorithm solutions and re-evaluating absorption, the distribution of final absorption values are shown in Figure 6.14. What is interesting to note is that for non-

deterministic algorithms, the 31 trials do not necessarily result in the same optimised shapes and the final absorption values are spread out. The boxes enclose first to third quartiles (i.e. 25 percentile to 75 percentile), the whiskers denote the span, and the crosses denote the outliers.

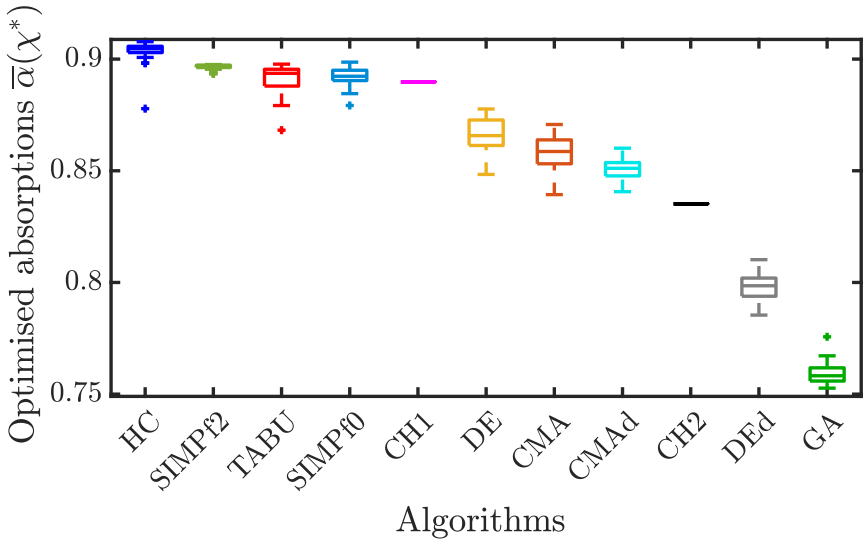

Figure 6.14: Distribution of best-solution absorption across trials for problem instance 6.

Often in practice, a particular topology optimisation strategy may be chosen, and one trial may be run to determine a near-optimal shape. In such cases, it is desirable to pick an algorithm that has the best median-performance across trials. Hence, using the median absorption across trials, the algorithms are sorted best to worst from left to right in Figure 6.14 for problem instance 6. HC and SIMPf2 turn out to be the top performing algorithms for this problem instance followed by TABU, SIMPf0 and CH1 in the second tier. DE, CMA and CMAd follow with all trials producing better solutions than the fully-filled CH2 solution. DEd and GA performed the poorest with no trials producing better than the fully-filled solution. The best fitness distribution for other problem instances are provided in the appendix B.2.

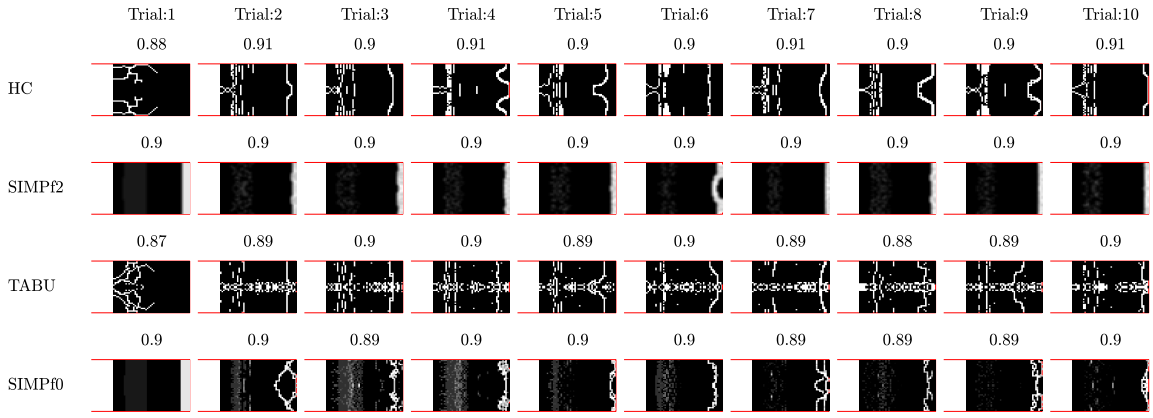

Figure 6.15: Impact of trials on the shapes produced from the top four algorithms for problem instance 6. A common attribute in these shapes is a thin air layer close to the rigid wall.

The shapes produced from 10 of the 31 trials from the top four algorithms are displayed in Figure 6.15. Most shapes seem to have a thin layer of air near the rigid backing as this allows removing elastic resonance around 500 Hz as can be observed from the absorption curves in Figure 6.16. Note that without filtering, SIMPf0 produces intricate designs near this thin air strip compared to SIMPf2.

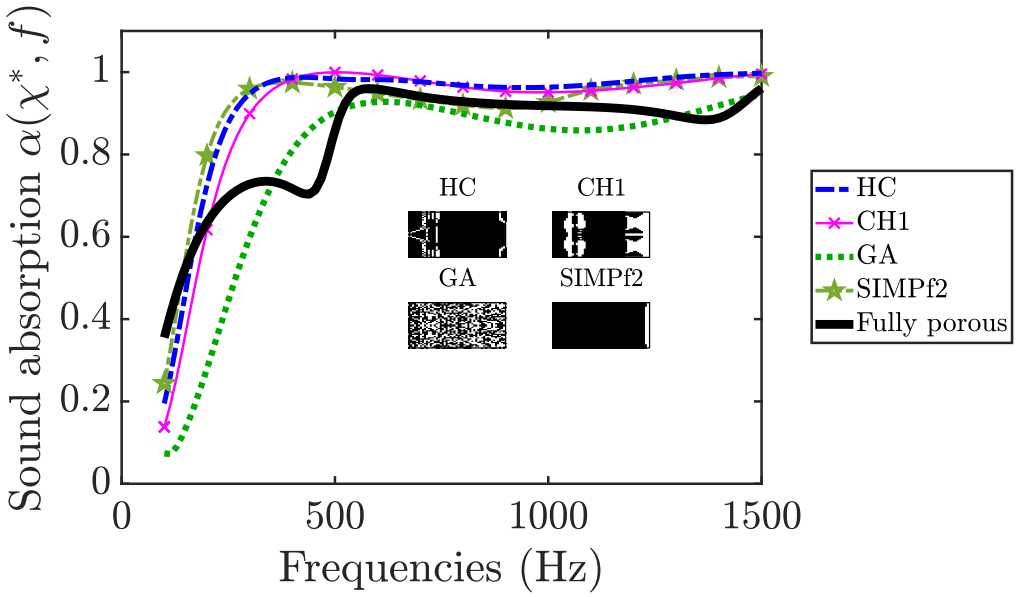

Figure 6.16: Sound absorption curves of optimal shapes from four selected algorithms for problem instance 6.

6.6.3 Performance across problem instances

For an overall comparison, the ranking is extended to other problem instances in Table 6.5. Such a comparison across many problem instances is essential as algorithms performing well on one problem instance need not necessarily perform well on other problem instances. The ranking scheme is such that if the median absorption values of two or more algorithms are the same correct to two decimal places, they are assigned the same rank. This ranking is only provided for a quick summary of the optimisation tests, and it is emphasised that the ranks may not be the same for a different set of problem instances.

Table 6.5: The algorithms are ranked based on median values of optimised shape absorption ($\overline{\alpha}*$) across trials. Lower the average rank, the better is the performance of the algorithm. Algorithms are sorted based on the average of the ranks across problem instances. This ranking scheme is provided for a quick look up only and not meant to be a precise indicator of the performance. The ranking could change if more problem instances and algorithms are considered.

Ranks	Problem instances →							Avg. rank
Algorithms ↓	1	2	3	4	5	6	7	
HC	**1**	**1**	3	**1**	**1**	**1**	**1**	**1.29***
CMAd	**1**	3	**1**	**1**	4	8	**1**	2.71
CH1	7	**1**	8	**1**	**1**	3	**1**	3.14
TABU	**1**	5	4	8	7	3	**1**	4.14
CH2	5	6	4	**1**	4	9	**1**	4.29
SIMPf0	8	3	10	**1**	4	3	9	5.43
SIMPf2	10	6	11	**1**	**1**	**1**	11	5.86
DEd	**1**	9	2	10	9	10	**1**	6
CMA	6	6	4	8	9	7	8	6.86
DE	11	11	9	**1**	7	6	9	7.71
GA	9	10	4	11	11	11	**1**	8.14

From Table 6.5, one can observe that HC, CMAd and CH1 rank among the top three in terms of the averaged rank. Although SIMPf0 and SIMPf2 performed well on problem instance 6 from Figure 6.11, they take respectively the 6^{th} and 7^{th} places overall. Surprisingly, the simple first-improvement hill climbing (HC) ranks among the best in all problem instances except the high-resistivity material instance (problem instance 3). This means that HC's potential can be exploited by using it in hybrid algorithms. CMAd and CH1 ranked first in four problem instances. Although CMAd ranked 8^{th} in problem instance 6, its overall performance across the problem instances puts the algorithm in the second place. Notably, in problem instance 3, which considers a high static airflow resistivity material, CMAd performed the best. This problem instance likely has many local optima and the performance of CMAd indicates its global topology optimisation potential. The poor performance of the SIMP algorithms in this problem instance is likely due to the multi-modality of the objective function and premature convergence to local optima. Although the progress of absorption in the initial stages of CH1 is slow compared to the other algorithms, the final absorption value makes CH1 one of the best algorithms. Notably, for many problem instances considered, the best absorption value from CH1 is higher than the absorption of the discretised solutions from both SIMPf0 and SIMPf2. CH1 seems to be better overall compared to CH2, indicating that constructing the solution from scratch may be better than removing material from a fully-filled solution. Performance of CMA and DE were relatively poor in this benchmark. One reason could be that the number of design variables is large and these strategies do not exploit the correlation of the neighbouring-element design variables, a special attribute in topology optimisation problems. Both CMAd and DEd seem to perform better than CMA and DE in general, indicating that rounding during the algorithm may be a better approach than rounding the solutions after the termination of continuous algorithms. While CMAd ranked among the top, the performance of DEd was similar to that of SIMP in terms of solutions quality. Among the algorithms considered, GA performed the poorest. Though, scope for improvement exists in terms of using better mutation and crossover operators adapted to topology optimisation [115, 135, 268], focus may be diverted to other strategies which show better promise.

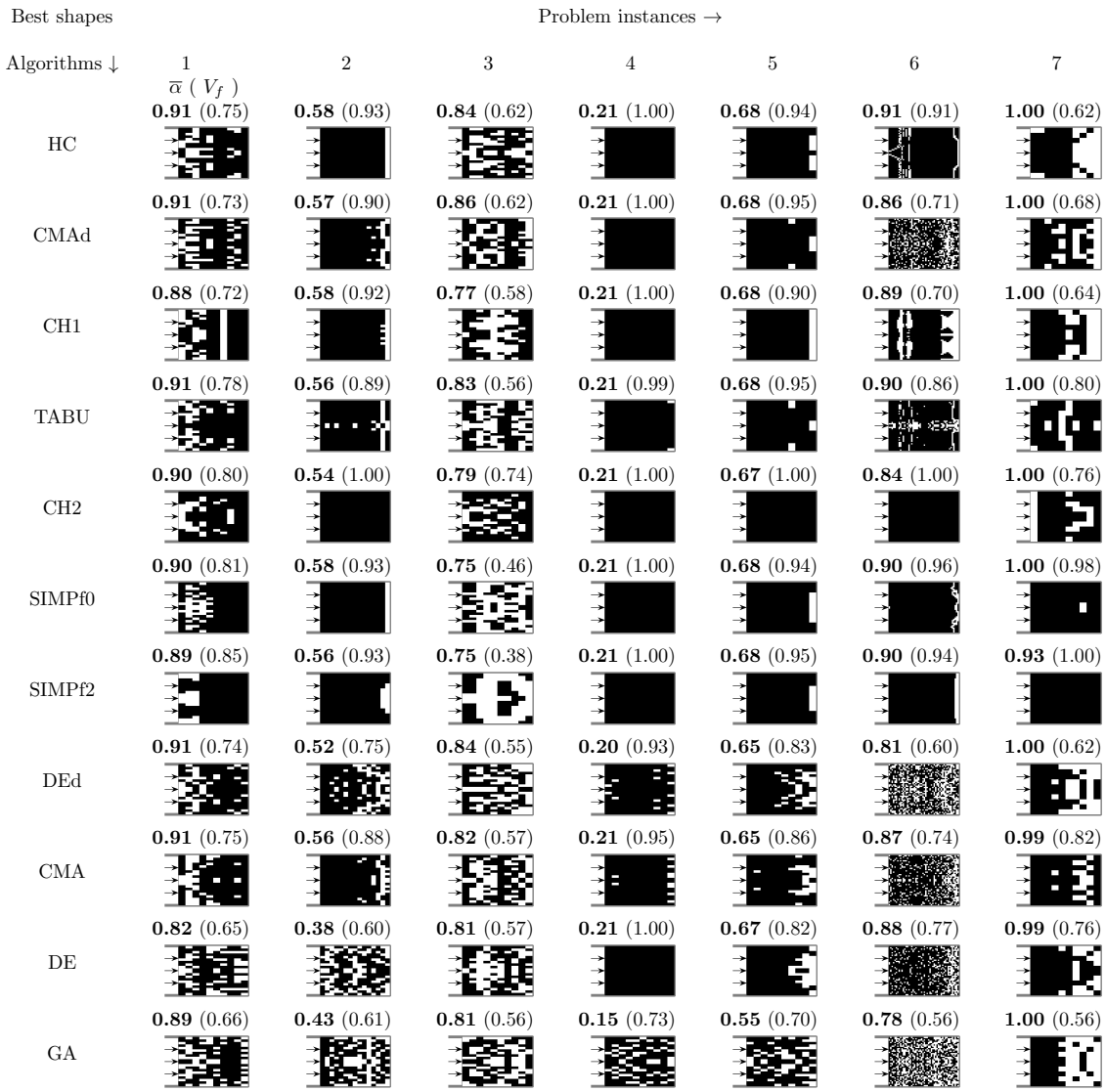

Figure 6.17: Optimised shapes obtained from all algorithms for each problem instance. The shapes are discretised by rounding for continuous algorithms. The values of mean absorption across frequencies ($\overline{\alpha}$) are printed at the top of each shape in bold font along with porous material volume fraction (V_f) in parentheses. White and black represent air and the porous, respectively, with the acoustic input on the left and rigid backing on the right.

6.6.4 Best shapes obtained from algorithms

The best solutions from all the algorithms for all problem instances are plotted in Figure 6.17. For non-deterministic algorithms, the solution with the highest absorption among the 31 trials is shown. It is recalled that manufacturability restrictions and morphological filters are not imposed in this study except for SIMPf2. Results show both SIMPf0 and SIMPf2 produce similar shapes for most problem instances.

For problem instance 1, all algorithms except SIMPf2 result in irregular shapes. The best quality shapes from most algorithms are flat layers of air and porous material towards the rigid wall with a somewhat circular air cavity in the front. GA and DE produced checker-box-like shapes. Moreover, shapes from GA for all problem instances are degenerate.

For problem instance 2, HC, CH1 and SIMPf0 produce the best shape with an almost porous material-filled design domain except for a layer of air next to the rigid wall. CH1, SIMPf2, CMA, CMAd, TABU produced similar shapes. CH2 resulted in a fully-filled shape with slightly less absorption.

In problem instance 3 which fills a high static airflow resistivity material, the shapes from all algorithms were seemingly random patterns but with sort of a cavity in the centre. SIMPf2 produces a result with a chunk of porous material suspended in air.

For problem instance 4, the optimal solution seems to be a fully-filled design domain and most algorithms are able to find this except for GA. The reason could be that GA is initiated from random bit arrays which would have volume fraction distributed near 50 percent (central limit theorem). Thus, initialising GA with solutions with a range of volume fractions might be a sounder approach.

For problem instance 5, many algorithms find a solution with a shape almost filled with the porous material except for air pockets near the rigid wall. CMA, DE and DEd seem to be approaching this solution. CH2 completely fills the design domain with the porous material.

For problem instance 6, the fully-filled solution has an elastic resonance in the frequency range considered, as may be seen from Figure 6.16. The elastic resonance forms a drop in the absorption near 500 Hz. The best solutions from different algorithms effectively remove this resonance. To do this, the algorithms seem to introduce air layers at the front and near the rigid backing. CMA, CMAd, DE and DEd give checker-board shapes which somewhat removes a layer near the rigid backing. Notably, CH1 gives a smooth shape even though no manufacturability restrictions were imposed. CH2 returns a filled design domain and is unable to get rid of the resonance.

For problem instance 7, many solutions have close to complete sound absorption ($\overline{\alpha} = 1$). Almost all algorithms find solutions with total sound absorption at 500 Hz. Notably, SIMPf0 and SIMPf2 seem to suggest a fully-filled solution.

In general, the algorithms which feature random move operations tend to produce degenerate shapes. Although hill climbing results in shapes with high sound absorption, the shapes obtained are sometimes irregular and need additional filtering. On the other hand, constructive heuristic with material addition (CH1) has both high performance and finds shapes with

smoother boundaries.

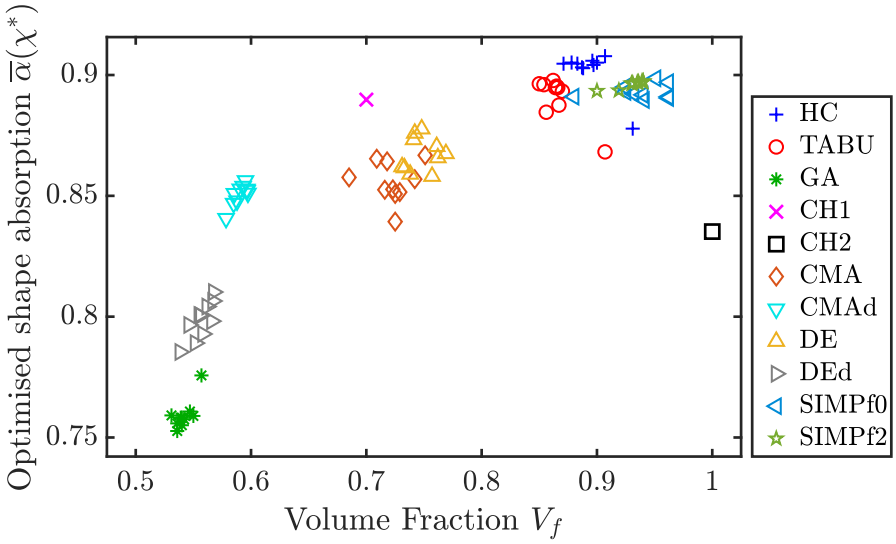

Figure 6.18: Absorption vs. volume fraction of optimal shapes for problem instance 6. For other problem instances refer Appendix B.

In summary, different algorithms seem to provide solutions from a unique pool. Figure 6.18 shows the distribution of final solutions in the absorption versus volume fraction plot. It may be observed that the solutions from various algorithms form clusters in specific regions. Again, this trend is not universal across problem instances. Plots for other problem instances are included in the appendix B.3. The reason for this is that each of the approaches use unique move operations during the optimisation. Thus it may be worth exploring various optimisation strategies to find unique solutions which may be of interest to the acoustic engineer. In addition, there exists significant scope for improving many of these methods. As an example, the performance of SIMP could be improved by using better strategies for avoiding local optima, and an appropriate morphological filter may be used in CMAd to overcome the drawback of producing unconnected shapes while speeding up the algorithm. The results outlined in this chapter provide an initial understanding of how various heuristics and metaheuristics perform on topology optimisation for absorption maximisation. Thus, guidelines for developing hybrid algorithms and hyperheuristics may be arrived at for devising more time-efficient strategies that also produce solutions closer to the true optima.

6.6.5 Statistical test: Wilcoxon signed-rank test

When sampling a set of values from the same distribution, we may obtain different results for the mean and standard deviation for the sampled sets when the sampling is repeated. These differences will tend to be higher for smaller sample sizes. When comparing two algorithms using the absorption values from various trials, it is of interest to know that any differences observed are significant or could happen due to random chance. In order to ensure that differences carry statistical significance, a Wilcoxon signed-rank test can be used. A null hypothesis that the distributions of the optimised absorption values from a chosen pair of algorithms are from the same distribution is assumed. Assuming that the optimised absorption values from each algorithm are normally distributed, we can estimate the probability (p-value) that two samples are indeed from the same distribution. A lower p-value suggests that there might be a significant difference in the distributions from which the best absorption values have been sampled. The null hypothesis

can be rejected if the p-value is low beyond a specific value. For a 95% confidence level, a p-value below 0.05 would suggest statistical significance of pairwise differences.

Table 6.6: Wilcoxon signed-rank test: p-values for problem instance 6.

	HC	TABU	GA	CH1	CH2	CMA	CMAd	DE	DEd	SIMPf0	SIMPf2
HC	-										
TABU	1.174e-06	-									
GA	1.174e-06	1.174e-06	-								
CH1	2.112e-06	**0.0548**	1.174e-06	-							
CH2	1.174e-06	1.174e-06	1.174e-06	1	-						
CMA	1.174e-06	1.174e-06	1.174e-06	1.174e-06	1.174e-06	-					
CMAd	1.174e-06	1.174e-06	1.174e-06	1.174e-06	1.174e-06	5.887e-05	-				
DE	1.174e-06	1.296e-06	1.174e-06	1.174e-06	1.174e-06	0.001142	1.578e-06	-			
DEd	1.174e-06	1.174e-06	1.174e-06	1.174e-06	1.174e-06	1.174e-06	1.174e-06	1.174e-06	-		
SIMPf0	8.651e-06	**0.4684**	1.174e-06	0.0006049	1.174e-06	1.174e-06	1.174e-06	1.174e-06	1.174e-06	-	
SIMPf2	2.114e-05	1.485e-05	1.174e-06	8.928e-07	8.928e-07	1.174e-06	1.174e-06	1.174e-06	1.174e-06	6.569e-06	-

Table 6.6 shows the p-values for paired comparison between the distributions of best absorption values from trials of two algorithms. Note that the p-values are generally much lower than 0.05 except for TABU vs. CH1 and TABU vs. SIMPf0 as can be confirmed from the distribution of absorption from these algorithms in Figure 6.18 and the boxplots in Figure 6.14. Although the differences between CMA and DE solutions from the box plot do not seem to be very different, the p-value of ≈0.001 indicates that the differences are indeed significant. The differences between other pairwise algorithms can thus be considered to be statistically significant. However, a note of caution is advised as these trends vary from one problem instance to another, and the performance of one algorithm over the other cannot be generalised from these p-values. In practise, the acoustic models used to determine absorption do not guarantee accuracy beyond two significant figures. Hence, the use of a rounding-based ranking scheme such as the one used to generate Table 6.5 could be effective.

6.6.6 Landscape analysis

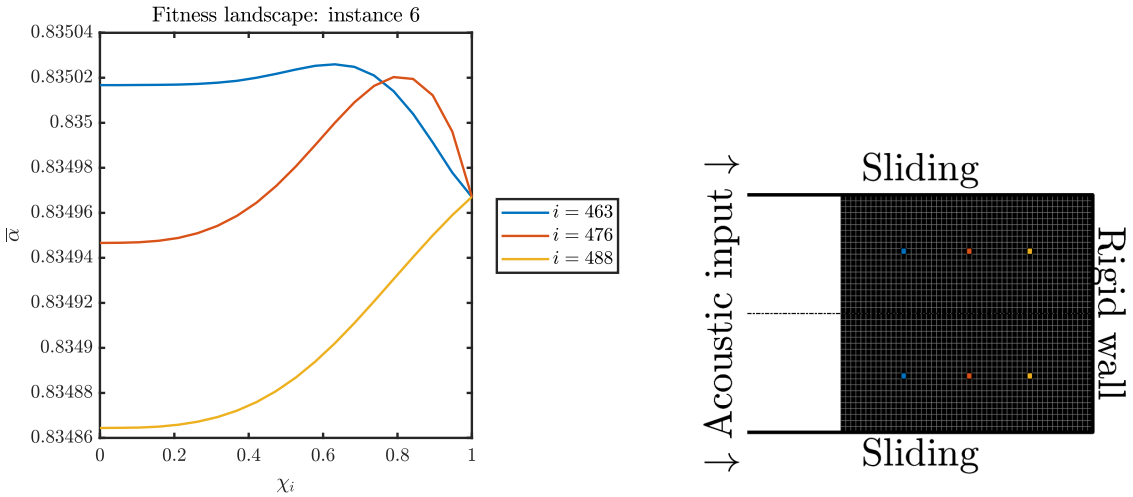

Figure 6.19: Landscapes for fully-filled shape problem instance 6

Objective function landscape for a problem is an important aspect to consider in choosing an optimisation approach. In this section, we will look at how the landscapes are for the acoustic

topology optimisation problem. We have observed that gradient algorithms have been outperformed by non-gradient methods such as hill climbing in terms of the best absorption found. Hence, it is of interest to carry out a deeper analysis of the fitness landscapes and assess the modality of the problem instances.

For this, we will consider a fully porous-filled solution and compute the variation of absorption when each of the elements is gradually changed to air. Figure 6.19 shows the variation of absorption values when three of the elements is gradually changed from porous $\chi_i = 1$ to air χ_i in problem instance 6. We observe that gradually removing porous material and replacing with air from various elements show a different absorption trend. The blue coloured element $i = 463$ which is closer to the acoustic source has a negative slope at $\chi_i = 1$, meaning that including a small fraction of air behaviour in the porous element would improve absorption. Indeed, this trend is retained as the porous material in that element is replaced with air, i.e., an increase in absorption $\overline{\alpha}$ is achieved when χ_{463} is changed from 1 to 0. Likewise, in the yellow-coloured element $i = 488$, the gradient is negative at $\chi_{488} = 1$ and as χ_{488} tends to 0, the absorption retains the decreasing trend. In these two elements, the gradients are considered to be helpful.

However, this is not the case for the element marked in red with $i = 476$. For this element, even though the gradient is negative, there exists a prominent peak closer to $\chi_i = 0.9$, and the absorption decreases rapidly as the porous material is completely removed. This is an example of an anomalous scenario where the gradients are misleading. Consider applying SIMP in this scenario. The algorithm would move towards the peak following the gradient and get stuck at a χ_i closer to one, which when rounded would make it 1. Even though, the gradient is deceiving, SIMP would succeed in this scenario in finding the right choice for the element. Overall, we observe that there is smoothness in the absorption landscape for this problem instance with less modality.

Gradient anomaly example When analysing the landscapes, there are occasions when the gradients are misleading and would lead to local optimal solutions. As an example, consider the optimised shape from Lee *et al.* for volume fraction 0.5 as shown in Figure 6.20a. The fitness landscape corresponding to the element marked by the arrow is shown in Figure 6.20b. At this element, while the gradient is positive, the fitness landscape reveals that a better solution could be obtained by removing the porous material. In these scenarios, a gradient method would get stuck at the local optimum whereas hill climbing would result in an improvement. This may explain the poor performance of gradient methods relative to non-gradient methods in certain problem instances. Upon studying the landscapes for many shapes, it was found that such an anomaly does not normally occur in most elements but do occur in a small fraction of elements in many optimised shapes from the SIMP algorithm.

Convexity does not guarantee optimality Many researchers have dedicated efforts to tune the fitness function to ensure the landscapes are convex with the consideration that convex functions have utmost one optimum across one design variable. While SIMP is expected to perform well for convex problems as opposed to problems with multiple modes and rugged landscapes, even if the function is convex, a gradient method could only find the exact optimum in the continuous space, but not necessarily in the discrete space. This is illustrated in Figure 6.21 using proof by contradiction. Consider a single variable topology optimisation where the fitness function is convex (i.e. a line joining any two points in the curve does not intersect the

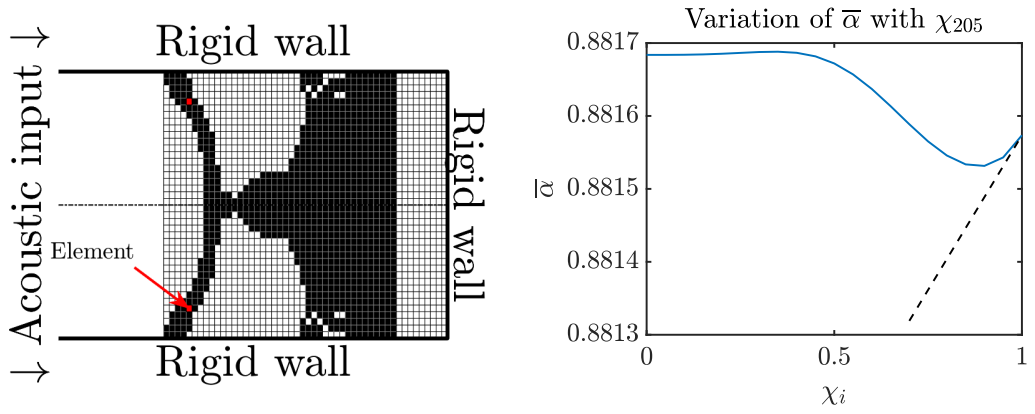

(a) Location of the anomalous element. *(b) Fitness landscape at an anomalous element.*

Figure 6.20: An example of a case where gradient algorithms may get stuck at a local optimum. (a) The optimised shape from Lee et al. [140] is considered as an example and one of the elements, marked by the arrow, is assessed. (b) The landscape for this element shows that gradients are misleading in this case.

curve). One can show that a gradient method can guarantee to reach the continuous optimum. However, topology optimisation is a unique problem domain where one is interested in the discrete optimum i.e. 0-1 solutions. Rounding the continuous solution to discrete using a simple rounding filter would result in 1 being chosen by the gradient algorithm. Whereas, in this example, the fitness value for 0 is better than that at 1 indicating that the discrete optimum is in fact 0. Thus, even for a single variable problem with a convex landscape, a gradient algorithm cannot guarantee optimality in the discrete space.

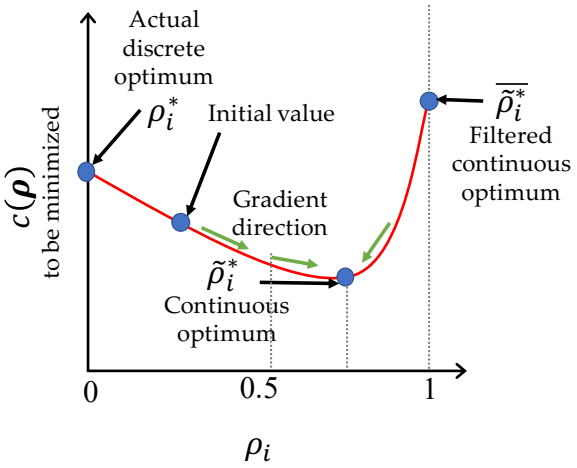

Figure 6.21: Proof that SIMP is a heuristic (inexact) even when the fitness function is convex. Convexity does not guarantee optimality when using gradient algorithms. For convex functions, gradient based methods like SIMP may find the continuous optimum but not necessarily the exact discrete optimum – an illustration using a one-design-variable system.

Does linearity guarantee optimality? The next natural question is, *if the fitness function is linear, does it guarantee optimality?* The answer is no. Consider a linear fitness function in topology optimisation expressed in equation 6.55.

$$\min_{\boldsymbol{\rho}} \quad c = \sum_i w_i \rho_i \qquad \rho \in \{0, 1\} \tag{6.55}$$

One may realise that the above problem is similar to the 0-1 Knapsack problem which is known to be NP-complete [120]. The NP-completeness of topology optimisation problems is unknown and is rarely discussed in topology optimisation literature.

6.7 Conclusions

In this chapter, results from topology optimisation experiments to maximise sound absorption under normal incidence in an impedance tube with a rigid backing was presented. Optimisation tests were conducted using 5 heuristic and 6 metaheuristic algorithms on 7 benchmark problem instances. The approaches include hill climbing (HC), constructive heuristics (CH1 and CH2), solid-isotropic-material-with-penalisation (SIMPf0 and SIMPf2), genetic algorithm (GA), tabu search (TABU), covariance-matrix-adaptation evolution strategy (CMA and CMAd), and differential evolution (DE and DEd). Unlike in usual structural topology optimisation problems, volume fraction constraint and manufacturability filters were not imposed. The highlights of the findings are as follows.

- Gradient algorithms (SIMPf0 and SIMPf2) are the most efficient in quickly converging to good quality solutions, but in some problems they either prematurely converge to local optima or produce shapes that have intermediate materials.
- No algorithm clearly outperformed all others on all of the problem instances. Ranking the algorithms based on median solution quality revealed that hill climbing (HC) performed the best, followed by the material-addition constructive heuristic (CH1), and the discrete variant of covariance-matrix-adaptation evolution strategy (CMAd).
- The optimal shapes produced by algorithms that use stochastic components (GA, CMA, CMAd, DE, DEd) tend to be irregular and unconnected, and hence they might need additional filtering techniques. Although hill climbing produced higher sound absorption solutions in general, the optimal shapes produced (particularly in problem instance 6 with fine mesh) were not smooth and crisp, which might pose difficulties in manufacturing.
- On the other hand, constructive heuristic with material addition (CH1) produces high-quality solutions that also have fewer irregularities than hill climbing. In addition to this, the sound absorption values of shapes produced by CH1 were at least as good as or better than those produced by SIMPf0. Moreover, the constructive heuristics proposed here can be easily modified to include volume fraction constraint by simply terminating the construction after the desired volume fraction is reached. The material removal heuristic (CH2) often returns a fully-filled design domain as the solution.
- Between the continuous algorithms (CMA and DE) and their discrete variants (CMAd and DEd), the discrete variants seem to perform better. This means using filtering techniques before each objective function evaluation works better than filtering the solutions at the end of the algorithm.

To conclude, the absorption maximisation topology optimisation problem seems to be rich with many local optimal solutions, and different strategies explore different regions of the search space producing unique set of solutions. Insights obtained may be valuable in designing hybrid strategies and hyperheuristics for general-purpose optimisation of sound absorbing materials.

Chapter 7

Multi-objective topology optimisation for absorption maximisation and weight minimisation

In the previous chapter, the performance of topology optimisation algorithms were studied only considering absorption maximisation objective. In this chapter, simultaneously maximising absorption and minimising material usage is considered. To identify efficient optimisation strategies for this multi-objective problem, several gradient, non-gradient and hybrid strategies are studied. For gradient approaches, the solid-isotropic-material-with-penalisation method (SIMP) and a novel gradient-based constructive heuristic (CHg) are considered. For gradient-free approaches, hill climbing with a weighted-sum scalarisation (HC) and a non-dominated sorting genetic algorithm II (NSGA-II) are considered. Optimisation trials are conducted on seven benchmark problems involving rectangular design domains in impedance tubes subject to normal-incidence sound loads. The results indicate that while gradient methods can provide quick convergence with high-quality solutions, often, gradient-free strategies are able to find improvements in specific regions of the Pareto front. Two novel hybrid approaches (HA1 and HA2) are proposed combining a gradient method (CHg) for initiation and a non-gradient method (respectively HC and NSGA-II) for local improvements. A novel and effective Pareto-slope-based weighted-sum hill climbing is introduced for local improvement. Results reveal that for a given computational budget, the hybrid methods can consistently outperform the parent gradient or non-gradient methods.

7.1 Introduction

In chapter 6, attributes of the single objective topology optimisation problem were discussed. Although topology optimisation is inherently a multi-objective problem, i.e., simultaneously maximising performance and minimising weight, it has been more common to treat topology optimisation as a single-objective problem, i.e., maximising the structural performance while using a constraint on the weight. Given that one of the main benefits of topology optimisation is the potential weight savings, it is of interest to treat it as a multi-objective problem and obtain multiple trade-off designs simultaneously. The acoustic designers can then decide from the set of Pareto optimal or trade-off solutions for manufacturing.

Identifying the most effective optimisation strategies to find these trade-off solutions in a specific problem domain is a challenging task. Without any testing or knowledge of the problem

domain, it is difficult to assure which algorithms would be more efficient in terms of finding better quality solutions in less time. If the optimisation strategy is not effective, sub-optimal designs may be chosen for manufacture.

Given that topology optimisation can be formulated using various search paradigms (discrete vs. continuous representation, finite element raster vs. moving morphable components [96], level set [5, 251], interpolation schemes etc.), it is helpful to study how various strategies compare against each other. However, there is a lack of such comparison studies specifically for multi-objective topology optimisation in the acoustics domain. Such studies would facilitate engineers to choose effective strategies for their use cases.

In this chapter, a few hand-picked approaches likely to be used by other researchers are tested and compared. The approaches include the following:

1. Solid-isotropic-material-with-penalisation (SIMP)
2. Constructive heuristic with gradient (CHg)
3. Hill climbing (HC) on scalarised objective
4. Non-dominated sorting genetic algorithm-II (NSGA-II)

As we have seen in chapters 4 and 6, SIMP is the state-of-the-art approach for structural topology optimisation [77, 206, 152]. A vital attribute of this approach is the relaxation of the discrete problem into a continuous problem by allowing intermediate materials and using a power-law interpolation scheme. Using continuous relaxation allows the possibility of computing the gradients quickly using adjoint-like methods, which can make the optimisation quite effective, notwithstanding certain drawbacks such as getting stuck at local optima or the presence of intermediate materials in the final solution. Its effectiveness and ease of implementation [217], have made it the most popular approach for topology optimisation.

At this point, some previous efforts toward extending SIMP for multi-objective topology optimisation are worth noting. Suresh [237] extended the 99-line Matlab code to a 199-line code for Pareto-optimal compliance minimisation and also studied the effect of restarts vs. hot starts. Mirzendehdel *et al.* [165] proposed a multi-objective algorithm for multi-material compliance minimisation removing the mass constraint and treating it as an objective. While the multi-objective consideration is prevalent, it constitutes a small fraction of the publications, and comparison studies are rare.

Constructive heuristics are a class of optimisation algorithms that start from empty solutions and build step by step using problem-specific move operations to reach a complete solution. An example is the nearest neighbour heuristic for the travelling salesman problem. For topology optimisation, the evolutionary structural optimisation (ESO) method introduced by Xie and Steven [256, 257] is a classic example of a constructive heuristic. ESO starts from a solid-filled design domain and incrementally removes material from low-stress regions. This procedure requires the knowledge of stress fields. For acoustic material topology optimisation, in chapter 6, we introduced two constructive heuristics: CH1, where the material is added incrementally to an empty domain in places of highest absorption increase; and CH2, where the material is incrementally removed from a filled domain from places where the decrease in absorption is minimal. These heuristics performed among the top strategies in the study. One of the drawbacks of CH1 and CH2 is that computing the numerical absorption increments is expensive. Fortunately, this can be overcome by making use of the gradients. Adopting this, a simple gradient-based constructive heuristic (CHg) is proposed in the current study.

Hill climbing is a single objective optimisation technique that starts with an initial solution and modifies it iteratively while accepting improving changes. A row-wise hill climbing approach was found to perform among the best strategies for acoustic material absorption maximisation in chapter 6. A common strategy to solve multi-objective problems using hill climbing is to combine the objectives into a scalar value in a process known as scalarisation [119], and apply the single-objective algorithm. A simple way to scalarise is to use the weighted sum of the objectives. By varying the weights, the relative importance of each objective can be controlled. In this study, hill climbing is used in conjunction with a weighted-sum scalarisation technique (HC) as a candidate for multi-objective topology optimisation.

The non-dominated sorting genetic algorithm-II (NSGA-II) introduced by Deb *et al.* [69] is a well-known multi-objective evolutionary algorithm. A notable attribute of NSGA-II is the use of a fast non-dominated sorting procedure in combination with a crowding-distance operator that allows finding multiple points in the Pareto front simultaneously, as opposed to having to run multiple trials of a single objective algorithm in combination with a scalarisation technique. The effectiveness of NSGA-II and its variants has made it the most popular multi-objective approach for solving combinatorial optimisation problems [247].

In addition to the above strategies, two hybrid approaches (HA1 and HA2) are proposed involving a gradient method for initialisation and a non-gradient method for local improvement. The aim is to find whether hybrid approaches are beneficial. The results will provide perspectives on each method and guide algorithm selection.

The remainder of the chapter is organised as follows. In section 7.2, the overall methodology, including problem description, optimisation formulation, modelling method, and details of the experimental design, is provided. In section 7.3, the overall experimental design is described. In section 7.4, a comparison of SIMP algorithms—SIMPsweep and SIMPrestart is provided. In section 7.5, a gradient-based constructive heuristic is detailed. In section 7.6, a comparison study between the gradient methods SIMPrestart, SIMPsweep and CHg is provided. In section 7.7, a hill climbing approach with two scalarisation methods are discussed. In section 7.8, the non-dominated sorting genetic algorithm is applied to the problem and results are discussed. Along with gradient-free algorithms, a random search procedure is also compared. In section 7.11, a hybrid approach with CHg as an initialiser and a hill climbing approach with Pareto-slope-based weighted sum scalarisation is introduced. In section 7.12, a hybrid approach with CHg as an initialiser and NSGA-II as the exploiter is detailed. In section 7.13, an overall comparison of all the multi-objective approaches is provided. Finally, in section 7.14, a summary of the findings and general guidelines for designing algorithms are provided.

7.2 Methodology

7.2.1 Problem formulation

Consider the problem of optimally filling a rectangular design domain with a given porous material such that the sound absorption is maximised while using minimal material. The design domain can be assumed to be backed by rigid walls with a normal-incidence acoustic source placed as shown in Figure 7.1a. Typically as more porous material is filled in the design domain, the absorption would increase, but this is not always the case. There are instances when

removing material would improve absorption [202]. Depending on the distribution of porous material and air in the design domain, sound absorption will be determined at different frequencies of the acoustic source. Thus, this is a classic bi-objective optimisation problem with trade-off solutions.

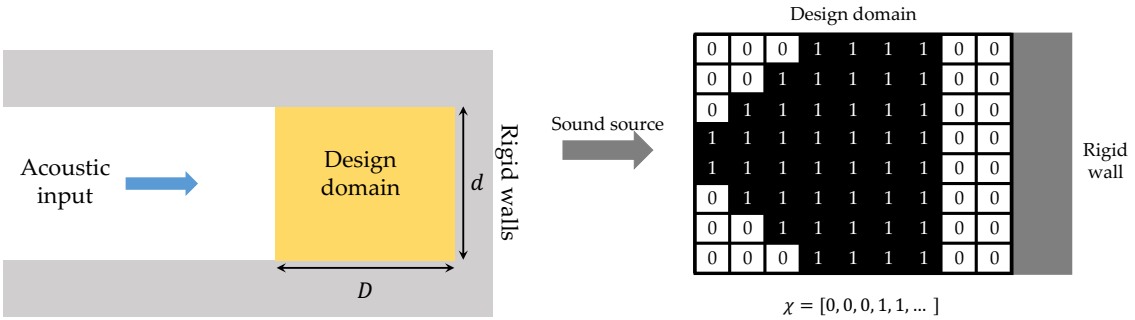

(a) Acoustic system with the design domain. *(b) Binary representation of a sample shape.*

Figure 7.1: Schematic of the problem and its representation.

While there are many ways to formulate the topology optimisation problem, one of the classical ways is to use a fixed discretisation of the system and optimise the material assigned to each finite element. The shape and topology can be represented by a vector χ with zeros and ones corresponding to the absence or presence of porous material in each element, respectively, as shown in Figure 7.1b. This is sometimes referred to as a bit-matrix representation [154]. At this point, it is also worth acknowledging other formulations such as moving morphable components [96], level set method [5, 251] etc. In moving morphable components-based topology optimisation, the structure is defined by a union of several components of the material with different shapes and sizes, while the design variables are the position, orientation and dimensions of these shapes. The design variables may then be converted to the presence or absence of material in each element in a finite element model and then solved to find the performance indicator. This representation reduces the number of design variables and simplifies the solution space. This approach is quick and robust in many cases, although in some cases, the true optimal solutions may be too intricate to be represented by this solution space. In the level set method, a scalar field is assumed in the design domain, and the iso-surfaces of this scalar field will determine the topology and shape, and the optimisation algorithm optimises this scalar field. While the above methods are more realistic for industrial applications, for the purposes of this study, the classical raster finite element representation is considered, i.e., optimising the presence or absence of material in each finite element.

In this study, the objective considered is to find the optimal discrete assignments of either air or a given poroelastic material to each finite element that simultaneously maximises the normal sound absorption and minimises the volume fraction of the porous material. Mathematically, this formulation can be written as:

Simultaneously,

$$\begin{aligned} \max_{\boldsymbol{\chi}} \quad & \overline{\alpha}(\boldsymbol{\chi}) = \frac{1}{n_f}\sum_{i=1}^{n_f}\alpha(\boldsymbol{\chi}, f_i) \\ \min_{\boldsymbol{\chi}} \quad & V_f(\boldsymbol{\chi}) = \frac{1}{n_e}\sum_{i=1}^{n_e}\chi_i \\ & \boldsymbol{\chi} \in \{0,1\}^{n_e} \\ & \overline{\alpha} \in [0,1] \\ & V_f \in [0,1] \end{aligned} \tag{7.1}$$

where $\boldsymbol{\chi}$ is the set of decision or design variables that determines whether the i^{th} element in the design domain is air or the given porous material, and thereby the shape of the acoustic structure. If χ_i is 0, the element is assigned the properties of air, and if it is 1, the element is assigned porous material. The first objective $\overline{\alpha} \in [0,1]$ is the sound absorption averaged across the target frequencies $(f_1, f_2, ...f_{n_f})$, and the second objective V_f is the volume fraction of the porous material in the design domain. Absorption $\overline{\alpha}$ is averaged over a number of target frequencies n_f, and porous material volume fraction V_f is averaged over the number of elements n_e in the design domain.

7.2.2 Computing the objective function

Computing the volume fraction V_f for a given shape $\boldsymbol{\chi}$ is less time consuming since it is simply the mean of an array, whereas computing absorption $\overline{\alpha}$ is expensive which requires solving a system of linear equations. The procedure followed in computing absorption is the same as outlined in chapter 6, and is briefly recalled here for the sake of completeness.

The acoustic system is modelled using the unified Biot-Helmholtz model introduced by Lee *et al.* [140], which considers air as a poroelastic material with negligible solid-part behaviour. In the unified model, air is considered to have $\chi_{air} = 0.001$ to avoid numerical issues when solving the system. Lee *et al.* also verified the validity of such modelling for poroelastic materials with mixed formulations [11]. The most expensive part of computing $\overline{\alpha}$ is finding the solution $\{\mathbf{X}\}$ to a system of linear equations $[\tilde{\mathbf{S}}(\boldsymbol{\chi}, f)]\{\mathbf{X}\} = \{\tilde{\mathbf{F}}\}$, where the system matrix $[\tilde{\mathbf{S}}(\boldsymbol{\chi}, f)]$ is a square symmetric complex-valued matrix with dimensions of the order of the number of finite elements in the design domain, and $\{\tilde{\mathbf{F}}\}$ is the dynamic forcing vector of the same dimension. The system matrix $[\tilde{\mathbf{S}}(\boldsymbol{\chi}, f)]$ is populated with material properties of air or porous material at specific submatrices depending on the shape $\boldsymbol{\chi}$. When considering continuous relaxation, for the intermediate materials i.e. $\chi_i \in (0,1]$, the material properties are interpolated using a power-law i.e. any material property, say ψ_i is given by $\psi_{air} + \chi_i^p(\psi_{por} - \psi_{air})$, where ψ_{por} and ψ_{air} are the properties of the porous material and air respectively.

Since evaluating absorption $\overline{\alpha}$ is the computational bottleneck, and other algorithmic processes take a relatively insignificant amount of time, this is an expensive optimisation problem, and hence it is reasonable to use the number of absorption evaluations to benchmark the performance of algorithms.

Computing the gradient of sound absorption with respect to the design variables takes approximately two more instances of solving the system of linear equations, making it twice as expensive as computing absorption (see equation 7.2), as explained in section 6.2.3.

$$\text{Time to compute } \left(\frac{\partial \overline{\alpha}}{\partial \boldsymbol{\chi}}\right) \approx 2 \times \text{Time to compute}(\overline{\alpha}) \tag{7.2}$$

Such a quick computation of the gradient is achieved using a fictitious load vector pre-multiplication, as explained in Lee *et al.* [138]. For more details, one may refer to section 6.2.3.

$$\text{Gradient algorithm fitness evaluation} \approx 3 \times \text{non-gradient fitness evaluation} \tag{7.3}$$

Thus, computing both absorption and the gradient is three times as expensive as computing just absorption as given in equation 7.3. Therefore, the gradient methods will be given one-third of the fitness evaluation budget.

7.2.3 Benchmark problem instances

To compare the optimisation approaches, seven benchmark problem instances introduced in chapter 6 are adopted. A modification has been made to the mesh size in problem instance 3 from 10×10 to 50×20 elements. The details of the problem instances are provided in Table 6.2. All the problem instances have a rectangular design domain, but with different dimensions, discretisation, porous material used and frequency range of interest. Table 6.3 provides the poroelastic material properties for the materials used in the problem instances. While problem instance 1 uses the same material as Lee *et al.* [140] with a high tortuosity, the third problem instance uses a fictitious material with high airflow resistivity, and all other problem instances use melamine.

7.2.4 Approaches for multi-objective topology optimisation

The multi-objective topology optimisation problem posed in equation 7.1 can be tackled in several ways. Table 7.1 gives the formulations for these approaches.

Table 7.1: A classification of multi-objective approaches for topology optimisation.

Single objective Restart/Adaptive	**Scalarisation**	**Direct multi-objective**
Repeat/Adapt for various $\bar{V}_f$:	Repeat for various w_1:	
$\max_{\boldsymbol{\chi}} \quad \overline{\alpha}(\boldsymbol{\chi})$	$\min_{\boldsymbol{\chi}} \quad C(\boldsymbol{\chi}) = -w_1\alpha(\boldsymbol{\chi}) + w_2 V_f(\boldsymbol{\chi})$	Simultaneously,
subject to: $V_f(\boldsymbol{\chi}) \leq \bar{V}_f$	subject to: $w_1, w_2 \in [0, 1]$	$\max_{\boldsymbol{\chi}} \quad \overline{\alpha}(\boldsymbol{\chi})$
	$w_1 + w_2 = 1$	$\min_{\boldsymbol{\chi}} \quad V_f(\boldsymbol{\chi})$
Examples: CHg, SIMPrestart, SIMPsweep	Example: HC	Example: NSGA-II

The more common approach has been to keep a limit on the volume fraction and start the algorithm with different values of volume fraction limit $\bar{V}_f$ in each trial to obtain several trade-off

designs. This approach can be called the *restart* approach. To speed the process, one can change $\bar{V_f}$ after an optimum is found and perturbatively explore various regions of the Pareto front, similar to Suresh [237].

Another approach is to use a *scalarisation* technique to combine the two objectives into an overall objective C and solve using a single objective algorithm. There exists several approaches to scalarise the objectives into a single value [119], whereas Table 7.1 only gives the formulation for weighted-sum scalarisation, one of the simplest. w_1 and w_2 are the weights that determine the importance of absorption and volume fraction, respectively. For example, the combination of weights $w_1 = 1$ and $w_2 = 0$ refers to only maximising absorption ignoring volume fraction. The overall cost function C is defined using a weight for each objective (α and V_f). The negative sign in front of α converts the maximisation goal into minimisation. Scalarisation approaches leave the designers to pick the weights w_1 and w_2 for which the relative importance of the corresponding objectives need to be known a priori. Typically, several sets of weights would be picked and multiple optimisation trials would be run, and the results can be combined to obtain the Pareto set approximation.

Finally, one can also use *direct* multi-objective methods that simultaneously optimise both objectives by keeping a record of the best trade-off solutions and pushing toward the true Pareto front (example: NSGA-II [69], SPEA-2 [278]). This is achieved using a crowding distance operator and a Pareto rank-based non-dominated sorting.

7.3 Experimental design

In Table 7.2, a summary of the optimisation approaches used in this study is provided, along with the attributes and hyper parameters of each approach. The reasoning behind the choice of multi-objective optimisation approaches picked for this study was briefed in the introduction section and hence not repeated here. Each algorithm used here is subject to basic tuning and used in the standard way unless otherwise stated. All the strategies are given the same arbitrarily-chosen computational budget of 4096 equivalent *gradient-free* fitness evaluations. Gradient algorithms are assigned $4096/3 \approx 1365$ fitness evaluations because each gradient-included fitness evaluation is thrice as expensive (equation 7.3), and the non-gradient methods are allowed 4096 fitness evaluations. For the hybrid algorithms, 25% of the computational effort was allotted for gradient-based search and 75% for non-gradient search i.e., $25\% \times 4096/3$ gradient-included and $75\% \times 4096$ gradient-free fitness evaluations. Each stochastic optimisation method is repeated 15 times by varying the random number seed. The number of trials 15 is chosen arbitrarily.

It should be noted that in some trials on some problem instances, the resulting SIMP solutions had intermediate materials. In such scenarios, only the non-dominated solutions are discretised by a round-off filter, and the fitnesses are recomputed. This is done so that all solutions compared in this study are from the discrete space to facilitate a fair comparison.

The experimental design involves firstly comparing the two gradient-based methods, namely SIMP and CHg in sections 7.4 and 7.5. The goal is to assess the quality of solutions produced by the two gradient methods and if the kind of shapes produced is similar for each problem instance. Then, the non-gradient methods HC, NSGA-II and random search (RAND) are compared separately in sections 7.7 and 7.8.

Table 7.2: Multiobjective optimisation approaches and their settings.

Algorithm	Description and pseudocode	Deterministic or stochastic	Trials	Fitness evaluation budget per trial
	Gradient-based approaches			
SIMPrestart	Solid isotropic material with penalisation (SIMP) restarted with different volume fraction constraints fixed for a trial: A gradient-based strategy with optimality criteria move-update following [10]; initialised with an empty design domain; Restarted with a new $\bar{V}_f$ until budget is used up.	Stochastic: multiple restarts within trial	1 (multiple restarts)	1365 (with gradient)
SIMPsweep	SIMP with adaptive volume fraction constraint: Initialised with an empty design domain; volume fraction constraint $\bar{V}_f$ updated after each fitness evaluation reaching 1 as budget approaches.	Deterministic	1	1365 (with gradient)
CHg	Gradient-based constructive heuristic: Start from an empty solution; add porous material in steps of 'm' elements where the gradient is highest, until all elements are porous.	Deterministic	1	min(N/m,1365) (with gradient)
	Non-gradient approaches			
HC	Hill climbing: Use a weighted-sum scalarisation technique to combine the two objectives into a single fitness value; apply first improvement hill climbing starting from a random discrete solution. Move order is like in a raster-scan.	Stochastic, since initial solution is random	15	4096 (non-gradient)
NSGA-II	Non-dominated sorting genetic algorithm - II [69]: Use a bit representation, tournament selection based on crowding distance and rank, uniform crossover, bitwise mutation probability of $1/N$.	Stochastic	15	4096 (non-gradient)
RAND	Random search algorithm: Pick a desired volume fraction uniformly $\in [0, 1]$; use this as the probability of porous material at each element and synthesise a solution; repeat budget number of times.	Stochastic	15	4096 (non-gradient)
	Hybrid approaches			
HA1	Hybrid approach 1: Run CHg using 25% of the budget, and run hill climbing for 75% of the budget starting from a selected solution with scalarisation weight such that the combined objective isoline at the solution point in objective space is tangential to the Pareto front.	Deterministic but depends on the point picked for hill climbing	15	4096 (equivalent non-gradient)
HA2	Hybrid approach 2: Run CHg using 25% of the budget, and run NSGA-II for 75% of the budget starting from an initial population from equispaced points in the CHg Pareto front.	Stochastic	15	4096 (equivalent non-gradient)

For comparing the performance of multi-objective algorithms, a hypervolume metric is adopted. Hypervolume for a set of solutions can be defined as the union of volumes of the objective space dominated by each solution in the set over and above the objective values of a reference solution. The larger the hypervolume of the solution set produced by an algorithm, the better supposedly is its performance according to this metric. For the problem in consideration, an illustration for this metric is provided in Figure 7.2. For the bi-objective problem under study, the hypervolume will be the *area* of the objective space dominated by the Pareto set from a chosen reference point given by $(\overline{\alpha}, V_f) = (0, 1)$.

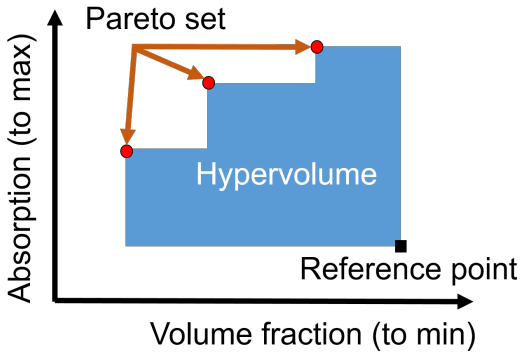

Figure 7.2: An illustration of the hypervolume metric: In this case it is the area of the objective function space dominated by the solutions from an algorithm. Larger the hypervolume of the solution set from an algorithm, better its performance can be considered to be.

Gradient algorithms

7.4 Solid-isotropic-material-with-penalisation

SIMP is a *single-objective* strategy for structural topology optimisation to maximise structural performance while keeping a soft constraint on volume fraction. SIMP has been discussed in detail in chapters 4 and 6. In this section, its extension to a multi-objective optimisation will be discussed. The main idea of SIMP is to allow a continuous relaxation of the material choices by using a power-law interpolation scheme. SIMP makes use of gradients to make incremental changes to the shape, followed by the application of morphological filters [218]. SIMP takes the desired volume fraction ($\bar{V}_f$) as one of its algorithmic parameters. By adapting this parameter, two variants for multi-objective optimisation are proposed, namely, SIMPrestart and SIMPsweep. For both these variants, the implementation is adapted from the efficient 88-line code for compliance minimisation by Andreassen *et al.* [10], replacing compliance and its gradients with absorption and its gradients.

7.4.1 SIMPrestart

In SIMPrestart, multiple trials of SIMP are run, with each trial using a different $\bar{V}_f$. For each of these trials, SIMP is initialised from a random solution normalised to have an overall initial volume fraction close to the chosen $\bar{V}_f$. Once convergence is achieved, SIMP is restarted with

a new $\bar{V}_f$ and a newly generated initial solution.

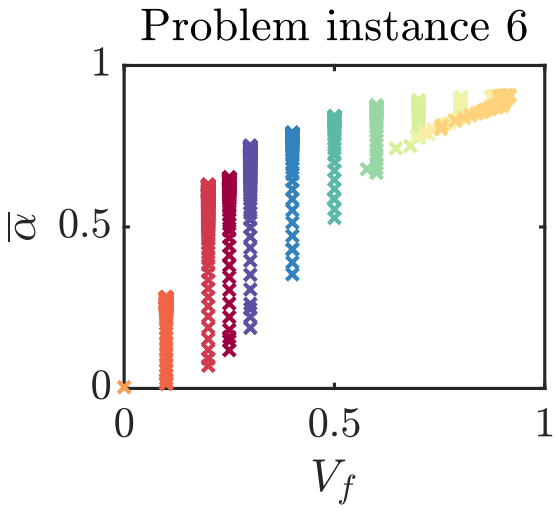

(a) Progress in objective space across trials. Each colour corresponds to a different trial.

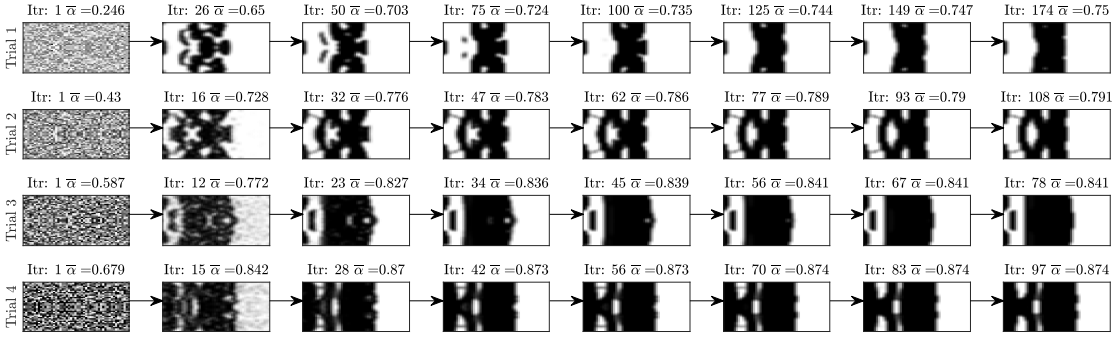

(b) Best shapes from the first 4 trials with volume fraction limits 0.3, 0.4, 0.5 and 0.6 respectively.

Figure 7.3: SIMPrestart applied on problem instance 6.

The solution progress in the objective space from SIMPrestart for each trial is shown in a different colour for problem instance 6 in Figure 7.3a. As iterations progress, better absorbing solutions with the same volume fraction are obtained as indicated by the vertical movement in the objective space. To populate the Pareto front, equispaced values of $\bar{V}_f$ are used in each trial. For trials with lower $\bar{V}_f$, the solutions tend to converge to lower absorption and for those with higher $\bar{V}_f$, higher absorptions are achieved. For higher volume fraction trials such as the ones in yellow, the initial volume fractions are slightly off because of the nature of initialisation, but as iterations progress, SIMP moves towards solutions with the prescribed $\bar{V}_f$.

Depending on the volume fraction limit, the algorithm converges to a variety of shapes for various volume fraction constraint values as can be seen in Figure 7.3b. For the first four trials, the volume fraction limits $(\bar{V}_f)$ are set to be 0.3, 0.4, 0.5, and 0.6, respectively, and it can be observed that the fraction of regions filled with porous material in the optimised solutions correspond to this value. The shapes seem to largely depend on the initial random solution used, as the final solutions closely resemble solutions in the initial iterations. The iteration number in which the shape is obtained is provided on top of each shape. Note that in each trial, the algorithm converges in about 100 iterations/fitness evaluations.

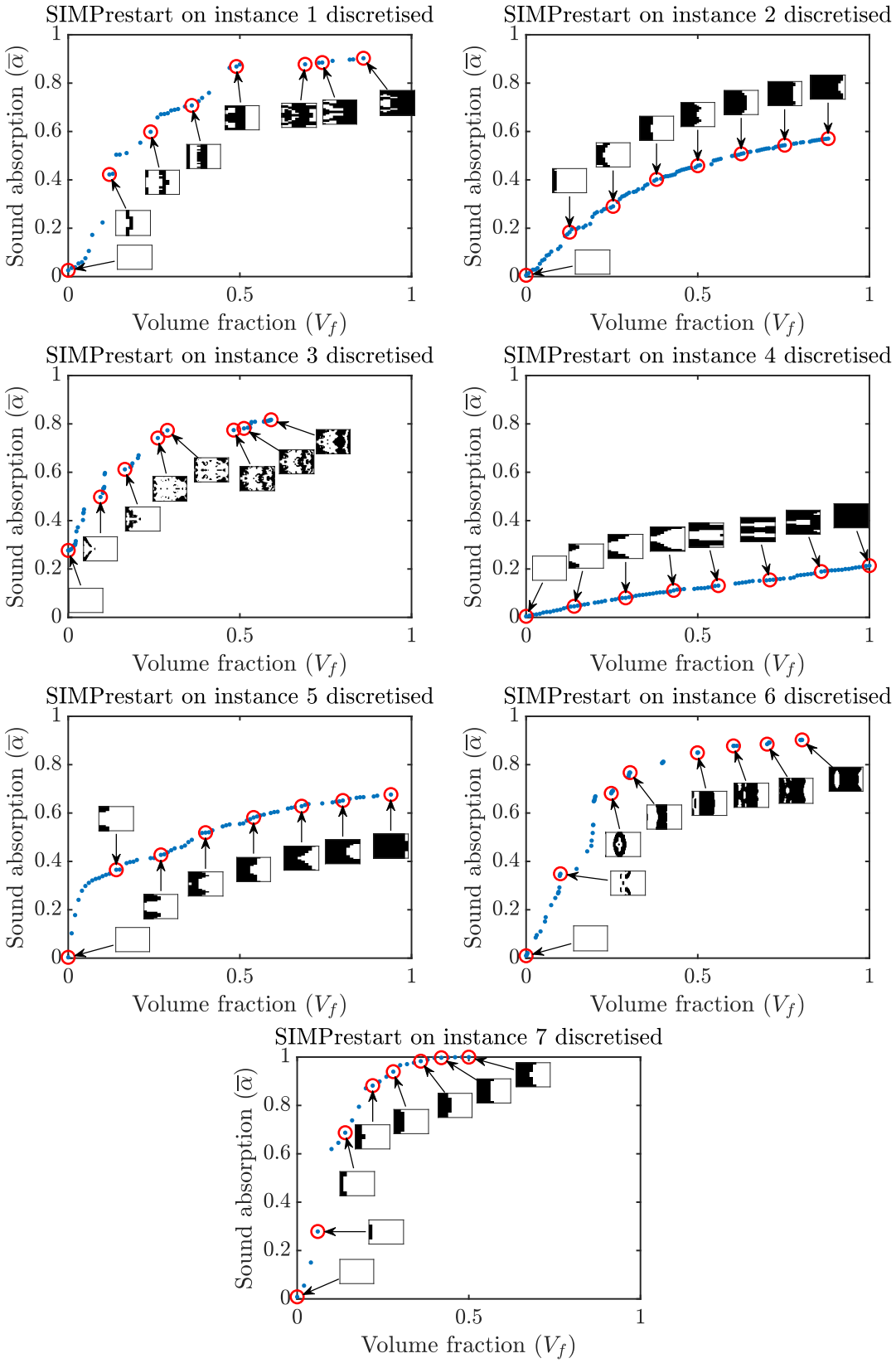

Figure 7.4: SIMPrestart trade-off solutions for all problem instances.

The Pareto optimal shapes produced by SIMPrestart for all problem instances are shown in

Figure 7.4. These shape plots show that typically as more porous material is present in the design domain, the absorption is high. For some problem instances, it seems to be better to place porous materials toward the acoustic source, leaving an air gap next to the rigid wall. For problem instance 1, the shapes seem to have porous-material walls in the middle of the design domain at low volume fractions, and shapes with intricacies in the front of the design domain for high volume fractions. For problem instances 2 and 7, SIMPrestart seems to find solutions that fill porous material in the front. For problem instance 3, the optimal shapes seem to have a large cavity in the centre. Interestingly, despite the morphological filters used as part of SIMP, many small features, which are a few elements wide, could be seen in the solutions. For problem instance 4, the shapes seem to indicate that a cavity of air enclosed by a perforated porous material facing the source need to be placed for a volume fraction around 0.3 to 0.4. Interestingly, around 0.7, the best shape seems to resemble porous material with macroscopic cylindrical pores. Such structures exhibiting both micro- and macro-pores are referred to as dual porosity materials [33]. For problem instance 6, intricate shapes with multiple circular macro-pores emerged in the solutions.

7.4.2 SIMPsweep

SIMPsweep starts from an empty or air-filled solution with an initial volume fraction limit $\bar{V}_f = 0$, and updates $\bar{V}_f$ in every iteration reaching 1 as the fitness evaluation budget is reached.

The solutions produced for all problem instances are plotted in the objective space in Figure 7.5, along with some of the shapes. A general trend across all problem instances is that as the volume fraction increases, absorption also increases. The Pareto solutions for problem instances 2, 4, 5 and 7 seem to be filling material away from the rigid backing with inverted wedge-like shapes. Whereas for problem instances 1 and 6, initially, the material placed in the middle of the domain seems to be favoured. Notably, for this melamine problem instance, some of the optimal shapes closely resemble flat layers. However, this is not always the case across problem instances. For example, in problem instance 3, which fills high airflow resistivity material, the resulting shapes resemble scattered blobs of porous material with a cavity in the middle. This pattern is somewhat similar to the optimal scatterer distribution found by Isakari *et al.* [106].

Discretisation issue: The raw solutions from SIMP algorithms did not always result in discrete 0 or 1 shapes, and the shapes had to be rounded, i.e., values less than 0.5 are set to 0, and more than 0.5 are set to 1, and the absorptions are recomputed. This involved additional fitness evaluations beyond the budget. To save on computational time, only the non-dominated solutions are discretised and recomputed. Nevertheless, the resulting changes in absorption due to rounding were insignificant in most cases. This is the reason why the points on the Pareto front do not seem to be subject to non-dominated sorting (especially for problem instance 3).

7.4.3 Comparison between SIMPsweep and SIMPrestart

The Pareto sets of SIMPsweep and SIMPrestart are compared in Figure 7.6. Overall, it may be noted that Pareto fronts produced are generally very close between the two algorithms, such as in problem instances 2, 4, and 5. Although in specific regions in some problem instances, one algorithm found slightly better solutions than the other (such as 1 and 6 and 7). Notably, in problem instance 3, the solutions from SIMPrestart significantly outperform SIMPsweep for

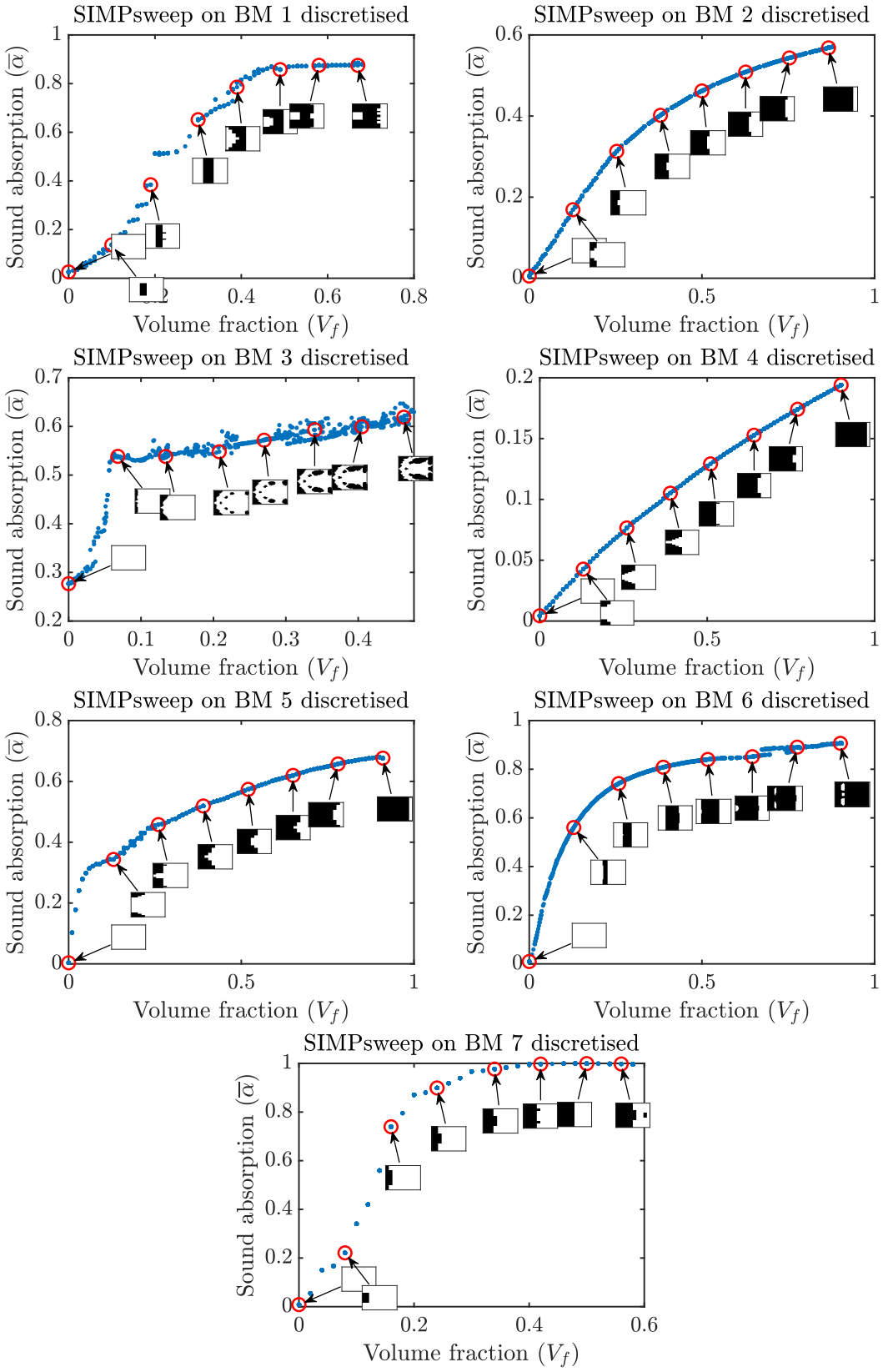

Figure 7.5: SIMPsweep trade-off solutions for all problem instances.

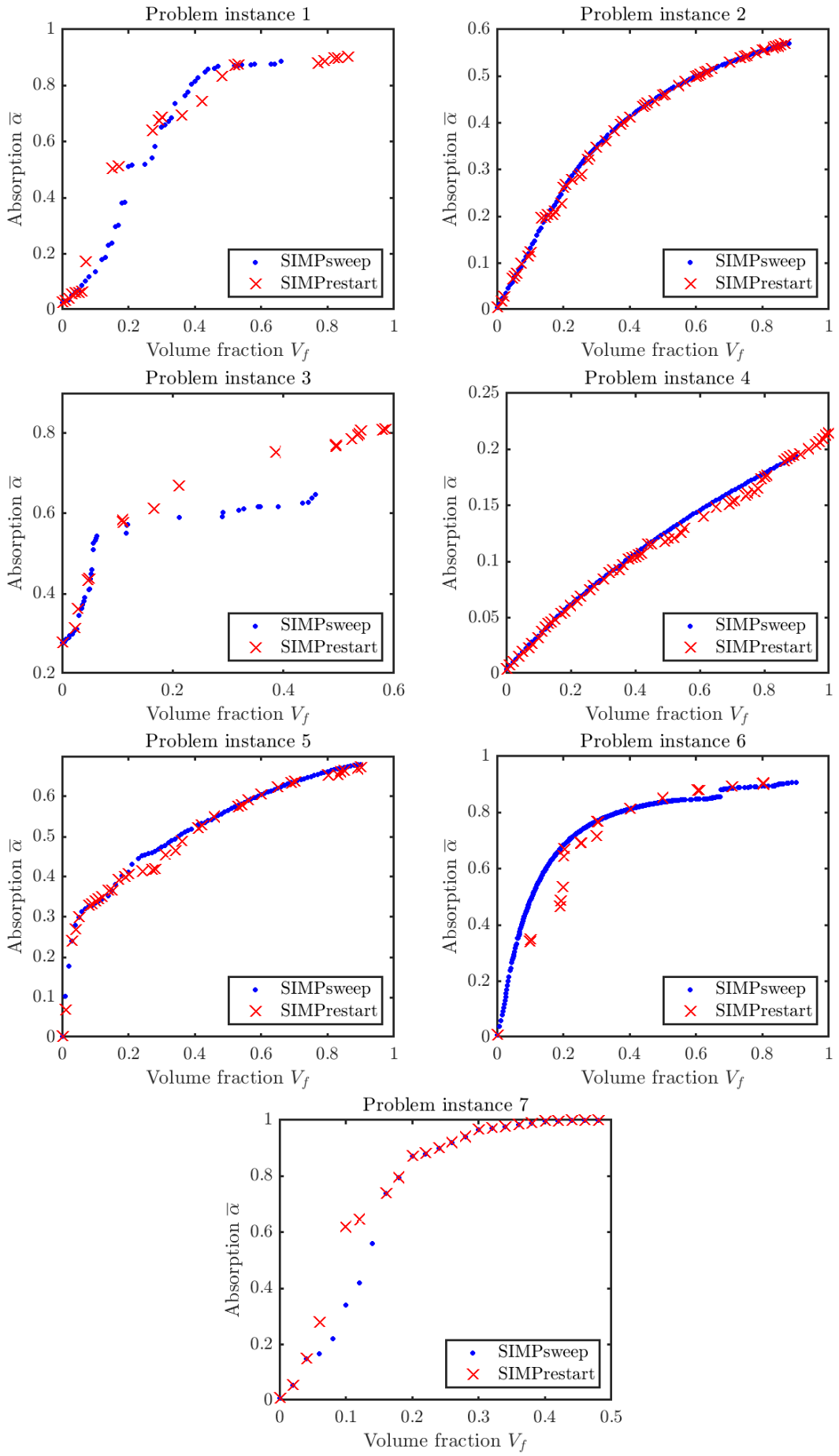

Figure 7.6: Comparison of Pareto fronts from SIMPrestart and SIMPsweep

high volume fractions. Comparing the shapes for problem instance 3 between Figure 7.4 and 7.5, we observe that SIMPrestart shapes are more intricate, whereas those produced by SIMPsweep have less intricacies. Overall, SIMPsweep seems to find solutions that are topologically simpler (with fewer holes) than SIMPrestart. Another observation to make in Figure 7.6 is that SIMPsweep finds closely-spaced solutions in the objective space, whereas SIMPrestart tends to leave larger gaps between solutions. While these results are true for the budget considered, for lower fitness evaluation budgets, SIMPsweep would be a better strategy since, less time will be spent on initially reaching good solutions, as also suggested by Suresh [237]. In other words, SIMPsweep would be more scalable to computational budgets and therefore be suited for problem instances with larger N.

7.5 Constructive heuristic using gradient (CHg)

Constructive heuristics are methods which incrementally build solutions to optimisation problems from scratch. In chapter 6, we observed that a material addition constructive heuristic (CH1) performed among the best approaches in topology optimisation for maximising sound absorption. In CH1, the procedure is to incrementally add materials in the locations where the increase in absorption is the highest. However, finding the change in absorption at every finite element, when toggling between air and porous material, is computationally expensive as this involves solving the finite element equations once for each element. In this approach (CHg), the absorption increments are replaced by gradients $(\frac{\partial \overline{\alpha}}{\partial \chi_i})$ which can be computed for all elements in the time it takes to solve the finite element problem three times. We call this variant *gradient-based constructive heuristics* (CHg). CHg starts from a fully-air design domain and fills porous material incrementally in the finite elements where the gradient of sound absorption $\frac{\partial \overline{\alpha}}{\partial \chi_i}$ is maximum.

At each step, m number of elements are chosen to fill with porous material after each gradient evaluation, and the total number of fitness evaluations necessary would be n_e/m where n_e is the total number of elements. m is chosen such that n_e/m does not exceed the budget. Note that in the seven problem instances considered, the number of elements is respectively 100, 150, 1000, 100, 100,1000, and 50. Since the budget considered is 1365, all problem instances can be completed in n_e fitness evaluations with $m = 1$. Hence, CHg will effectively utilise fewer fitness evaluations than the budget in the cases considered. Note that CHg always will search for solutions in the discrete space since an element is either filled or not filled. In this way, it is different from SIMPsweep.

The progress of solutions found by CHg applied in the objective space along with a few shapes is shown in Figure 7.7 for all problem instances . One of the first things to note is that, in many problem instances (2, 4 and 7), the best shapes tend to have porous materials away from the rigid backing. Having an air gap next to the rigid backplane seems to be favourable. Placing an air gap between the wall and porous package is an already known strategy to improve absorption. In many anechoic chambers, the foam wedges are placed a few centimetres in front of the wall [24]. Moreover, in problem instances 2, 5 and 7, some of the shapes resemble an inverted wedge similar to the ones found by SIMPsweep. Notably, the occurrence of such inverted wedges is less in CHg than in the SIMP algorithms, wherein such shapes occurred in five out of seven problem instances. For problem instance 1, the shapes produced by CHg have mainly flat surfaces as opposed to wedge like surfaces in SIMPsweep. For problem instance

3, there are stark differences in the shapes between CHg and SIMPsweep: while the SIMPsweep optimal solutions have patches of porous materials in the design domain resembling scattering structures, CHg solutions are more intricate and difficult to manufacture. For problem instance 6, the shapes from CHg seem to have two flat layers as opposed to one layer found by SIMPsweep. Overall, one can consider that CHg and SIMPsweep algorithms performances are similar. A unique attribute of CHg is that the algorithm traverses through good solutions with various volume fractions, resulting in a quick approximation of the Pareto front.

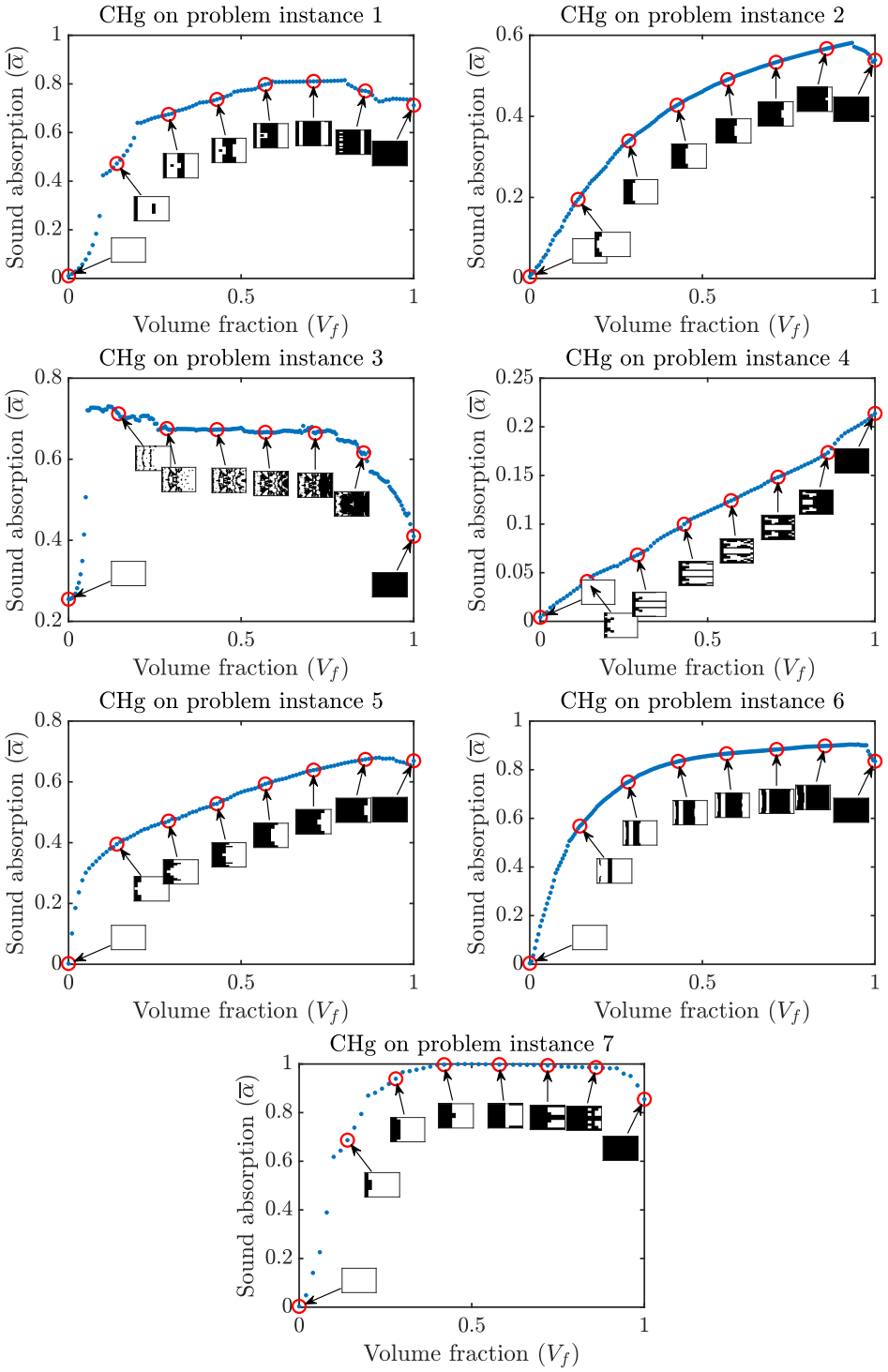

Figure 7.7: Constructive heuristic using gradients (CHg): Solution progress for all problem instances.

Table 7.3: Hypervolume comparison of gradient based approaches SIMPrestart, SIMPsweep and CHg.

Instance	SIMPrestart	SIMPsweep	CHg
1	**0.7065**	0.6835	0.6724
2	0.4014	0.4047	**0.4066**
3	0.7317	0.6063	**0.7412**
4	0.1160	**0.1188**	0.1087
5	0.5208	0.5292	**0.5323**
6	0.7202	**0.7607**	0.7512
7	0.8727	0.8567	**0.8733**

7.6 Comparison of gradient-based algorithms

First, we will consider a comparison of the gradient algorithms —SIMPrestart, SIMPsweep and CHg. Figure 7.8 shows the Pareto front approximations produced by these two algorithms for all the problem instances. There are specific regions in each problem instance where one algorithm performs better than the other. Only for a few problem instances, there were significant differences in the Pareto fronts. In problem instance 1, at low volume fractions, CHg performed better, whereas SIMP performed better at high volume fractions. For problem instance 3, a few solutions from CHg near 0.1 volume fraction have very high absorption and dominate other solutions. Overall, these three approaches may be considered to be similar in terms of the performance with respect to covering the Pareto front.

The hypervolumes covered by solutions from the gradient approaches are shown in Table 7.3. Among the three methods, SIMPrestart covered the most hypervolume in one problem instance, SIMPsweep in two problem instances and CHg in the other four, as emphasised by the bold font. However, the values are not significantly different among the three approaches.

Note that it is the possible to speed up SIMPsweep and CHg if required. As an example, if the fitness evaluation budget is reduced by 10 times, in SIMPsweep, the volume fraction constraint $\bar{V}_f$ can be adapted 10 times quickly. Similarly, in CHg, the number of elements filled m can be increased 10 times. Though this risks potentially missing several trade-off solutions, the quality of the solutions would not be significantly affected. This is because, every next solution found by SIMPsweep or CHg is an incremental perturbation from an already good solution. Although, for SIMPrestart, speed-up can be achieved by tuning the move limit parameter m, there are some caveats such as the occurrence of numerical oscillations.

Non-gradient algorithms

7.7 Hill climbing with scalarisation (HC)

Hill climbing with a raster-scan move ordering discussed in chapter 6 is extended for multi-objective optimisation. In this implementation, a weighted-sum scalarisation is used to convert the two objectives into one and hill climbing is applied. Here, a Davis-bit hill climbing [64] is used wherein consecutive elements are toggled between air and porous, and the change is accepted if it improves the scalarised objective. The initial solution is generated randomly

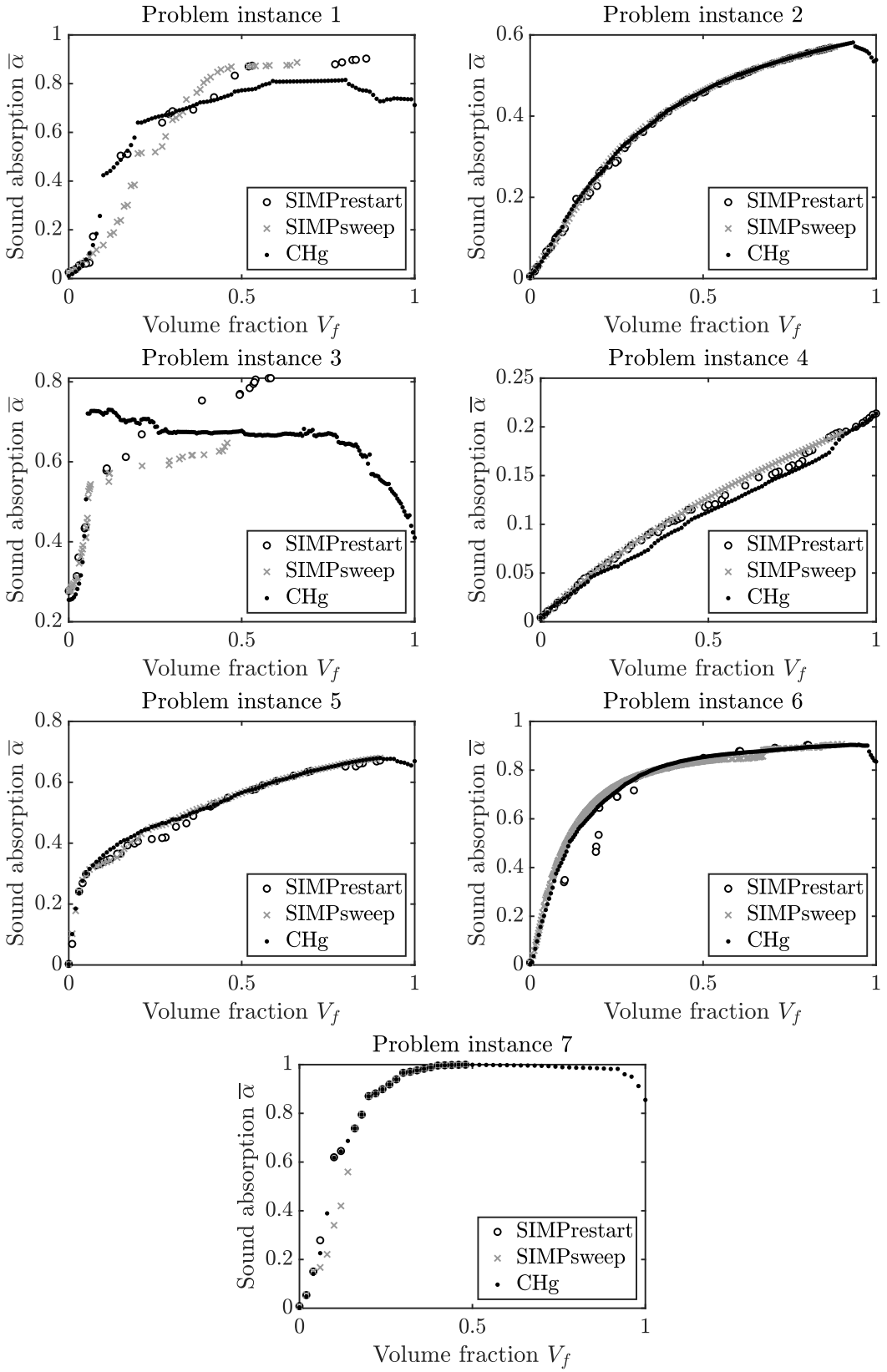

Figure 7.8: Comparison of solutions from gradient algorithms in the objective space: Trade-off solutions from SIMPrestart vs. all solutions from SIMPsweep and CHg.

by first picking the desired volume fraction between 0 and 1, and filling each element with a probability equal to the desired volume fraction value. This approach allows choosing initial solutions spread out in volume fractions. From the initial solution, an element is bitflipped i.e. air becomes porous and porous becomes air, and the change is accepted as the current solution if the scalarised objective function decreases. Then, the next element is bitflipped. The order in which the elements are flipped in this implementation, is like in a raster scan. This is similar to HC in chapter 6 along with a weighted-sum scalarisation. The scalarisation function used is as follows:

$$\min_{\boldsymbol{x}} \quad C = -w\overline{\alpha} + (1-w)V_f \tag{7.4}$$

The weight w corresponds to the importance of maximising absorption as opposed to minimising volume fraction and can take values between 0 and 1. A weight of 1 implies maximising only absorption irrespective of volume fraction, and likewise, a weight of 0 corresponds to only minimising volume fraction. An illustration of the effect of choosing w on the scalarised objective is shown in Figure 7.9. Note that w governs the slope of the isolines of the scalarised objective. This will be relevant later.

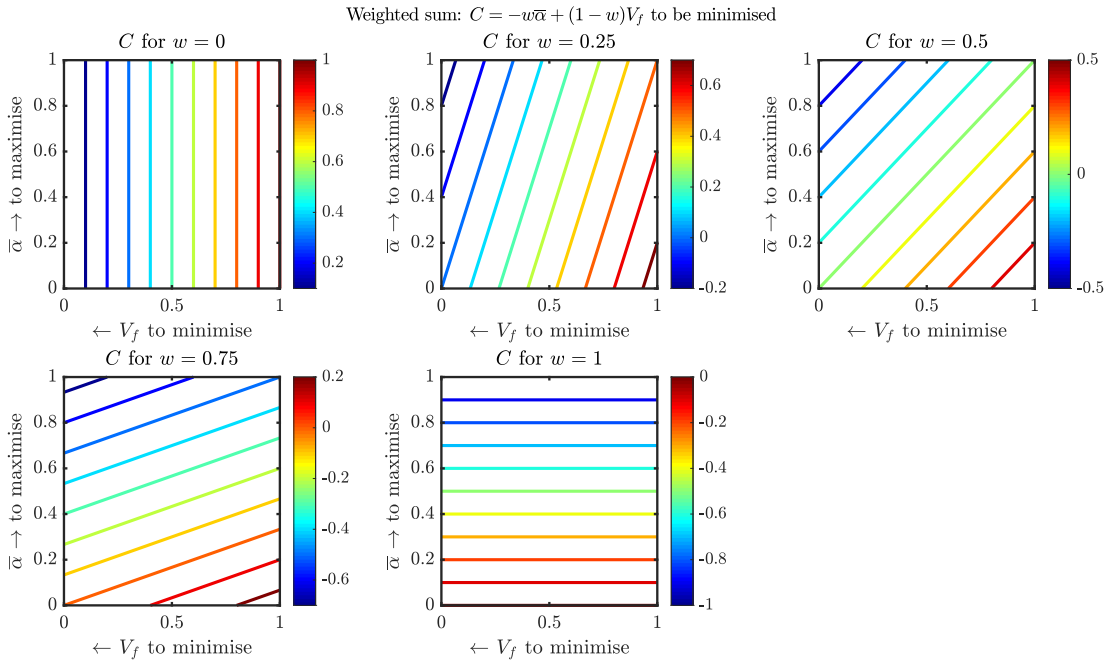

Figure 7.9: Isolines of scalarised objective in weighted sum scalarisation. Depending on the weight chosen, the slope of the combined objective C isoline will vary.

For each trial run of HC, a random starting solution is picked and a fixed weight is chosen. Then, the elements are toggled between air and porous material consecutively and the new solution is accepted if and only if there is an improvement in the combined objective. This hill climbing process is continued until the fitness evaluation budget is used up. Fifteen such trials are run with different weights, and Figure 7.10 shows all solutions from these trials of HC compared with CHg solutions. The trails of points in the figure correspond to individual trials improving solutions in a specific direction depending on the chosen weight. The combined results from HC are better than those of CHg in some regions in both $\overline{\alpha}$ and V_f, indicating that the gradient methods do often converge to local-optimal solutions, and potential for improvements exist.

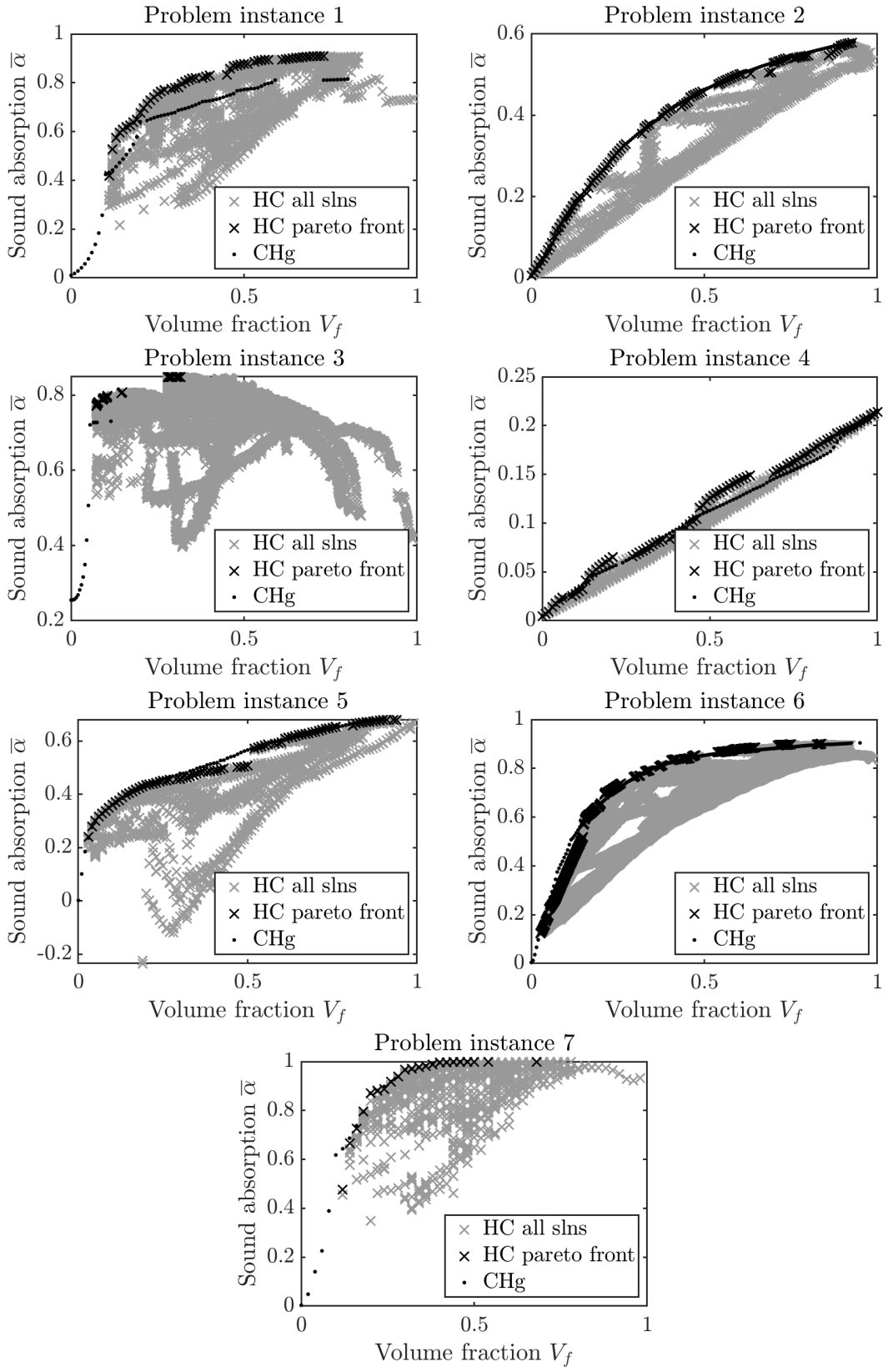

Figure 7.10: Figures showing all solutions from 15 trials of HC for each problem instance benchmarked with CHg solutions. HC finds solutions in specific regions better than CHg but the per-trial the amount of hypervolume dominated by the solution set is not as good as that of CHg.

Table 7.4: Hypervolumes covered by hill climbing when using weighted sum vs. Chebyshev scalarisation methods.

Instance	Weighted sum	Chebyshev
1	**0.6177**	0.5098
2	**0.3629**	0.2574
3	**0.7672**	0.5528
4	0.0554	**0.0793**
5	**0.4859**	0.3202
6	**0.6961**	0.5325
7	**0.8000**	0.6594

An issue with HC is that only one specific region in the Pareto front will be explored. While this results in solutions better than CHg in some regions, on a per-trial basis, the overall hypervolume obtained turns out to be poor. This is because using a set scalarisation weight for a trial will guide the search towards a specific region in the Pareto front. The trial-averaged hypervolumes are significantly lower than the combined hypervolume over 15 trials as may be observed by comparing the HC columns in Tables 7.5 in page 152 and 7.6 in page 153.

7.7.1 Weighted-sum vs. Chebyshev scalarisation

Many scalarisation techniques are available to combine the objectives in a multi-objective problem [119]. In this study, two scalarisation methods were tested, namely, weighted sum and Chebyshev. While weighted sum is a simple and popular technique where a linear sum of the objectives is used as the combined objective, Chebyshev scalarisation uses the following expression to combine the objectives:

$$\min_{\boldsymbol{x}} \qquad C_{ch} = \text{maximum}\Big(-w_1(\overline{\alpha} - \overline{\alpha}_{target}),\ w_2(V_f - V_{f,target})\Big) \tag{7.5}$$

where C_{ch} must be minimised. For Chebyshev scalarisation, a target value needs to be assigned for each objective, i.e., $\overline{\alpha}_{target}$ and $V_{f,target}$ in the equation for sound absorption and volume fraction, respectively. The combined objective to be minimised is then the maximum of weighted deviations from the target. A utopian set of target values one could choose is $\overline{\alpha}_{target} = 1$ and $V_{f,target} = 0$. Even though targets are impossible to achieve simultaneously since, mathematically it provides a way to assign a single performance scalar for a given shape that can be optimised. The concept behind such a scalarisation technique is that a trade-off solution between two neighbouring solutions in the objective space may not have a better combined scalarisation when weighted-sum scalarisation is used, whereas Chebyshev scalarisation would give it a higher combined objective value. This essentially is an exploration of the neighbourhood of the Pareto front. The isolines of the scalarised objective using Chebyshev scalarisation are plotted for various values of weights and targets in Figure 7.11.

During testing, we observed that weighted-sum scalarisation outperformed Chebyshev scalarisation consistently. Table 7.4 shows a comparison of the hypervolumes obtained by the two techniques empirically on the problem instances. Hence, a decision is made to use the weighted-sum scalarisation method. Although many other scalarisation methods exist, performing comparison studies using them may be considered in future works. Within this chapter, unless otherwise stated, HC will refer to a multi-objective hill climbing with a weighted-sum scalarisation technique.

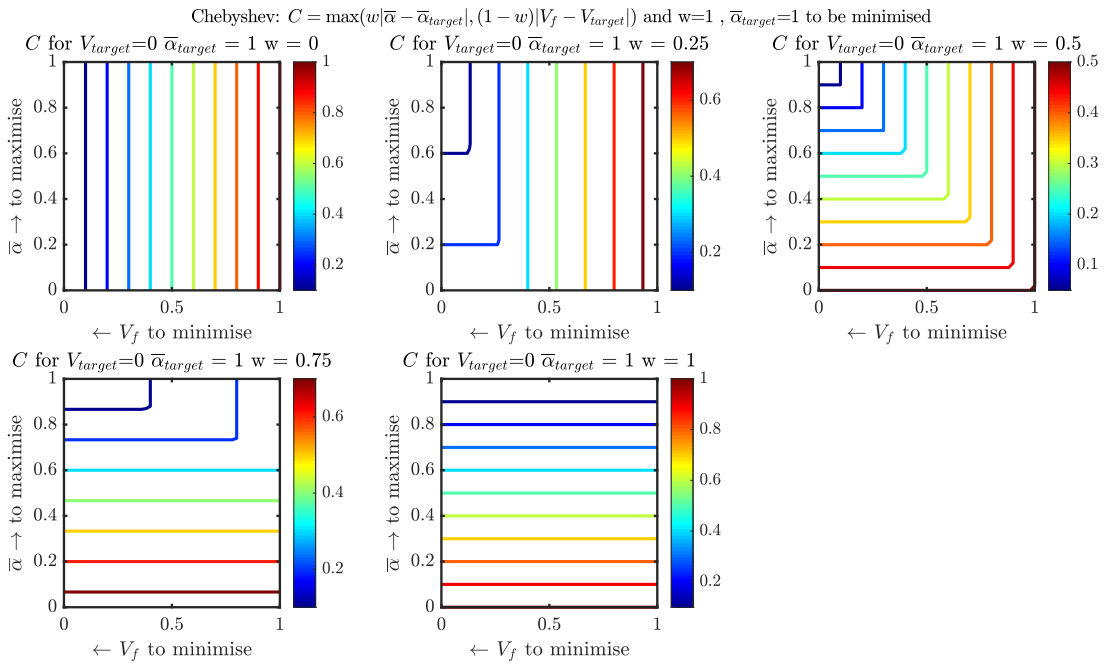

Figure 7.11: Isolines of combined objective in Chebyshev scalarisation. In this example, when the objective function targets are fixed and the weights are varied, the aspect ratios of the rectangular isolines vary.

The reason for the poor performance of Chebyshev scalarisation is explored further. It is found that for some solutions that hill climbing crosses through, none of the bitflips resulted in an improvement in Chebyshev fitness. Referring to Figure 7.12, a bitflip operation on the current solution (denoted by a red dot) may result in a new solution (yellow dot) that has a better fitness according to weighted-sum scalarisation but not in Chebyshev due to the sharp rectangular isoline (blue dashed line). When none of the bitflips produce solutions that cross the Chebyshev isoline (towards top left of blue dashed lines), the algorithm gets stuck. However, this is not the case for weighted-sum scalarisation which has a relatively liberal acceptance isoline (towards the top left of the brown dotted line). In essence, such solutions are local optimal for Chebyshev scalarisation, whereas in weighted-sum scalarisation, the new solution is accepted, allowing the possibility to find better solutions as indicated by the green point in Figure 7.12.

7.8 Non-dominated sorting genetic algorithms (NSGA-II)

NSGA-II is a popular multi-objective optimisation strategy introduced by Deb *et al.* [69]. It has been effectively used in solving multi-criteria decision-making problems across a plethora of domains. In this implementation, a single-point cross over with an individual cross-over probability of 0.9 is applied with a bit-wise mutation rate of 1/ (chromosome length). The CPU time for non-dominated sorting is insignificant compared to the objective function evaluation time, and hence the function evaluation budget consideration remains valid for comparing NSGA-II with other algorithms. Figure 7.13 shows the progress of solutions in the objective function space for one trial of NSGA-II for all problem instances. In the figure, each point refers to a particular shape, and the colour corresponds to the generation in which it is found. We can observe that as the generations progress (from blue to red), the solution set tends towards the top

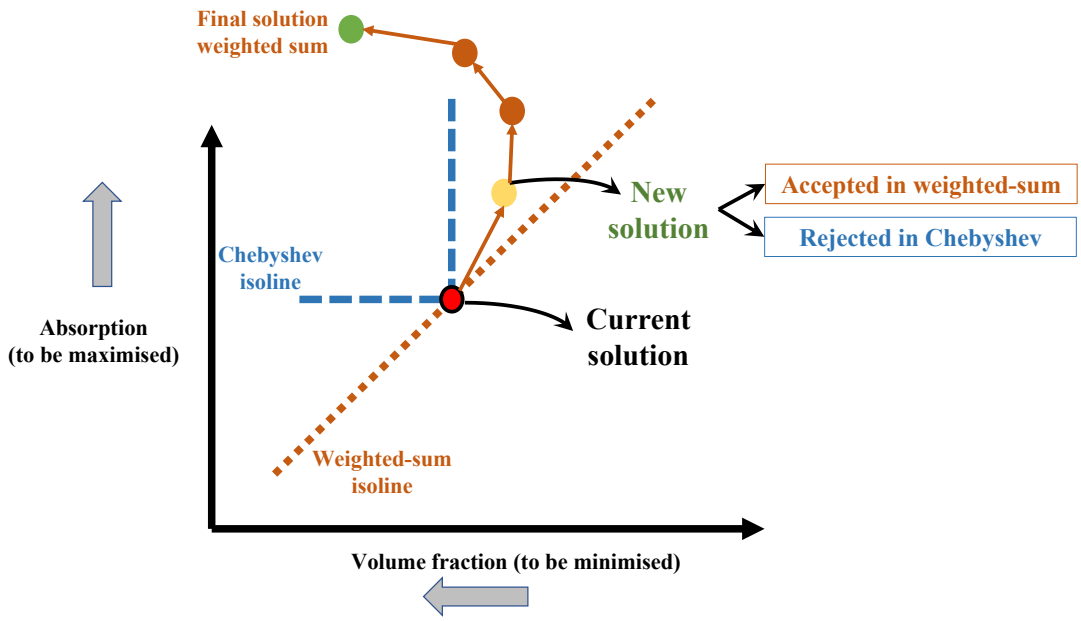

Figure 7.12: An illustration as to why weighted sum scalarisation performs better compared to Chebyshev scalarisation.

left corresponding to more sound absorption and less volume fraction. While the improvement in the quality of solutions over the generations is more prominent in problem instances 1, 3, 5 and 7, it is not significant in others.

In Figure 7.14, the final Pareto front after applying non-dominated sorting across all solutions in a given trial is shown. For problem instance 1, it seems that better quality solutions tend to have porous materials at the back of the domain closer to the rigid wall. For problem instances 2, 5 and 7, at low volume fractions, the shapes seem to fill material closer to the acoustic source, and for higher volume fractions, a cavity is formed closer to the rigid wall. For problem instance 3 and 6, the shapes found are too intricate that they did not have any overall feature. This is a drawback for NSGA-II as the shapes are not manufacturable when no filtering techniques are considered. For problem instance 4, the optimal shapes have an inverted-wedge-like shapes.

7.9 Random Search (RAND)

For establishing a baseline, a random search algorithm is also included in the pool of strategies compared. In this implementation, the random solutions are obtained across various volume fractions by choosing the desired volume fraction uniformly between 0 and 1, and using this value as the probability to fill porous material at each element. The solutions are generated at random until the budget is used up and the best results are returned.

The results from RAND for all problem instances are shown in Figure 7.15. On examining all the solutions picked by RAND, we observe that at a particular volume fraction, the spread of absorption values of the solutions is distinct for each problem instance. Two trials are shown with different coloured dots to highlight that multiple trials do not significantly change the distribution of solutions in the objective space. In problem instance 6, the spread of absorption at any picked volume fraction is small, indicating that a random solution picked at that volume

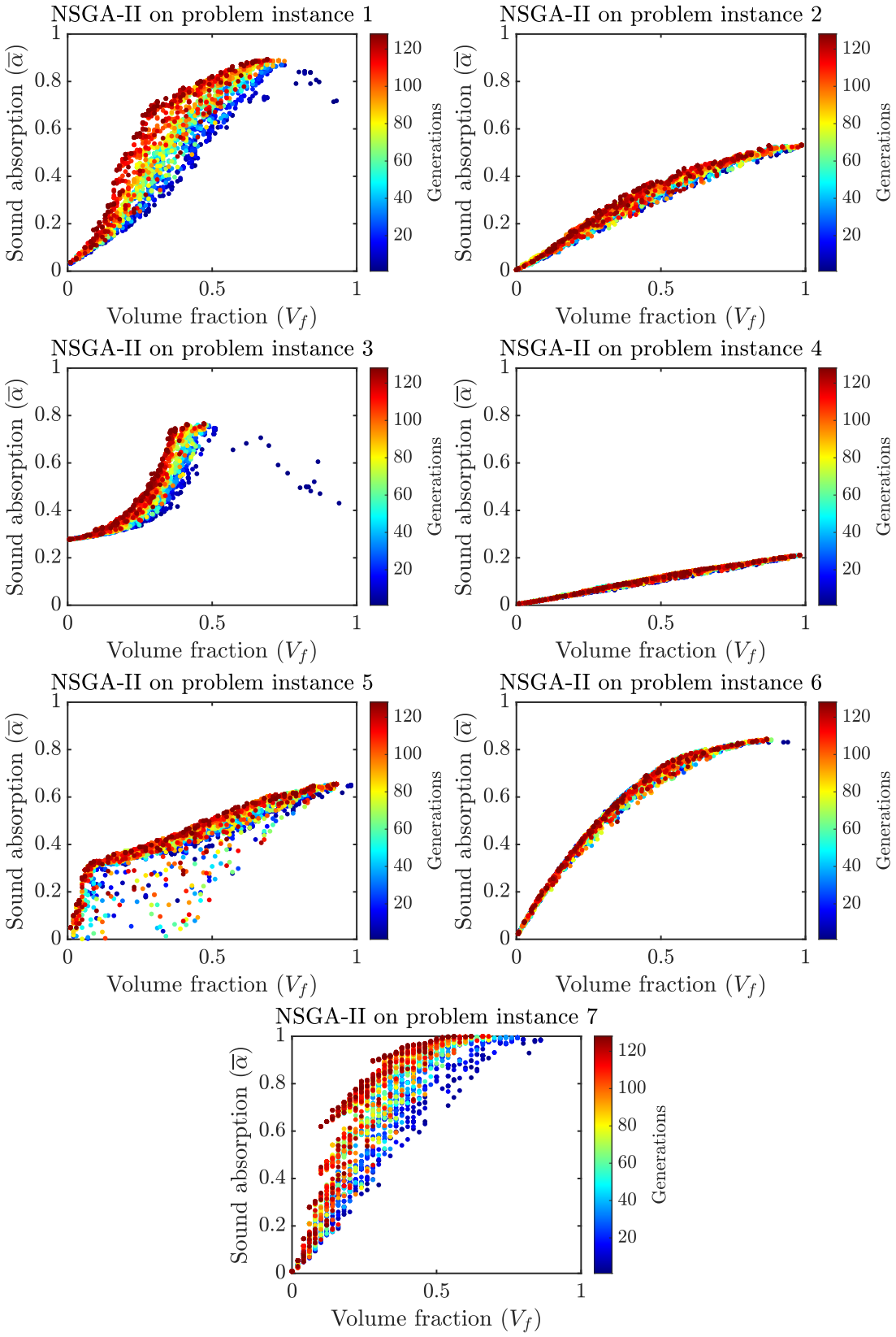

Figure 7.13: NSGA-II on problem instance 6: Pareto front with trade-off shapes.

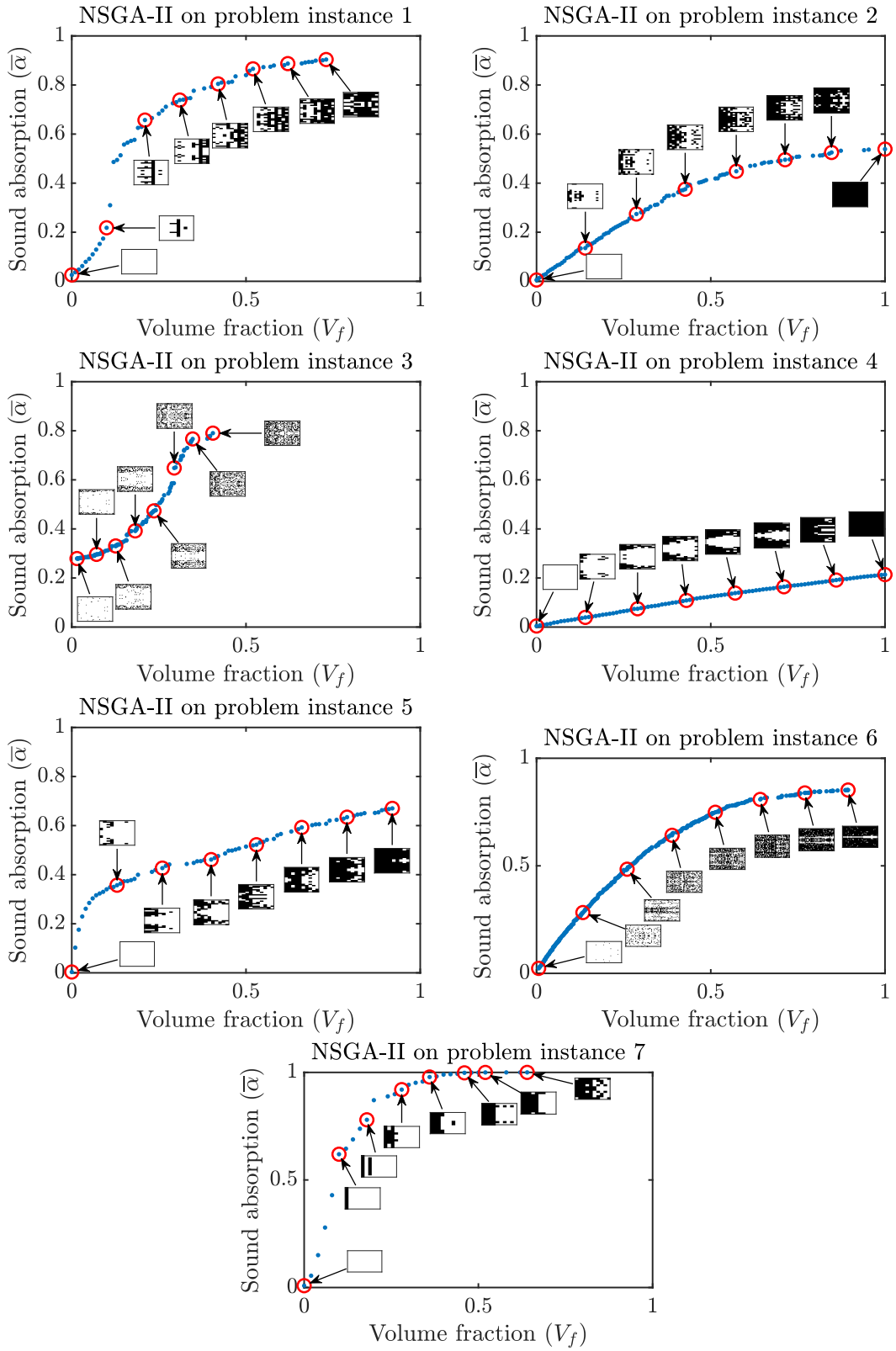

Figure 7.14: NSGA-II trade off shapes in the objective function space for all problem instances.

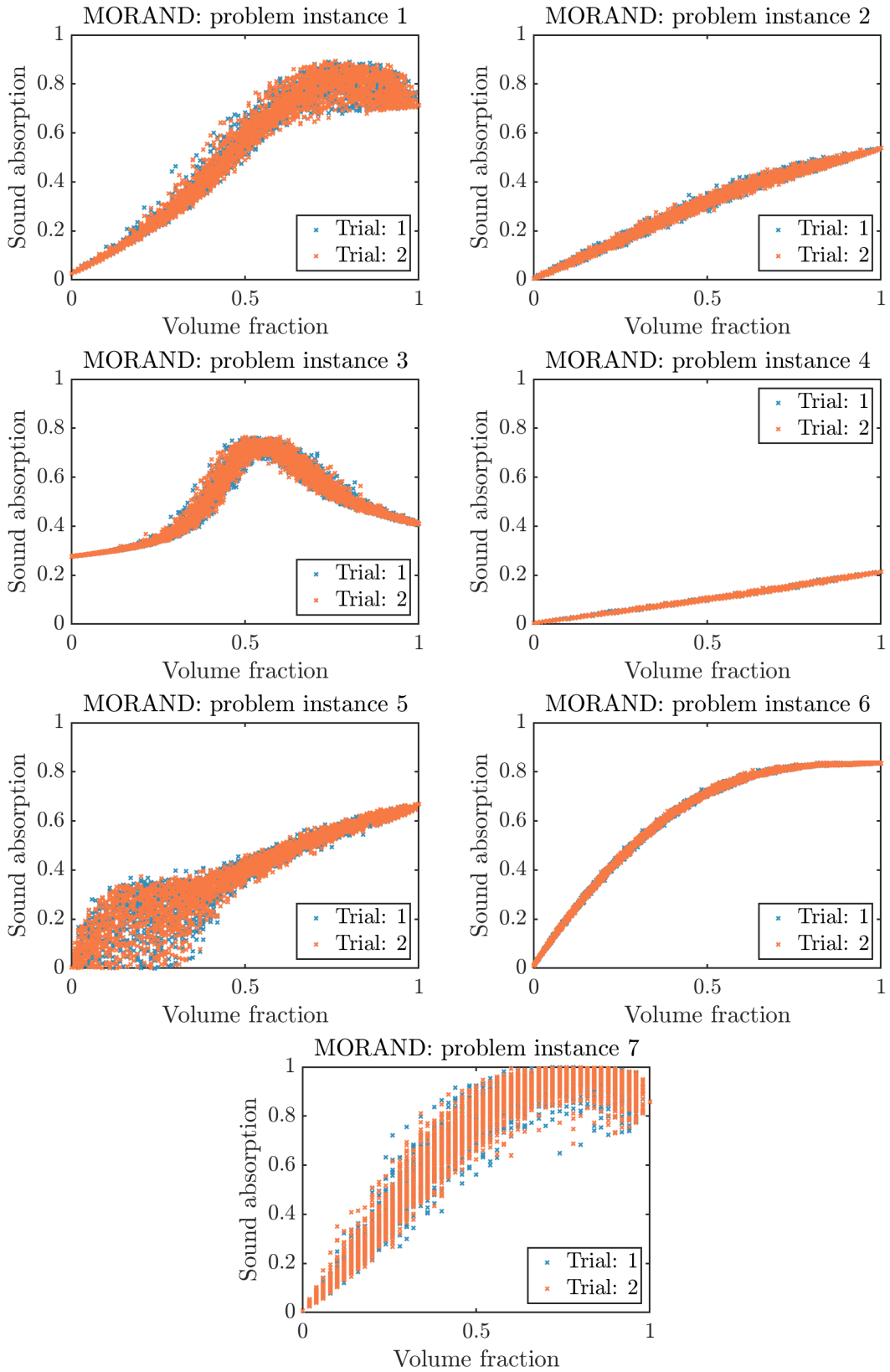

Figure 7.15: Pareto solutions from RAND on all problem instances. Notice the unique spread of absorption values at a given volume fraction for each problem instance. For instances 2, 4 and 6, the spread is less indicating either that there may be little benefit to optimising or that the best solutions are outliers which may be hard to find using search methods.

fraction may be expected to have similar quality. However, this is not the case in other problem instances such as 1, 3 and 7, where solutions at a particular volume fraction seem to have a reasonable spread in absorption. By studying the improvement obtained by an algorithm in comparison to a random search, some aspects of the fitness landscape can be uncovered. For instance, if RAND performs better than a gradient approach, it indicates that the landscape might be highly rugged and multimodal. Problems identified to have rugged landscapes may benefit from population-based strategies.

7.10 Comparison of non-gradient algorithms

7.10.1 Performance per trial

As we now understand, in a given HC trial, based on the choice of the scalarisation weight, only a specific region of the Pareto front will be explored. Hence, if only one trial of the algorithm is allowed, HC can cover the specific region of the Pareto front well but not cover much of the other regions resulting in a Pareto set with a poor hypervolume. On the other hand, in one trial, NSGA-II solutions can span the objective space effectively due to the crowding distance control mechanism in the algorithm.

Comparing the median-trial hypervolumes from HC and NSGA-II in Table 7.5, it is clear that NSGA-II is consistently better across all problem instances. This is because based on the choice of scalarisation weight, in a given trial, HC only explores a specific region in the Pareto front. Whereas, NSGA-II spans the objective space effectively due to the crowding distance-based selection mechanism. NSGA-II also outperforms RAND in all problem instances, but interestingly, HC, on a per-trial basis, does not outperform even RAND. Moreover, RAND outperforms HC across all problem instances. This is because HC in a single trial is essentially a single-objective algorithm that does not incentivise spanning the hypervolume.

7.10.2 Performance across 15 trials

It is of interest to see which algorithms have achieved a better combined performance across the 15 trials. If all regions of the objective space are explored by repeated trials of HC, different regions of the Pareto front can be explored. Figure 7.16 shows the combined Pareto fronts from 15 trials of HC, NSGA-II and RAND, involving 15×4096 function evaluations. To arrive at this plot, first, a non-dominated sorting is done for all the solutions searched in a trial. Then, the Pareto solutions from each trial are combined, and a final non-dominated sorting is performed. The results show that solutions from HC are often superior for a given volume fraction value across problem instances.

Combining 15 trials of HC run with different weights results in a better hypervolume than the combined results of 15 trials of NSGA-II consistently across all problem instances, as can be observed in Table 7.6 (see columns HC vs. NSGA-II). While the performance of NSGA-II is similar to HC in some problem instances, in others, NSGA-II performed relatively poorly.

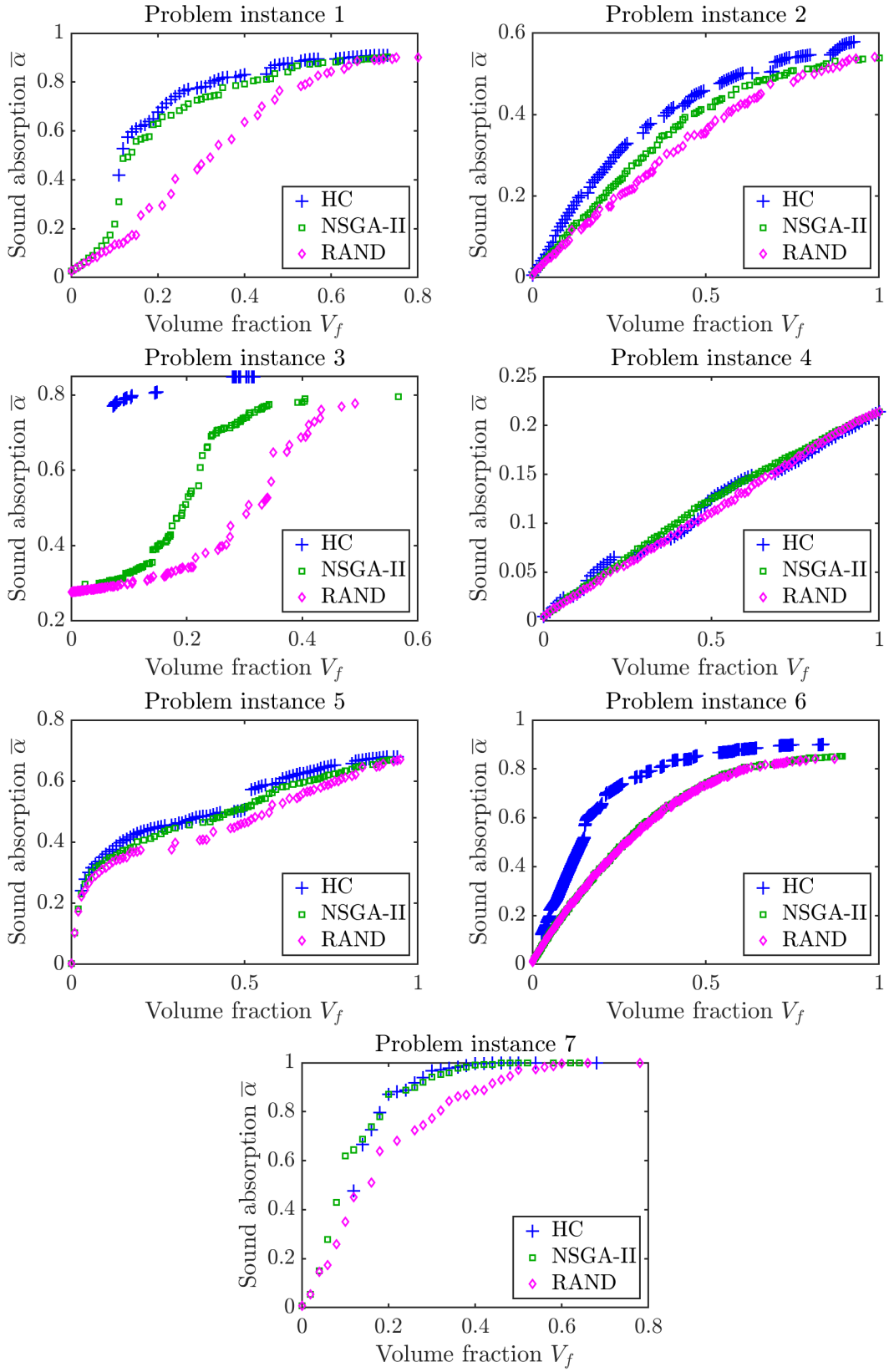

Figure 7.16: Combined Pareto fronts from 15 trials of HC, NSGA-II and RAND on all 7 problem instances.

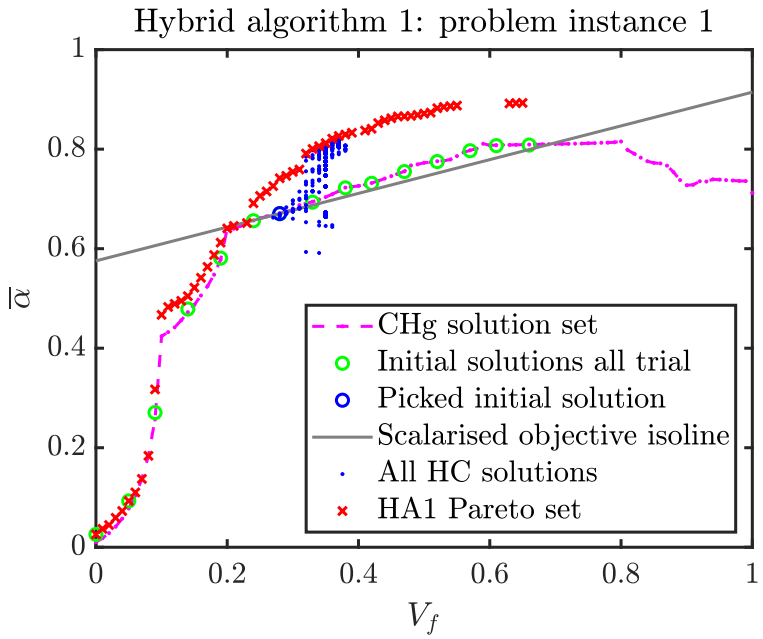

Figure 7.17: Illustration of one trial of hybrid algorithm 1. Procedure: Apply CHg for 25% of the trials. Pick a point on the CHg Pareto set. Find the slope of the Pareto front using central difference. Set scalarisation weight such that the isolines of the combined objective are parallel to the tangent of the Pareto front at the selected CHg point. Apply hill climbing for rest of the fitness evaluation budget. The final Pareto set after 15 such trials each starting from equispaced points on the CHg Pareto set are shown using red 'x' markers.

Hybrid algorithms

From the studies on the gradient and non-gradient algorithms, there are a few points to take away. Gradient methods, while they are quick to approximate the Pareto front, they are often outperformed by HC when interested in solutions with a specific volume fraction. However, using non-gradient algorithms can be quite time-consuming to explore all regions in the Pareto front. In order to obtain the benefits of both, two hybrid approaches combining a gradient-based algorithm for the initiation and a non-gradient algorithm for improvement are presented and compared. The first hybrid approach is a combination of CHg and HC, denoted as HA1, and the second hybrid approach is a combination of CHg and NSGA-II, denoted as HA2. We picked CHg as the initiator mainly because it guarantees discrete solutions and allows the possibility to speed up (see section 7.6).

7.11 Hybrid algorithm 1: CHg+HC

In the first algorithm, we introduce a novel adaptive scalarisation technique that considers the isolines of the scalarised objective function to be tangential to the Pareto front. Similar approaches that use adaptive weighted-sum scalarisation have been shown to perform well [145, 255].

Hybrid approach 1 (HA1) combines the use of CHg for 25% of the budget and HC for the remaining 75% of the budget. These numbers are arbitrarily chosen with some basis on experience. Since CHg is gradient-based, and gradient-included evaluations are thrice as expensive as non-gradient fitness evaluations (equation 7.2), the rationing is such that CHg uses $25\% \times (\frac{4096}{3})$

fitness evaluations and HC uses $75\% \times (\frac{4096}{1})$.

Figure 7.17 illustrates the procedure involved in HA1. Firstly, CHg is run to obtain a trade-off solution set. Then, 15 solutions are selected from the CHg trade-off set equispaced in volume fraction to use as initial solutions for each of the 15 HC trials. For each HC trial, a different scalarisation weight w is used such that the isolines of the combined objective C has a slope tangential to CHg Pareto front at the initial solution. The slope of the Pareto front at the initial solution is obtained using a simple central difference of adjacent points. This *Pareto-slope-based scalarisation* effectively guides HC to find improvements to the Pareto front. Then, HC is run until the remaining budget is used up. As seen in Figure 7.17, in each trial, only a specific region is explored. The hypervolumes covered after each trial and after combining all 15 trials are computed. The per-trial median hypervolumes and 15-trials-combined hypervolumes obtained by HA1 are provided in Tables 7.5 and 7.6 for all problem instances.

In Figure 7.18, the final Pareto front across 15 trials of hybrid algorithm 1 is shown. For problem instance 1, HA1 seems to include a middle porous layer and gradually grows into a wedge-like shape, although with intricate holes which are difficult to manufacture. For problem instance 2, HA solutions are simplest to explain among the algorithms so far discussed. All the Pareto shapes have a flat layer of porous material as far away from the rigid backing as possible. For problem instance 3, however, the shapes exhibit checkerboard patterns with no clear shape. Within the checkerboard pattern, there seems to emerge a gross pattern, which encloses three air cavities along the vertical axis. This pattern does not resemble any of the solutions produced by SIMPsweep or SIMPrestart, which in turn were able to find shapes with reasonable patterns. For problem instance 4, the shapes seemed to resemble inverted wedges. But these shapes seem to be slightly better than the shapes produced by CHg in terms of manufacturability. For problem instance 5, there were clear patterns of inverted wedges in optimal shapes. For problem instance 6, the optimal shapes were predominantly two simple flat porous layered with air gaps. The shapes for problem instance 7 suggest the addition of porous material away from the rigid backing, similar to all other algorithms.

7.12 Hybrid algorithm 2: CHg+NSGA-II

Hybrid approach 2 (HA2) combines CHg and NSGA-II in a similar fashion, i.e., CHg uses 25% of the budget, and NSGA-II uses the remaining 75%. The rationing of fitness evaluations is similar to that in HA1.

Originally, the final solution set from CHg was meant to be used as the initial population for NSGA-II in each trial. However, on some occasions, the CHg Pareto front contained more or less solutions than the population size assigned for NSGA-II. Hence, when there were more solutions in CHg Pareto set, only 32 solutions equispaced in volume fraction were considered as the initial population for NSGA-II, and when there were fewer than 32 solutions, they were duplicated using the selection process in the first generation. Then NSGA-II is run for the remainder of the budget.

Figure 7.19 shows the solutions searched in an example trial out of the 15 trials that were run for problem instance 1. The combined Pareto front from 15 trials is then plotted using red crosses. It may be observed that in the low volume fraction regions, the solutions from NSGA-II never

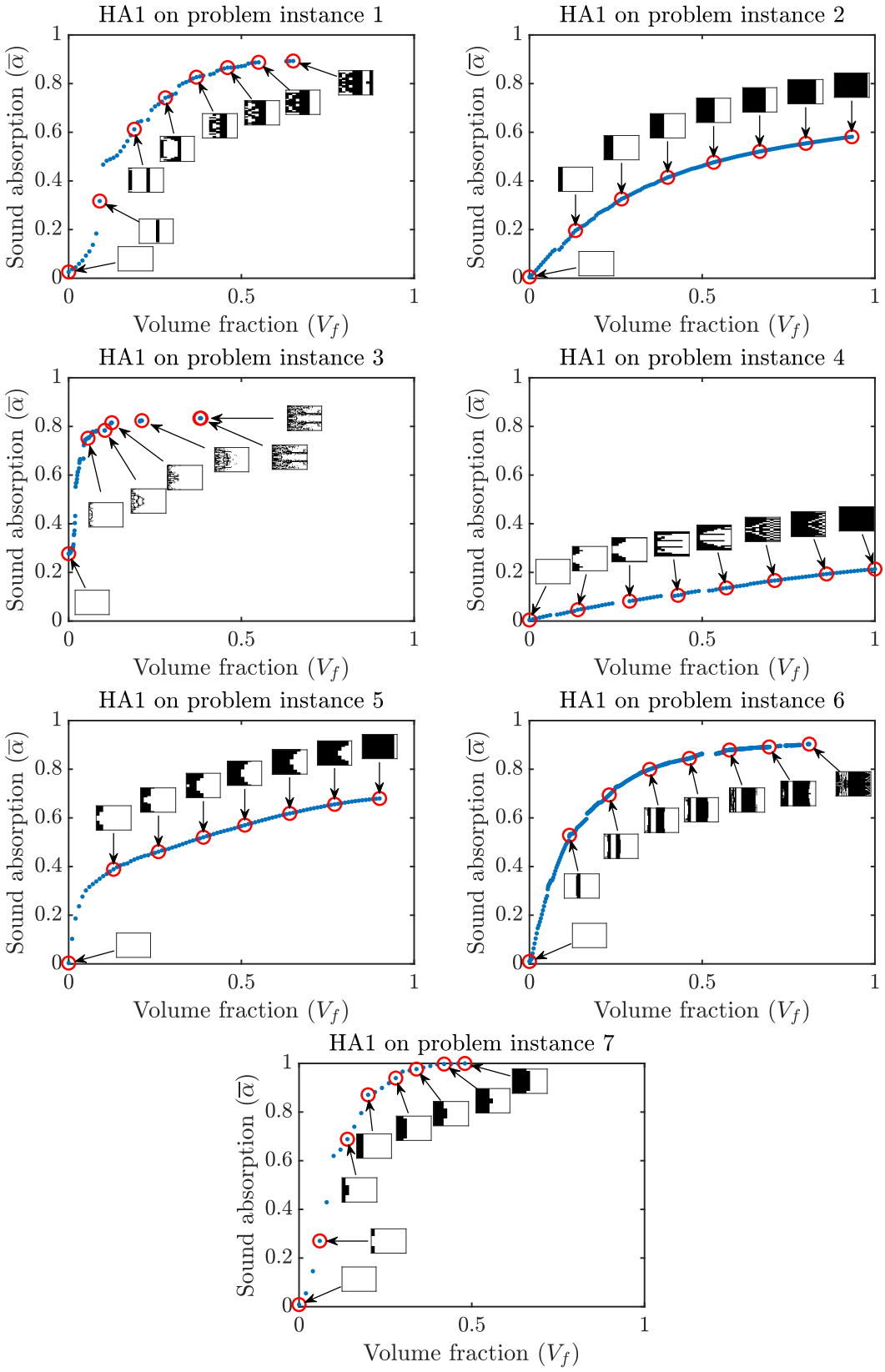

Figure 7.18: HA1 trade off shapes in the objective function space for all problem instances.

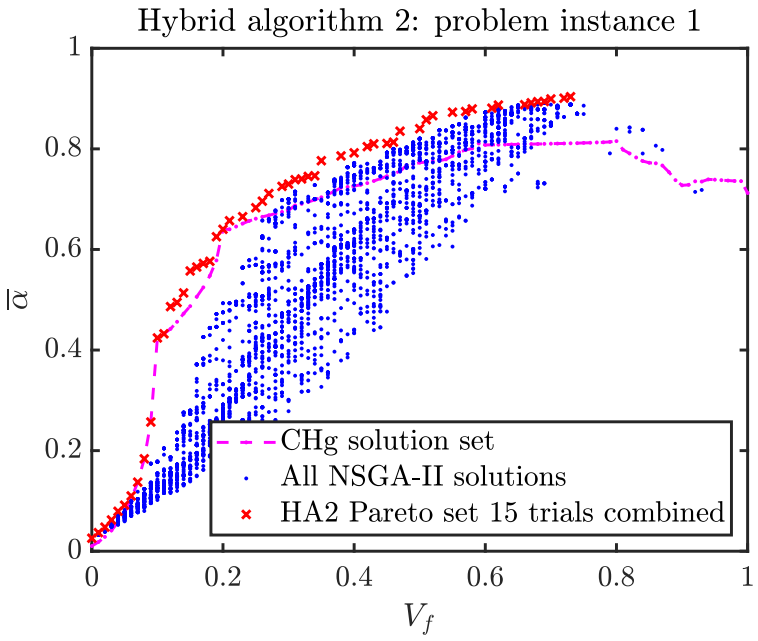

Figure 7.19: Illustration of one trial of hybrid algorithm 2. Procedure: A combination of CHg run for 25% of computational budget, and then using the Pareto set as the initial population, NSGA-II is run for 15 trials and the resulting combined Pareto front is found.

seem to improve. This is because crossover and mutation operations always produce worse solutions. The hypervolumes covered by the median trial and the overall hypervolume of the combined non-dominated solutions across 15 trials of HA2 are provided in Tables 7.5 and 7.6.

Figure 7.20 shows the final Pareto front across 15 trials of hybrid algorithm 2. For problem instance 1, HA2 includes porous layers towards the rigid backing end with no apparent pattern emerging in the front end facing the acoustic wave. These shapes are even more intricate than HA1 and are worse in terms of manufacturability. For problem instance 2, it is interesting to note that HA2 solutions exactly resemble those of HA1. Both HA1 and HA2 produce simple flat layers away from the rigid wall for this problem instance. For problem instance 3, however, unlike HA1, the shapes from HA2 seemed to fill material only close to the left edge of the design domain and exhibit checkerboard patterns with no precise shape. For problem instance 4, the shapes seemed to resemble inverted wedges, like in many other algorithms. However, the shapes have almost a clear cavity, which is easier to manufacture relative to those of CHg and HA1. For problem instance 5, there were patterns of inverted wedges in optimal shapes similar to HA1. For problem instance 6, the optimal shapes were predominantly two simple flat porous layers with air gaps. The shapes for problem instance 7 suggest adding porous material away from the rigid backing, but the shape pattern is a bit clearer than those from other algorithms, especially HA1.

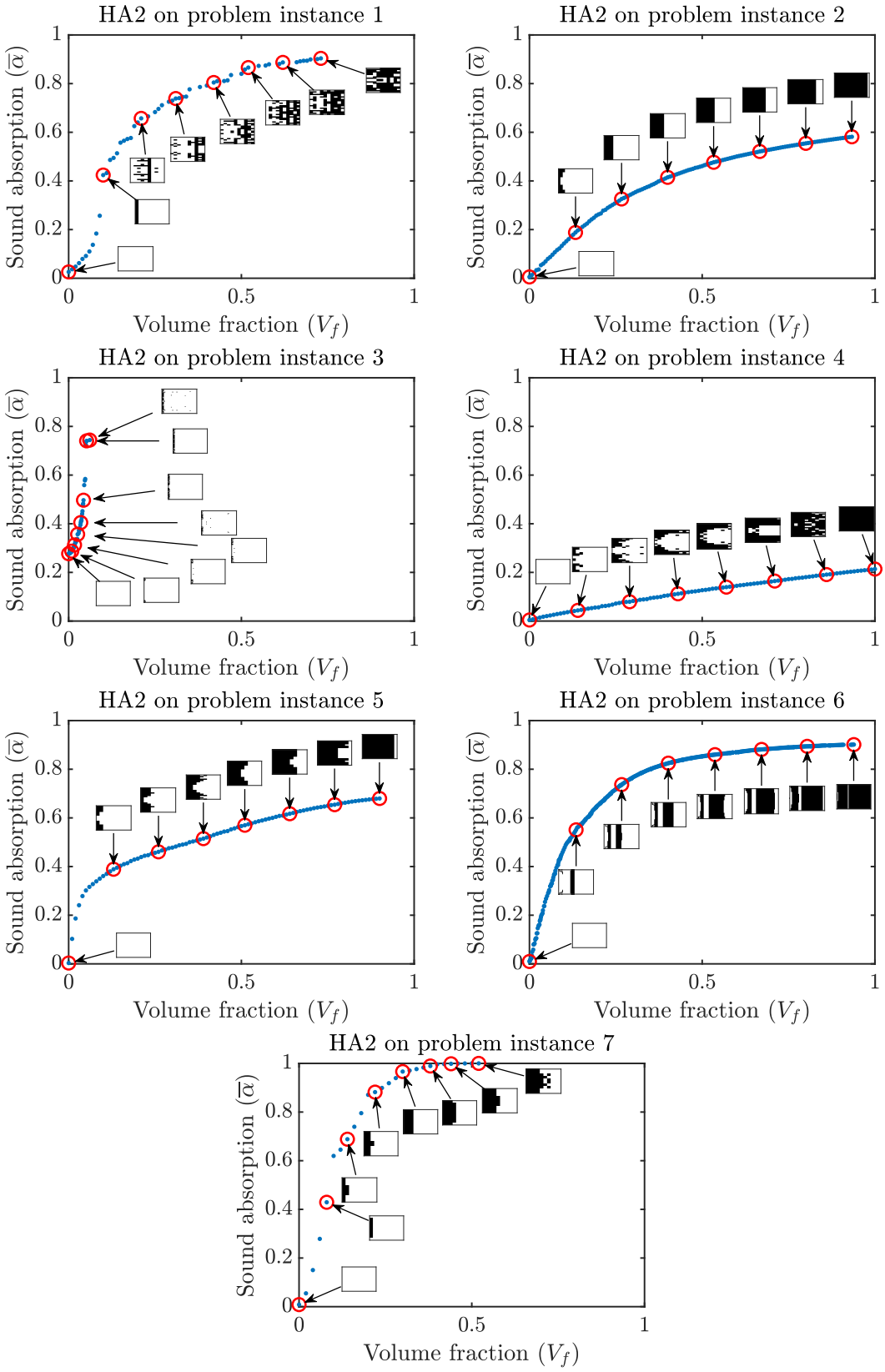

Figure 7.20: HA2 trade off shapes in the objective function space for all problem instances.

Table 7.5: Median hypervolumes obtained while running one trial with a budget equivalent to 4096 gradient-free fitness evaluations. HA2 seems to perform best when considering the trial-averaged performance for 4096 fitness evaluations.

	Gradient-based			Gradient-free			Hybrid	
Fitness evaluations	1365	1365	min(n_e/m,1365)	4096	4096	4096	4096	4096
Instance/ Alg.	SIMPrestart	SIMPsweep	CHg	HC	NSGA-II	RAND	HA1	HA2
1	0.7065	0.6835	0.6724	0.5622	0.6824	0.5915	0.7013	**0.7170**
2	0.4014	0.4047	0.4066	0.2684	0.3427	0.3212	0.4066	**0.4068**
3	0.7317	0.6063	**0.7412**	0.5908	0.6336	0.6061	0.7343	0.7184
4	0.1160	**0.1188**	0.1087	0.0893	0.1148	0.1085	0.1122	0.1174
5	0.5208	0.5292	0.5323	0.3798	0.4847	0.4561	0.5324	**0.5327**
6	0.7202	**0.7607**	0.7512	0.5430	0.6159	0.6211	0.7603	0.7601
7	0.8727	0.8567	0.8733	0.7133	0.8531	0.7677	0.8733	**0.8758**

7.13 Overall comparison

7.13.1 Trial-averaged performance for 4096 budget

For a computational budget of 4096 gradient-free fitness evaluations, Table 7.5 shows the resulting hypervolumes covered by all algorithms used in this study. It should be noted that CHg did not need to use the entire budget. Since in each iteration, CHg has to fill at least one element, the entire design domain can be filled with only {100, 150, 1000, 100, 100, 1000, 50} fitness evaluations respectively for problem instances 1 through 7.

Keeping this in mind, the table shows that HA2, a combination of CHg and NSGA-II, covers the most hypervolume in 4 out of 7 problem instances on average per trial. Note that HA2 also performs better than stand-alone NSGA-II for the same budget. While it is evident that gradient-based initialisation boosts the performance of NSGA-II, it is interesting to note that HA2 can perform better than SIMPrestart or SIMPsweep, which are normally used in practice. Thus, if one has a fixed computational budget to cover the most hypervolume, a reliable strategy is to use a combination of CHg followed by NSGA-II.

Also, it is worth noting that SIMPsweep performs the best in two problem instances, and CHg performs best in one problem instance. Notably, SIMPsweep and CHg are also scalable for lower budgets. These three algorithms may be recommended for applications such as software implementations in the initial stages of design that need to quickly come up with trade-off acoustic solutions within a set computational budget.

7.13.2 Combined performance of 15 trials each with 4096 budget

*Table 7.6: Combined 15-trial hypervolumes covered by all algorithms for all problem instances. Hybrid algorithm 1 (CHg + HC) covers the most hypervolume across 6 out of 7 problem instances given the same budget of 15*4096 equivalent gradient-free fitness evaluations.*

	Gradient-free			Hybrid	
Instance	HC	NSGA-II	RAND	HA1	HA2
Budget	15*4096	15*4096	15*4096	15*4096	15*4096
1	0.7436	0.7302	0.6221	**0.7438**	0.7307
2	0.4029	0.3613	0.3329	**0.4081**	0.4074
3	0.7772	0.6878	0.6219	**0.8104**	0.7295
4	0.1144	0.1169	0.1107	**0.1195**	0.1190
5	0.5212	0.5034	0.4708	**0.5343**	0.5337
6	0.7509	0.6310	0.6269	**0.7646**	0.7606
7	0.8407	0.8725	0.8021	0.8755	**0.8759**

It is also of interest to identify effective strategies that find solutions with the best attainable quality with relaxed computational time budgets, such as for manufacturing the best acoustic designs. Table 7.6 shows the resulting hypervolumes covered by a combination of 15 trials which is equivalent to 15*4096 gradient-free function evaluations. For this comparison, we do not include the gradient methods as they did not use the same budget.

In this study, HC shows a significant improvement as it is able to combine the good solutions from various regions of the Pareto front. For the same reason, HA1 (CHg+HC) also performs exceptionally well, producing the best hypervolumes in 6 out of 7 problem instances. This shows that the proposed Pareto-slope-based weighted-sum scalarisation technique with a simple greedy hill climbing algorithm can be used as an effective local improvement strategy. A takeaway is that before manufacturing an optimal shape using any multi-objective topology optimisation approach, it is worth ensuring that there exists no other dominating solution that HC can find.

Between NSGA-II and its hybrid counterpart HA2, the latter seems to cover more hypervolumes across all problem instances. This is again an example of a hybrid approach performing better than its parent approach. HA2 also performed the best in one of the seven problem instances and comes close to the performance of HA1. This show that there is a benefit to using hybrid strategies involving gradient initialisers with non-gradient improvers.

7.13.3 Pareto front comparison for all algorithms combined across 15 trials

The problem of topology optimisation has no exact algorithms that run in practical times to confirm the true Pareto-optimal solutions. Nevertheless, it is of interest to see which algorithms contribute to finding the best-known solutions in the Pareto diagram.

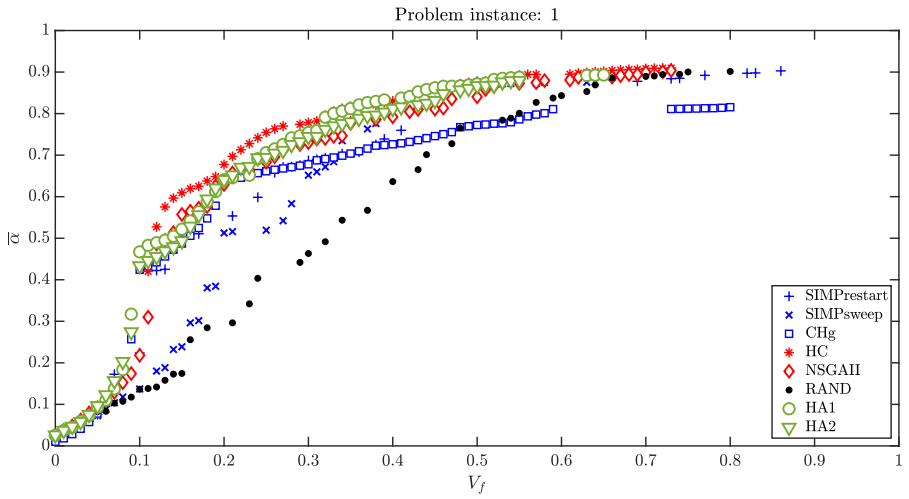

Figure 7.21: Comparison of all Pareto fronts in problem instance 1. The gradient algorithms are marked in blue, non gradient algorithms in red, and hybrid algorithms in green.

Hence, we compare the Pareto fronts obtained from all algorithms in one place. As an example, this is shown for problem instance 1 in Figure 7.21. The gradient algorithms are marked in blue, non-gradient in red and hybrid in green. For other problem instances, the figures are included in Appendix C.

It should be noted that the Pareto fronts for gradient algorithms are obtained from only one trial, while results for other algorithms are from a combination of 15 trials. Hence, one cannot draw a direct comparison between gradient strategies and others.

Among the three gradient algorithms, it may be observed that CHg finds better absorbing solutions in lower volume fractions up to 0.3, and the SIMP algorithms found better solutions after $V_f = 0.3$.

Among non-gradient algorithms, it is clear that all approaches perform better than random search, but there is no single clear winner between HC and NSGA-II.

Hybrid algorithms work best to cover the most hypervolume, but interestingly, there are some regions where HC produces better non-dominated solutions (see between $V_f = 0.1$ and 0.3). This shows that one cannot ignore HC just because the hypervolume spanned is poor. The potential of HC for local exploration needs to be recognised.

7.14 Conclusions

In this chapter, several multi-objective strategies were compared to identify effective approaches for quickly obtaining lightweight and high-absorbing acoustic shape designs within a given amount of computational effort. Three gradient strategies—SIMPrestart, SIMPsweep and CHg, two gradient-free strategies—HC and NSGA-II, and two hybrid strategies—HA1 (CHg+HC) and HA2 (CHg+NSGA-II), were studied. The findings are highlighted as follows.

1. Gradient algorithms often get stuck at local-optimal shapes, indicated by the fact that non-gradient approaches have been able to find better solutions in terms of both absorption and volume fraction objectives.
2. Reusing solutions from SIMP with an adaptive volume fraction constraint (SIMPsweep) is better at finding closely spaced points in the Pareto front than restarting SIMP at various volume fraction constraints (SIMPrestart).
3. A simple new gradient-based constructive heuristic (CHg) is introduced that guarantees discrete solutions while also being scalable and as performant as SIMP algorithms.
4. NSGA-II proves to be most effective in spanning the hypervolume on a per-trial basis for a fixed computational budget, among gradient and non-gradient methods.
5. Hybrid approaches using gradient algorithms as initialisers and non-gradient algorithms as exploiters seem to be more effective than any parent gradient or non-gradient algorithm for the same computational budget.
6. Hill climbing with a Pareto-slope-based weighted-sum scalarisation proves to be an effective local search technique to improve solutions near the Pareto front.

Some guidelines for choosing an algorithm from the results are provided as follows: If the goal is to quickly find a set of trade-off shapes, such as to use in software applications, then any gradient approach or a hybrid approach with CHg and NSGA-II would be more suitable. If the goal is to obtain the optimised shape designs of the best attainable quality for manufacture, then a hybrid approach with CHg and hill climbing with a Pareto-slope-based scalarisation seems to be more suitable. If the interest is to find the best attainable trade-off solutions to a problem, then no algorithm is a clear winner. Algorithms such as HC occasionally find better solutions in specific regions than their hybrid counterpart and cannot be ignored.

Chapter 8

Conclusions and perspectives

The work carried out as part of this thesis and the contributions to the field are highlighted in this chapter. The chapter is organised as follows. Section 8.1 covers the work on multilayered sound package optimisation, section 8.2 covers with single objective topology optimisation for absorption maximisation, and section 8.3 covers the multi-objective topology optimisation work is summarised. Section 8.4 discusses some perspectives and future work prospects, and a final concluding remark is provided in section 8.5.

8.1 Multilayered sound package optimisation study

8.1.1 Summary

Flat multilayered acoustic material packages are more widely used in the industry as sound panels for sound absorption and isolation. Studies on optimising multilayered sound packages, especially for absorption maximisation, have last been reported in 2006 and since then many recent materials and models have been introduced. The fitness landscapes have not been studied previously in this problem domain. This thesis presented substantial progress in this regard as reported in chapter 5. For multilayered sound package optimisation, the material choices for each layer are the decision variables and the thicknesses and acoustic properties are the design variables. Initially, the fitness landscapes over the acoustic properties in two-layered systems were studied. Then, for a three-layered system, the exploration of optimal material choices from 29 available materials and the thicknesses for each layer was considered. A steady-state genetic algorithm with integer representation was applied to find near-optimal solutions. The effects of various parameters of GA were studied. To analyse the fitness landscape over the material configurations and thicknesses, a brute-force search on all possible material configurations for a fixed equal-thickness three-layered system was carried out. For the best material configuration, all possible thickness configurations for a total thickness constraint were explored to study the fitness landscape across thickness variables. The insights gained were used to arrive at some guidelines for algorithm selection.

8.1.2 Contributions

The main contributions are highlighted as follows.

1. The fitness function landscapes across the acoustic design variables—static airflow resistivity and porosity—were assessed for the first time in the absorption maximisation

problem and were found to be smooth and uni-modal or with a few modes. The implication is that the optimising across those parameters can be performed quickly using simple steepest-descent hill climbing or CMA-ES etc.
2. Genetic algorithms were able to quickly find good quality solutions when material choices and thickness variables were optimised for a three-layered system. However, the improvements after a specific absorption value were insignificant or hard to obtain.
3. The choice of GA parameters such as population size, selection strategy and replacement seemed to have little effect on the performance.
4. Some materials (especially FoamR1) featured in the final best solutions more frequently than others over 30 GA trials.
5. A brute-force search over the material configuration for the three-layered system revealed that there exist many solutions which had a near-optimal absorption for the problem instance. The best solution found by GA trials was one among the many near-optimal solutions that were only insignificantly worse than the true optimum.
6. Across the thickness variables, the fitness landscape was observed to be smooth and unimodal.
7. From the insights obtained, as more layers are considered, a memetic algorithm with a combination of GA over the material choices and a hill climbing or a fast continuous approach such as hill climbing or CMA-ES seems to be a natural choice to explore.

8.2 Single objective topology optimisation study

8.2.1 Summary

A more challenging topology optimisation problem was tackled in chapter 6. This problem is significantly more challenging as the number of design variables usually involved is much larger, and the fitness evaluations are more expensive relative to multilayered optimisation. While there exist a few publications on acoustic topology optimisation, which mainly deal with implementation for various problem case studies, none exists that compares many different approaches. In this novel venture, fitness landscapes have been explored for the first time, and many domain-specific insights have been obtained. A single-objective optimisation problem involving maximising absorption was considered, without including any constraint on the volume fraction or manufacturability. The computations involved in fitness and gradient evaluation were investigated to understand the problem structure. Based on this, techniques to improve fitness evaluation speed without compromising on accuracy were implemented. A discussion on the practical time complexity of the fitness and gradient computations was provided. Further, empirical comparison studies were conducted using seven different optimisation approaches, including state-of-the-art heuristics and popular metaheuristics. The approaches tested are hill climbing, constructive heuristics, SIMP, GA, tabu search, CMA-ES and differential evolution. In total, eleven algorithms were tested that included variants of some of the approaches listed above. Firstly, the runtime performance of the algorithms was compared, which revealed that gradient methods quickly find good quality solutions. Then, the best solution performance for a given computational budget was compared over 31 trials. Some non-gradient algorithms such as hill climbing, a material addition constructive heuristic and a discrete variant of CMA-ES consistently outperformed SIMP variants across 7 problem instances. Different shapes produced by each algorithm and their frequency vs. absorption curves were discussed. Then, a fitness landscape analysis was carried out to assess why gradient algorithms are outperformed by non-gradient ones.

8.2.2 Contributions

The main contributions are highlighted as follows.

1. A detailed exploration of the fitness evaluation computation was used to estimate the theoretical and practical time complexities of both absorption and its gradient. This revealed that, in absorption maximisation, fitness and gradients have a similar time complexity, whereas in compliance minimisation, the gradient evaluation has a smaller time complexity than fitness.
2. The gradient-based SIMP algorithms were typically faster in reaching good quality solutions for low computational budgets.
3. When comparing over longer fitness-evaluation budgets, non-gradient algorithms were able to find better solutions than the optimised solutions produced by the state-of-the-art SIMP algorithms, meaning that gradient methods do converge to local optima and that the fitness landscapes might be rugged.
4. Hill climbing, a material addition constructive heuristic, and a discrete variant of CMA-ES were the top three across the seven problem instances when comparing the median value of best absorption obtained over several trials.
5. The convergence rate of a standard GA was found to be poor, and the final solution qualities were outperformed by other algorithms.
6. Among CMA-ES and DE, CMA-ES seems to be more suitable in this problem domain. Among continuous vs. discrete variants of CMA-ES and DE, discrete variants were found to be better. Hence, discretising before fitness evaluation may be considered for continuous algorithms.
7. When using CMA-ES, the shapes produced were not smooth, and using additional morphological filters may be necessary. Although the solution qualities were high for CMA-ES, the shapes produced were not smooth in this study which did not consider manufacturing. On the other hand, constructive heuristics, SIMP, hill climbing and tabu search produced shapes with distinguishable features.
8. The distribution of the absorption vs. volume fraction plot revealed that different algorithms tend to find solutions from different regions, indicating that the absorption maximisation problem is rich with unique varieties of solutions.
9. The general lesson is that no algorithm studied can be considered to be the best for all of the problem instances. If the interest is to quickly find good quality solutions, gradient methods are recommended. If the interest is to find the best quality shapes for manufacture, then using multiple effective methods and choosing from the best solutions may be a better overall strategy.

8.3 Multi-objective topology optimisation study

8.3.1 Summary

A multi-objective topology optimisation involving simultaneous maximisation of absorption and minimisation of porous-material volume fraction was considered in chapter 7. Multi-objective treatment has not been done previously in acoustic material shape design. In a first of its kind study, several multi-objective approaches were compared, resulting in an understanding of the balance between gradient and non-gradient methods. Based on the results and

insights obtained from chapter 6, only select algorithms were included in this study. The main theme was comparing gradient and non-gradient methods, and their hybrids. In a comparison among gradient methods, a new gradient-based constructive approach (CHg) was compared with two variants of multi-objective SIMP. In a comparison among non-gradient methods, a weighted-sum hill climbing and NSGA-II were studied. In empirical optimisation trials, it was observed that gradient algorithms were fast to reach an approximation of the Pareto front in less iterations. On the other hand, non-gradient approaches, for example, a hill climbing approach using a scalarisation technique, seemed to find better solutions in specific regions of the Pareto front. On a per-trial basis, NSGA-II was found to have a better performance. For hill climbing, two scalarisation techniques—weighted-sum and Chebyshev were compared, and weighted-sum performed consistently better. Two hybrid algorithms were proposed combining a gradient-based initialiser and a non-gradient improver. A simple yet effective Pareto-slope-based weighted-sum scalarisation was used in one of the hybrid algorithms. This algorithm consistently outperformed all other strategies for a given higher computational budget. The two hybrid strategies were able to perform better than their parent algorithms for the same computational budget. These hybrid algorithms combined the benefits of both gradient and non-gradient algorithms, resulting in a better overall performance in terms of a hypervolume metric.

8.3.2 Contributions

The main contributions are highlighted as follows.

1. Among the gradient methods, which included two variants of SIMP and a gradient-based constructive heuristic (CHg), overall, the performance was similar in terms of the dominated area in the objective space. Although in some problem instances, in some regions of the Pareto front, one of these algorithms performed better than the others, indicating that using only one of the algorithms leads to missing out on better solutions.
2. Between weighted-sum and Chebyshev scalarisation methods used with the hill climbing approach, weighted sum consistently performed better, and the reason for this was identified to be the highly selective nature of the Chebyshev isoline that rejects solutions on the path to better solutions.
3. Among non-gradient methods, hill climbing with weighted-sum scalarisation and NSGA-II, while hill climbing required many trials to span the Pareto front, NSGA-II consistently outperformed hill climbing on a per-trial basis. However, when combining more trials (i.e. a longer computational budget), hill climbing performs consistently better.
4. Hybrid algorithm 1, which is a combination of CHg and hill climbing with a Pareto-slope-based weighted-sum scalarisation outperformed all other algorithms consistently for a combination of 15 trials with the same computational budget. This highlights the effectiveness of such a simple yet novel adaptive scalarisation technique.
5. Hybrid algorithm 2, which is a combination of CHg and NSGA-II, was the winner on a per-trial basis, including among gradient methods when considering the same computational budget. Again, this highlighted the effectiveness of hybrid methods over their parent gradient or non-gradient strategies.
6. The general lesson is that hybrid methods with a gradient initialiser and a non-gradient exploiter is a better alternative for multi-objective topology optimisation in acoustic porous materials.

8.4 Reflections and future work prospects

Manufacturability-oriented topology optimisation: In the current work, one of the main limitations is that manufacturability was not considered so as to allow more algorithms to be tested. We have observed that filtering techniques play a significant role in the performance of algorithms by significantly modifying the fitnesses of the optimal shapes. Even a simple round-off filter is sufficient to change the evaluated fitness values significantly. Manufacturing-oriented topology optimisation is a well-studied topic in structural compliance minimisation [153] but has not been explored yet in the acoustics domain. Manufacturability is an objective on its own, and hence in future work, a penalty term may be introduced in the fitness function, and the performance of algorithms may be studied based on this new fitness function. Exploring various filtering techniques is also a topic of interest in the future. Additionally, manufacturing and testing such designs remain a challenge. While additive manufacturing has been used to fabricate porous materials with specific properties [155, 110], the reproducibility of such manufacturing techniques is also a challenge [276]. Only recently, researchers have manufactured topology optimised shapes of rigid structures in melamine foam obtained using a genetic algorithm [147]. The availability of such new and advanced fabrication techniques is also limited and is an area for further investigation.

Incremental evaluation: Evaluation of sound absorption indicators is computationally expensive for certain problem instances, which involve diffused sound fields and intricate shapes, which need finer discretisation. For purposes of optimisation, it is beneficial to have ways to quickly evaluate the change in the performance indicator for a given perturbation in the input variables. While there are efficient ways to find the sensitivities of fitness, such as conjugate gradient [81] and adjoint methods [87], an unexplored area is to perform incremental evaluation analogous to 2-opt for the travelling salesman problem [62]. In 2-opt, when crossing routes are reordered, the change in tour distance can be computed quickly by only considering the incremental change obtained when reordering the routes. Currently, when an element is bitflipped, the full linear system is solved again to compute absorption. When an optimisation move such as a bit flip is made, only a small submatrix (or a block) is modified in the system finite element matrices. Incremental evaluation in topology optimisation may involve, for instance, using block matrix operations [53] to compute fitness for perturbed solutions to make the computation faster. There is an immense potential benefit to exploring existing mathematical methods such as Cholesky decomposition to quickly estimate the new fitness by making use of data structures from the previous computation.

Multi-material topology optimisation: Composites involving a porous material with embedded solid scattering materials have been shown to have enhanced low-frequency sound absorption even with a layer of thickness much less than one-fourth wavelength required by theory [41]. Researchers have recently studied to design such sound absorbing systems [268] using topology optimisation. Topology optimisation in acoustic materials have already been extended to multi-material topology optimisation [138], but only a SIMP variant has been tested. There is potential for improving the quality of solutions using more effective strategies by combining with non-gradient operators such as Pareto-slope-based scalarisation.

Gradient-based metaheuristics and hybrid strategies: Developments in metaheuristics have focussed mainly on blackbox optimisation methods that do not use any domain information other than fitness. There exists a growing need for theoretical and empirical studies on metaheuristic strategies that use gradient information. An example of a gradient-based heuristic is stochastic gradient descent which has found immense application in machine learning [172]. While stochastic gradient descent has been applied to other topology optimisation problems [67, 73], they are yet to be tested on acoustics problems. Developing and testing metaheuristics that embed gradient-based search operators on mathematical benchmarks is an area which has received less attention. An example would be a memetic algorithm that embeds a gradient-based local search or other gradient-based variants and hybrids of different metaheuristics. Such research would have direct application in the field of topology optimisation and others alike. Moreover, in the current work, while single point-based and population-based metaheuristics were tested, other constructive metaheuristics such as ant colony [55], GRASP [158] or their hybrids with gradient strategies are yet to be investigated.

Machine learning models as surrogates for fitness evaluation: Machine learning methods such as convolutional neural networks have been successful in pattern recognition in images [28]. From the current study, it is observed that good-quality acoustic shapes exhibit specific patterns. A potential future work is to explore the use of machine learning-based regression techniques as surrogate models to quickly predict the expensive fitness function. Such models could be used to guide algorithms to identify porous material shape designs that tend to have high absorption properties. Efforts towards using deep learning for approximating the fitness are gaining interest in the compliance minimisation domain [211] but are yet to be applied to porous material problems.

Informed heuristics: Another potential future work topic is to identify if any domain-specific information other than fitness or gradients could be used to implement faster topology optimisation methods. Incorporating domain-specific knowledge into metaheuristics has been shown to be beneficial in other domains [187]. The BESO algorithm [257] uses stress information to make moves, and whether there exists a parameter analogous to stress in acoustics is a question of interest. In this regard, the acoustic pressure and velocity fields in the design domain were explored during this thesis. These fields are computed during the fitness evaluation and do not require any additional computational effort, unlike gradients. Even though correlations between these fields and the sensitivity to absorption were observed at each element, there were exceptions, especially near the elastic resonance frequency of the solid part. This line of research needs to be further explored to lead to designing *informed* heuristics that make use of the domain-specific structure.

Graded materials: Topology optimisation can be extended to optimise the material property distribution in acoustic materials. A recent work by Boulvert *et al.* [32] presents a strategy for optimising the graded properties and manufacturing 3D-printed graded acoustic materials. In their work, a graded porosity acoustic structure is additively manufactured using ABS plastic demonstrating the proof of concept. Currently, there is a lack of comparative studies on various strategies for such graded materials, which makes this a potential topic for future research.

8.5 Final remarks

To conclude, the purpose of this line of research is to have at our disposal efficient tools to reduce excess sound-absorbing materials in weight-critical applications such as aircraft and space launch vehicles and the cost of noise reduction solutions in urban environments. In the short to medium term, efficient acoustic topology optimisation and the resulting weight savings can reduce the operating costs of air travel and reduce costs of sound-proofing solutions, and in the long term, expand the horizons of space transport, benefiting humanity at large.

Bibliography

[1] AAGE, N., NOBEL-JØRGENSEN, M., ANDREASEN, C. S., AND SIGMUND, O. Interactive topology optimization on hand-held devices. *Structural and Multidisciplinary Optimization 47*, 1 (2013), 1–6.

[2] AARTS, E., AARTS, E. H. L., AND LENSTRA, J. K. *Local search in combinatorial optimization*. Princeton University Press, 2003.

[3] AGUILAR-RIVERA, R., VALENZUELA-RENDÓN, M., AND RODRÍGUEZ-ORTIZ, J. J. Genetic algorithms and darwinian approaches in financial applications: A survey. *Expert Systems with Applications 42*, 21 (2015), 7684–7697.

[4] ALLAIRE, G., DE GOURNAY, F., JOUVE, F., AND TOADER, A.-M. Structural optimization using topological and shape sensitivity via a level set method. *Control and Cybernetics 34*, 1 (2005), 59.

[5] ALLAIRE, G., JOUVE, F., AND TOADER, A.-M. A level-set method for shape optimization. *Comptes Rendus Mathematique 334*, 12 (2002), 1125–1130.

[6] ALLAIRE, G., JOUVE, F., AND TOADER, A.-M. Structural optimization using sensitivity analysis and a level-set method. *Journal of Computational Physics 194*, 1 (2004), 363–393.

[7] ALLARD, J., AND ATALLA, N. *Propagation of sound in porous media: modelling sound absorbing materials 2e*. John Wiley & Sons, 2009.

[8] ALLARD, J. F., CHAMPOUX, Y., AND DEPOLLIER, C. Modelization of layered sound absorbing materials with transfer matrices. *The Journal of the Acoustical Society of America 82*, 5 (1987), 1792–1796.

[9] AMINE, K. Insights into simulated annealing. In *Handbook of Research on Modeling, Analysis, and Application of Nature-Inspired Metaheuristic Algorithms*. IGI Global, 2018, pp. 121–139.

[10] ANDREASSEN, E., CLAUSEN, A., SCHEVENELS, M., LAZAROV, B. S., AND SIGMUND, O. Efficient topology optimization in MATLAB using 88 lines of code. *Structural and Multidisciplinary Optimization 43*, 1 (2011), 1–16.

[11] ATALLA, N., PANNETON, R., AND DEBERGUE, P. A mixed displacement-pressure formulation for poroelastic materials. *The Journal of the Acoustical Society of America 104*, 3 (1998), 1444–1452.

[12] ATALLA, N., AND SGARD, F. Modeling of perforated plates and screens using rigid frame porous models. *Journal of Sound and Vibration 303*, 1-2 (2007), 195–208.

[13] ATTENBOROUGH, K. Acoustical characteristics of rigid fibrous absorbents and granular materials. *The Journal of the Acoustical Society of America 73*, 3 (1983), 785–799.

[14] AZEVEDO, F. M., MOURA, M. S., VICENTE, W. M., PICELLI, R., AND PAVANELLO, R. Topology optimization of reactive acoustic mufflers using a bi-directional evolutionary optimization method. *Structural and Multidisciplinary Optimization 58*, 5 (2018), 2239–2252.

[15] BASU, S. Tabu search implementation on traveling salesman problem and its variations: a literature survey. *American Journal of Operations Research 2*, 2 (2012), 163.

[16] BEASLEY, J. E. Or-library: distributing test problems by electronic mail. *Journal of the operational research society 41*, 11 (1990), 1069–1072.

[17] BÉCOT, F.-X., AND JAOUEN, L. An alternative Biot's formulation for dissipative porous media with skeleton deformation. *The Journal of the Acoustical Society of America 134*, 6 (2013), 4801–4807.

[18] BÉCOT, F.-X., JAOUEN, L., AND GOURDON, E. Applications of the dual porosity theory to irregularly shaped porous materials. *Acta Acustica united with Acustica 94*, 5 (2008), 715–724.

[19] BENDSØE, M. P. Optimal shape design as a material distribution problem. *Structural Optimization 1*, 4 (1989), 193–202.

[20] BENDSØE, M. P., AND KIKUCHI, N. Generating optimal topologies in structural design using a homogenization method. *Computer Methods in Applied Mechanics and Engineering 71*, 2 (1988), 197–224.

[21] BENDSØE, M. P., AND SIGMUND, O. *Optimization of structural topology, shape, and material*, vol. 414. Springer, 1995.

[22] BENDSØE, M. P., AND SIGMUND, O. Material interpolation schemes in topology optimization. *Archive of Applied Mechanics 69*, 9-10 (1999), 635–654.

[23] BENDSØE, M. P., AND SIGMUND, O. *Topology optimization: theory, methods, and applications*. Springer Science & Business Media, 2013.

[24] BERANEK, L. L., AND SLEEPER JR, H. P. The design and construction of anechoic sound chambers. *The Journal of the Acoustical Society of America 18*, 1 (1946), 140–150.

[25] BIOT, M. A. Theory of deformation of a porous viscoelastic anisotropic solid. *Journal of Applied Physics 27*, 5 (1956), 459–467.

[26] BIOT, M. A. Theory of elastic waves in a fluid-saturated porous solid I. low frequency range. *The Journal of the Acoustical Society of America 28*, 1 (1956), 168–178.

[27] BIOT, M. A. Theory of propagation of elastic waves in a fluid-saturated porous solid II. higher frequency range. *The Journal of the acoustical Society of America 28*, 2 (1956), 179–191.

[28] BISHOP, C. M., AND NASRABADI, N. M. *Pattern recognition and machine learning*, vol. 4. Springer, 2006.

[29] BOLTON, J. S., SHIAU, N.-M., AND KANG, Y. J. Sound transmission through multi-panel structures lined with elastic porous materials. *Journal of Sound and Vibration 191*, 3 (1996), 317–347.

[30] BOREL, P. I., HARPØTH, A., FRANDSEN, L. H., KRISTENSEN, M., SHI, P., JENSEN, J. S., AND SIGMUND, O. Topology optimization and fabrication of photonic crystal structures. *Optics express 12*, 9 (2004), 1996–2001.

[31] BORN, M., AND WOLF, E. *Principles of optics: electromagnetic theory of propagation, interference and diffraction of light*. Elsevier, 2013.

[32] BOULVERT, J., CAVALIERI, T., COSTA-BAPTISTA, J., SCHWAN, L., ROMERO-GARCÍA, V., GABARD, G., FOTSING, E. R., ROSS, A., MARDJONO, J., AND GROBY, J.-P. Optimally graded porous material for broadband perfect absorption of sound. *Journal of Applied Physics 126*, 17 (2019), 175101.

[33] BOUTIN, C., ROYER, P., AND AURIAULT, J.-L. Acoustic absorption of porous surfacing with dual porosity. *International Journal of Solids and Structures 35*, 34-35 (1998), 4709–4737.

[34] BRADLEY, A. M. PDE-constrained optimization and the adjoint method. 2019. *URL https://cs.stanford.edu/ãmbrad/adjoint_tutorial.pdf* (2021).

[35] BROUARD, B., LAFARGE, D., AND ALLARD, J.-F. A general method of modelling sound propagation in layered media. *Journal of Sound and Vibration 183*, 1 (1995), 129–142.

[36] BUNCH, J. R., AND HOPCROFT, J. E. Triangular factorization and inversion by fast matrix multiplication. *Mathematics of Computation 28*, 125 (1974), 231–236.

[37] BUREERAT, S., AND LIMTRAGOOL, J. Performance enhancement of evolutionary search for structural topology optimisation. *Finite Elements in Analysis and Design 42*, 6 (2006), 547–566.

[38] BURGER, M., HACKL, B., AND RING, W. Incorporating topological derivatives into level set methods. *Journal of Computational Physics 194*, 1 (2004), 344–362.

[39] BURKE, E. K., GENDREAU, M., HYDE, M., KENDALL, G., OCHOA, G., ÖZCAN, E., AND QU, R. Hyper-heuristics: A survey of the state of the art. *Journal of the Operational Research Society 64*, 12 (2013), 1695–1724.

[40] BURKE, E. K., NEWALL, J. P., AND WEARE, R. F. A memetic algorithm for university exam timetabling. In *International Conference on the Practice and Theory of Automated Timetabling* (1995), Springer, pp. 241–250.

[41] CAMBONIE, T., MBAILASSEM, F., AND GOURDON, E. Bending a quarter wavelength resonator: Curvature effects on sound absorption properties. *Applied Acoustics 131* (2018), 87–102.

[42] CHAKRABORTY, U. K. *Advances in differential evolution*, vol. 143. Springer, 2008.

[43] CHAMPOUX, Y., AND ALLARD, J.-F. Dynamic tortuosity and bulk modulus in air-saturated porous media. *Journal of Applied Physics 70*, 4 (1991), 1975–1979.

[44] CHANG, Y.-C., YEH, L.-J., AND CHIU, M.-C. Numerical studies on constrained venting system with side inlet/outlet mufflers by GA optimization. *Acta Acustica united with Acustica 90*, 6 (2004), 1159–1169.

[45] CHANG, Y.-C., YEH, L.-J., AND CHIU, M.-C. Optimization of double-layer absorbers on constrained sound absorption system by using genetic algorithm. *International Journal for Numerical Methods in Engineering 62*, 3 (2005), 317–333.

[46] CHEN, L., LIU, C., ZHAO, W., AND LIU, L. An isogeometric approach of two dimensional acoustic design sensitivity analysis and topology optimization analysis for absorbing material distribution. *Computer Methods in Applied Mechanics and Engineering 336* (2018), 507–532.

[47] CHEN, L., LU, C., LIAN, H., LIU, Z., ZHAO, W., LI, S., CHEN, H., AND BORDAS, S. P. Acoustic topology optimization of sound absorbing materials directly from subdivision surfaces with isogeometric boundary element methods. *Computer Methods in Applied Mechanics and Engineering 362* (2020), 112806.

[48] CHEN, L. L., LIAN, H., LIU, Z., GONG, Y., ZHENG, C. J., AND BORDAS, S. P. A. Bi-material topology optimization for fully coupled structural-acoustic systems with isogeometric FEM–BEM. *Engineering Analysis with Boundary Elements 135* (2022), 182–195.

[49] CHEN, L. L., LIAN, H., NATARAJAN, S., ZHAO, W., CHEN, X. Y., AND BORDAS, S. P. A. Multi-frequency acoustic topology optimization of sound-absorption materials with isogeometric boundary element methods accelerated by frequency-decoupling and model order reduction techniques. *Computer Methods in Applied Mechanics and Engineering 395* (2022), 114997.

[50] CHEN, W., LIU, S., TONG, L., AND LI, S. Design of multi-layered porous fibrous metals for optimal sound absorption in the low frequency range. *Theoretical and Applied Mechanics Letters 6*, 1 (2016), 42–48.

[51] CHEN, Y., DAVIS, T. A., HAGER, W. W., AND RAJAMANICKAM, S. Algorithm 887: CHOLMOD, supernodal sparse Cholesky factorization and update/downdate. *ACM Transactions on Mathematical Software (TOMS) 35*, 3 (2008), 1–14.

[52] CHENG, A. H.-D., AND CHENG, D. T. Heritage and early history of the boundary element method. *Engineering Analysis with Boundary Elements 29*, 3 (2005), 268–302.

[53] CHOI, Y. New form of block matrix inversion. In *2009 IEEE/ASME International Conference on Advanced Intelligent Mechatronics* (2009), IEEE, pp. 1952–1957.

[54] CHUNG, J. Y., AND BLASER, D. A. Transfer function method of measuring in-duct acoustic properties. I. Theory. *The Journal of the Acoustical Society of America 68*, 3 (1980), 907–913.

[55] COLORNI, A., DORIGO, M., MANIEZZO, V., ET AL. Distributed optimization by ant colonies. In *Proceedings of the first European conference on artificial life* (1991), vol. 142, Paris, France, pp. 134–142.

[56] COPPERSMITH, D., AND WINOGRAD, S. Matrix multiplication via arithmetic progressions. In *Proceedings of the nineteenth annual ACM symposium on Theory of computing* (1987), pp. 1–6.

[57] COURANT, R. *Variational methods for the solution of problems of equilibrium and vibrations*. Verlag nicht ermittelbar, 1943.

[58] COWLING, P., KENDALL, G., AND SOUBEIGA, E. A hyperheuristic approach to scheduling a sales summit. In *International Conference on the Practice and Theory of Automated Timetabling* (2000), Springer, pp. 176–190.

[59] CRAGGS, A. A finite element model for rigid porous absorbing materials. *Journal of Sound and Vibration 61*, 1 (1978), 101–111.

[60] CRAINIC, T. G., AND GENDREAU, M. Towards an evolutionary method—cooperating multi-thread parallel tabu search hybrid. In *Meta-Heuristics*. Springer, 1999, pp. 331–344.

[61] CRAINIC, T. G., TOULOUSE, M., AND GENDREAU, M. Toward a taxonomy of parallel tabu search heuristics. *INFORMS Journal on Computing 9*, 1 (1997), 61–72.

[62] CROES, G. A. A method for solving traveling-salesman problems. *Operations Research 6*, 6 (1958), 791–812.

[63] DAS, S., MULLICK, S. S., AND SUGANTHAN, P. N. Recent advances in differential evolution–an updated survey. *Swarm and Evolutionary Computation 27* (2016), 1–30.

[64] DAVIS, L. Bit-climbing, representational bias, and test design. In *Proceedings of the International Conference on Genetic Algorithms* (1991), pp. 18–23.

[65] DBOUK, T. A review about the engineering design of optimal heat transfer systems using topology optimization. *Applied Thermal Engineering 112* (2017), 841–854.

[66] DE, S., HAMPTON, J., MAUTE, K., AND DOOSTAN, A. Topology optimization under uncertainty using a stochastic gradient-based approach. *Structural and Multidisciplinary Optimization 62*, 5 (2020), 2255–2278.

[67] DE, S., MAUTE, K., AND DOOSTAN, A. Reliability-based topology optimization using stochastic gradients. *Structural and Multidisciplinary Optimization 64*, 5 (2021), 3089–3108.

[68] DEATON, J. D., AND GRANDHI, R. V. A survey of structural and multidisciplinary continuum topology optimization: post 2000. *Structural and Multidisciplinary Optimization 49*, 1 (2014), 1–38.

[69] DEB, K., AGRAWAL, S., PRATAP, A., AND MEYARIVAN, T. A fast elitist non-dominated sorting genetic algorithm for multi-objective optimization: NSGA-II. In *International Conference on Parallel Problem Solving from Nature* (2000), Springer, pp. 849–858.

[70] DELANY, M. E., AND BAZLEY, E. N. Acoustical properties of fibrous absorbent materials. *Applied Acoustics 3*, 2 (1970), 105–116.

[71] DILGEN, C. B., DILGEN, S. B., AAGE, N., AND JENSEN, J. S. Topology optimization of acoustic mechanical interaction problems: a comparative review. *Structural and Multidisciplinary Optimization* (2019), 1–23.

[72] DILGEN, S. B., AAGE, N., AND JENSEN, J. S. Three dimensional vibroacoustic topology optimization of hearing instruments using cut elements. *Journal of Sound and Vibration* (2022), 116984.

[73] DILLEN, W., LOMBAERT, G., AND SCHEVENELS, M. A hybrid gradient-based/metaheuristic method for eurocode-compliant size, shape and topology optimization of steel structures. *Engineering Structures 239* (2021), 112137.

[74] DOLAN, E. D., AND MORÉ, J. J. Benchmarking optimization software with performance profiles. *Mathematical programming 91* (2002), 201–213.

[75] DUDA, J. Basic design considerations for anechoic chambers. *Noise Control Engineering Journal 9* (1977), 60–67.

[76] DÜHRING, M. B., JENSEN, J. S., AND SIGMUND, O. Acoustic design by topology optimization. *Journal of Sound and Vibration 317*, 3-5 (2008), 557–575.

[77] ESCHENAUER, H. A., AND OLHOFF, N. Topology optimization of continuum structures: a review. *Applied Mechanics Reviews 54*, 4 (2001), 331–390.

[78] FANG, J., SUN, G., QIU, N., KIM, N. H., AND LI, Q. On design optimization for structural crashworthiness and its state of the art. *Structural and Multidisciplinary Optimization 55*, 3 (2017), 1091–1119.

[79] FEOKTISTOV, V. *Differential evolution*. Springer, 2006.

[80] FERRARI, F., AND SIGMUND, O. A new generation 99 line matlab code for compliance topology optimization and its extension to 3d. *Structural and Multidisciplinary Optimization 62*, 4 (2020), 2211–2228.

[81] FLETCHER, R., AND REEVES, C. M. Function minimization by conjugate gradients. *The computer journal 7*, 2 (1964), 149–154.

[82] FLEURENT, C., AND FERLAND, J. A. Genetic and hybrid algorithms for graph coloring. *Annals of Operations Research 63*, 3 (1996), 437–461.

[83] FREISLEBEN, B., AND MERZ, P. A genetic local search algorithm for solving symmetric and asymmetric traveling salesman problems. In *Proceedings of IEEE International Conference on Evolutionary Computation* (1996), IEEE, pp. 616–621.

[84] GAO, H., LIANG, J., LI, B., ZHENG, C., AND MATSUMOTO, T. A level set based topology optimization for finite unidirectional acoustic phononic structures using boundary element method. *Computer Methods in Applied Mechanics and Engineering 381* (2021), 113776.

[85] GENDREAU, M. Recent advances in tabu search. In *Essays and surveys in metaheuristics*. Springer, 2002, pp. 369–377.

[86] GENLIN, J. Survey on genetic algorithm. *Computer Applications and Software 2* (2004), 69–73.

[87] GILES, M. B., AND SÜLI, E. Adjoint methods for pdes: a posteriori error analysis and postprocessing by duality. *Acta numerica 11* (2002), 145–236.

[88] GLOVER, F. Future paths for integer programming and links to artificial intelligence. *Computers & Operations Research 13*, 5 (1986), 533–549.

[89] GLOVER, F., AND LAGUNA, M. Tabu search. In *Handbook of Combinatorial Optimization*. Springer, 1998, pp. 2093–2229.

[90] GONÇALVES, J. F., MOREIRA, J. B. D., SALAS, R. A., GHORBANI, M. M., RUBIO, W. M., AND SILVA, E. C. N. Identification problem of acoustic media in the frequency domain based on the topology optimization method. *Structural and Multidisciplinary Optimization 62*, 3 (2020), 1041–1059.

[91] GÖRANSSON, P. A weighted residual formulation of the acoustic wave propagation through a flexible porous material and a comparison with a limp material model. *Journal of Sound and Vibration 182*, 3 (1995), 479–494.

[92] GÖRANSSON, P., CUENCA, J., AND LÄHIVAARA, T. Parameter estimation in modelling frequency response of coupled systems using a stepwise approach. *Mechanical Systems and Signal Processing 126* (2019), 161–175.

[93] GOURDON, E., AND SEPPI, M. Extension of double porosity model to porous materials containing specific porous inclusions. *Acta Acustica united with Acustica 96*, 2 (2010), 275–291.

[94] GUIRGUIS, D., AULIG, N., PICELLI, R., ZHU, B., ZHOU, Y., VICENTE, W., IORIO, F., OLHOFER, M., MATUSIK, W., COELLO, C. A. C., AND SAITOU, K. Evolutionary black-box topology optimization: challenges and promises. *IEEE Transactions on Evolutionary Computation* (2019), 613–633.

[95] GUO, J., ZHANG, X., AND FANG, Y. Topology optimization design and experimental validation of an acoustic metasurface for reflected wavefront modulation. *Journal of Sound and Vibration 520* (2022), 116631.

[96] GUO, X., ZHANG, W., AND ZHONG, W. Doing topology optimization explicitly and geometrically—a new moving morphable components based framework. *Journal of Applied Mechanics 81*, 8 (2014).

[97] GUPTA, D., LANGELAAR, M., BARINK, M., AND VAN KEULEN, F. Topology optimization of front metallization patterns for solar cells. *Structural and Multidisciplinary Optimization 51*, 4 (2015), 941–955.

[98] HAERTEL, J. H. K., ENGELBRECHT, K., LAZAROV, B. S., AND SIGMUND, O. Topology optimization of thermal heat sinks. In *Proceedings of COMSOL Conference* (2015), vol. 2015.

[99] HANSEN, N. References to CMA-ES applications. *URL http://www.cmap.polytechnique.fr/ñikolaus.hansen/cmaapplications.pdf* (2005).

[100] HANSEN, N. The CMA evolution strategy: A tutorial. *arXiv preprint arXiv:1604.00772* (2016).

[101] HASSANI, B., AND HINTON, E. A review of homogenization and topology optimization III—topology optimization using optimality criteria. *Computers & Structures 69*, 6 (1998), 739–756.

[102] HOLLAND, J. H. *Adaptation in natural and artificial systems: an introductory analysis with applications to biology, control, and artificial intelligence*. MIT press, 1992.

[103] HOOS, H. H., AND STÜTZLE, T. *Stochastic local search: Foundations and applications*. Elsevier, 2004.

[104] HOSSEINKHANI, A., YOUNESIAN, D., KRUSHYNSKA, A. O., RANJBAR, M., AND SCARPA, F. Full-gradient optimization of the vibroacoustic performance of (non-) auxetic sandwich panels. *Transport in Porous Media* (2021), 1–18.

[105] HRENNIKOFF, A. Solution of problems of elasticity by the framework method. *Journal of Applied Mechanics* (1941).

[106] ISAKARI, H., KURIYAMA, K., HARADA, S., YAMADA, T., TAKAHASHI, T., AND MATSUMOTO, T. A topology optimisation for three-dimensional acoustics with the level set method and the fast multipole boundary element method. *Mechanical Engineering Journal 1*, 4 (2014), CM0039–CM0039.

[107] JAOUEN, L. Acoustical porous material recipes. *Website URL: http://apmr. matelys. com, ISSN 2606-4138* (2000-2020).

[108] JAOUEN, L., AND BÉCOT, F.-X. Acoustical characterization of perforated facings. *The Journal of the Acoustical Society of America 129*, 3 (2011), 1400–1406.

[109] JENSEN, J. S., AND SIGMUND, O. Topology optimization for nano-photonics. *Laser & Photonics Reviews 5*, 2 (2011), 308–321.

[110] JIANG, C., MOREAU, D., AND DOOLAN, C. Acoustic absorption of porous materials produced by additive manufacturing with varying geometries. In *Proceedings of Acoustics* (2017), vol. 19.

[111] JOHNSON, D. L., KOPLIK, J., AND DASHEN, R. Theory of dynamic permeability and tortuosity in fluid-saturated porous media. *Journal of Fluid Mechanics 176* (1987), 379–402.

[112] JONES, D. R., SCHONLAU, M., AND WELCH, W. J. Efficient global optimization of expensive black-box functions. *Journal of Global Optimization 13*, 4 (1998), 455–492.

[113] JONES, T., FORREST, S., ET AL. Fitness distance correlation as a measure of problem difficulty for genetic algorithms. In *ICGA* (1995), vol. 95, pp. 184–192.

[114] JOSHI, S. K., AND BANSAL, J. C. Parameter tuning for meta-heuristics. *Knowledge-Based Systems 189* (2020), 105094.

[115] KANE, C., AND SCHOENAUER, M. Topological optimum design using genetic algorithms. *Control and Cybernetics 25*, 5 (1996), 1059–1088.

[116] KANG, Y. J., AND BOLTON, J. S. Finite element modeling of isotropic elastic porous materials coupled with acoustical finite elements. *The Journal of the Acoustical Society of America 98*, 1 (1995), 635–643.

[117] KARAKATIČ, S., AND PODGORELEC, V. A survey of genetic algorithms for solving multi depot vehicle routing problem. *Applied Soft Computing 27* (2015), 519–532.

[118] KARIMI-MAMAGHAN, M., MOHAMMADI, M., MEYER, P., KARIMI-MAMAGHAN, A. M., AND TALBI, E.-G. Machine learning at the service of meta-heuristics for solving combinatorial optimization problems: A state-of-the-art. *European Journal of Operational Research 296*, 2 (2022), 393–422.

[119] KASIMBEYLI, R., OZTURK, Z. K., KASIMBEYLI, N., YALCIN, G. D., AND ERDEM, B. I. Comparison of some scalarization methods in multiobjective optimization. *Bulletin of the Malaysian Mathematical Sciences Society 42*, 5 (2019), 1875–1905.

[120] KELLERER, H., PFERSCHY, U., AND PISINGER, D. Introduction to NP-Completeness of knapsack problems. In *Knapsack problems*. Springer, 2004, pp. 483–493.

[121] KHAJAH, T., LIU, L., SONG, C., AND GRAVENKAMP, H. Shape optimization of acoustic devices using the scaled boundary finite element method. *Wave Motion 104* (2021), 102732.

[122] KIM, K. H., AND YOON, G. H. Optimal rigid and porous material distributions for noise barrier by acoustic topology optimization. *Journal of Sound and Vibration 339* (2015), 123–142.

[123] KIM, K. H., AND YOON, G. H. Acoustic topology optimization using moving morphable components in neural network-based design. *Structural and Multidisciplinary Optimization 65*, 2 (2022), 1–28.

[124] KIRCHHOFF, G. Ueber den einfluss der wärmeleitung in einem gase auf die schallbewegung. *Annalen der Physik 210*, 6 (1868), 177–193.

[125] KIRKPATRICK, S., GELATT, C. D., AND VECCHI, M. P. Optimization by simulated annealing. *Science 220*, 4598 (1983), 671–680.

[126] KNOWLES, J. D., AND CORNE, D. W. M-paes: A memetic algorithm for multiobjective optimization. In *Proceedings of the 2000 Congress on Evolutionary Computation. CEC00 (Cat. No. 00TH8512)* (2000), vol. 1, IEEE, pp. 325–332.

[127] KOIDAN, W., HRUSKA, G. R., AND PICKETT, M. A. Wedge design for national bureau of standards anechoic chamber. *The Journal of the Acoustical Society of America 52*, 4A (1972), 1071–1076.

[128] KOOK, J. Evolutionary topology optimization for acoustic-structure interaction problems using a mixed u/p formulation. *Mechanics Based Design of Structures and Machines 47*, 3 (2019), 356–374.

[129] KOOK, J., AND JENSEN, J. S. Topology optimization of periodic microstructures for enhanced loss factor using acoustic–structure interaction. *International Journal of Solids and Structures 122* (2017), 59–68.

[130] KOOK, J., JENSEN, J. S., AND WANG, S. Acoustical topology optimization of Zwicker's loudness with Padé approximation. *Computer Methods in Applied Mechanics and Engineering 255* (2013), 40–66.

[131] KOOK, J., KOO, K., HYUN, J., JENSEN, J. S., AND WANG, S. Acoustical topology optimization for Zwicker's loudness model–Application to noise barriers. *Computer Methods in Applied Mechanics and Engineering 237* (2012), 130–151.

[132] KRASNOGOR, N., AND SMITH, J. Memetic algorithms: The polynomial local search complexity theory perspective. *Journal of Mathematical Modelling and Algorithms 7*, 1 (2008), 3–24.

[133] KROG, L., TUCKER, A., KEMP, M., AND BOYD, R. Topology optimisation of aircraft wing box ribs. In *10th AIAA/ISSMO Multidisciplinary Analysis and Optimization Conference* (2004), p. 4481.

[134] LAFARGE, D., LEMARINIER, P., ALLARD, J. F., AND TARNOW, V. Dynamic compressibility of air in porous structures at audible frequencies. *The Journal of the Acoustical Society of America 102*, 4 (1997), 1995–2006.

[135] LAGARRIGUE, C., GROBY, J.-P., DAZEL, O., AND TOURNAT, V. Design of metaporous supercells by genetic algorithm for absorption optimization on a wide frequency band. *Applied Acoustics 102* (2016), 49–54.

[136] LEE, C.-M., AND XU, Y. A modified transfer matrix method for prediction of transmission loss of multilayer acoustic materials. *Journal of Sound and Vibration 326*, 1-2 (2009), 290–301.

[137] LEE, C.-Y., LEAMY, M. J., AND NADLER, J. H. Frequency band structure and absorption predictions for multi-periodic acoustic composites. *Journal of Sound and Vibration 329*, 10 (2010), 1809–1822.

[138] LEE, J. S., GÖRANSSON, P., AND KIM, Y. Y. Topology optimization for three-phase materials distribution in a dissipative expansion chamber by unified multiphase modeling approach. *Computer Methods in Applied Mechanics and Engineering 287* (2015), 191–211.

[139] LEE, J. S., KIM, E. I., KIM, Y. Y., KIM, J. S., AND KANG, Y. J. Optimal poroelastic layer sequencing for sound transmission loss maximization by topology optimization method. *The Journal of the Acoustical Society of America 122*, 4 (2007), 2097–2106.

[140] LEE, J. S., KIM, Y. Y., KIM, J. S., AND KANG, Y. J. Two-dimensional poroelastic acoustical foam shape design for absorption coefficient maximization by topology optimization method. *The Journal of the Acoustical Society of America 123*, 4 (2008), 2094–2106.

[141] LEE, J.-S., KIM, Y.-Y., KIM, J.-S., KANG, Y.-J., AND KIM, E.-I. One-dimensional topology optimization for transmission loss maximization of multi-layered acoustic foams. In *Proceedings of the Korean Society for Noise and Vibration Engineering Conference* (2006), The Korean Society for Noise and Vibration Engineering, pp. 938–941.

[142] LEE, J. W., AND KIM, Y. Y. Rigid body modeling issue in acoustical topology optimization. *Computer Methods in Applied Mechanics and Engineering 198*, 9-12 (2009), 1017–1030.

[143] LEE, J. W., AND KIM, Y. Y. Topology optimization of muffler internal partitions for improving acoustical attenuation performance. *International Journal for Numerical Methods in Engineering 80*, 4 (2009), 455–477.

[144] LENZI, M. S., LEFTERIU, S., BERIOT, H., AND DESMET, W. A fast frequency sweep approach using Padé approximations for solving helmholtz finite element models. *Journal of Sound and Vibration 332*, 8 (2013), 1897–1917.

[145] LI, M., YANG, S., LI, K., AND LIU, X. Evolutionary algorithms with segment-based search for multiobjective optimization problems. *IEEE transactions on cybernetics 44*, 8 (2013), 1295–1313.

[146] LI, N., TAHAR, M. B., AND SUI, F. Optimization of sound transmission loss of open acoustic barriers with respect to unit cell topology. *Proceedings of the Institution of Mechanical Engineers, Part C: Journal of Mechanical Engineering Science 235*, 22 (2021), 5962–5974.

[147] LI, Z., HOU, X., KE, Y., AND TAO, M. Topology optimization with a genetic algorithm for the structural design of composite porous acoustic materials. *Applied Acoustics 197* (2022), 108917.

[148] LIND-NORDGREN, E., AND GÖRANSSON, P. Optimising open porous foam for acoustical and vibrational performance. *Journal of Sound and Vibration 329*, 7 (2010), 753–767.

[149] LIPTON, R. J., AND REGAN, K. W. David johnson: Galactic algorithms. In *People, Problems, and Proofs*. Springer, 2013, pp. 109–112.

[150] LIPTON, R. J., ROSE, D. J., AND TARJAN, R. E. Generalized nested dissection. *SIAM Journal on Numerical Analysis 16*, 2 (1979), 346–358.

[151] LIU, B., WANG, L., AND JIN, Y.-H. An effective PSO-based memetic algorithm for flow shop scheduling. *IEEE Transactions on Systems, Man, and Cybernetics, Part B (Cybernetics) 37*, 1 (2007), 18–27.

[152] LIU, J., GAYNOR, A. T., CHEN, S., KANG, Z., SURESH, K., TAKEZAWA, A., LI, L., KATO, J., TANG, J., WANG, C. C. L., CHENG, L., LIANG, X., AND TO, A. C. Current and future trends in topology optimization for additive manufacturing. *Structural and Multidisciplinary Optimization 57*, 6 (2018), 2457–2483.

[153] LIU, J., AND MA, Y. A survey of manufacturing oriented topology optimization methods. *Advances in Engineering Software 100* (2016), 161–175.

[154] LIU, W., ZHU, H., WANG, Y., ZHOU, S., BAI, Y., AND ZHAO, C. Topology optimization of support structure of telescope skin based on bit-matrix representation NSGA-II. *Chinese Journal of Aeronautics 26*, 6 (2013), 1422–1429.

[155] LIU, Z., ZHAN, J., FARD, M., AND DAVY, J. L. Acoustic properties of a porous polycarbonate material produced by additive manufacturing. *Materials Letters 181* (2016), 296–299.

[156] LOURENÇO, H. R., MARTIN, O. C., AND STÜTZLE, T. Iterated local search. In *Handbook of Metaheuristics*. Springer, 2003, pp. 320–353.

[157] MAEDA, Y., NISHIWAKI, S., IZUI, K., YOSHIMURA, M., MATSUI, K., AND TERADA, K. Structural topology optimization of vibrating structures with specified eigenfrequencies and eigenmode shapes. *International Journal for Numerical Methods in Engineering 67*, 5 (2006), 597–628.

[158] MARQUES-SILVA, J. P., AND SAKALLAH, K. A. Grasp: A search algorithm for propositional satisfiability. *IEEE Transactions on Computers 48*, 5 (1999), 506–521.

[159] MARTÍNEZ-MARADIAGA, D., DAMONTE, A., MANZO, A., HAERTEL, J. H. K., AND ENGELBRECHT, K. Design and testing of topology optimized heat sinks for a tablet. *International Journal of Heat and Mass Transfer 142* (2019), 118429.

[160] MATHWORKS. Matlab *mldivide* operator. *URL: https://uk.mathworks.com/help/matlab/ref/mldivide.html* (2020).

[161] MATLAB. *version 9.7.0.1216025 (R2019b) Update 1*. The MathWorks Inc., Natick, Massachusetts, 2019.

[162] MEYER, E., BUCHMANN, G., AND SCHOCH, A. Eine neue schallschluckanordnung hoher wirksamkeit und der bau eines schallgedämpften raumes. akustische zeitschrift 5 (6)(dezember 1940) 352–364. Review in English: A novel, highly effective sound-absorbing arrangement and the construction of a dead room. *Journal of the Acoustical Society of America 13*, 2 (1941), 191–193.

[163] MIKI, Y. Acoustical properties of porous materials-generalizations of empirical models. *Journal of the Acoustical Society of Japan (E) 11*, 1 (1990), 25–28.

[164] MIKI, Y. Acoustical properties of porous materials-modifications of Delany-Bazley models. *Journal of the Acoustical Society of Japan (E) 11*, 1 (1990), 19–24.

[165] MIRZENDEHDEL, A. M., AND SURESH, K. A Pareto-optimal approach to multimaterial topology optimization. *Journal of Mechanical Design 137*, 10 (2015).

[166] MOSCATO, P., AND NORMAN, M. G. A memetic approach for the traveling salesman problem implementation of a computational ecology for combinatorial optimization on message-passing systems. *Parallel Computing and Transputer Applications 1* (1992), 177–186.

[167] MUNJAL, M. L. *Acoustics of ducts and mufflers with application to exhaust and ventilation system design*. John Wiley & Sons, 1987.

[168] MÜNZEL, T., GORI, T., BABISCH, W., AND BASNER, M. Cardiovascular effects of environmental noise exposure. *European Heart Journal 35*, 13 (2014), 829–836.

[169] MÜNZEL, T., SØRENSEN, M., AND DAIBER, A. Transportation noise pollution and cardiovascular disease. *Nature Reviews Cardiology 18*, 9 (2021), 619–636.

[170] NERI, F., AND COTTA, C. Memetic algorithms and memetic computing optimization: A literature review. *Swarm and Evolutionary Computation 2* (2012), 1–14.

[171] NERI, F., AND TIRRONEN, V. Recent advances in differential evolution: a survey and experimental analysis. *Artificial intelligence review 33*, 1 (2010), 61–106.

[172] NETRAPALLI, P. Stochastic gradient descent and its variants in machine learning. *Journal of the Indian Institute of Science 99*, 2 (2019), 201–213.

[173] NOGUCHI, Y., YAMADA, T., IZUI, K., AND NISHIWAKI, S. Optimum design of an acoustic metamaterial with negative bulk modulus in an acoustic-elastic coupled system using a level set–based topology optimization method. *International Journal for Numerical Methods in Engineering 113*, 8 (2018), 1300–1339.

[174] NORRIS, A. N. On the viscodynamic operator in Biot's equations of poroelasticity. *J. Wave Mat. Interact 1* (1986), 365–380.

[175] OCHOA, G., HYDE, M., CURTOIS, T., VAZQUEZ-RODRIGUEZ, J. A., WALKER, J., GENDREAU, M., KENDALL, G., MCCOLLUM, B., PARKES, A. J., PETROVIC, S., ET AL. Hyflex: A benchmark framework for cross-domain heuristic search. In *Evolutionary Computation in Combinatorial Optimization: 12th European Conference, EvoCOP 2012, Málaga, Spain, April 11-13, 2012. Proceedings 12* (2012), Springer, pp. 136–147.

[176] OLNY, X., AND BOUTIN, C. Acoustic wave propagation in double porosity media. *The Journal of the Acoustical Society of America 114*, 1 (2003), 73–89.

[177] OLNY, X., PANNETON, R., AND TRAN-VAN, J. An indirect acoustical method for determining intrinsic parameters of porous materials. *Poromechanics II, Proceedings of the 2nd Biot Conference, Grenoble (France)* (2002).

[178] OLSON, H. F. Acoustic laboratory in the new RCA laboratories. *The Journal of the Acoustical Society of America 15*, 2 (1943), 96–102.

[179] ÖZCAN, E. Memetic algorithms for nurse rostering. In *International Symposium on Computer and Information Sciences* (2005), Springer, pp. 482–492.

[180] ÖZCAN, E., AND BAŞARAN, C. A case study of memetic algorithms for constraint optimization. *Soft Computing 13*, 8-9 (2009), 871.

[181] ÖZCAN, E., BILGIN, B., AND KORKMAZ, E. E. A comprehensive analysis of hyper-heuristics. *Intelligent Data Analysis 12*, 1 (2008), 3–23.

[182] PANNETON, R., AND ATALLA, N. Numerical prediction of sound transmission through finite multilayer systems with poroelastic materials. *The Journal of the Acoustical Society of America 100*, 1 (1996), 346–354.

[183] PANNETON, R., AND ATALLA, N. An efficient finite element scheme for solving the three-dimensional poroelasticity problem in acoustics. *The Journal of the Acoustical Society of America 101*, 6 (1997), 3287–3298.

[184] PANNETON, R., AND OLNY, X. Acoustical determination of the parameters governing viscous dissipation in porous media. *The Journal of the Acoustical Society of America 119*, 4 (2006), 2027–2040.

[185] PARRA MARTINEZ, J. P., DAZEL, O., GÖRANSSON, P., AND CUENCA, J. Acoustic analysis of anisotropic poroelastic multilayered systems. *Journal of Applied Physics 119*, 8 (2016), 084907.

[186] PARRINELLO, A., AND GHIRINGHELLI, G. L. Transfer matrix representation for periodic planar media. *Journal of Sound and Vibration 371* (2016), 196–209.

[187] PASSONE, S., CHUNG, P. W., AND NASSEHI, V. Incorporating domain-specific knowledge into a genetic algorithm to implement case-based reasoning adaptation. *Knowledge-Based Systems 19*, 3 (2006), 192–201.

[188] PAULINAS, M., AND UŠINSKAS, A. A survey of genetic algorithms applications for image enhancement and segmentation. *Information Technology and Control 36*, 3 (2007).

[189] PEREIRA, R. L., LOPES, H. N., AND PAVANELLO, R. Topology optimization of acoustic systems with a multiconstrained BESO approach. *Finite Elements in Analysis and Design 201* (2022), 103701.

[190] PERROT, C., CHEVILLOTTE, F., TAN HOANG, M., BONNET, G., BÉCOT, F.-X., GAUTRON, L., AND DUVAL, A. Microstructure, transport, and acoustic properties of open-cell foam samples: Experiments and three-dimensional numerical simulations. *Journal of Applied Physics 111*, 1 (2012), 014911.

[191] PICHON, H., PIOLLET, E., AND ROSS, A. An acoustic trade-off chart for the design of multilayer acoustic packages. *Applied Acoustics 148* (2019), 9–18.

[192] PILLAY, N., AND QU, R. *Hyper-heuristics: theory and applications*. Springer, 2018.

[193] PITZER, E., AND AFFENZELLER, M. A comprehensive survey on fitness landscape analysis. *Recent advances in intelligent engineering systems* (2012), 161–191.

[194] PLONA, T. J. Observation of a second bulk compressional wave in a porous medium at ultrasonic frequencies. *Applied Physics Letters 36*, 4 (1980), 259–261.

[195] PRICE, K., STORN, R. M., AND LAMPINEN, J. A. *Differential evolution: a practical approach to global optimization*. Springer Science & Business Media, 2006.

[196] PRIDE, S. R., MORGAN, F. D., AND GANGI, A. F. Drag forces of porous-medium acoustics. *Physical Review B 47*, 9 (1993), 4964.

[197] QIN, J., ISAKARI, H., TAJI, K., TAKAHASHI, T., AND MATSUMOTO, T. A robust topology optimization for enlarging working bandwidth of acoustic devices. *International Journal for Numerical Methods in Engineering 122*, 11 (2021), 2694–2711.

[198] QIN, J., ISAKARI, H., TAKAHASHI, T., AND MATSUMOTO, T. A robust topology optimisation for wideband structures in acoustic–elastodynamic coupled fields. *Engineering Analysis with Boundary Elements 140* (2022), 544–561.

[199] QU, R. A general model for automated algorithm design. In *Automated Design of Machine Learning and Search Algorithms*. Springer, 2021, pp. 29–43.

[200] RADCLIFFE, N. J., AND SURRY, P. D. Formal memetic algorithms. In *AISB Workshop on Evolutionary Computing* (1994), Springer, pp. 1–16.

[201] RAMAMOORTHY, V. T., ÖZCAN, E., PARKES, A. J., LUC, J., AND BÉCOT, F.-X. Metaheuristic optimisation of sound absorption performance of multilayered porous materials. *Proceedings of the 23rd International Congress on Acoustics (ICA2019.org), Aachen, Germany* (2019).

[202] RAMAMOORTHY, V. T., ÖZCAN, E., PARKES, A. J., SREEKUMAR, A., JAOUEN, L., AND BÉCOT, F.-X. Comparison of gradient-based and gradient-free heuristics and metaheuristics for topology optimisation in acoustic porous materials. *The Journal of the Acoustical Society of America 150*, 4 (2021), 3164–3176.

[203] REINELT, G. Tsplib—a traveling salesman problem library. *ORSA journal on computing 3*, 4 (1991), 376–384.

[204] RHAZI, D., AND ATALLA, N. Transfer matrix modeling of the vibroacoustic response of multi-materials structures under mechanical excitation. *Journal of Sound and Vibration 329*, 13 (2010), 2532–2546.

[205] ROSTAMI, P., AND MARZBANRAD, J. Identification of optimal topologies for continuum structures using metaheuristics: A comparative study. *Archives of Computational Methods in Engineering* (2021), 1–28.

[206] ROZVANY, G. I., AND LEWIŃSKI, T. *Topology optimization in structural and continuum mechanics*. Springer, 2014.

[207] ROZVANY, G. I. N. Aims, scope, methods, history and unified terminology of computer-aided topology optimization in structural mechanics. *Structural and Multidisciplinary Optimization 21*, 2 (2001), 90–108.

[208] RUMPLER, R., GÖRANSSON, P., AND DEÜ, J.-F. A finite element approach combining a reduced-order system, Padé approximants, and an adaptive frequency windowing for fast multi-frequency solution of poro-acoustic problems. *International Journal for Numerical Methods in Engineering 97*, 10 (2014), 759–784.

[209] RUMPLER, R., GÖRANSSON, P., AND RICE, H. J. An adaptive strategy for the bivariate solution of finite element problems using multivariate nested Padé approximants. *International Journal for Numerical Methods in Engineering 100*, 9 (2014), 689–710.

[210] SADOUKI, M. Experimental measurement of the porosity and the viscous tortuosity of rigid porous material in low frequency. *Journal of Low Frequency Noise, Vibration and Active Control 37*, 2 (2018), 385–393.

[211] SASAKI, H., AND IGARASHI, H. Topology optimization accelerated by deep learning. *IEEE Transactions on Magnetics 55*, 6 (2019), 1–5.

[212] SCHOENBERG, M. Wave propagation in alternating solid and fluid layers. *Wave Motion 6*, 3 (1984), 303–320.

[213] SGARD, F. C., OLNY, X., ATALLA, N., AND CASTEL, F. On the use of perforations to improve the sound absorption of porous materials. *Applied Acoustics 66*, 6 (2005), 625–651.

[214] SHARMA, C., SABHARWAL, S., AND SIBAL, R. A survey on software testing techniques using genetic algorithm. *International Journal of Computer Science Issues 10*, 1 (2013), 381.

[215] SHEIKH, R. H., RAGHUWANSHI, M. M., AND JAISWAL, A. N. Genetic algorithm based clustering: A survey. In *2008 First International Conference on Emerging Trends in Engineering and Technology* (2008), IEEE, pp. 314–319.

[216] SIGMUND, O. On the design of compliant mechanisms using topology optimization. *Journal of Structural Mechanics 25*, 4 (1997), 493–524.

[217] SIGMUND, O. A 99 line topology optimization code written in Matlab. *Structural and Multidisciplinary Optimization 21*, 2 (2001), 120–127.

[218] SIGMUND, O. Morphology-based black and white filters for topology optimization. *Structural and Multidisciplinary Optimization 33*, 4-5 (2007), 401–424.

[219] SIGMUND, O. On the usefulness of non-gradient approaches in topology optimization. *Structural and Multidisciplinary Optimization 43*, 5 (2011), 589–596.

[220] SIGMUND, O., AND CLAUSEN, P. M. Topology optimization using a mixed formulation: an alternative way to solve pressure load problems. *Computer Methods in Applied Mechanics and Engineering 196*, 13-16 (2007), 1874–1889.

[221] SIGMUND, O., AND MAUTE, K. Topology optimization approaches. *Structural and Multidisciplinary Optimization 48*, 6 (2013), 1031–1055.

[222] SIGMUND, O., AND PETERSSON, J. Numerical instabilities in topology optimization: A survey on procedures dealing with checkerboards, mesh-dependencies and local minima. *Structural Optimization 16*, 1 (1998), 68–75.

[223] SILVER, D., SCHRITTWIESER, J., SIMONYAN, K., ANTONOGLOU, I., HUANG, A., GUEZ, A., HUBERT, T., BAKER, L., LAI, M., BOLTON, A., CHEN, Y., LILLICRAP, T., HUI, F., SIFRE, L., VAN DEN DRIESSCHE, G., GRAEPEL, T., AND HASSABIS, D. Mastering the game of Go without human knowledge. *Nature 550*, 7676 (2017), 354–359.

[224] SONG, B. H., AND BOLTON, J. S. A transfer-matrix approach for estimating the characteristic impedance and wave numbers of limp and rigid porous materials. *The Journal of the Acoustical Society of America 107*, 3 (2000), 1131–1152.

[225] SÖRENSEN, K. Metaheuristics—the metaphor exposed. *International Transactions in Operational Research 22*, 1 (2015), 3–18.

[226] SÖRENSEN, K., AND GLOVER, F. W. Metaheuristics. *Encyclopedia of Operations Research and Management Science* (2013), 960–970.

[227] SÖRENSEN, K., SEVAUX, M., AND GLOVER, F. A history of metaheuristics. *Handbook of Heuristics* (2018), 1–18.

[228] SRINIVAS, M., AND PATNAIK, L. M. Adaptive probabilities of crossover and mutation in genetic algorithms. *IEEE Transactions on Systems, Man, and Cybernetics 24*, 4 (1994), 656–667.

[229] SRINIVAS, M., AND PATNAIK, L. M. Genetic algorithms: A survey. *Computer 27*, 6 (1994), 17–26.

[230] STINSON, M. R. The propagation of plane sound waves in narrow and wide circular tubes, and generalization to uniform tubes of arbitrary cross-sectional shape. *The Journal of the Acoustical Society of America 89*, 2 (1991), 550–558.

[231] STOLPE, M., AND BENDSØE, M. P. Global optima for the Zhou–Rozvany problem. *Structural and Multidisciplinary Optimization 43*, 2 (2011), 151–164.

[232] STORN, R. On the usage of differential evolution for function optimization. In *Proceedings of North American Fuzzy Information Processing* (1996), IEEE, pp. 519–523.

[233] STORN, R., AND PRICE, K. Differential evolution–a simple and efficient heuristic for global optimization over continuous spaces. *Journal of Global Optimization 11*, 4 (1997), 341–359.

[234] STRASSEN, V. Gaussian elimination is not optimal. *Numerische mathematik 13*, 4 (1969), 354–356.

[235] SUDHOLT, D. Memetic algorithms with variable-depth search to overcome local optima. In *Proceedings of the 10th Annual Conference on Genetic and Evolutionary Computation* (2008), ACM, pp. 787–794.

[236] SUMAN, B., AND KUMAR, P. A survey of simulated annealing as a tool for single and multiobjective optimization. *Journal of the Operational Research Society 57*, 10 (2006), 1143–1160.

[237] SURESH, K. A 199-line Matlab code for Pareto-optimal tracing in topology optimization. *Structural and Multidisciplinary Optimization 42*, 5 (2010), 665–679.

[238] SVANBERG, K. The method of moving asymptotes—a new method for structural optimization. *International Journal for Numerical Methods in Engineering 24*, 2 (1987), 359–373.

[239] SVANBERG, K. A class of globally convergent optimization methods based on conservative convex separable approximations. *SIAM Journal on Optimization 12*, 2 (2002), 555–573.

[240] TANNEAU, O., CASIMIR, J. B., AND LAMARY, P. Optimization of multilayered panels with poroelastic components for an acoustical transmission objective. *The Journal of the Acoustical Society of America 120*, 3 (2006), 1227–1238.

[241] THENGADE, A., AND DONDAL, R. Genetic algorithm-survey paper. In *MPGI National Multi Conference* (2012), Citeseer, pp. 7–8.

[242] TIMMIS, A. J., HODZIC, A., KOH, L., BONNER, M., SOUTIS, C., SCHÄFER, A. W., AND DRAY, L. Environmental impact assessment of aviation emission reduction through the implementation of composite materials. *The International Journal of Life Cycle Assessment 20*, 2 (2015), 233–243.

[243] TREFETHEN, L. N., AND BAU III, D. *Numerical linear algebra*, vol. 50. SIAM, 1997.

[244] TVEIT, A. On the complexity of matrix inversion. *Mathematical Note* (2003), 1.

[245] UTSUNO, H., TANAKA, T., FUJIKAWA, T., AND SEYBERT, A. F. Transfer function method for measuring characteristic impedance and propagation constant of porous materials. *The Journal of the Acoustical Society of America 86*, 2 (1989), 637–643.

[246] VERDIÈRE, K., PANNETON, R., ELKOUN, S., DUPONT, T., AND LECLAIRE, P. Transfer matrix method applied to the parallel assembly of sound absorbing materials. *The Journal of the Acoustical Society of America 134*, 6 (2013), 4648–4658.

[247] VERMA, S., PANT, M., AND SNASEL, V. A comprehensive review on NSGA-II for multi-objective combinatorial optimization problems. *IEEE Access 9* (2021), 57757–57791.

[248] VILLOT, M., GUIGOU, C., AND GAGLIARDINI, L. Predicting the acoustical radiation of finite size multilayered structures by applying spatial windowing on infinite structures. *Journal of sound and vibration 245*, 3 (2001), 433–455.

[249] WADBRO, E., AND BERGGREN, M. Topology optimization of an acoustic horn. *Computer Methods in Applied Mechanics and Engineering 196*, 1-3 (2006), 420–436.

[250] WANG, C., ZHAO, Z., ZHOU, M., SIGMUND, O., AND ZHANG, X. S. A comprehensive review of educational articles on structural and multidisciplinary optimization. *Structural and Multidisciplinary Optimization 64*, 5 (2021), 2827–2880.

[251] WANG, M. Y., WANG, X., AND GUO, D. A level set method for structural topology optimization. *Computer Methods in Applied Mechanics and Engineering 192*, 1-2 (2003), 227–246.

[252] WANG, X., WANG, D., AND LIU, B. Efficient acoustic topology optimization using vibro-acoustic coupled Craig–Bampton mode synthesis. *Acoustics Australia* (2020), 1–12.

[253] WEYLAND, D. A critical analysis of the harmony search algorithm—How not to solve sudoku. *Operations Research Perspectives 2* (2015), 97–105.

[254] WILSON, D. K. Relaxation-matched modeling of propagation through porous media, including fractal pore structure. *The Journal of the Acoustical Society of America 94*, 2 (1993), 1136–1145.

[255] XIANG, Y., ZHOU, Y., LI, M., AND CHEN, Z. A vector angle-based evolutionary algorithm for unconstrained many-objective optimization. *IEEE Transactions on Evolutionary Computation 21*, 1 (2016), 131–152.

[256] XIE, Y. M., AND STEVEN, G. P. A simple evolutionary procedure for structural optimization. *Computers & Structures 49*, 5 (1993), 885–896.

[257] XIE, Y. M., AND STEVEN, G. P. Evolutionary structural optimization for dynamic problems. *Computers & Structures 58*, 6 (1996), 1067–1073.

[258] XU, J., NANNARIELLO, J., AND FRICKE, F. R. Optimising flat-walled multi-layered anechoic linings using evolutionary algorithms. *Applied Acoustics 65*, 11 (2004), 1009–1026.

[259] XU, Y., ZHAO, W., CHEN, L., AND CHEN, H. Distribution optimization for acoustic design of porous layer by the boundary element method. *Acoustics Australia* (2020), 107–119.

[260] XU, Z.-X., GAO, H., DING, Y.-J., YANG, J., LIANG, B., AND CHENG, J.-C. Topology-optimized omnidirectional broadband acoustic ventilation barrier. *Physical Review Applied 14*, 5 (2020), 054016.

[261] YAMAMOTO, T., MARUYAMA, S., NISHIWAKI, S., AND YOSHIMURA, M. Topology design of multi-material soundproof structures including poroelastic media to minimize sound pressure levels. *Computer Methods in Applied Mechanics and Engineering 198*, 17-20 (2009), 1439–1455.

[262] YANG, X. Y., XIE, Y. M., STEVEN, G. P., AND QUERIN, O. M. Topology optimization for frequencies using an evolutionary method. *Journal of Structural Engineering 125*, 12 (1999), 1432–1438.

[263] YEDEG, E. L., WADBRO, E., AND BERGGREN, M. Interior layout topology optimization of a reactive muffler. *Structural and Multidisciplinary Optimization 53*, 4 (2016), 645–656.

[264] YEH, L.-J., CHANG, Y.-C., AND CHIU, M.-C. Numerical studies on constrained venting system with reactive mufflers by GA optimization. *International Journal for Numerical Methods in Engineering 65*, 8 (2006), 1165–1185.

[265] YI, W., QU, R., JIAO, L., AND NIU, B. Automated design of metaheuristics using reinforcement learning within a novel general search framework. *IEEE Transactions on Evolutionary Computation* (2022).

[266] YOON, G. H. Acoustic topology optimization of fibrous material with Delany–Bazley empirical material formulation. *Journal of Sound and Vibration 332*, 5 (2013), 1172–1187.

[267] YOON, G. H., JENSEN, J. S., AND SIGMUND, O. Topology optimization of acoustic–structure interaction problems using a mixed finite element formulation. *International Journal for Numerical Methods in Engineering 70*, 9 (2007), 1049–1075.

[268] YOON, W. U., PARK, J. H., LEE, J. S., AND KIM, Y. Y. Topology optimization design for total sound absorption in porous media. *Computer Methods in Applied Mechanics and Engineering 360* (2020), 112723.

[269] YU, Y., ZHAO, G., REN, S., AND WANG, B. Layout optimization of porous sound-absorbing material in mid-frequency vibro-acoustic systems. *Journal of Fluids and Structures 100* (2021), 103197.

[270] ZARGHAM, S., WARD, T. A., RAMLI, R., AND BADRUDDIN, I. A. Topology optimization: a review for structural designs under vibration problems. *Structural and Multidisciplinary Optimization 53*, 6 (2016), 1157–1177.

[271] ZHAO, W., CHEN, L., ZHENG, C., LIU, C., AND CHEN, H. Design of absorbing material distribution for sound barrier using topology optimization. *Structural and Multidisciplinary Optimization 56*, 2 (2017), 315–329.

[272] ZHOU, M., AND ROZVANY, G. I. N. The COC algorithm, Part II: Topological, geometrical and generalized shape optimization. *Computer Methods in Applied Mechanics and Engineering 89*, 1-3 (1991), 309–336.

[273] ZHOU, M., AND ROZVANY, G. I. N. On the validity of ESO type methods in topology optimization. *Structural and Multidisciplinary Optimization 21*, 1 (2001), 80–83.

[274] ZHOU, M., AND SIGMUND, O. Complementary lecture notes for teaching the 99/88-line topology optimization codes. *Structural and Multidisciplinary Optimization 64*, 5 (2021), 3227–3231.

[275] ZHU, Z., ONG, Y.-S., AND DASH, M. Wrapper–filter feature selection algorithm using a memetic framework. *IEEE Transactions on Systems, Man, and Cybernetics, Part B (Cybernetics) 37*, 1 (2007), 70–76.

[276] ZIELIŃSKI, T. G., OPIELA, K. C., PAWŁOWSKI, P., DAUCHEZ, N., BOUTIN, T., KENNEDY, J., TRIMBLE, D., RICE, H., VAN DAMME, B., HANNEMA, G., ET AL. Reproducibility of sound-absorbing periodic porous materials using additive manufacturing technologies: Round robin study. *Additive Manufacturing 36* (2020), 101564.

[277] ZIENKIEWICZ, O. C., TAYLOR, R. L., NITHIARASU, P., AND ZHU, J. Z. *The finite element method*, vol. 3. McGraw-hill London, 1977.

[278] ZITZLER, E., LAUMANNS, M., AND THIELE, L. SPEA2: Improving the strength Pareto evolutionary algorithm. *TIK-report 103* (2001).

[279] ZUO, W., AND SAITOU, K. Multi-material topology optimization using ordered SIMP interpolation. *Structural and Multidisciplinary Optimization 55*, 2 (2017), 477–491.

[280] ZWIKKER, C., AND KOSTEN, C. W. *Sound absorbing materials*. Elsevier publishing company, 1949.

Appendix A

Database of porous materials

In this appendix, a database of material properties of existing porous materials used in the optimisation studies in chapter 5 is provided. These material properties have been obtained from Matelys research lab's standard database for the Alphacell software.

Table A.1: Air

Property	Value
Speed of sound (m/s)	340

Table A.2: Air dissipative

Property	Value
Speed of sound (m/s)	340
Dissipation factor	0.05

Table A.3: Felt 62 kg·m^{-3}

Property	Value
Acoustic model	JCAL
Open porosity ϕ	0.97
Static airflow resistivity σ (N· s · m^{-4})	38500
Viscous characteristic length Λ (m)	4.2e-5
Thermal characteristic length Λ' (m)	8.6e-5
High frequency limit of tortuosity α_∞	1.02
Static thermal permeability k'_o	6.4e-9
Elastic model	Elastic (isotropic)
Density ρ (kg·m^{-3})	62
Young's modulus E (N·m^{-2})	35000
Poisson's ratio ν	0
Equivalent viscous damping coefficient η	0.12

Table A.4: Felt 93 kg·m^{-3}

Property	Value
Acoustic model	JCAL
Open porosity ϕ	0.94
Static airflow resistivity σ (N· s · m^{-4})	37800
Viscous characteristic length Λ (m)	2.8e-5
Thermal characteristic length Λ' (m)	10.5e-5
High frequency limit of tortuosity α_∞	1.01
Static thermal permeability k'_o	3.0e-9
Elastic model	Elastic (isotropic)
Density ρ kg·m^{-3}	62
Young's modulus E (N·m^{-2})	35000
Poisson's ratio ν	0
Equivalent viscous damping coefficient η	0.12

Table A.5: Foam 55 kg·m^{-3}

Property	Value
Acoustic model	JCAL
Open porosity ϕ	0.97
Static airflow resistivity σ (N· s · m^{-4})	50000
Viscous characteristic length Λ (m)	3.9e-5
Thermal characteristic length Λ' (m)	22.0e-5
High frequency limit of tortuosity α_∞	1.0
Static thermal permeability k'_o	6.9e-9
Elastic model	Elastic (isotropic)
Density ρ (kg·m^{-3})	55
Young's modulus E (N·m^{-2})	43000
Poisson's ratio ν	0.4
Equivalent viscous damping coefficient η	0.3

Table A.6: Foam Agglomerate, Gourdon and Seppi [93]

Property	Value
Acoustic model	JCAL
Open porosity ϕ	0.9
Static airflow resistivity σ (N· s · m^{-4})	47700
Viscous characteristic length Λ (m)	2.4e-5
Thermal characteristic length Λ' (m)	20.0e-5
High frequency limit of tortuosity α_∞	1.29
Static thermal permeability k'_o	2.9e-9
Elastic model	Elastic (isotropic)
Density ρ (kg·m^{-3})	55
Young's modulus E (N·m^{-2})	43000
Poisson's ratio ν	0.4
Equivalent viscous damping coefficient η	0.3

Table A.7: Foam Backrest

Property	Value
Acoustic Model	Miki
Open porosity ϕ	0.98
Static airflow resistivity σ (N· s · m^{-4})	12000
High frequency limit of tortuosity (α_∞)	1.1

Table A.8: Foam Agglomerate, Gourdon and Seppi [93]

Property	Value
Elastic model	Elastic (isotropic)
Density ρ (kg·m^{-3})	60
Young's modulus E (N·m^{-2})	80000
Poisson's ratio ν	0.41
Equivalent viscous damping coefficient η	0.3

Table A.9: Foam cushion

Property	Value
Acoustic model	Miki
Open porosity ϕ	0.97
Static airflow resistivity σ (N· s · m^{-4})	50000
High frequency limit of tortuosity (α_∞)	1.2

Table A.10: Foam Headliner

Property	Value
Acoustic model	Delany-Bazley-Miki
Static airflow resistivity σ (N· s · m^{-4})	46000

Table A.11: Foam R1 Perrot et al. 2012 [190]

Property	Value
Acoustic model	JCAPL
Open porosity ϕ	0.9
Static airflow resistivity σ (N· s · m^{-4})	700
Viscous characteristic length Λ (m)	12.9e-5
Thermal characteristic length Λ' (m)	44.0e-5
High frequency limit of tortuosity α_∞	1.12
Static thermal permeability k'_o	3e-9
Static viscous tortuosity (α_o)	1.22
Static thermal permeability (α'_o)	1.13

Table A.12: Glasswool Thermal

Property	Value
Acoustic model	Miki
Open porosity ϕ	0.97
Static airflow resistivity σ (N· s · m^{-4})	5000
High frequency limit of tortuosity (α_∞)	1.0
Density ρ (kg·m^{-3})	35

Table A.13: Glasswool 16 kg·m^{-3}

Property	Value
Acoustic model	JCAL
Open porosity ϕ	0.99
Static airflow resistivity σ (N· s · m^{-4})	20000
Viscous characteristic length Λ (m)	2.6e-5
Thermal characteristic length Λ' (m)	13.5e-5
High frequency limit of tortuosity α_∞	1.11
Static thermal permeability k'_o	2.4e-9
Elastic model	Limp
Density ρ (kg·m^{-3})	16

Table A.14: Glasswool 18 kg·m^{-3}

Property	Value
Acoustic model	JCAL
Open porosity ϕ	0.96
Static airflow resistivity σ (N· s · m^{-4})	11500
Viscous characteristic length Λ (m)	10.8e-5
Thermal characteristic length Λ' (m)	8e-5
High frequency limit of tortuosity α_∞	1.01
Static thermal permeability k'_o	2.4e-9
Elastic model	Elastic (isotropic)
Density ρ (kg·m^{-3})	18
Young's modulus E (N·m^{-2})	3000
Poisson's ratio ν	0.3
Equivalent viscous damping coefficient η	0.21

Table A.15: Glasswool 18 kg·m^{-3} visco

Property	Value
Acoustic model	JCAL
Open porosity ϕ	0.96
Static airflow resistivity σ (N· s · m^{-4})	11500
Viscous characteristic length Λ (m)	10.8e-5
Thermal characteristic length Λ' (m)	13.8e-5
High frequency limit of tortuosity α_∞	1.01
Static thermal permeability k'_o	2.4e-9
Elastic model	Visco (isotropic)
Density ρ (kg·m^{-3})	18
Young's Modulus E (N·m^{-2})	3000
Poisson's ratio ν	0.3
Frequency (Hz)	Equivalent viscous damping coefficient (η)
10	0.3312
1000	.0463
5000	0.029
10000	0.025

Table A.16: Glasswool 27 kg·m^{-3}

Property	Value
Acoustic model	JCAL
Open porosity ϕ	0.98
Static airflow resistivity σ (N· s · m^{-4})	17500
Viscous characteristic length Λ (m)	10.6e-5
Thermal characteristic length Λ' (m)	15.1e-5
High frequency limit of tortuosity α_∞	1.0
Static thermal permeability k'_o	5.6e-9

Table A.17: Glasswool 8 kg·m^{-3}

Property	Value
Acoustic model	JCAL
Open porosity ϕ	0.99
Static airflow resistivity σ (N· s · m^{-4})	19300
Viscous characteristic length Λ (m)	8.5e-5
Thermal characteristic length Λ' (m)	12.5e-5
High frequency limit of tortuosity α_∞	1.21
Static thermal permeability k'_o	23e-9
Elastic model	Limp
Density ρ (kg·m^{-3})	8

Table A.18: Melamine foam

Property	Value
Acoustic model	JCA
Open porosity ϕ	0.99
Static airflow resistivity σ (N· s · m^{-4})	10000
Viscous characteristic length Λ (m)	9.8e-5
Thermal characteristic length Λ' (m)	19.6e-5
High frequency limit of tortuosity α_∞	1.01
Elastic model	Elastic (isotropic)
Density ρ (kg·m^{-3})	8
Young's modulus E (N·m^{-2})	160000
Poisson's ratio ν	0.44
Equivalent viscous damping coefficient η	0.1

Table A.19: Mineral wool Villot et al. 2001 [248]

Property	Value
Acoustic model	JCA
Open porosity ϕ	0.96
Static airflow resistivity σ (N· s · m^{-4})	34000
Viscous characteristic length Λ (m)	4e-5
Thermal characteristic length Λ' (m)	8e-5
High frequency limit of tortuosity α_∞	1.0
Elastic model	Elastic (isotropic)
Density ρ (kg·m^{-3})	90
Young's modulus E (N·m^{-2})	400000
Poisson's ratio ν	0.0
Equivalent viscous damping coefficient η	0.18

Table A.20: Perforated Plate circular

Property	Value
Acoustic model	Perf. Plate Circular
Open porosity ϕ	0.1
Radius (m)	1e-4
Correction	dynamic
Inclination	0

Table A.21: Polymer foam 27 kg·m^{-3}

Property	Value
Acoustic model	JCAL
Open porosity ϕ	0.98
Static airflow resistivity σ (N· s · m^{-4})	43900
Viscous characteristic length Λ (m)	1.9e-5
Thermal characteristic length Λ' (m)	26.7e-5
High frequency limit of tortuosity α_∞	2.81
Static thermal permeability k'_o	25.5e-9
Elastic model	Limp
Density ρ (kg·m^{-3})	27

Table A.22: PU foam Groby et al., JASA 2010

Property	Value
Acoustic model	JCA
Open porosity ϕ	0.98
Static airflow resistivity σ (N· s · m^{-4})	2830
Viscous characteristic length Λ (m)	31.9e-5
Thermal characteristic length Λ' (m)	62.1e-5
High frequency limit of tortuosity α_∞	1.06

Table A.23: PU foam Groby et al., JASA 2010

Property	Value
Acoustic model	JCAL
Open porosity ϕ	0.95
Static airflow resistivity σ (N· s · m^{-4})	13500
Viscous characteristic length Λ (m)	3.9e-5
Thermal characteristic length Λ' (m)	22e-5
High frequency limit of tortuosity α_∞	1.0
Static thermal permeability k'_o	6.9e-9

Table A.24: Rock wool

Property	Value
Acoustic model	JCAL
Open porosity ϕ	0.95
Static airflow resistivity σ (N· s · m^{-4})	120000
Viscous characteristic length Λ (m)	1.2e-5
Thermal characteristic length Λ' (m)	7.2e-5
High frequency limit of tortuosity α_∞	1.08
Static thermal permeability k'_o	1.1e-9

Table A.25: Screen 10

Property	Value
Acoustic model	Screen
Open porosity ϕ	0.1
Static airflow resistivity σ (N· s · m^{-4})	200000
Correction	Dynamic

Table A.26: Screen with high porosity, Jaouen & Bécot 2011 [108]

Property	Value
Acoustic model	Screen
Open porosity ϕ	0.72
Static airflow resistivity σ (N· s · m^{-4})	87000
Correction	Dynamic
Elastic model	Rigid body
Density ρ (kg·m^{-3})	171

Table A.27: Screen with low porosity, Jaouen & Bécot 2011 [108]

Property	Value
Acoustic model	Screen
Open porosity ϕ	0.04
Static airflow resistivity σ (N· s · m^{-4})	720000
Correction	Dynamic
Elastic model	Rigid body
Density ρ (kg·m^{-3})	809

Table A.28: Scrim headliner

Property	Value
Acoustic model	Screen
Open porosity ϕ	0.2
Static airflow resistivity σ (N· s · m^{-4})	170000
Correction	Dynamic
Elastic Model	Limp
Density ρ (kg·m^{-3})	250

Table A.29: Wood fiber

Property	Value
Acoustic model	JCAL
Open porosity ϕ	0.97
Static airflow resistivity σ (N· s · m^{-4})	400000
Viscous characteristic length Λ (m)	1.5e-5
Thermal characteristic length Λ' (m)	13.8e-5
High frequency limit of tortuosity α_∞	1.28
Static thermal permeability k'_o	32.3e-9

Appendix B

Topology optimisation

B.1 Runtime progress: all problem instances

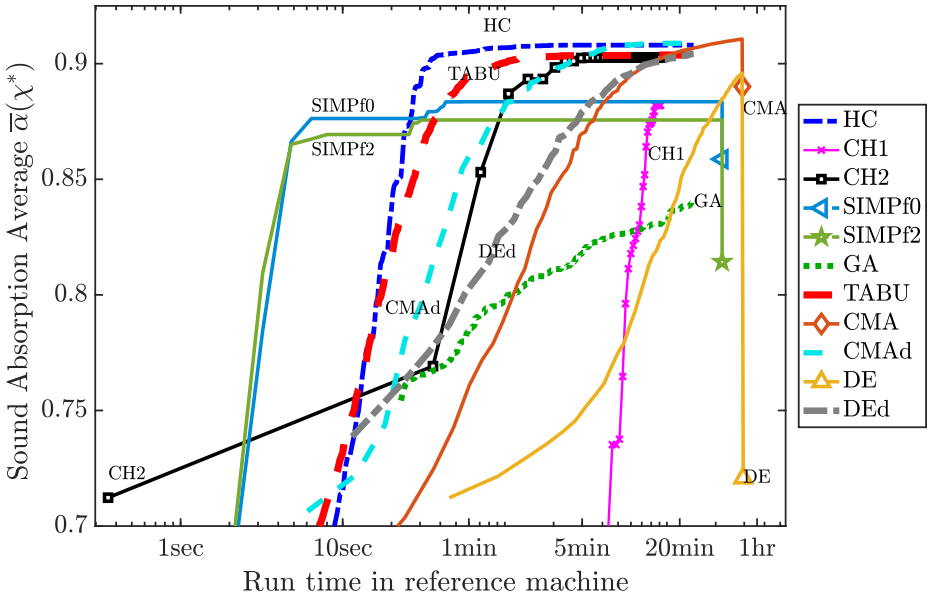

Figure B.1: Runtime progress of all algorithms on problem instance 1

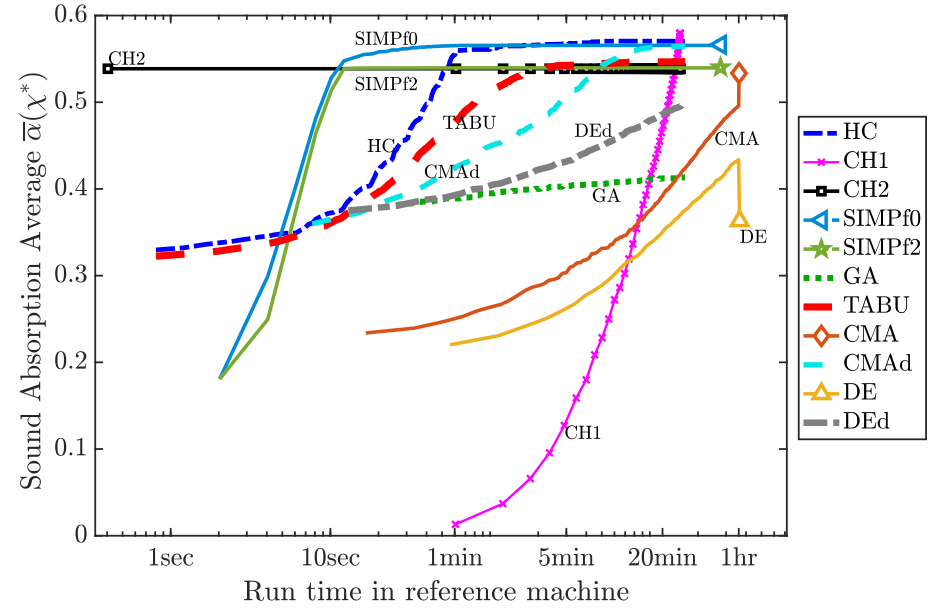

Figure B.2: Runtime progress of all algorithms on problem instance 2

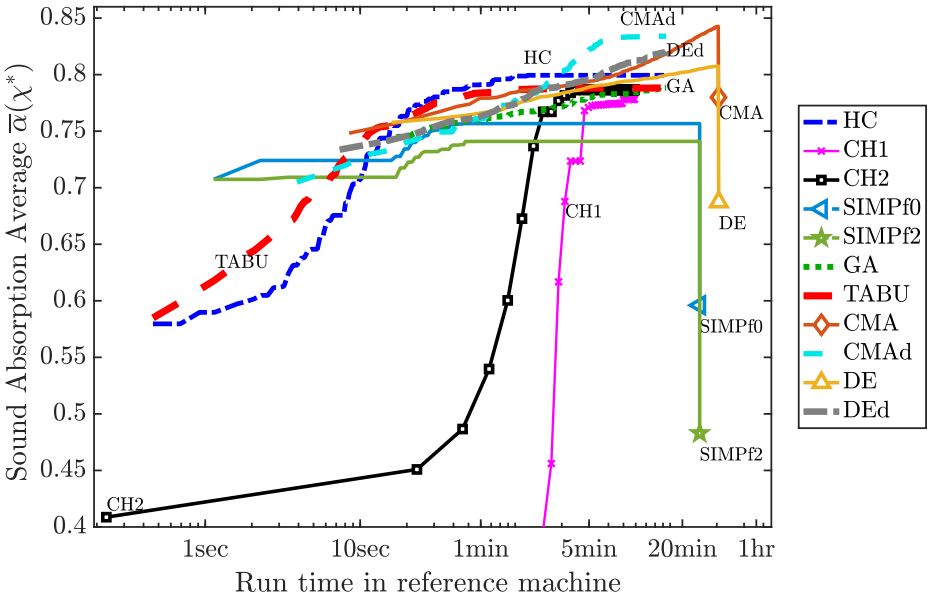

Figure B.3: Runtime progress of all algorithms on problem instance 3

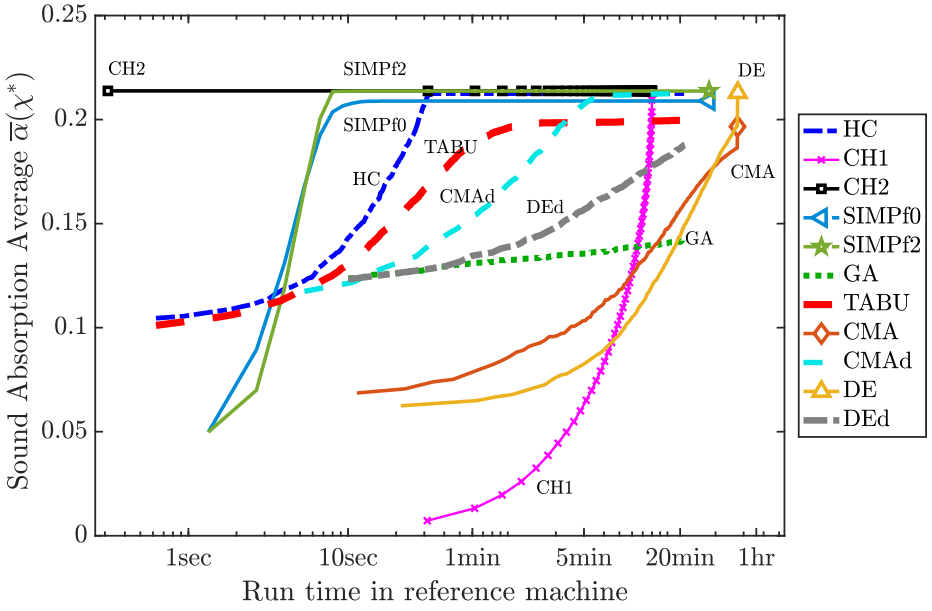

Figure B.4: Runtime progress of all algorithms on problem instance 4

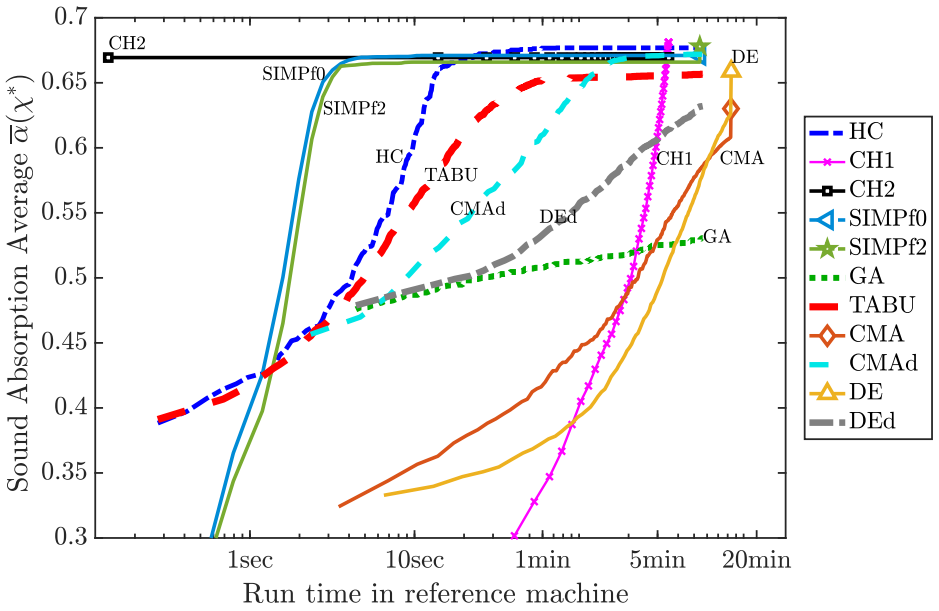

Figure B.5: Runtime progress of all algorithms on problem instance 5

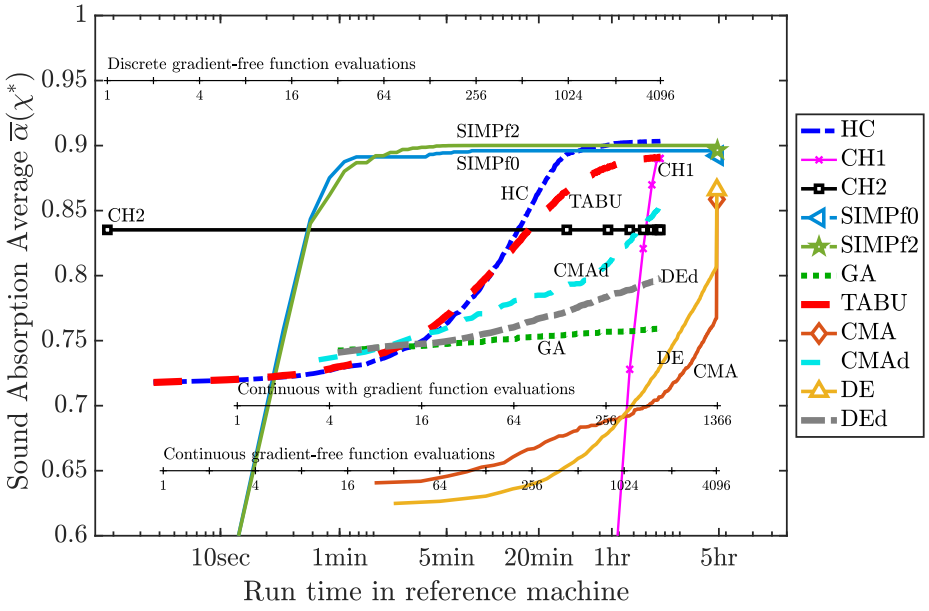

Figure B.6: Runtime progress of all algorithms on problem instance 6

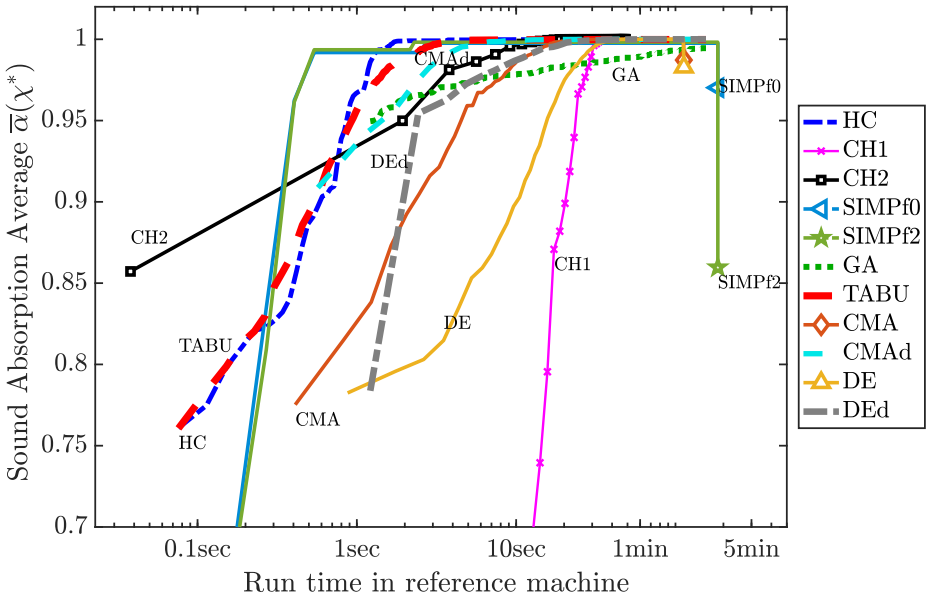

Figure B.7: Runtime progress of all algorithms on problem instance 7

B.2 Final solution absorption-distribution from trials

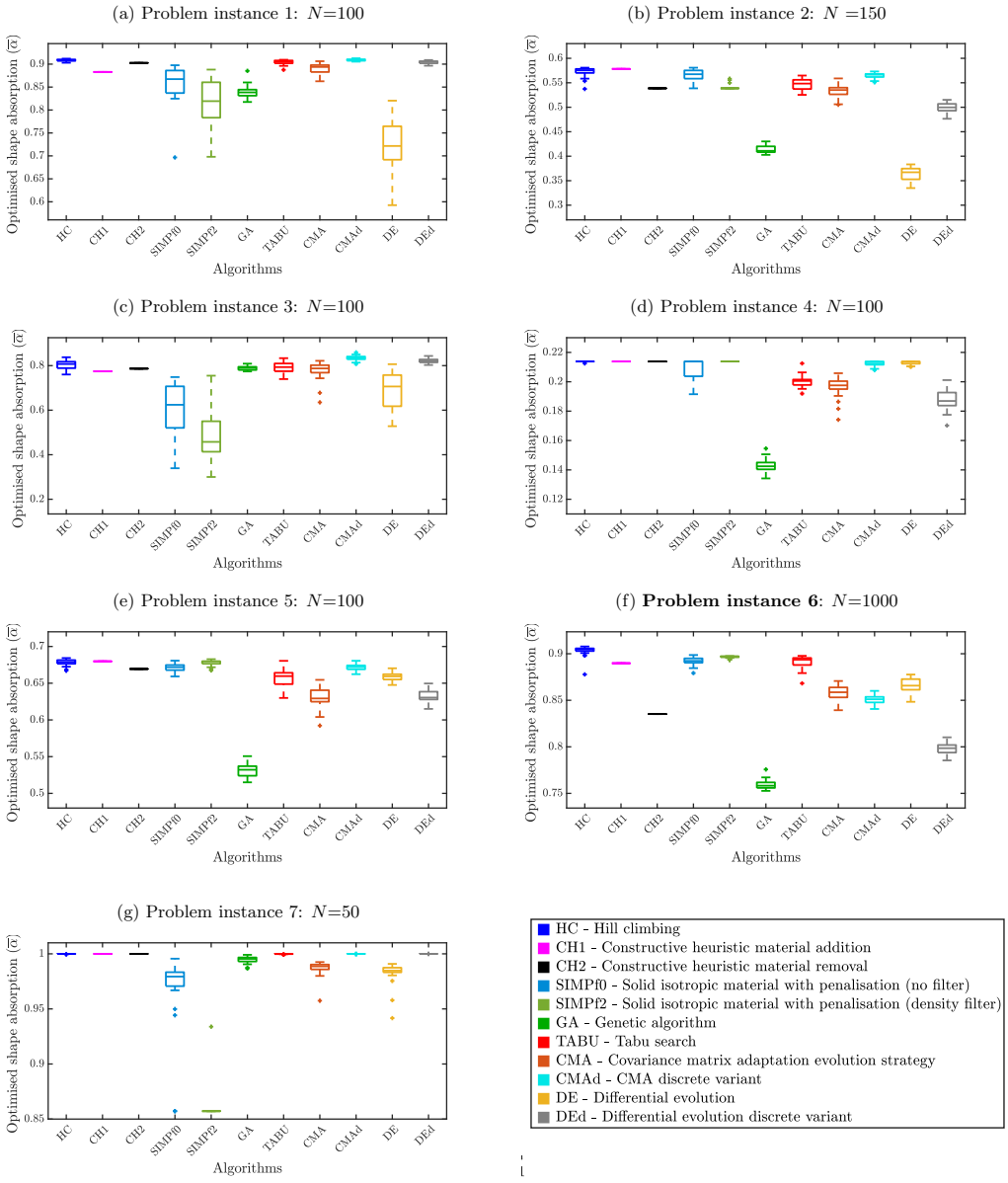

Figure B.8: Distribution of absorption of solutions from all trials of all algorithms for each problem instance.

B.3 Final solution absorption vs. volume fraction

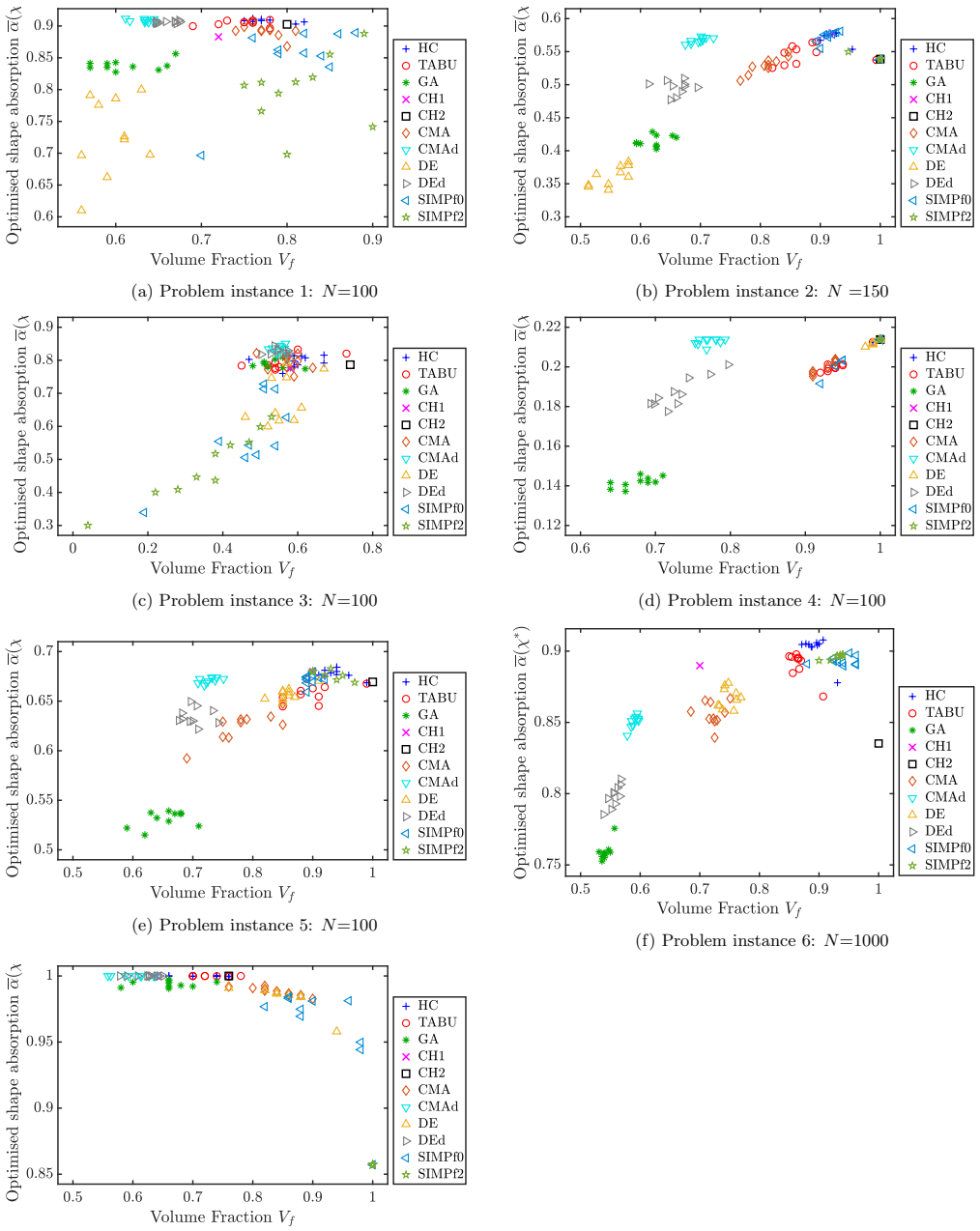

(a) Problem instance 1: N=100

(b) Problem instance 2: N =150

(c) Problem instance 3: N=100

(d) Problem instance 4: N=100

(e) Problem instance 5: N=100

(f) Problem instance 6: N=1000

Figure B.9: Absorption versus volume fraction of solutions from all trials of all algorithms for each problem instance. Observe the solutions from each algorithm being clustered in this space.

B.4 Final solutions across trials

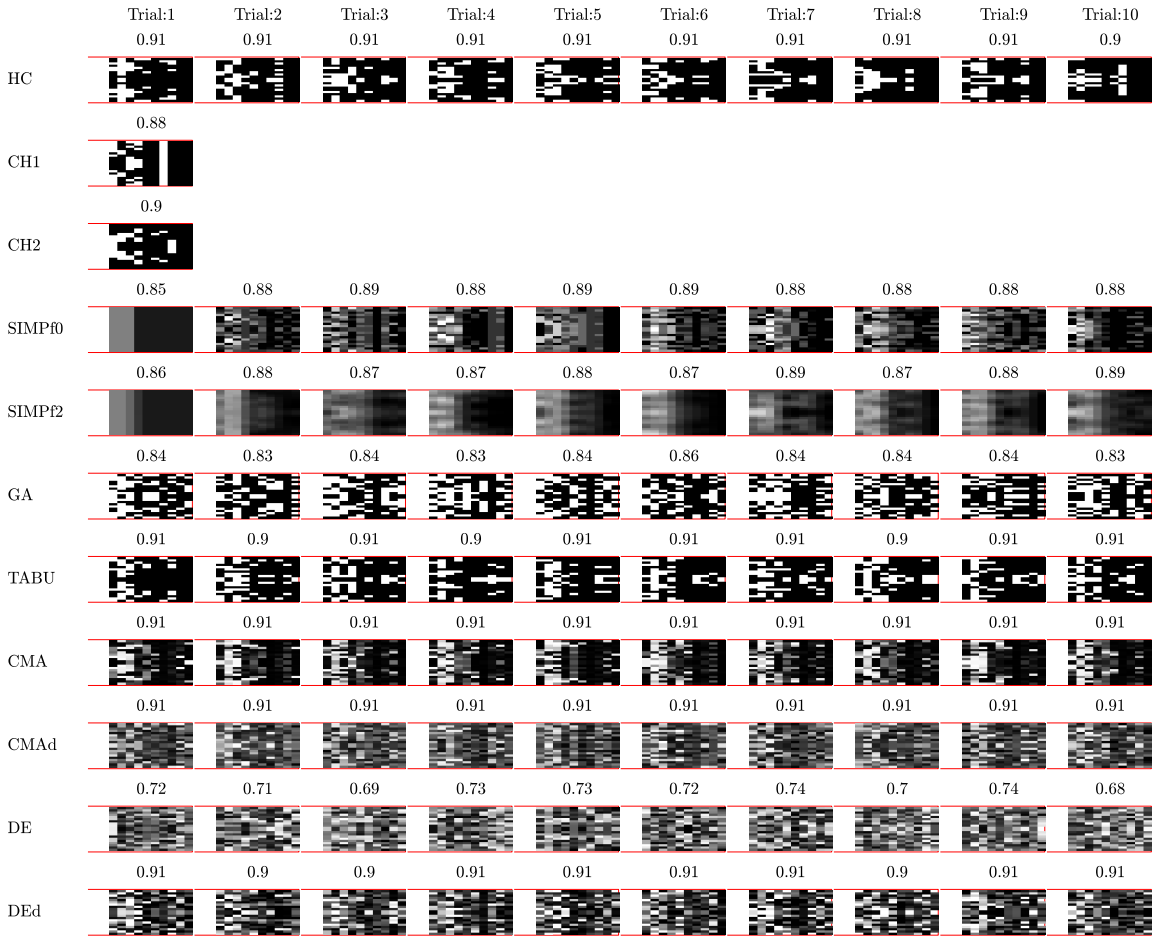

Figure B.10: Final solutions for problem instance 1

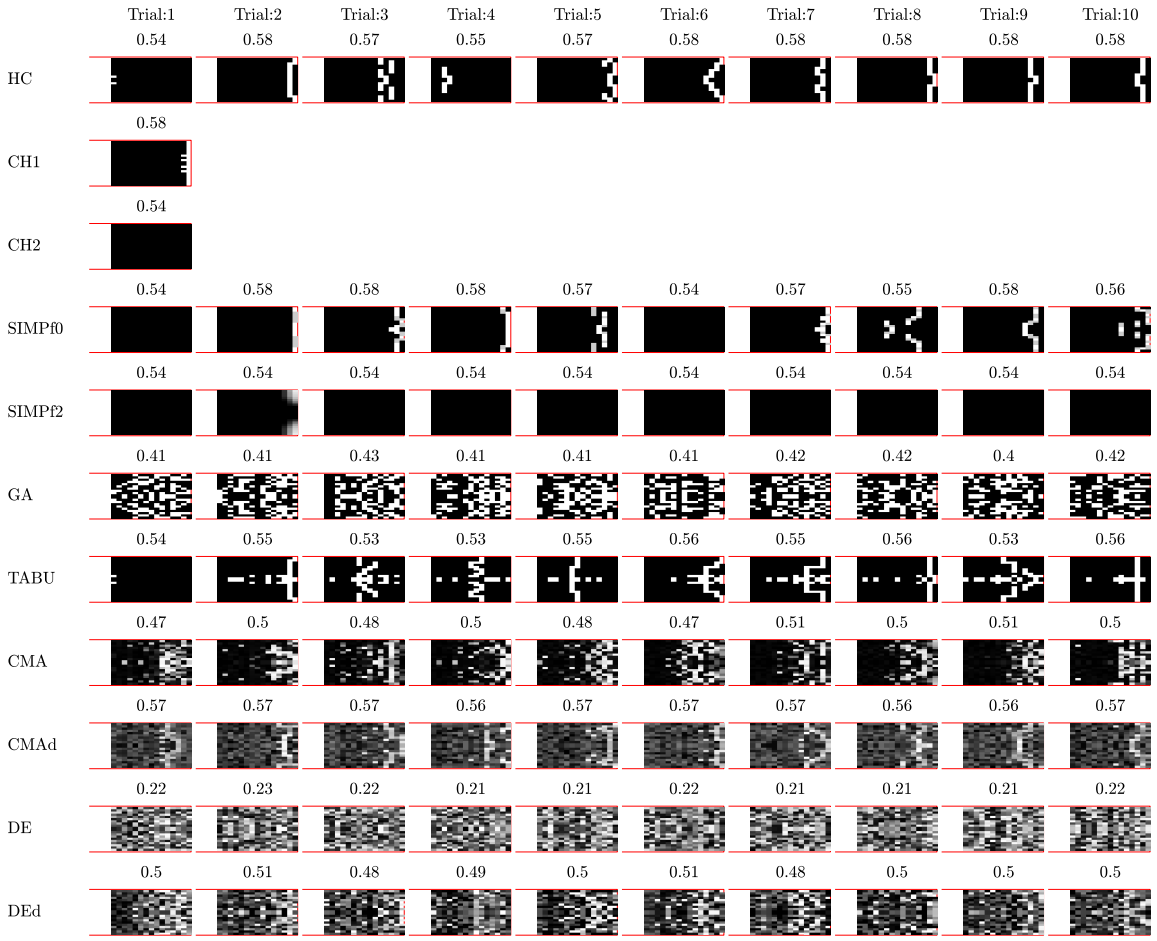

Figure B.11: Final solutions for problem instance 2

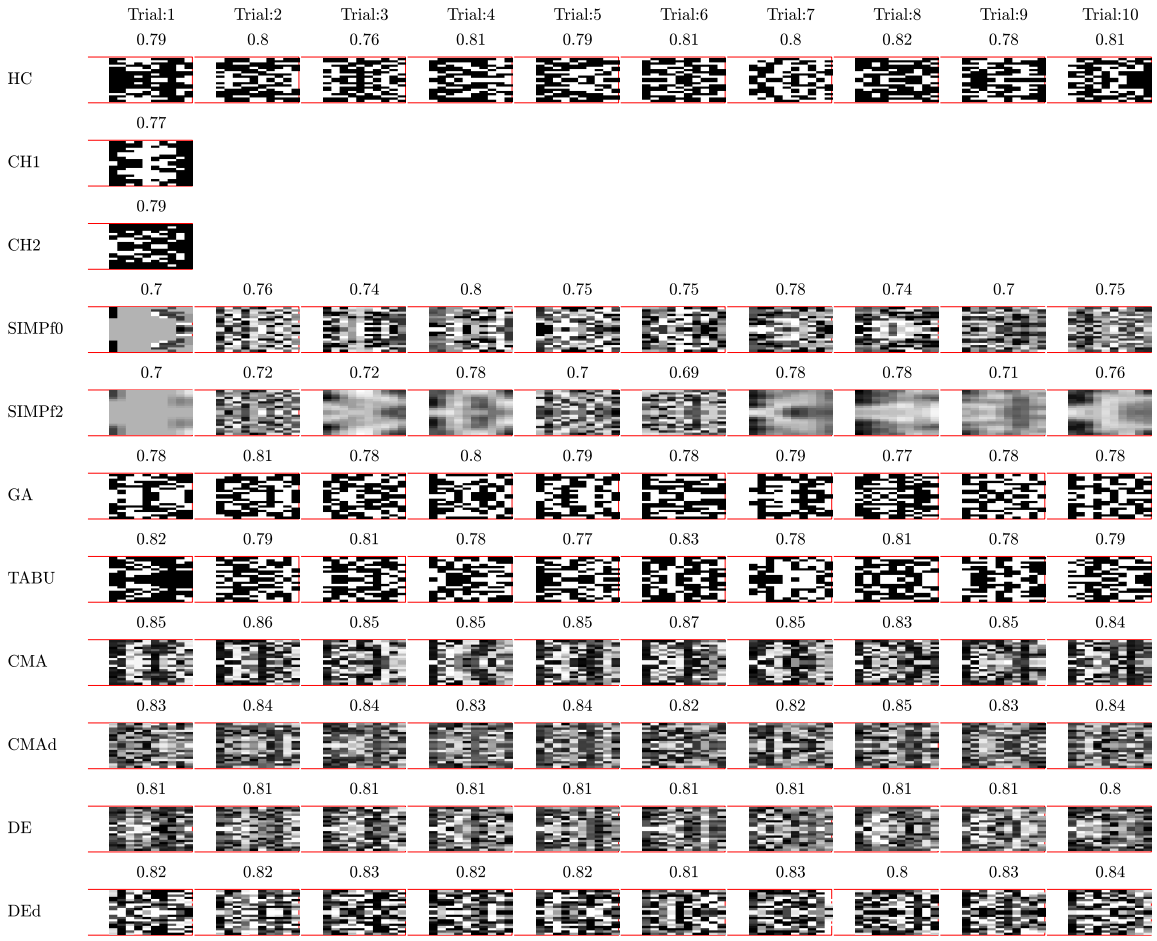

Figure B.12: Final solutions for problem instance 3

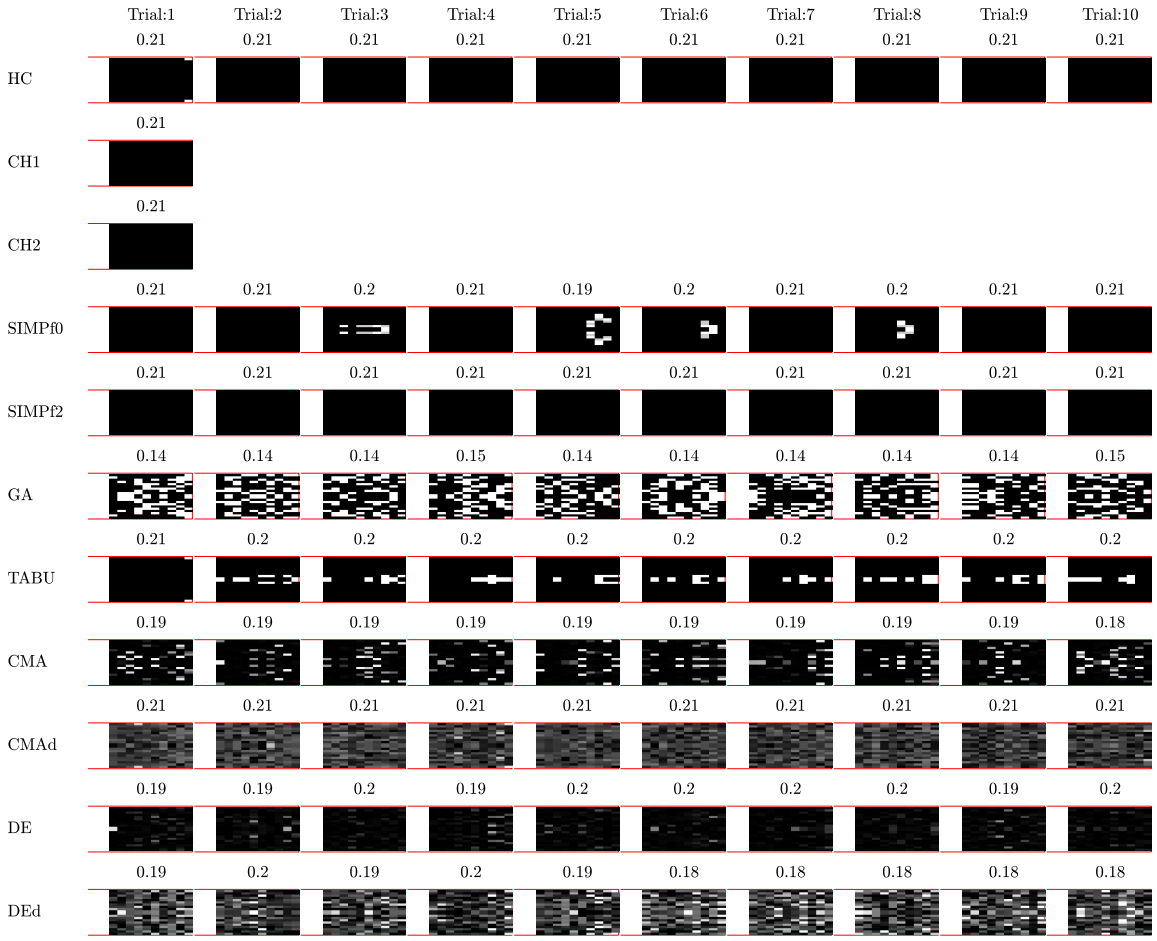

Figure B.13: Final solutions for problem instance 4

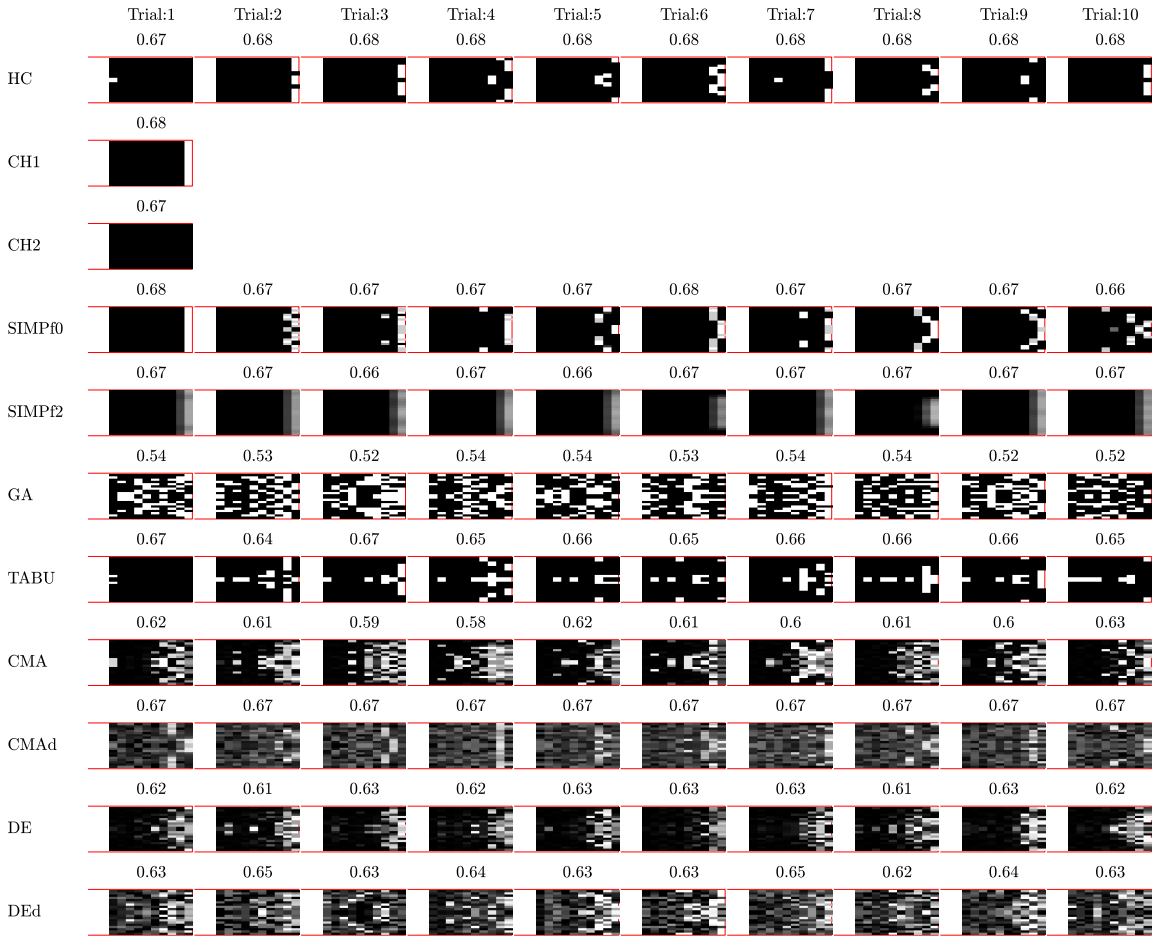

Figure B.14: Final solutions for problem instance 5

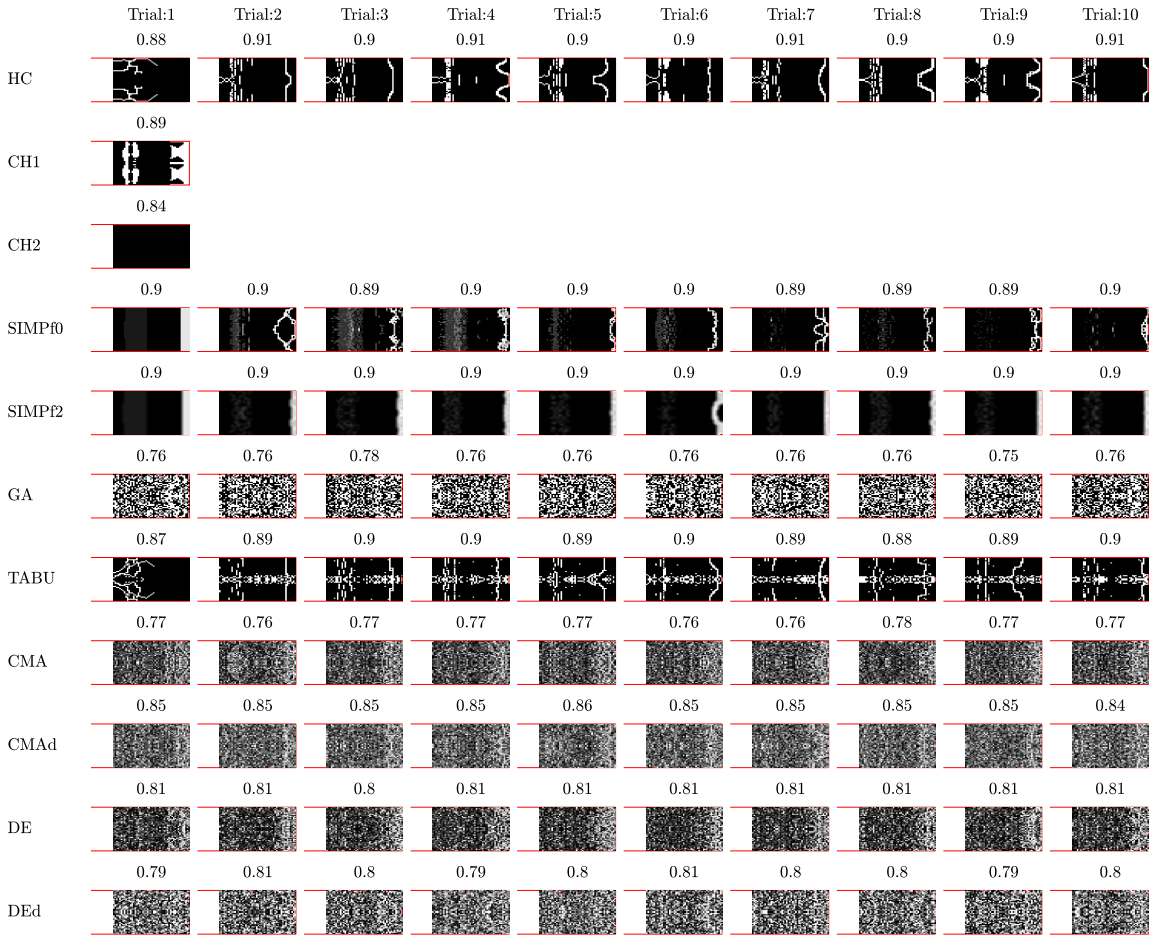

Figure B.15: Final solutions for problem instance 6

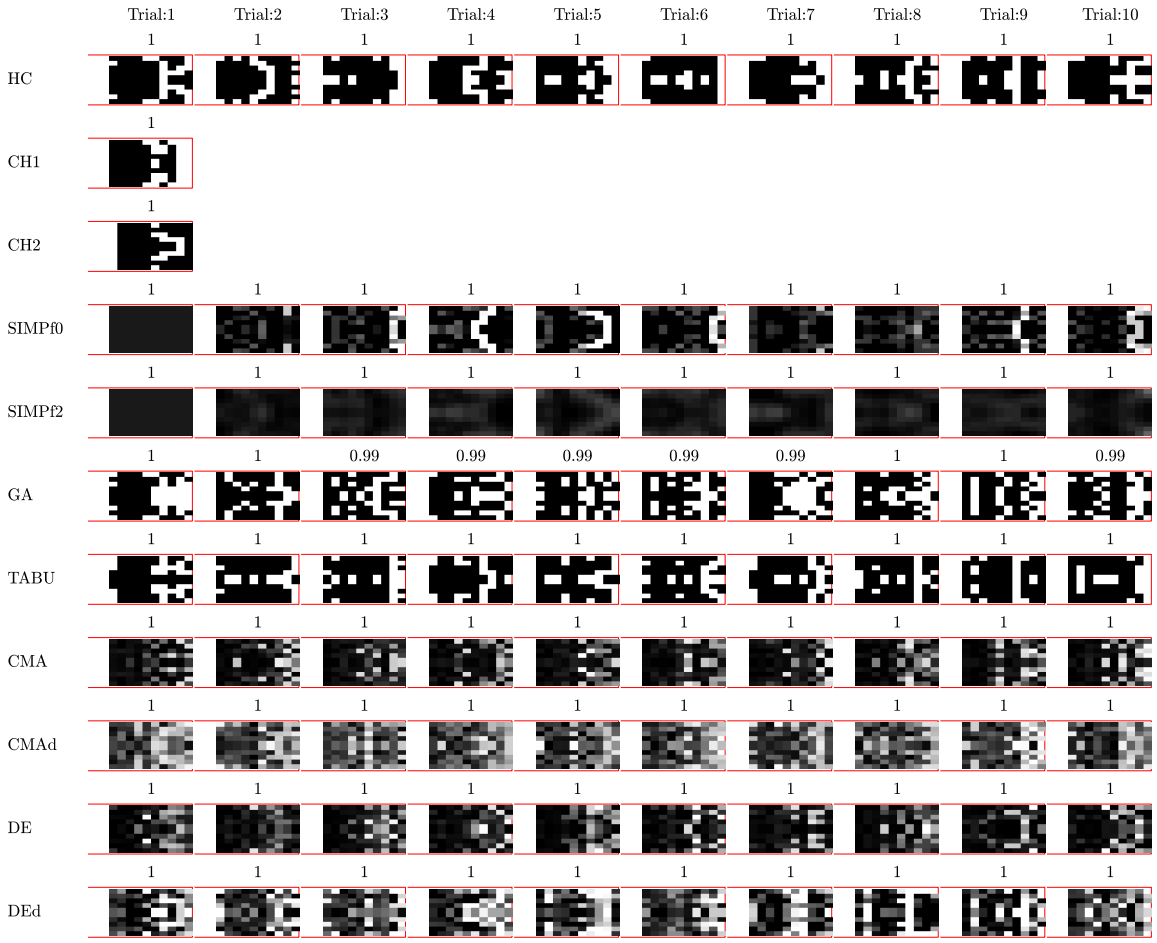

Figure B.16: Final solutions for problem instance 7

Appendix C

Multi-objective optimisation

C.1 Pareto plots for 15-trial-combined results

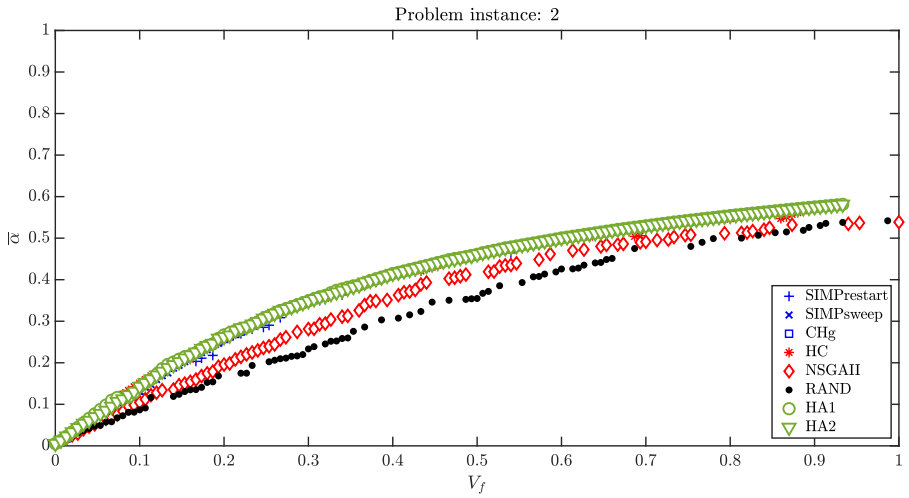

Figure C.1: Comparison of all Pareto fronts in problem instance 2

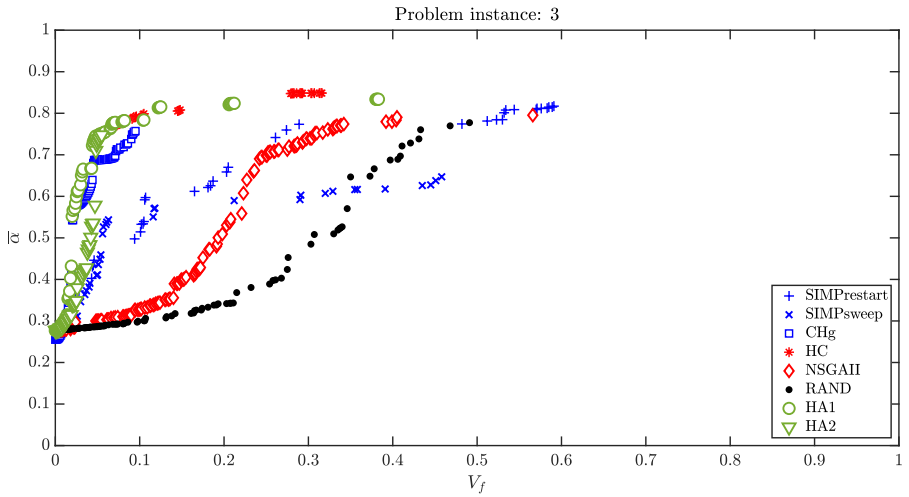

Figure C.2: Comparison of all Pareto fronts in problem instance 3

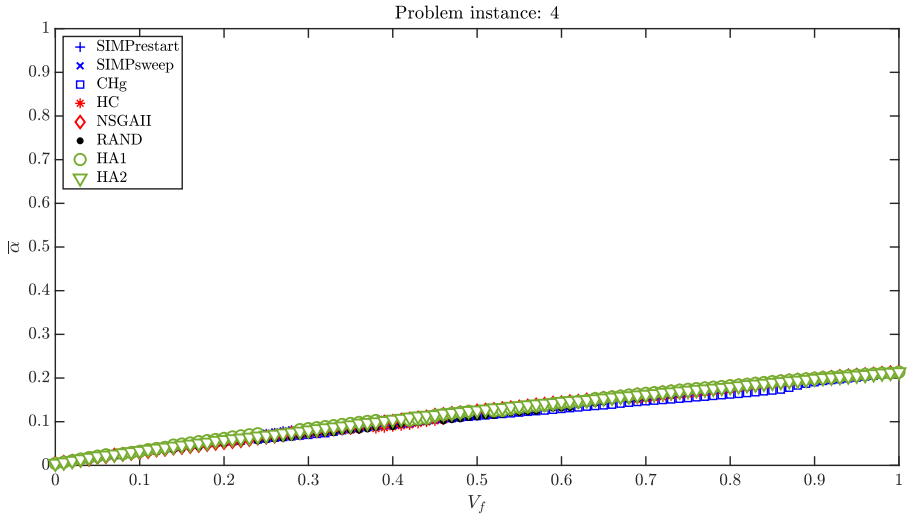

Figure C.3: Comparison of all Pareto fronts in problem instance 4

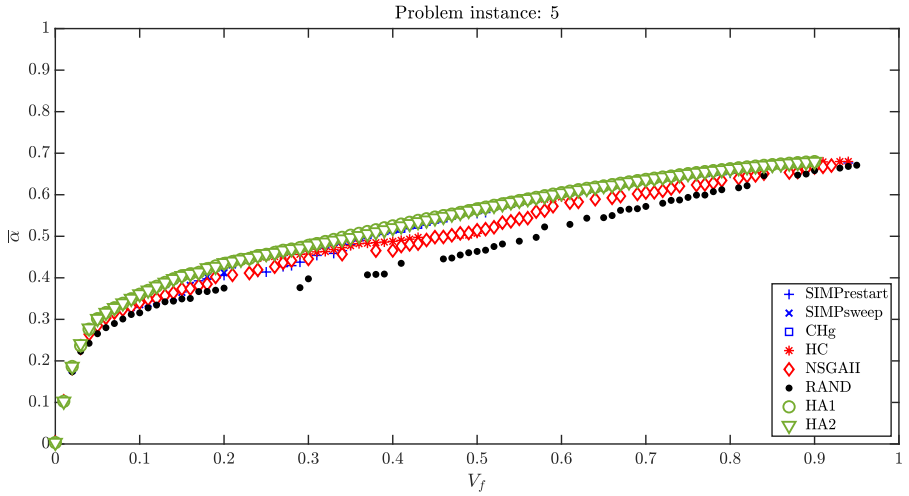

Figure C.4: Comparison of all Pareto fronts in problem instance 5

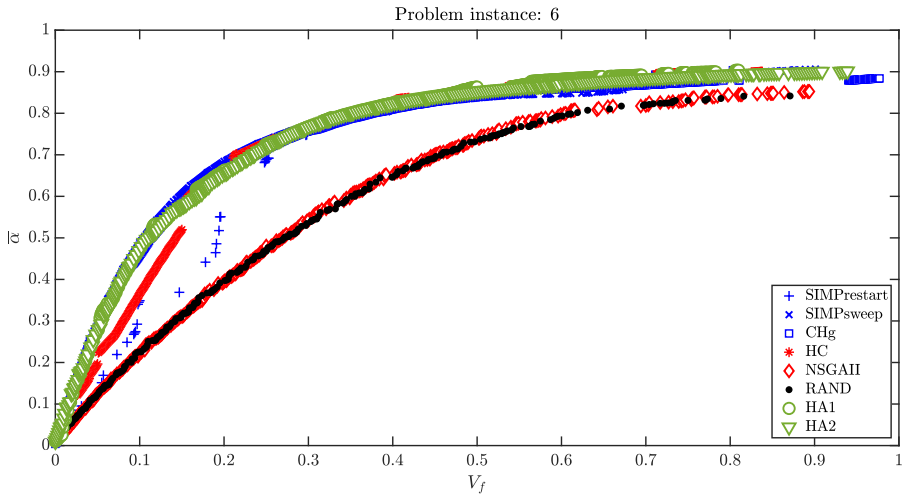

Figure C.5: Comparison of all Pareto fronts in problem instance 6

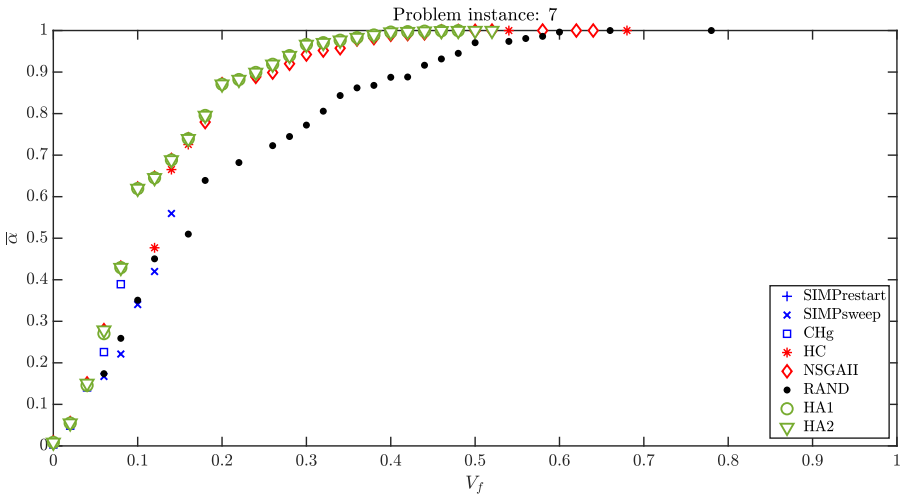

Figure C.6: Comparison of all Pareto fronts in problem instance 7